Viscoelastic Behavior of Water-Blown Flexible Polyurethane Foams

by

John C. Moreland

Dissertation submitted to the Faculty of the

Virginia Polytechnic Institute and State University

in partial fulfillment of the requirements for the degree of

Doctor of Philosophy

in

Chemical Engineering

APPROVED:

G.L. Wilkes, Chairman

M.E. Davis

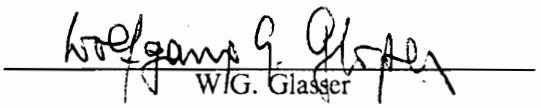

W.G. Glasser

J.S. Riffle

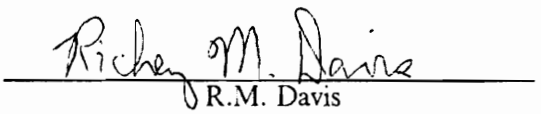

R.M. Davis

April, 1991

Blacksburg, Virginia

Viscoelastic Behavior of Water-Blown Flexible Polyurethane Foams

by

John C. Moreland

G.L. Wilkes, Chairman

Chemical Engineering

(ABSTRACT)

The main focus of this dissertation was on characterizing the viscoelastic behavior of a set of four flexible slabstock water-blown polyurethane foams with varying hard segment content as well as solid plaques made from these foams. Three viscoelastic tests; tensile stress relaxation, compression load relaxation, and compression creep, were utilized to evaluate the behavior of these materials at constant temperature and/or relative humidity, RH. The tensile stress relaxation tests were performed at a 25 percent strain level. The majority of the compression load relaxation tests were conducted at a 65 percent level since this is the strain level used for the common indentation load deflection test for flexible foams and the relaxation behavior was rather independent of strain at this level. Over a three hour testing period, a near linear relationship for the log of tensile stress or compressive load versus log time is observed for most conditions. The slope from this linear relationship in tension or the stress decay rate is similar for all the foams and their respective plaques; thus indicating that the tensile stress relaxation of these materials is governed by the solid portion of the foams and is therefore independent of the cellular textures. In addition, the rates of relaxation for rather linear behavior in tension and compression are also comparable for these foams and this implies that the relaxation in compression is mostly independent of the cellular texture of the foams at a 65 percent strain level. After a short induction period, the compressive creep behavior exhibits rather linear behavior for linear strain vs log time over a three hour period. The slope of this relationship is dependent on the initial strain level and goes through a maximum with initial strain at 40 percent. This maximum is believed to be due to the buckling of the foam's struts. The results for the creep behavior were evaluated at a 65 percent initial strain since the creep behavior is believed to be mostly independent of the cellular texture of the foam at this level and greater. A greater amount of viscoelastic decay, i.e. tensile stress relaxation, compression load relaxation and com-

pression creep is observed for the higher hard segment foams. Temperature has a similar effect on the results obtained from the three viscoelastic tests. Likewise, relative humidity at a constant temperature also has a similar effect on the viscoelastic behavior of the three tests. Up to 100°C, temperature accelerates the viscoelastic decay of these foams over a three hour time period. For all three viscoelastic tests, a significant increase in the viscoelastic decay at temperatures greater than 100°C is observed. The FTIR thermal analysis of the plaques indicated that this significant increase is due to additional hydrogen bond disruption as well as possible degradation in the urea and urethane links. Increasing relative humidity at a given temperature does bring about a steady decrease in the initial load or initial stress as well as a small increase in the rate of viscoelastic decay. Overall, the effects of temperature are greater on the viscoelastic decay than humidity.

The morphology and the viscoelastic behavior of another set of flexible slabstock foams were characterized. These additional foams are rather unique in that some of their morphological features, the urea aggregate structure in particularly, are altered by adding a small amount of LiCl to the formulation. As discussed within the body of this dissertation, these observed changes in morphology are believed to have a significant effect on the viscoelastic nature.

Acknowledgements

I would like to thank my advisor, Dr. G.L. Wilkes, for his guidance, patience and encouragement, throughout my graduate work at Virginia Tech. In addition, I thank him for giving me the opportunity to work on my own and to develop as an individual.

I would also like to thank Dr. W.G. Glasser, Dr. M.E. Davis, Dr. R.M. Davis and Dr. J.S. Riffle for their suggestions and interest in my work as well as for reading this document.

A special thanks goes to Dow Chemical for sponsoring this project and their collaboration over the years. I am also grateful to Bob Turner of Dow Chemical for his efforts towards this project as well as the opportunities he has given me to interact with others who work in the area of polyurethane foams. I extend a special thanks to Bob Kuklies for his efforts in making the foams for the latter part of this study. I would also like to thank Ralph Priester for his help on the interpretation of the FTIR data presented in this dissertation. Finally, I would like to thank Gene Parks for making the LiCl foams and supplying necessary data on these materials as well as Ed Rightor for his TEM work on several of the foams studied in this dissertation.

I would like to thank Riley Chan and Billy Williams for their assistance in constructing the equipment that was utilized for obtaining the viscoelastic behavior on the flexible foams.

I would like to thank S.S. Sankar and C.G. Moreland(my dad) for carrying out the solid state NMR measurements on the foams as well as for their input on interpreting the results.

I would like to thank my fellow workers in the lab, both past and present, for their interest in this work, helpful discussions, support, friendship, encouragement and for all the good times in the lab as well as away from the lab.

Finally, I am grateful for the support and encouragement that I received from my family, my fiancee, Cheryl Whitfield, and other friends during my stay at Virginia Tech and especially over the last few months while I was writing my dissertation.

Table of Contents

List of Illustrations

List of Tables

Chapter I

1.0 Introduction

Polyurethanes are often made by reacting an isocyanate group of an aromatic diisocyanate with a hydroxyl group of a polyether or polyester polyol. In polyurethanes, the urethane group (NH-CO-O) serves as the chemical linkage between the flexible unit(e.g. polyol) and the more rigid unit(e.g. aromatic diisocyanate). The different types of polyurethane products can be classified under foams, elastomers, adhesives, binders, coatings and paints. Within these categories there are a wide range of properties leading to numerous applications. Five of the most important areas of applications are automotive, furniture, construction, thermal insulation, and footwear. Of the different types of polyurethanes, flexible foams are dominant and have been chosen for this investigation because of their extensive usage. The main focus of this investigation is on the viscoelastic behavior of flexible slabstock water-blown foams due to its importance in understanding load bearing and long term properties of these materials.

From a historical point of view, urethane chemistry dates back to 1849 when the reaction between an isocyanate and hydroxyl compound was first reported. However, not until 1937 did the first commercial polyurethanes become available by Otto Bayer and co-workers. During World

War II polyurethane elastomers, coatings and adhesives were also developed due to the demand for new materials.

In 1953, the first flexible polyurethane foams were produced based on a Bayer patent system using toluene-diisocyanate (TDI) and a polyester polyol. It was in 1956 that the first polyether based-flexible polyurethane foam was developed in the United States using a two stage process. Three years later flexible foams were produced by mixing all chemical components at the same time and then dispensing the mixture. This process is better known as the "one shot" system and still remains the common way of producing flexible foams. In 1959 improvements in the polyether polyol were made that cut costs and brought about improved properties. One other major development for the advancement of flexible foam technology was the introduction of the silicone surfactant into the "one-shot" system. From here, improvements in the physical properties in flexible foams have been continuously made by several approaches. All of these improvements have resulted in flexible foams constituting 50% or more of the polyurethanes made today.

Flexible foams are manufactured either by a continuous method or by a batch operation. The batch operation consists of molding foams in a hot-cure or in cold-cure process. The most efficient batch operation is the cold-cure process and high-resilient (HR) foams are most often made by this process. These foams are used in the automotive and furniture industries. Molded foams make up about 20% of the flexible foams while slabstock foams make up the rest. Flexible slabstock foams are usually manufactured by a continuous method and in few cases by a batch operation (e.g. complex shapes and sizes). They are also used in the furniture and automotive industries as well as for packaging material.

As was mentioned earlier, improvements in the performance and in the physical properties of flexible foams have been made since their market introduction in the 1950's. Most of these improvements were made by adjusting the chemical and processing variables and these types of improvements are still being made today. However, the more recent approaches are beginning to focus on understanding why a particular physical property results. One of these approaches has involved comprehending the sequence of reactions and their mechanisms that take place during the foam formation. Furthermore, studies have and are being carried out to model or predict mechanical

behavior in hopes of understanding the contributions from the cell structure and the solid portion of flexible foams. One of the more recent studies has concentrated on understanding the morphology of the solid portion of flexible water-blown polyurethane foams by utilizing several structural techniques. In the latest work, the technique of linear IR-dichroism with a simultaneous mechanical response was utilized to better understand the structure-property behavior in the solid portion of these same materials.

In summary, the approach to obtaining more economical flexible foams possessing better physical properties has changed somewhat in the last ten to fifteen years. Instead of continuously changing the chemical and processing variables to obtain the preferred physical properties, foams are being studied on the macroscopic and the microscopic levels. With this in mind, Dow Chemical and Virginia Tech have initiated a joint venture to hopefully obtain a better understanding of the resulting physical properties in flexible water-blown polyurethane foams. A part of this venture is presented in this dissertation with the main emphasis on evaluating the viscoelastic behavior in both compression and tension modes of deformation under controlled testing conditions(temperature and relative humidity) for a series of four variable hard segment flexible slabstock water-blown polyurethane foams as well as the compression molded plaques of these same foams. In continuation of an earlier investigation(author's Masters Thesis), the effects of temperature on the segmental orientation behavior for one of the four compression molded plaques is also presented to aid in the understanding the viscoelastic nature of flexible foams. In addition, work on a special set of flexible water-blown foams with unique morphological features is also discussed.

Chapter II

2.0 Literature Review

In this chapter, a summary is given on works reported in the literature on flexible polyurethane foams and in a few cases, for comparison purposes, on thermoplastic polyurethane elastomers. The areas that will be reviewed concerning these two polyurethanes are (1) chemistry, (2) morphology, (3) mechanical properties, and (4) FTIR applications. Since the work presented in this dissertation is a continuation of the author's Master Thesis, parts of the literature review have been taken from this earlier document. In particularly, sections on the chemistry and the morphology of polyurethane foams are mostly from the review presented in that thesis. However, where possible and relevant, additional and more recent publications have been reviewed. In the section on mechanical properties, a more thorough review is presented with special emphasis on the viscoelastic properties. Also, for the section on FTIR applications and in particular linear IR- dichroism, a summary is provided from the author's Masters work which concentrated on the orientation-deformation behavior of plaques compression molded from foams.

2.1 Chemistry

In this section, the focus will be on flexible polyurethane foams, although some comparisons to thermoplastic polyurethane elastomers are made in some instances. The general chemical reactions as well the specific components and their significance in the foaming process are discussed. Furthermore, the foaming process and some of the most recent work concerning the chemistry of flexible water-blown polyurethane foams are also covered.

2.1.1 General Chemical Reactions

There are three primary reactions that take place in the formation of polyurethane foams. The first(see Figure 2.1a) takes place between an isocyanate group and water to give an unstable intermediate group, carbamic acid, which then degenerates to form a primary amine and carbon dioxide gas. The carbon dioxide created from this reaction serves as the principal source of blowing the foam mixture. Thus, this reaction is commonly referred to as the blowing reaction. In the second as shown in Figure 2.1b, the primary amine created from the first reacts with another isocyanate group to give a disubstituted urea. This reaction serves as a means to chain extend the aromatic groups of the diisocyanates by urea linkages. These first two reactions are highly exothermic (1-3).

The third takes place between an isocyanate group and a hydroxyl group to give a urethane as shown in Figure 2.1c. The urethane serves as a link between the chains of a polyol and an aromatic diisocyanate. This reaction is called the gelling reaction due to its ability to develop a network from the polymerizing foam mixture. Furthermore, the gelling reaction is also highly exothermic.

Secondary reactions can also take place upon reaction of urea or urethane groups with isocyanate to give biuret or allophanate groups, respectively (see Figure 2.2). These reactions can cause further crosslinking in foams with the biuret formation being more likely of the two, since

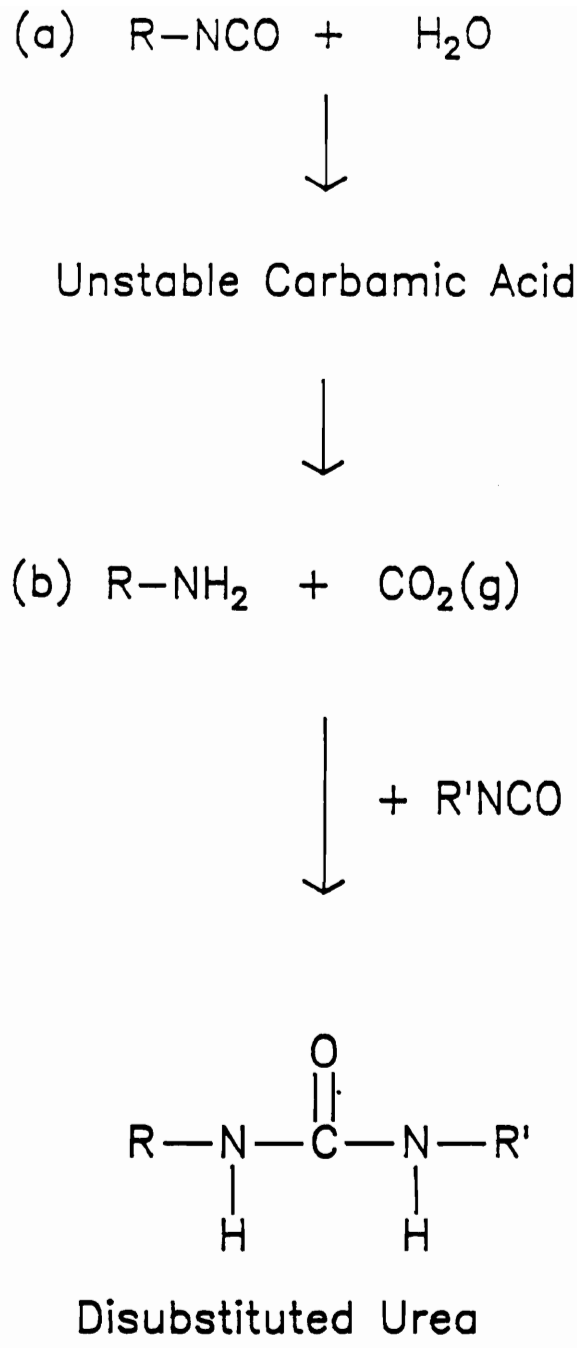

Figure 2.1. Primary Reactions in Flexible Foam Formation: (a) blowing reaction (b) chain extension (c) gelling reaction (next page)

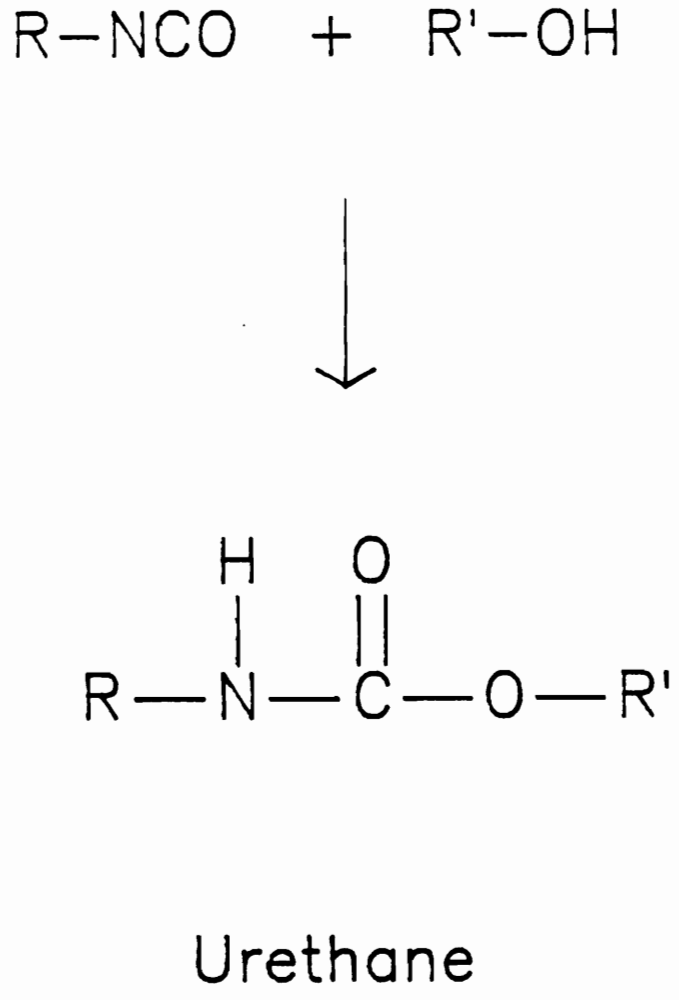

Figure 1, cont'd: Gelling Reaction

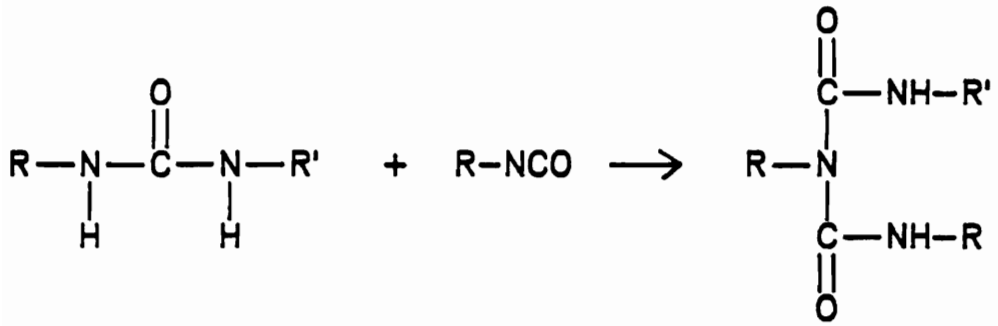

Biuret

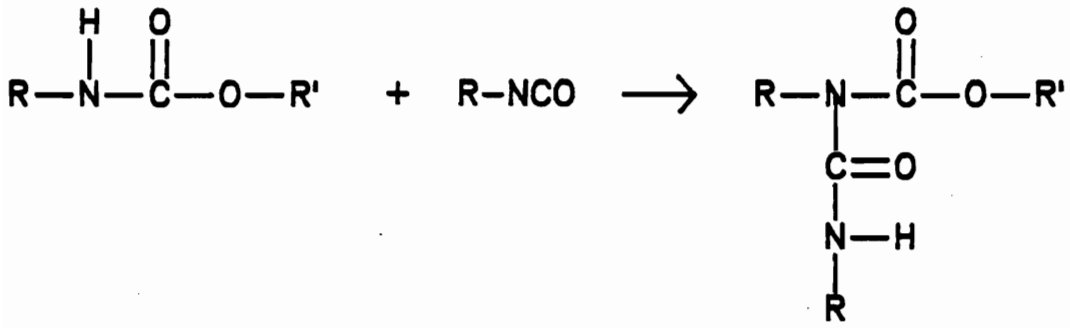

Allophanate

Figure 2.2. Secondary Reactions in Flexible Foam Formation

urea groups are more reactive to isocyanate than urethanes. Furthermore, temperatures greater than 120°C in uncatalyzed systems are necessary to have any significant allophanate crosslinking. However, both of these reactions are less likely to occur in flexible polyurethane foams due to steric hindrance in the reacting components as will become clearer when the chemical structures of the formulation components in flexible foams are reviewed.

Polyurethane elastomers are made by a one or two step reaction. The two step procedure is the more preferred.The first step is similar to the gelling reaction described above and consists of reacting a polyol and diisocyanate to give an encapped prepolymer. The prepolymer and the excess isocyanate mixture are then reacted with a chain extender to give the final product. This step is similar to the primary amine-isocyanate reaction given above. Depending on the type of chain extender, urea(diamine) or urethane(diol) linkages are formed between the aromatic groups of the diisocyanates. Thus, if a diamine is used, a polyurea-urethane is made; if a diol is used, a polyurethane is made.

The chemistry of foams and elastomers differ in several ways. First, two reactions are taking place simultaneously in the formation of foams, while it usually takes two separate stagewise reactions to form an elastomer. Also, the conditions for the foam reaction are less controllable in comparison to that of the polyurethane elastomers. This is due to the elastomer being formed in solution, where such conditions as temperature are more controllable. Furthermore, a network polymer is generally formed in flexible foams and a linear polymer forms in polyurethane elastomers. Some of the other differences and the similarities of the resulting chemistries for the two polyurethanes are covered later in this dissertation.

2.1.2 Formulation Components

There are many different components that go into making polyurethane foams. The five major ones are diisocyanate, polyol, catalysts, surfactant, and blowing agent. The different chemical

names as well as their function in the formation of the foams are given below. Comparisons to the formulation components of polyurethane elastomers are also provided in the following paragraphs.

Diisocyanates

The two most important diisocyanates are toluene diisocyanate (TDI) and diphenylmethane diisocyanate (MDI) with the latter being more dominant in the production of elastomers and the former in the manufacture of foams (1). TDI is manufactured from toluene via nitration and followed by phosgenation. It is mainly sold in the liquid form as a mixture of 2,4 and 2,6 isomers at ratios of 80:20 and 65:35, respectively. The structures of the two isomers are shown in Figure 2.3. The order of reactivity of the isocyanate groups from highest to lowest is as follows: (1) #4 group on the 2,4 isomer, (2) #2 and #6 groups of the 2,6 isomer and (3) #2 group of the 2,4 isomer. The 80:20 mixture of TDI which is called TDI-80 is used most often in producing flexible slabstock foams, and in some cases, hot-molded foams as well as cast elastomers (1-4).

Polymeric MDI (shown in Figure 2.3) and mixtures of polymeric MDI and TDI-80 are also used to manufacture flexible molded polyurethane foams. Pure MDI also shown in Figure 2.3 is used in making thermoplastic polyurethane and polyurea-urethane elastomers. The main difference in polymeric MDI and pure MDI is the level of functionality is higher in the polymeric form (1,3).

In the production of flexible foams and in some cases for elastomers, the amount of isocyanate(s) used is expressed as the isocyanate index. An index of 110 indicates an excess of 10 percent diisocyanate over the stoichiometric amount required by the polyol and water (3). The isocyanate index in flexible foams is generally overindexed in order to obtain the optimum physical properties. The effect of isocyanate index on the physical properties in flexible foams will be shown later in the literature review.

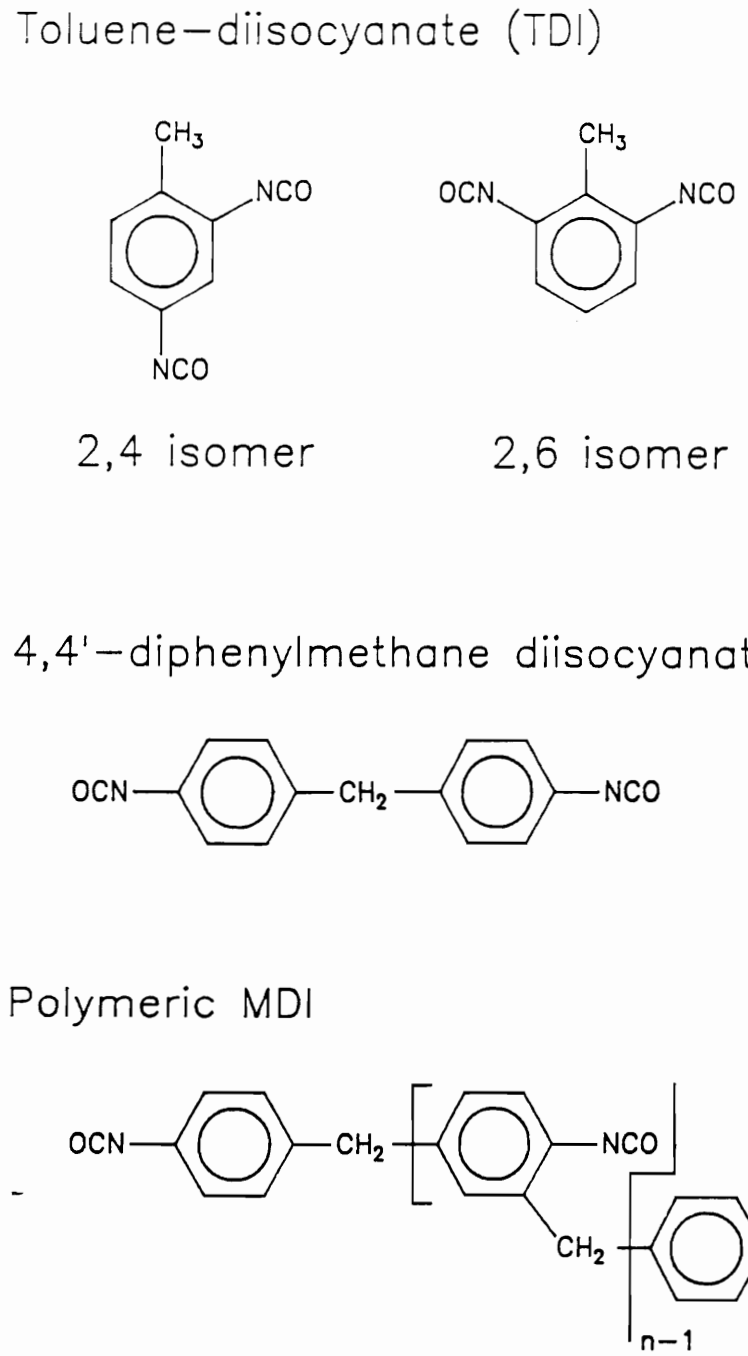

Figure 2.3. Stuctures of Diisocyanates Commonly Used in Manufacture of Foams and Elastomers

Polyols

The two most important polyols are hydroxyl terminated polyethers and hydroxyl terminated polyesters. Polyether polyols are generally chosen over polyester polyols because they are cheaper and more hydrolytically stable. Polyether polyols are generally made from cylic oxides of propylene(PO) and ethylene(EO). The repeat units for these polyether polyols are shown in Figure 2.4. Polyether polyols used in flexible foams are of functionalities from 3 to 5 and in the molecular weight range of 1000 to 4000. Polyether polyols used for manufacturing polyurethane elastomers are generally of functionality equal to 2 and in a molecular weight range of 1000 to 6500. An example of a commonly used polyol in polyurethane elastomers is polytetramethylene oxide (PTMO) and its repeat unit is shown in Figure 2.4 (1,2).

The first polyether polyol used to manufacture flexible foams was a 2900 molecular weight propylene oxide/glycerine initiated polyol (2). However, there have been modifications in composition to improve the polyol performance. Duffy and Whitman report that through the years modifications have been made by changing the functionality, using an ethylene/propylene oxide composition, capping polypropylene polyols with ethylene oxide, and using a glycerine/oxypropylene/oxyethylene polyol(5). Today, most flexible polyurethane foam formulations use a copolymer made from an approximately 80:20 mixture of ethylene and propylene oxide which is then glycerine initiated. Two important aspects in synthesizing this copolymer are the amount and the placement of the oxyethylene groups amongst the oxypropylene groups to give the particular foam of interest without any processing difficulties (1). One reason for this is that the reactivity of secondary hydroxyl group of the oxypropylene groups is lower than that of the oxyethylene. Furthermore, the oxypropylene groups are more hydrolytically stable and thus they make up a higher percentage in the copolymer. A third aspect in synthesizing the above copolymer polyol is that PO is subject to the formation of unsaturated allyl end groups. These groups are undesirable due to increasing the molecular weight of the polyol and lowering its functionality. Furthermore, these unsaturated groups are not reactive with isocyanate groups.

(a) Polypropylene oxide (PPO)

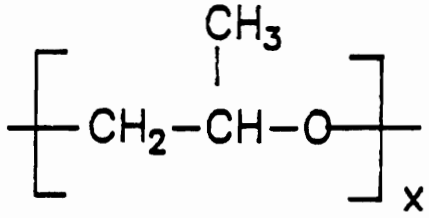

Polyethylene oxide (PEO)

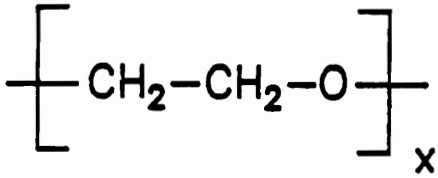

(b) Poly(tetramethylene oxide) (PTMO)

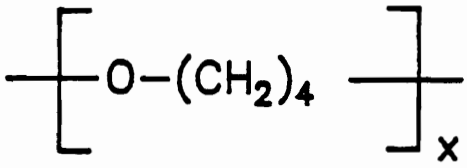

Figure 2.4. Repeat Units for the Most Common Polyether Polyols: (a) flexible foams and (b) elastomers

Modifications on polyether polyols are generally made to provide foams of higher hardness. One example is the polyurea-modified polyols (PHD) which contain polyurea dispersions. These dispersions may react with an isocyanate group to give increased crosslinking i.e., higher hardness. Polyester polyols are also used in special instances where higher levels of tensile strength, stiffness, and compressive strength are necessary. These higher levels in the above physical properties are obtained due to hydrogen bonding between the ester carbonyl and urea and urethane groups (1). Furthermore, this hydrogen bonding also raises the soft segment glass transition temperature (T_g) by promoting phase mixing between the hard and soft segments (phase mixing is covered in more detail later in this dissertation).

Most polyester polyols used in making flexible foams are lightly branched poly(diethylene adipates) An example of such a structure is shown in Figure 2.5. Polyester polyols are also used in the manufacture of polyurethane elastomers. They usually consist of adipates made from aliphatic diols(see Figure 2.5) and in some cases the more expensive polycaprolactone diols.

Chain Extenders

Chain extenders are used in the manufacture of thermoplastic polyurethane elastomers and are very rarely added to the formulation for flexible polyurethane foams. As stated earlier, chain extenders are either diols or diamines and serve as a link between chains in the diisocyanate-polyol prepolymer. An example of a diol is butanediol(BD) as shown in Figure 2.6. This diol is often utilized for elastomers. One common diamine is ethylenediamine(ED) - see Figure 2.6. The use of a diamine extender clearly produces a polyurea-urethane elastomer. Chain extenders also serve as curing agents and especially in TDI cast elastomers. The most commonly used curing agent was 3,3′ dichloro-4-4′- diaminodiphenylmethane (MOCA) until some years ago when it was considered a possible carcinogen (2,4). The structure of MOCA is also given in Figure 2.6.

(a) Poly(oxydiethylene adipate)

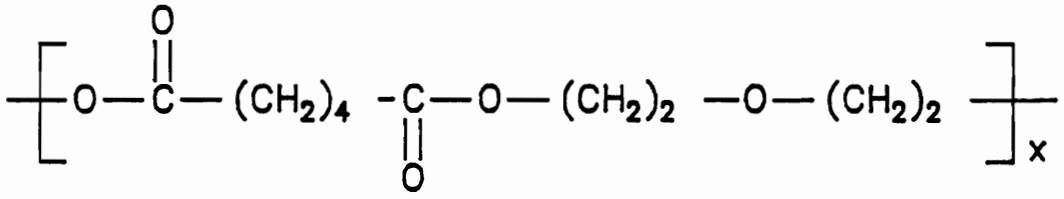

(b) Poly(tetramethylene adipate)

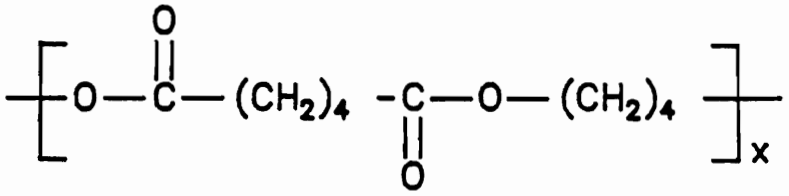

Figure 2.5. Repeat Units for Most Common Polyester Polyols: (a) flexible foams and (b) elastomers

1,4 Butanediol (BD)

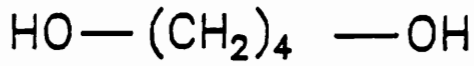

Ethyldiamine

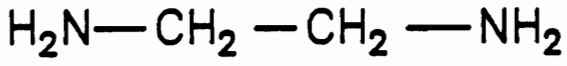

Methylene–bis(2–chloroaniline) (MOCA)

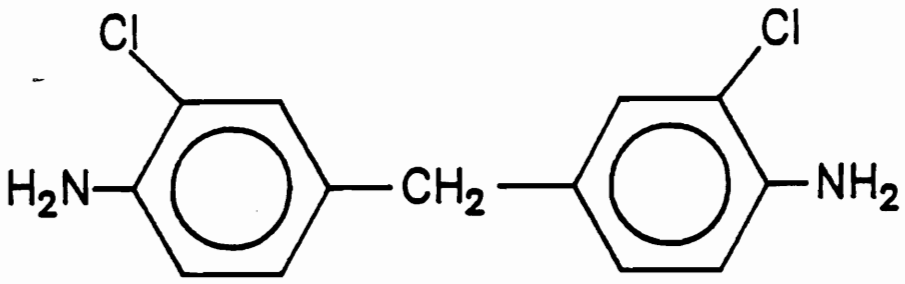

Figure 2.6. Most Common Chain Extenders Used in Manufacture of Elastomers

Catalysts

The two main catalysts used in making flexible foams are a tertiary amine and an organotin compound. The importance of these catalysts are to balance the blowing and gelling reactions. The correct balance is needed due to the possibility of foam collapse if the blowing reaction is too fast. On the other hand, if the gelling reaction is too fast, foams with closed "crosslinked" cells result and foam shrinkage or "pruning" occurs. In general, a catalyst system should allow for a sufficient induction period, appropriate timing in the foaming reaction and the curing process, and the possibility to adjust the foam properties. The catalyst system should not affect the properties such as the stability of the foam (3,6).

The tertiary amine enhances the blowing reaction the most, since it is able to form stable hydrogen bonds with water. The reactivity of the tertiary amine increases with its level of basicity. On the other hand, the organotin compound acts as Lewis acid that can attack the oxygen of a polyol and thus exhibits its ability to enhance the gelling reaction (6).

The tin and the amine catalyst can also activate the blowing and the gelling reaction, respectively as shown by Burkhart and co-workers (6). They have reported that the tin compound catalyzes the blowing reaction as much as the amine compound. Thus, the tin compound sets the reactivity of the formulation. On the other hand, the amine compound is referred to as a fine tuning catalyst and its level is adjusted most often to obtain the right balance between the two competing reactions (6).

Some of the different tertiary amines for flexible polyurethane foams are triethylenediamine (DABCO), trimethyl-hydroxylethyl ethylenediamine and dimethethylamine (DMEA). Stannous octate is the primary organotin compound used in making flexible foams.

Blowing Agents

Blowing agents are used to bring about the foaming and to help control the density of the foam. There are chemical and physical blowing agents. Water acts as the chemical blowing agent and reacts with an isocyanate group leading to the formation of a primary amine. By increasing the level of water in the formulation and adjusting other component levels the density of the foam will decrease because of an increased blowing reaction that occurs. Furthermore, the hard segment content in the foam is also increased due to reacting more water and isocyanate. However, the amount of water added to the formulation is limited by the exothermic heat of reaction which depends on numerous factors such as the scale of manufacture, rate of heat dissipation, and the amount of excess diisocyanate present (2).

Physical or auxiliary blowing agents are used to lower the density and thus produce softer foams. Auxiliary blowing reagents are low boiling solvents and are inert in the chemical reactions. Chloroflourocarbons (CFC's) are most commonly used in flexible polyurethane foams. CFC 11 and in some cases CFC 12 are normally used. However, the production of these two CFC's has been reduced in the past few years due to the Montreal Protocol and due to environmental concerns. CFC's in general have been reported as depleting the Earth's protective ozone layer - especially over the Antarctica (7). Two replacements, HCFC-123 and HCFC 141b, are most likely to replace CFC 11 for use in foam manufacture and especially in rigid foams used for thermal insulation. These halogenated chlorinated flourocarbons(HCFC) are reported as having the potential to deplete the Earth's ozone layer by only 1 to 2% of the fully chlorinated CFC's(such as CFC 11). Along with the reduced effect on the environment, rigid foams made with the HCFC's(123 and 141b) have shown comparable results for various physical properties to that of foams made with CFC 11(8,9). The main problem in utilizing these HCFC's, is that manufacturers do not have the capability to produce these blowing agents on a large scale and are not expected to until 1993 (8,9). Thus, other alternatives are being considered to reduce and or eliminate the use of CFC 11 for the meantime. One common approach amongst the many producers of polyurethane foams(flexible and rigid) who have used CFC's in the past, has been to produce foams blown partially or fully

by CO_2 which is produced by the reaction of isocyanate and water as discussed above. This approach, as reported at the most recent SPI meeting on Polyurethanes, has led to modifications in both the chemical components(mainly the polyols, surfactants and catalysts) as well as the processing of the foams in order to retain the physical properties that are obtained by producing 100 percent CFC 11 blown foams(9). Although, it appears that CFC's will not be totally eliminated from foam production in the immediate future, steps by foam manufacturers are continually being made to reduce its use and in a few instances, chemical and processing modifications have led to its complete removal in the production of flexible foams(9).

Surfactants

With the introduction of the "one-shot" system versus foam systems based on prepolymers, new surfactants were developed for producing flexible polyurethane foams. The new surfactants are primarily siloxane-polyether block and graft copolymers. Their introduction was necessary due to the lower viscosity in the foam mixture and the need for foam stabilization. Thus, the surfactants used today serve many functions in the production of one-shot flexible polyurethane foams. Some of which are not well understand and agreed upon. For the most part, surfactants help in stabilizing the foam structure and the cell size. In doing so, the surfactants play an important role in many of the stages in the foam formation as shown below.

The first stage in the foam process is nucleation and here the surfactants act as a dispersion agent by regulating the air bubbles in the liquid mixture. In the second stage, called creaming, the air bubbles are enlarged and the surfactant acts in a similar manner as in the first stage. The foam now begins to rise as more gases are given off and the foam mixture becomes more viscous. The surfactant acts as a stabilizing agent here by reducing the surface tension; thus preventing the bubbles from coalescing. The mechanism(s) by which the surfactants performs this role are not well understood. One mechanism that seems to hold true is the surfactant slows the drainage of the cell membranes into the plateau borders by increasing the surface viscosity. This delay in the thinning

of the struts enables the foam to gain some of its mechanical strength before bubble breakage occurs. Another possible mechanism that could be taking place due to surface viscosity build-up, is the Gibbs-Marangoni effect. This effect calls for elasticity in the membrane which serves to maintain the membrane at uniform thickness; thus preventing rupture (12). Rossmy et. al. have also suggested that upon precipitation of polyurea (more explanation on the development of precipitated polyurea is given later) the stability of the rising foam was affected (10). In order to overcome this instability, the surfactant becomes a dispersing agent by incorporating the precipitated polyurea into the liquid foam matrix. The last two events in the formation of the foam are the blow-off or cell rupture point which establishes the full rise in the foam and the gelation step (3). The surfactants role in these steps has not been reported on heavily. However, it is believed that the surfactants possibly assist in the cell opening process, but the actual mechanism is not known. Finally, the surfactant is thought to help to control the precise timing in the foam process (2-3).

The amount of surfactant used in the formulation governs the quality of the final foam. For example, if too much surfactant is used a closed cell foam results due to the possibility of little drainage in plateau borders; thus preventing cell rupture. On the other hand, if not enough surfactant is added the foam collapses due to cell opening occurring to soon (3).

As mentioned earlier, surfactants used today in flexible polyurethane foams are generally polysiloxane-polyoxyalkylene block and graft copolymers. These surfactants generally have two different structures. The first is a linear polysiloxane with attached polyoxyalkylene chains. The second is a branched trifunctional polysiloxane polymer which contains pendant polyether chains. The surfactants used in flexible foams are usually non-hydrolyzable and thus consist of Si-C linkages between the polyether and the siloxane. The polyether portion of the surfactants are adjusted to meet the requirements of the particular foam being produced (11,13). Generally the polyether consists of 75 percent or more of oxypropylene and the rest oxyethylene (4).

2.1.3 Foam Process

The flexible polyurethane foam formation is a difficult process to follow in detail. However, most of the main mechanisms in the foam process are understood and for the most part agreed upon. A discussion of the foam process from the mixing of the five or more chemical components, until the final product is obtained is given below.

Flexible polyurethane foams are made by a "one-shot" process. The chemical components are usually metered into a mixing head in appropriate quantities and at well controlled temperature conditions. During mixing it is essential that nucleation sites are formed. The level of nucleation is reflected in the cell size and the cell structure. Normally in flexible foam formation, the amount of nucleation is controlled by bubbling air or nitrogen gas into the mixing head through a polyol or isocyanate meter. The mixing agitation speed is also important in the level of nucleation.

After mixing for less than one second, the nucleated liquid mixture is dispensed into a mold or onto the bottom lining of a continuous trough. For a short induction period, the bubbles begin to grow and decrease in number. Furthermore, the mixture turns opaque at the end of the induction period(6-15 seconds) and this time is referred to as the "cream time." The longer the "cream time" the larger the cell size. Furthermore, by using a surfactant the bubble loss is lowered due to reducing the surface tension and thus lowering the pressure differential between the dissolved gas and the dispersed gas. By increasing the catalyst levels, the cream time is shorter and the cells are fewer in number and in size.

After the cream time, the foam mixture begins to rise and the small spherical bubbles are elongated. The expansion of the bubble is in the blow direction and is caused by the increasing amounts of CO_2 that are produced by the isocyanate-water reaction. The bubbles will continue to expand until they eventually contact to form planar membranes, if the bubbles are equal in size (usually the case for water-blown slabstock foams). The planar membrane is formed by three bubbles and produces a triangular shaped rib at the point of contact.

At temperatures near 100°C, the wall-membranes of the cells rupture and the gas is released. The temperature of the cell opening depends on the foam formulation. However, the actual mechanism that brings about the cell opening is not well understood. At the point of cell opening which is also known as blow-off, the foam reaches full rise. This time generally occurs 100-200 seconds after mixing the chemical formulation.

The remaining isocyanate groups continue to react after blow off and furthermore, the temperature of the foam continues to increase. After the maximum temperature(30 minutes- 1hour), is reached the foams are taken to storage areas where they cure. The time for curing will depend on the size of the foam. Large foams which are generally produced in a continuous process take approximately forty-eight hours. The smaller foams (e.g. molded cushions) can take up to seven days before the properties stabilize (1-4).

2.1.4 Reaction Sequences in Foam Formation

As was alluded to earlier, the chemical reactions are difficult to follow in polyurethane foams due to the high rates of reaction, the large exotherms, the high rate of viscosity and volume changes, and the heterogeneity of the reacting mixtures (2). Thus, it has only been in the last 10-15 years that steps toward a better understanding of the reaction sequences in foams has been obtained. Some of the techniques that have been used in following the sequence of reactions are FTIR, weight loss of certain components, and temperature profiles.

The water-isocyanate reaction has been observed by several investigators in the early stages of the foam reaction by using FTIR (10,11,14,16). Rossmy et. al. reported seeing at the beginning of the reaction an absorption at 1710 cm^{-1} which increased in the early stages of the reaction (10). They also observed absorptions at 1660 cm^{-1} at 50% of the rise time and for 75% of the rise time a band at 1645 cm^{-1} then appeared. Bailey and Critchfield also reported observing an absorption at 1710 cm^{-1} in the beginning of the reaction as well as at 1645 cm^{-1} at approximately 75% of the rise time (14). Both of the investigators agreed that the 1645 cm^{-1} is due to a disubstituted urea,

but they were not in full agreement on the band at 1710 cm^{-1}. It appears, as Rossmy et. al. first suggested, that the band at 1710 cm^{-1} is due to soluble urea while that at 1645 cm^{-1} is due to insoluble urea. This hypothesis was supported by Hauptman et. al. and Hocker who reported observing a IR shift from 1710 cm^{-1} to 1645 cm^{-1} for a diphenyl urea model compound dissolved in a good solvent(DMF) and a poor solvent (THF), respectively. Rossmy et. al. gave further justification by replacing the surfactant in their formulation with a defoamer. In this experiment, the authors observed the foam mixture going from a clear mixture to an opaque mixture at the same time they observed the 1645 cm^{-1} band in the regular foam mixture (10). Furthermore, in the clear mixture the IR absorption at 1710 cm^{-1} was only observed, and as the mixture turned opaque, the 1645 cm^{-1} was detected. Thus, with this evidence there appears that at some time during the foam reaction a precipitated urea phase is formed.

The isocyanate-polyol reaction has been reported as occurring in the later stages in the foam reaction (near blow-off) (10,11,14-17). Bailey and Critchfield reported observing during foam rise a slow increase in the urethane absorption band at 1730 cm^{-1} in comparison to the urea absorption band at 1645 cm^{-1} (14). A steady increase in the urethane absorption was observed after foam rise for 30 minutes while the urea absorption remained practically constant. Rossmy et. al. reported observing the urethane band at 1725 cm^{-1} for the first time at 75% of the foam rise(11).

In a different study, Illeger et. al. followed the relative weight loss of isocyanate and water. With this approach, it was also concluded that the isocyanate-water reaction was the dominant reaction in the early stages of foam formation. They did report observing a small amount of isocyanate-polyol reaction at the beginning of the foam reaction as did Bailey and Critchfield(17).

Bailey and Critchfield also used gel/rise profiles to follow the foam formation(14). The gel/rise profiles give a qualitative idea of the balance of the gelling and blowing reactions, respectively (18). The rise profile measures the height of the rising foam mixture, while the gel profile gives a measure of the strength of the rising foam. The authors observed that the rate of rise was going through a maximum upon the first detection of the urea groups at 1645 cm^{-1} (14). It was suggested that the urea groups could be aggregating and thus retarding the foam rise. On the other hand, the gel profile occurred during the period of time when the urea formation was predominant and as the rate of rise

was decreasing. This also suggested that the urea groups were forming domains due to the added strength in the foam mixture (14). Rossmy et. al. have also suggested in another study that the urethane formation does not play an important role in the foam stabilization (11).

Van Gheluwe and Leroux have followed the temperature rise during the foam formation (19). In doing so, they determined the maximum rate of temperature rise as a function of varying water content and tertiary amine catalyst concentration for two different polyether polyols. Two temperature curves were obtained for the two different chemical reactions. The temperature rate for the blowing reaction was generally greater than that of the gelling reaction. This observation further supports the fact that the blowing reaction is more reactive in the early stages of foam formation (19).

The results of Van Gheluwe and Leroux work also showed an increase in the temperature rate curves with increasing water content. This is expected due to more extensive blowing reaction occurring at higher water contents. However, they did note the temperature rate levels off at the higher water level contents for the blowing reaction, but a steady increase in the temperature rate was observed for the gelling reaction. This observation was not fully understood, but was related to the formation of the polyurea precipitates. An increase in the temperature rate was also seen with increasing levels of tin catalysts. On the other hand, only slight increases in temperature rate were observed by increasing the levels of tertiary amine. These last two results suggest as stated earlier that the tin catalysts activate the gelling and blowing reactions more. These authors also reported observing higher temperature rates upon reaction for the primary hydroxyl polyol than that of the secondary hydroxyl. This is to be expected since primary hydroxyls are more reactive (19).

In short, this section has provided a semi-quantitative outlook on the reaction sequences as well as some details on the foaming mixture for flexible foams. One of the basic conclusions is that the isocyanate-water reaction is dominant in the early stages of the foam formation. On the other hand, the gelling reaction becomes more effective when the foam approximately reaches its maximum height. One other important feature, is that the polyurea is soluble in the foam mixture in the early stages of foam formation and at 75% of the rise time it begins to aggregate as well as precipitate out of solution.

2.2 Morphology

Until the past five to six years very little work had been done towards understanding the morphology of flexible foams (20-24). In the past, the study of the morphology in polyurethanes has been concentrated on thermoplastic elastomers. A typical polyurethane elastomer consists of a MDI chain extended hard segments and a linear polyether or polyester soft segment. The hard segments generally aggregate due to hydrogen bonding to form crystalline or amorphous domains. These domains serve as physical crosslinks in a soft segment matrix. Thus, a two phase morphology consisting of hard domains randomly dispersed in a soft segment matrix is normally depicted in polyurethane elastomers (1,25).

For the past five to six years, Dow Chemical and Virginia Tech have undertaken a joint venture to investigate the morphology of flexible water-blown polyurethane foams using many of the different techniques that were also utilized in defining the morphology of polyurethane elastomers (20-24). The techniques that have provided the most useful information in this recent joint study have been scanning electron microscopy (SEM), transmission electron microscopy (TEM), dynamic mechanical spectroscopy (DMS), differential scanning calorimetry (DSC), wide angle X-ray scattering (WAXS), small angle X-ray scattering (SAXS), and the most recent infrared(IR)-dichroism. A series of four TDI-80 - polypropylene oxide water blown foams of varying hard segment content(21 to 34 by wt%) were studied. These foams are referred to as F1-F4 with one having the lowest hard segment content. Compression molded plaques of these same foams were also studied and were made by compressing the foams at 204°C for 10 minutes at 250 tons of pressure. A summary of the recent work form the first five techniques listed above is given below. The work utilizing IR-dichroism is summarized in a separate section, since this work was done as a continuation to the initial morphological study and it provides information that not only leads to understanding the morphological features, but also how these features are affected by different deformation processes.

2.2.1 Macroscopic Structure

The cellular structure of foams F1 and F4 are shown in Figure 2.7 looking down the blow direction and along the blow direction. Looking down or parallel to the blow direction the cells appear spherically shaped in both foams and more in foam F1. Along or perpendicular to the blow direction the cells appear ellipsoidal in shape with the major axis aligned with the blow direction. This anisotropy of the cells is reflected in the foam's properties. For example, the compressive strength parallel to the blow direction is generally much greater than that in the perpendicular direction.

The cells in foam F4 looking along the blow direction are more elongated in comparison to foam F1 (see Figure 2.7). This is due to more blowing action taking place in the formation of foam F4. With the increased blowing action, a more open foam (more ruptured windows) and thinner struts results. It was suggested that the above trends could also be attributed to greater nucleation taking place in the formation of higher water content foams as in the case of foam F4 (20).

2.2.2 Thermal Characterization

Spell et. al. used dynamic mechanical spectroscopy (DMS) to investigate the thermal behavior in foams F1-F4 and the corresponding plaques (24). The DMS spectra for the foams are shown in Figure 2.8 and resemble the spectra of soft ideal elastomers. Each spectra exhibits a fairly sharp glass transition, a rubbery modulus, and thermal stability up to 200°C. At or above 200°C the modulus drops off due to thermal degradation. The soft segment glass transition is approximately -40°C for for all the foams and thus did not change significantly upon increasing the hard segment content.

The DMS spectrum for the foams are similar to that of TDI-polyurea-urethane elastomers. This was somewhat surprising due to the network structure of the foams versus the linear segmented structure of the elastomers (21). However, as the authors pointed out the intramolecular

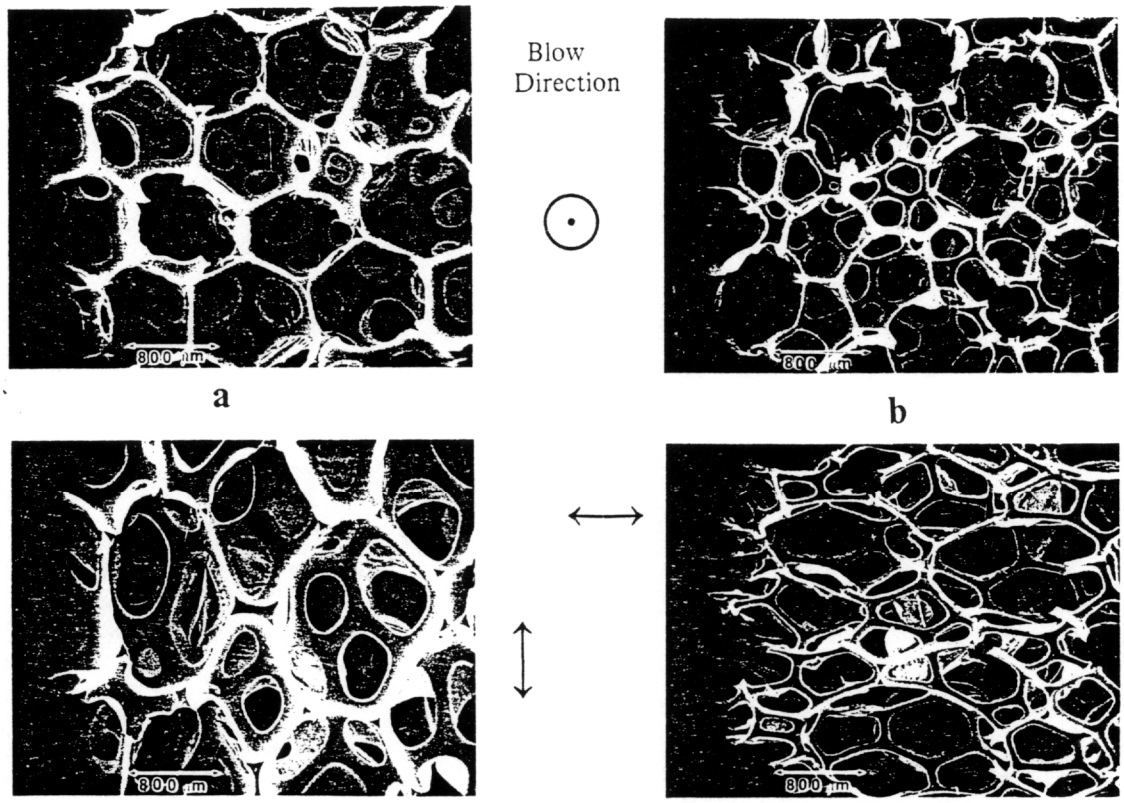

Figure 2.7. SEM Micrographs of Foam F1(a) and F4(b): observation direction is perpendicular(bottom) and parallel(top) to the blow axis (ref. 21)

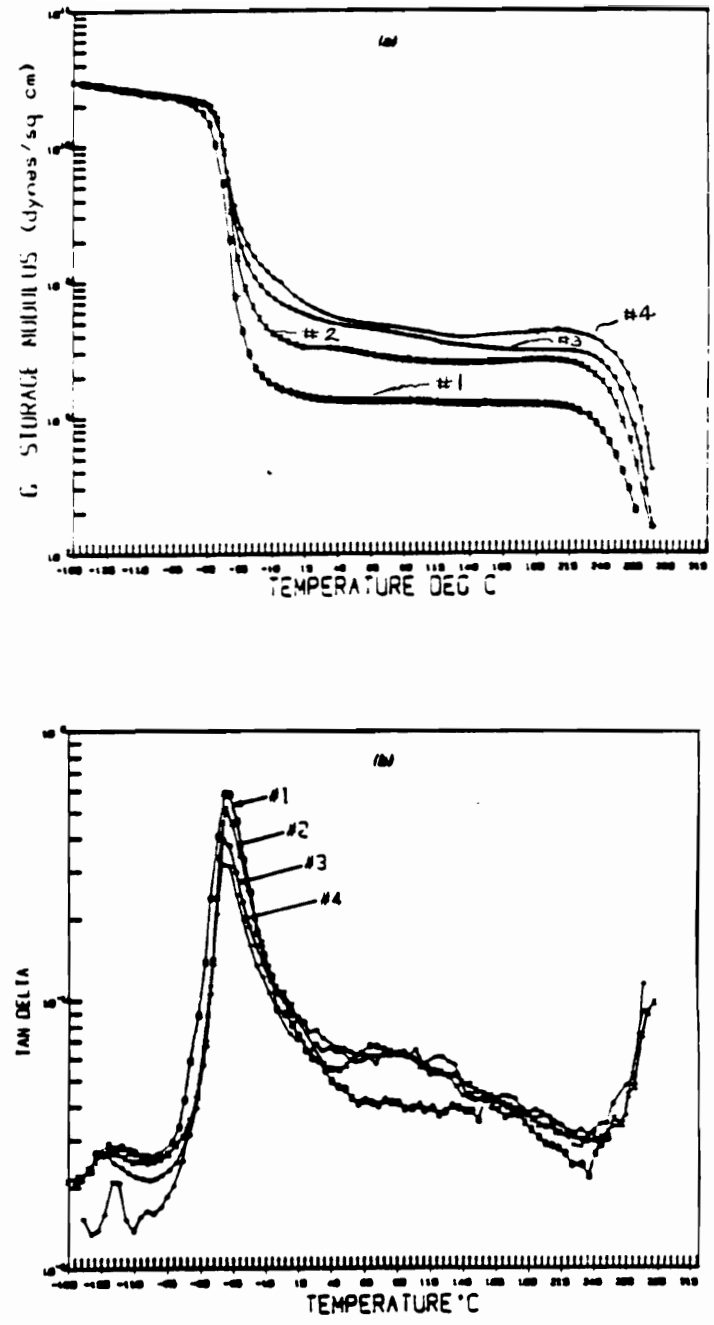

Figure 2.8. Storage Moduli(a) and Tan Delta(b) Curves for Foams F1-F4: The storage moduli are normalized at -160°C based on a typical polyurethane plaque in the glassy state (ref. 24).

and the intermolecular forces that govern the two different polyurethane systems appear to be similar.

A comparison of the DMS spectra for foam F3 and plaque P3 is shown in Figure 2.9. The spectra are very similar with the plaque having a slightly lower soft segment T_g and higher temperature stability. The differences were attributed to the plaques having possibly better phase separation induced upon compression molding.

In comparison to the DMS data, the differential scanning calorimetry results showed slightly higher soft segment T_g's for the foams. Again the difference in the soft segment T_g's was small (21).

2.2.3 Microphase Structure

Transmission and high magnification scanning electron microscopy were both used to detect any form of phase separation in the foams and the plaques. The TEM results for foam F1 showed a diffuse grainy texture at the 100 nm level. It was thought, due to the weak contrast and different levels of contrast that the grains are randomly dispersed and can be attributed to features less than 120 nm in size. On the other hand, the contrast systematically improved in foams F2-F4 showing what appeared to be larger urea based aggregations. The aggregates are randomly dispersed and vary in size. The largest aggregates in foam F2 were ca. 100 nm in diameter and for foam F4 were ca. 300 nm in diameter. Similar results as described for foams F1-F4 were also observed in their respective plaques.

The SEM micrographs also gave evidence of a multiphase morphology on the cold fracture surfaces of the plaques. The micrograph of plaque 1 showed a smooth fracture surface indicating no observable microstructure at the 100 nm level. Increasing surface texture was observed in plaques P2-P4. In plaques P3 and P4, 100-300 nm protuberances were observed. Further evidence of the microphrase morphology was seen in the compression molded plaques with the naked eye. Plaque P1 is transparent while the other plaques increase in opaqueness from plaque P2 to P4.

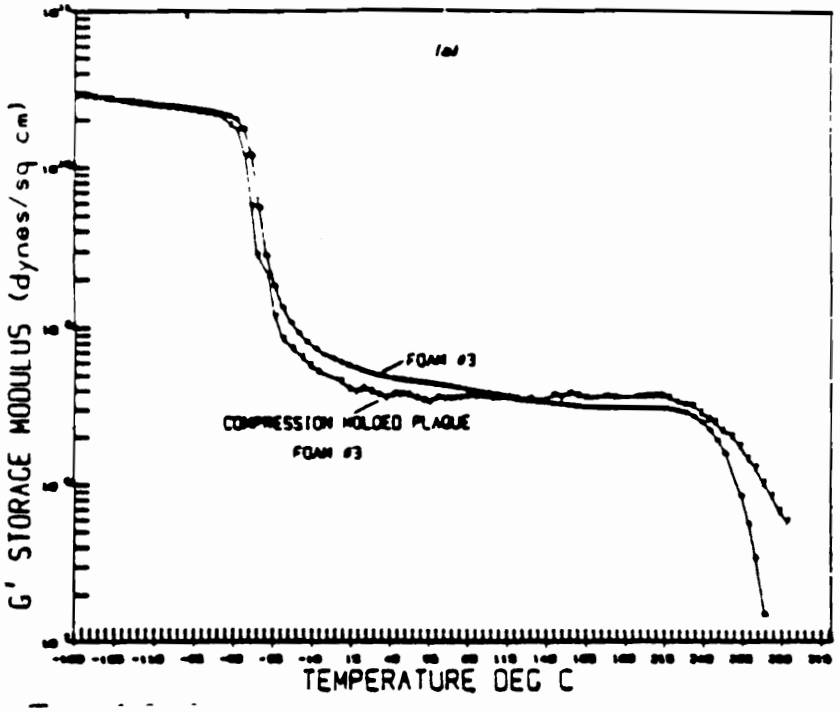

Figure 2.9. Comparison of DMS spectra for Foam F3 and its Compression Molded Plaque:

The microscopy results gave further indication that the precipitated urea phase detected by Rossmy and co-workers(10-11) in the their IR kinetic study is most likely present in the resulting foam. Thus, it was speculated that the agglomerations observed in the TEM micrographs are due to this precipitated urea phase (21).

2.2.4 Extraction Study

The extraction studies were carried out after swelling foams F1-F4 in THF and DMF to determine if such species as urea were apart of the polymer network (20). The sol fractions from both the DMF and THF solutions are small and increase with hard segment content with the highest fraction being 7 percent. The sol fractions were higher for the DMF extracts which indicated the hard segment was extracted the most. This observation was further supported by analyzing the extract with IR and detecting that urea was the predominant species. Overall, the swelling study showed that there exist a well-formed network in all of the foams (20).

2.2.5 Wide and Small Angle X-Ray Scattering

The WAXS patterns for foams F1-F4 exhibited a diffuse halo and a corresponding reasonably sharp diffraction peak at 0.45 nm. Foams F2-F4 have another weaker peak at 0.59 nm. The sharpness of the peaks increased with hard segment content. The peaks were also distinct, thus indicating a certain degree of order and not just a typical maxima of the amorphous halos. The plaques exhibited very similar patterns to that of the foams.

In comparison to the diffraction results of a TDI- 80 based water extended polyurea (27) and other WAXS studies of amorphous polyurea-urethane elastomers with similar hard segments (26), it was suggested that the amorphous halo was due to the randomness associated with the hard and soft segments. The diffraction peaks at 0.45 and 0.59 nm indicate an increase in the hard segment

order. This was surprising due to the hard segments consisting of both 2,4 and 2,6 TDI isomers. The origin of these diffraction peaks, based on an earlier study of MDI-BD urethanes(28), were thought to be caused by hydrogen bonding in the hard segments (20-21).

The WAXS patterns did not appear to change significantly upon compression molding, thus indicating the thermal process did not have a significant effect on the hard segment order. However, after swelling plaque P4 in DMF, the hard segment ordering did appear to decrease due to the increased diffuseness in the diffraction pattern. It was suspected that the swelling removed some of the polyurea rich phase and/or may have disrupted the hydrogen bonding between the hard domains leading to some rearrangement in microphase separation.

The results from the SAXS study were obtained from the scattering profiles, the correlation function analysis and the interfacial boundary thickness between the hard and the soft segment regions. The scattering profiles for the foams and the plaques did not exhibit sharp peaks, but shoulders that appeared nearly in the same place for the foams or plaques. The shoulders were a result of the morphological features not having the same shape, size and distance from one another. Bragg's law was applied to the shoulders and estimates of the center-to-center (interdomain) spacing between the scattering particles, approximately equal to 10 nm for the plaques and 9 nm for the foams were obtained. The difference in the Bragg law spacings for the foams and the plaques can possibly be attributed to better phase separation and formation of slightly larger domains in the plaques (20-21).

The correlation functions (1-dimensional and 3-dimensional) also provide additional information on the scattering particles. In short, the correlation function gives the probability that a rod of length r will have both ends in the same electron density. The 3-dimensional(3-D) correlation function gives an estimate of the center-to-center particle spacing. The 1-dimensional(1-D) correlation function provides the distance between scattering centers assuming a lamellar morphology. The results of the 1-D and 3-D showed no long range order. The results of the first maxima in the 3-D correlation function were lower than that of the Bragg-spacing's and are believed to be a better estimate of the interdomain spacing.

In comparison to polyurea-urethanes of similar hard segment structure, the interparticle spacings in the foams and the plaques were 20-50 percent lower (25,29-30). This was attributed to the shorter and stiffer hard segments and the use of a trifunctional polyol in the foams. Where as in the urea-urethanes, an ethylenediamine chain extender exist in the hard segments and a linear soft segment is used (26).

The diffuse boundary between the hard and soft segments was characterized assuming a sigmodial gradient and by utilizing Porod's law. Such an analysis lead to an index of interfacial thickness, denoted as sigma, where sigma represents half-width of the diffuse boundary where the smoothing function has a value of 0.606. The results showed an increase in sigma from 0.23 to 0.53 nm for increasing hard segment content. This trend, though unexpected, implies that the ends of the hard segments are more phase mixed with increasing water content due to the their asymmetry. One might predict, as the authors suggested, higher ordered domains with increasing hard segment content (25).

The plaques followed the same trend as the foams did with increasing water content, but with slightly higher sigma values. This again implies that larger domains are formed upon compression molding. The authors also pointed out that the sigma values are comparable to that of TDI-based urethane and urea-urethane elastomers (28-29). Furthermore, the results by the SAXS analysis suggested that the hard segment domains in the foams have many rather similar features to that of the urethane and urea/urethane elastomers (20-21).

With the above results in mind the authors proposed a simplified morphological model as shown in Figure 2.10 (21). The urea balls in the model represent the precipitates seen in the TEM micrographs and are believed to be bonded to the matrix. The remaining structure appears to be very similar to that of urea and urea/urethane elastomers. That is, the smaller hard segments form amorphous domains through hydrogen bonding and are dispersed randomly in the soft segment matrix.

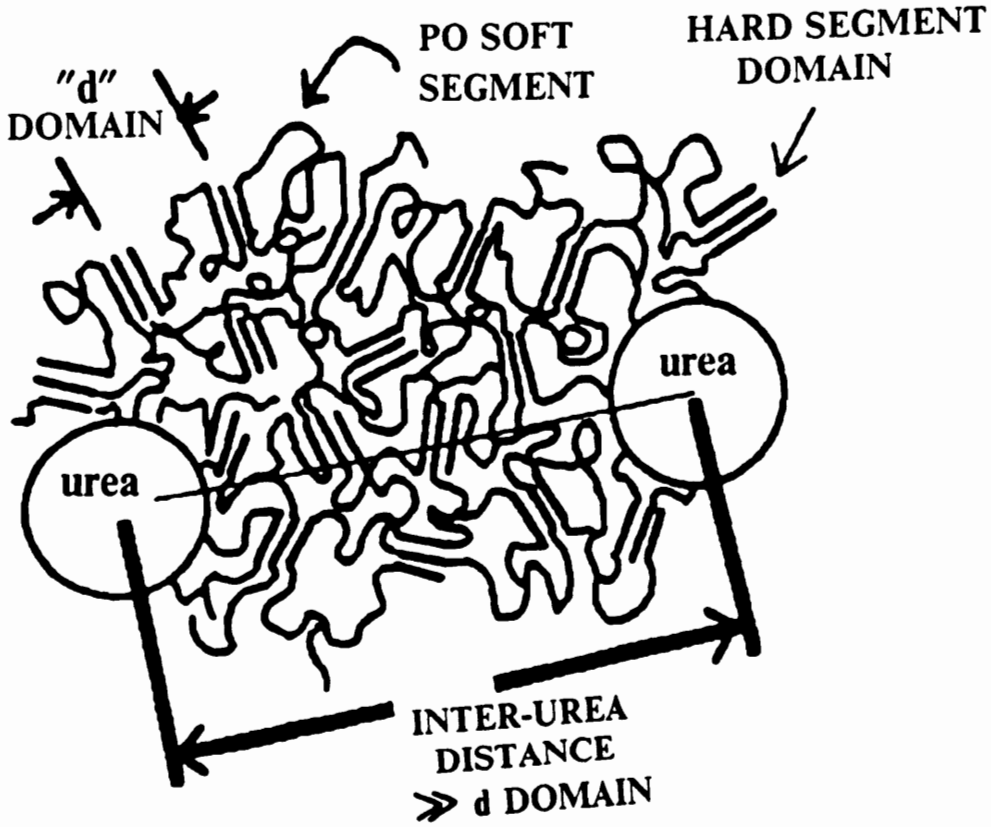

Figure 2.10. Proposed Morphological Model for the Solid Portion of Flexible Water-Blown Foam: The urea represents the polyurea aggregates; "d" is the interdomain distance between the smaller hard domains represented by the "sticklike" hard segments (ref. 21)

2.3 Mechanical Properties of Polyurethane Foams

Flexible polyurethane foams like other cellular materials are complex material systems which can be characterized as having a mechanical response that is a function of deformation, time and the surrounding conditions. The mechanical response also depends on the cell structure as well as the morphology of the cell matrix material. As was discussed earlier, both are dependent on the foam formulation. This in itself exhibits the complexity of characterizing the mechanical response of these materials and probably why very few systematic studies have been reported on the stress strain properties of flexible polyurethane foams. As a result, some of the reports on these properties for flexible foams have involved theoretical analyses. In other studies, the formulation components influence on the different stress strain properties have been evaluated. Two of the stress strain properties that are discussed in this section are the ultimate properties and the load bearing properties. Furthermore, a few of the theoretical models are qualitatively presented to give a structural interpretation of the mechanical response as well as the structural dependence on the mechanical response. Finally, a section is devoted to the viscoelastic properties which become important when considering the long-term behavior of the physical properties in flexible foams. Where possible, some comparisons to polyurethane elastomers are also made.

2.3.1 Stress-Strain Behavior

The stress-strain behavior like many other mechanical properties of flexible foams are usually measured in compression. The compression stress-strain behavior is measured on a small rectangular piece of foam with uniform thickness and a width to thickness ratio of not less than 2 to 1. The rate of deformation in this test, as well as other mechanical tests, is important due to the viscoelastic nature of flexible foams. In the paragraphs to follow, the stress-strain behavior in compression is described using predictions from structural models and an empirical model analysis.

In addition, some comparisons to stress-strain behavior in tension of flexible foams and polyurethane elastomers are given.

Gent and Thomas and more recently Gibson and Ashby have used structural models to predict the stress-strain behavior in compression (31-34). The authors generally evaluate the modes of deformation to model the stress-strain behavior for a given foam. Gent and Thomas used a cubic strut model (Figure 2.11a), while Gibson and Ashby used a similar model, but slightly different as shown in Figure 2.11b (31-33).

In modeling the behavior, two different deformation modes were developed to describe the stress-strain behavior as depicted in Figure 2.12 (34). The first mode occurs when the cells bend, and this represents the linear elastic region. This region occurs over the first 5-10 percent of compressive strain and is much higher in tension. The non- linear region represents the buckling of the cell walls for flexible foams. The buckling of the cell walls occurs elastically if the cell wall material does not have a plastic yield point. A plastic yield point is usually not observed in flexible foams, but is observed in rigid foams. The last region is the densification of the foam which occurs when the cell walls are crushed together. The differences in the stress-strain behavior in tension and compression as shown in Figure 2.13 are two-fold: (1) A longer linear-elastic region in tension and (2) only a small non-linear region in tension before rupture (33-35).

Rusch evaluated the effects of the structural features on the compressive stress-strain behavior of low density flexible foams using an empirical model (36). Some of his results are shown in Figure 2.14. Using his nomenclature, curves Q and L represent low density reticulated polyurethane foams that have a regular cell structure, for which Q is of higher density. Curve R is for a rubber latex foam that has irregular cell structure and a higher density than the other foams shown in Figure 2.14. Foam E is a nonreticulated polyurethane flexible foam which contains some closed cells and has an irregular cell structure.

From his empirical model analysis (given in ref. 36), Rusch came to some basic conclusions. First, the cell structure (specific matrix geometry) has the greatest effect on the compressive stress-strain behavior. This can be seen in Figure 2.14 by comparing the non- linear regions of foam L or Q to foam E and recalling the description given above for the different cell structures. The density

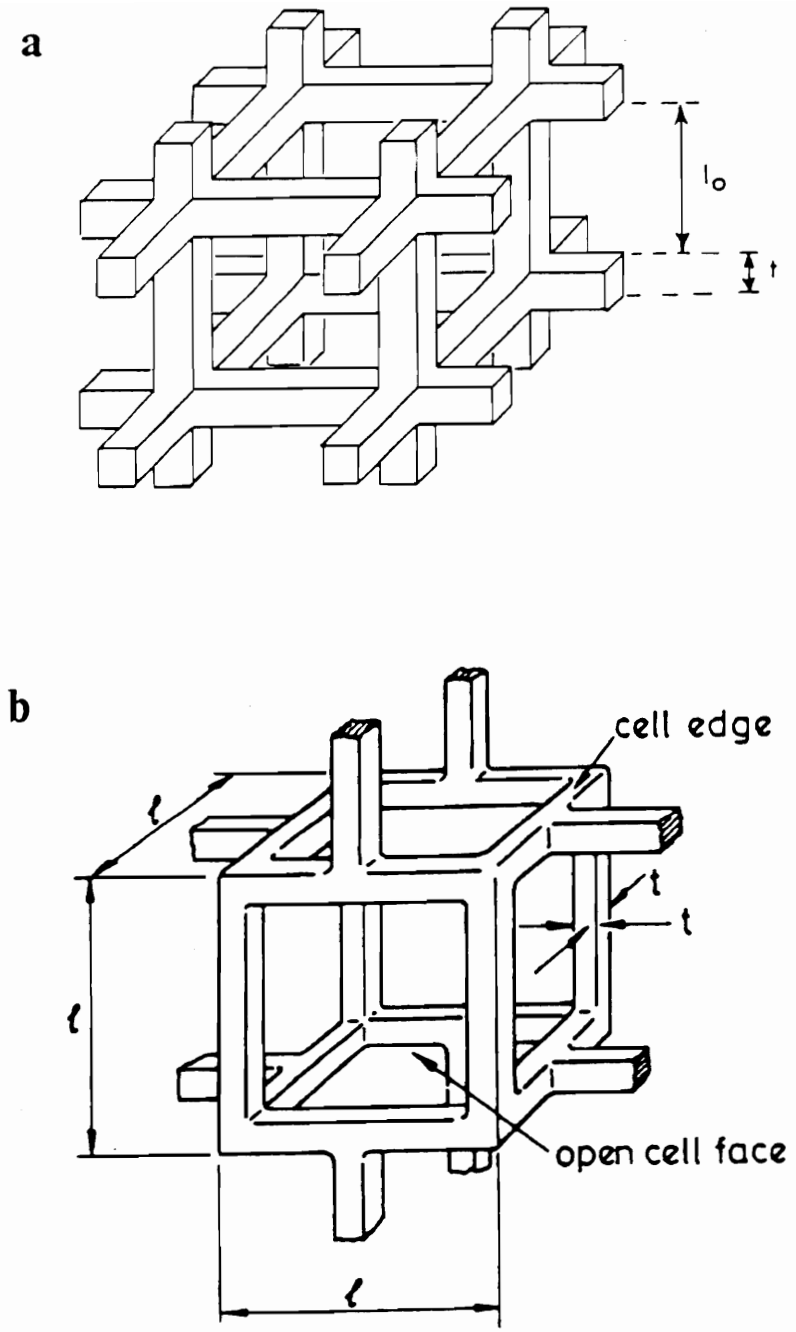

Figure 2.11. Cubic Models for Open-Cellular Materials: (a) Gent and Thomas (ref. 31) and (b) Gibson and Ashby (ref. 34)

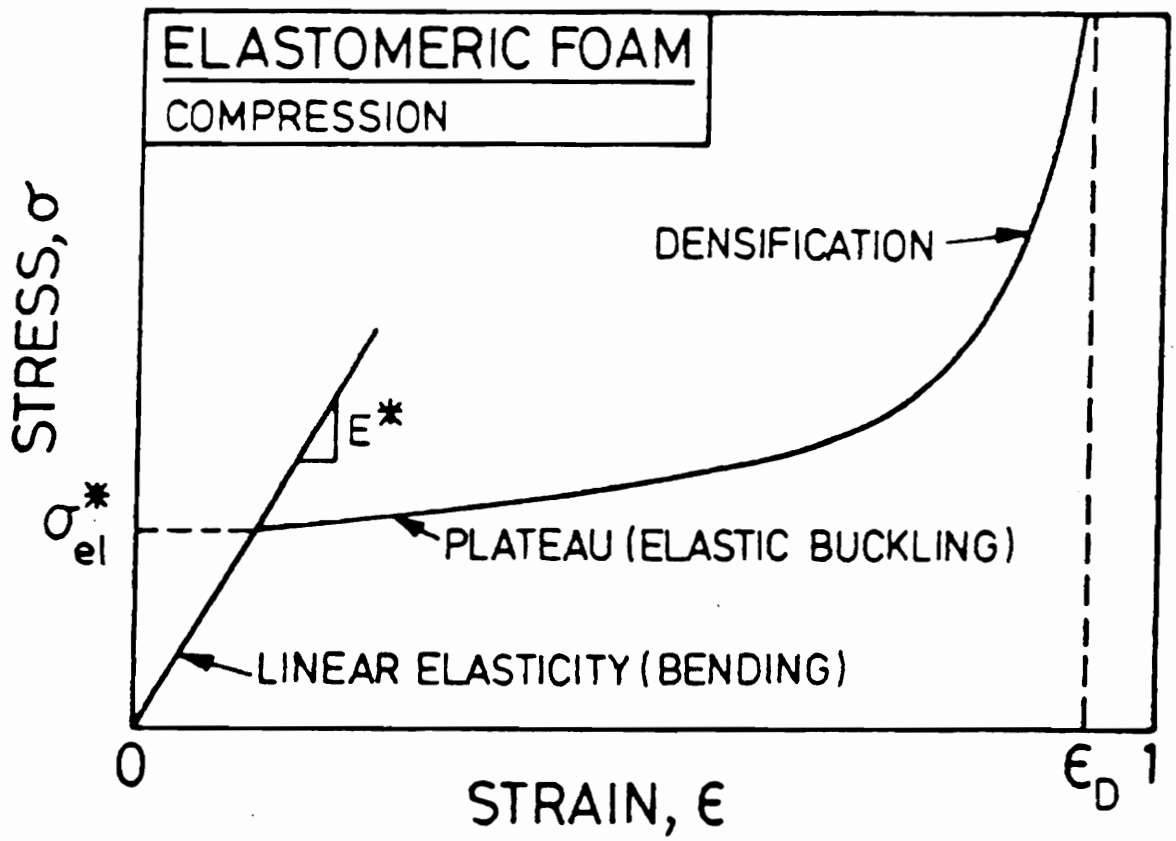

Figure 2.12. Typical Shape of the Compressive Stress-Strain Curve for a Foam: taken from ref. (33)

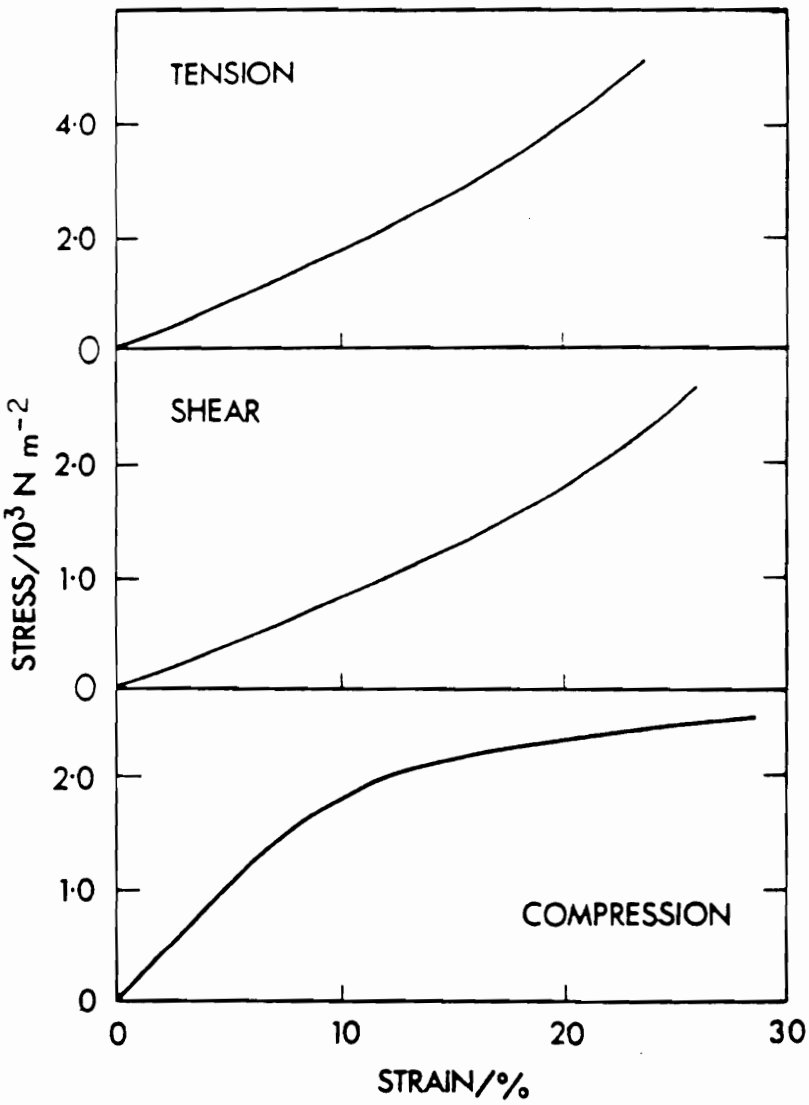

Figure 2.13. Stress-Strain Behavior for Flexible Foams in Compression, Shear, and Tension: taken from ref. (35)

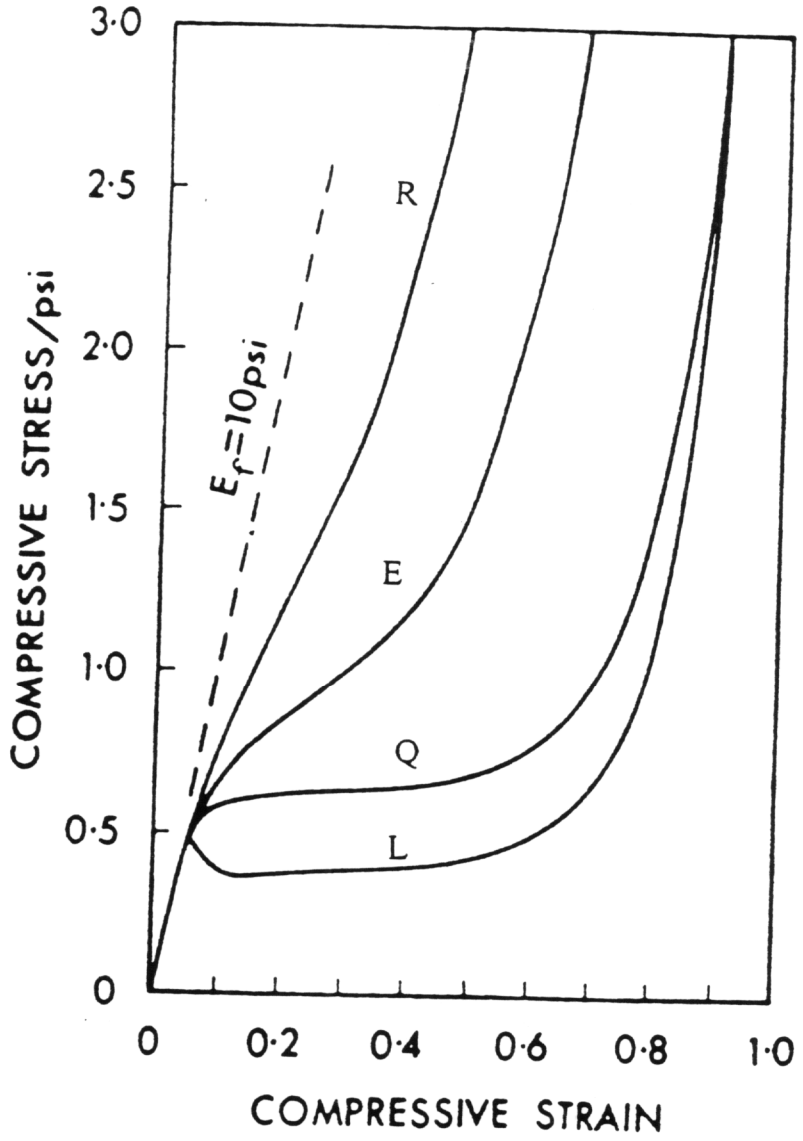

Figure 2.14. Compressive Stress-Strain Curves for Four Different Flexible Foams: taken from ref. (36)

or volume fraction of the matrix polymer and the cell size showed secondary effects on the stress-strain behavior. These effects are seen by comparing foam L and Q for which Q has the higher density and the smaller cell size.

One common industrial application of compressive stress-strain curves or the more commonly used indentation load-deflection curves (described later) is in predicting the performance of a cushion. Generally speaking, a comfortable foam is represented by a cushion curve that is characterized as having an increase in stress or load with increasing deflection. An example of a representative cushion curve, but with a slightly lower initial modulus is shown in Figure 2.14 for foam E (36). The cushion curve for foam E exhibits a constant force of "fight back" when compressed. In contrast, the cushion curve for foam L shows a sharp rise in stress and then reaches a constant level of stress which is indicative of a foam with a low comfort rating (35).

The shape of the stress-strain behavior in tension for polyurethane elastomers is similar in many cases to that in compression of the foams. The stress-strain curve has a small linear region and then becomes non-linear. The non-linearity in the elastomers is caused by stress softening which could be due to a number of factors. Four of these are;(1) disruption of hard segment domains by rearrangement of hydrogen bonding, (2) movement of polymer chains, crosslinks and entanglements, (3) potential strain induced crystallization in some elastomers - especially those with PTMO, and (4) the reformation of domains after being stressed mechanically and then taking on different geometrical configurations as a result.

2.3.2 Ultimate Properties

The tensile strength and the tear strength as well as the elongation of flexible polyurethane foams have been shown to increase by increasing the water content (hard segment content) up to a certain level (4 parts/100 parts polyol) and then leveling off (2,38). This of course assumes that the formulation is adjusted to obtain a reasonable foam. By normalizing these results based on the density of the foam, the tensile strength increases with water content. Thus, the decrease in density

of the foam appears to have caused the leveling off of the ultimate properties. In addition, Patten et. al. has shown for a set of variable water-constant density HR foams that an increase in tensile strength and a decrease in elongation are observed with increasing water content(39).

Sung et. al. reported for a set of 2,4 TDI-ED-PTMO amorphous urea-urethane elastomers as having higher moduli and tensile strength with increasing hard segment content at a given PTMO MW(26). Cooper and Wang have also observed the same behavior for a set of MDI-ED-PTMO urea-urethanes that have semicrystalline hard segments (37). Both investigators also observed lower elongation at break with increasing hard segment content.

2.3.3 Load Bearing Properties

Another important mechanical property of flexible foams is their load bearing capacity which is measured by the hardness of the foam. The hardness is typically measured by indentation load deflection (ILD) and in some cases by compressive stress (compression hardness) which was discussed earlier. The difference between the two is illustrated in Figure 2.15. The indentation hardness is performed on a larger piece of foam (standard cushion size) as shown in Figure 2.15. Furthermore, the indentation hardness is reported as a load and not as a stress as in the case of compression hardness. Thus, the thickness of the sample, the tensile strength and the sample size effect the level of indentation hardness, but have little or no effect on the compression hardness. The rate of deformation is also of importance as stated earlier.

As mentioned earlier and shown in Figure 2.15, the indentation hardness can be reported in the form of ILD-deflection curves. The ILD value is also reported at different levels of deflection or at a percentage of the original height of the foam in the form of %ILD. An example of the latter, is by calculating the ratio of the 65% to 25% ILD values (sag factor) to give an indication of a cushion's expected performance. A sag factor of 2.8 or greater usually suggests a good cushion. However, it could be misleading without the ILD values when considering the level of comfort (35).

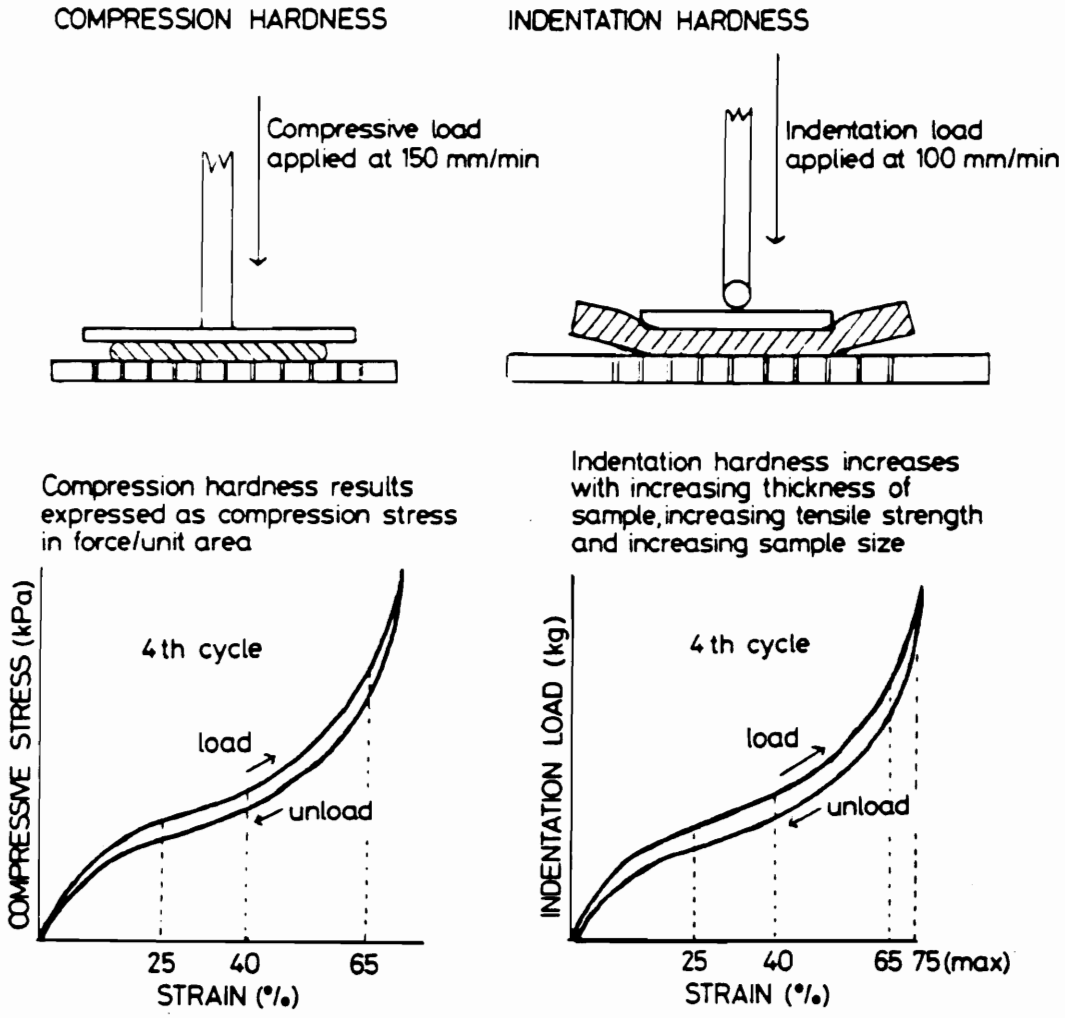

Figure 2.15. Characteristics of Compression Hardness and Indentation Hardness in Flexible Foams: taken from ref. 2

The hardness depends like some of the other stress-strain properties on different formulation variables (2-4,35,38,40). The hardness (65% ILD value) decreases with increasing water content (decreasing density) for flexible slabstock foams (2,4,41) and in high resilient(HR) foams (38). This trend, though somewhat different to that of the tensile strength, is explainable. First, the cell structure and possibly the density play a more important role in the compression mode than in tension. Furthermore, there are two opposing factors with increasing water content; increasing modulus of the matrix and the decreasing density of the foam. It appears the density is the controlling factor. However, Patten and co-workers showed if the density is held constant by using a physical blowing agent, the hardness increases with water content (38-39). This again shows the strength of the foam is effected greater by the urea content. Furthermore, this is also a good example of the difficulties that can arise if both the structure and the matrix material are not considered when evaluating the mechanical properties of foams.

Some of the other formulation variables that effect the hardness are the isocyanate index and the polyol structure. An isocyanate index of 105 or greater results in a harder foam. The level of hardness for high isocyanate indexes will also depend on the humidity during foam processing(42). With humid conditions, a decrease in the level of hardness is observed due to excess isocyanate being reacted; thus preventing biuret and allophanate structures from being formed or additional crosslinking taking place. A softer foam will be produced for either a lower functionality or higher molecular weight polyol.

One of the many factors of the foam geometry that effects the hardness as well as tensile strength is the direction of cell elongation. As mentioned earlier, the cells appear ellipsoidal in shape when looking perpendicular to the blow direction. The maximum loads in tension and compression occur by deforming along the major axis of these ellipsoidal cells as would be expected (2,35). For a 50 percent deflection, for example, the indentation load deflection force in newtons was reported as 414 along the major axis and 325 perpendicular to the axis(35).

2.3.4 Viscoelastic Properties

In most cases, the viscoelastic properties of polymers are characterized by measuring the stress decay or strain increase with time at a constant strain or load, respectively. These two types of tests are better known as stress relaxation and creep. However, with flexible foams, tests that more realistically consider the application of foams have been generally used to characterize their viscoelastic nature. Such tests include compression set as well as static and dynamic fatigue. These tests are done in compression under a constant load or constant deflection and also under dynamic conditions. Furthermore, these tests are carried out under accelerated conditions such as high temperature and humidity in order to predict the long term durability and/or fatigue resistance.

Before discussing the different responses, a brief description of each is necessary. Compression set is a measure of the recovery of the foam height after subjecting a foam to a constant deflection at a given set of conditions (usually 23 °C and 50% relative humidity) for an extended period of time (usually 22 hours). The static fatigue test is generally reported as indentation load(%ILD) loss after subjecting a foam to similar conditions to those of the compression set test. Dynamic fatigue is also reported as %ILD loss, but involves cycling the foam under a constant load or deflection up to 20,000 cycles. The %ILD loss is a measure of the load loss i.e., stress relaxation after subjecting a foam to a static or dynamic fatigue test.

Several authors have measured the compression set in slabstock flexible foams and more so in HR flexible foams (36- 41,43-48). Most of these studies have concentrated on the effects of the formulation variables as well as temperature and humidity effects on compression set. The water content has shown the largest effect on compression set and especially under humid conditions (38-39,43-44). Herrington and Klarfeld reported humid aged compression set(HASET) values increasing with water content after exposing the foams for 5 hours at 121°C and 100 percent relative humidity(RH) conditions and then a 50% deflection for 22 hours at the usual compression set conditions or 50% RH and 23°C(43). Patten and Seefried also observed the same trend for 50% HASET values under similar testing conditions (40). In addition, Saotome reported a more signif-

icant increase in compression set with increasing water content for compression set tests that were carried out under conditions of 50°C and 95%RH for 22 hrs (44). Patten and co-workers also reported slight changes in compression set at different levels of density (constant water content) and isocyanate index (38-39). The above results indicate that the urea content or the hard segment content has a significant effect on the humid aged compression set. A possible mechanism will be given later.

Several investigators have also studied the recovery of the foam's thickness after subjecting the foam to a 22 hour compression set. For the same testing conditions described above, Herrington and Klarfeld observed that the foams recover with time upon removal from the compression jig, reaching a 10 percent loss in original height in about 120 hours (43). The time to reach the 10 percent loss was accelerated by storing the sample in a 70°C oven rather than at ambient conditions. Dwyer also reported similar recovery behavior upon storing the foam at different temperatures(47). Saotome et. al., on the other hand, observed very little recovery in the thickness of the foams which were subjected to high humidity during the compression set test. This type of recovery was also seen by these same authors after storing the foams at higher temperatures(low %RH)(44). In another study, Hogan et. al. looked at the effect of humidity during the recovery of the foam's thickness after subjecting the foam to HASET conditions(45). These authors reported an increase in compression set with decreasing humidity level at 23°C. Kane also observed a similar effect of humidity on the recovery of %ILD loss values for static fatigue tests(49). Kane suggested that the water was acting as a plasticizer and thus was allowing for more load loss upon compression as well as a faster recovery of the foams strength. This explanation also appears to hold in the case of Hogan et. al.'s results for recovery of the foam's thickness. Overall, these results suggest that the compression set is practically reversible and the bonding involved is mostly secondary and not primary when the foams are compressed at 23°C and 50%RH. However, in the case of Saotome et. al.'s study at high humidity and temperature, it appears that some primary bonding may have been disrupted during compression.

The effects of temperature and humidity on the compression set, before and during compression, have been studied to some extent. Herrington and Klarfeld reported that there were lower

50% HASET values upon humid aging at 104°C rather than at 121°C as well as by exposing the foams to low humidity versus high humidity at 121°C(43). In addition, the change in 50% HASET values were almost negligible with increasing water content at the lower temperature and there were no changes with water content at the lower humidity. Upon flex testing flexible foams for 20,000 cycles in the range of 85°F to 100°F and 60 to 100%RH., Dwyer reported observing an increase in thickness loss with increasing humidity and temperature(47). Saotome also reported observing a significant increase in compression set by compressing the foam at 70°C and 95%RH versus 70°C under dry conditions(42). These results indicate that both temperature and humidity are effecting the recovery of the foam's thickness. At elevated temperatures it appears the hydrogen-bonding between the hard segments is weakened to a greater extent. This hypothesis is supported by IR-thermal studies. For example, Cooper et. al. reported observing a decrease in the absorption of the hydrogen bonded carbonyl group with increasing temperature in the range of 80°C to 120°C for polyurethane elastomers (50). On the other hand, at higher humidities the water appears to be acting as a plasticizer and allowing for more chain slippage to occur. A possible mechanism for this plasticizing effect is given in the next paragraph.

In their study, Herrington and Klarfeld also discovered that there was a direct correlation between the urea concentration and the 50% HASET values(43). In explaining this result, the authors utilized attenuated internal reflectance-infrared spectroscopy (ATR-IR) and revealed a more distinct urea carbonyl at 1640 cm^{-1} for the humid aged sample. Thus, it was proposed during humid aging that the hydrogen bonds to the urea carbonyls of the hard segments were replaced by water molecules as described schematically in Figure 2.16. From these results and the proposed model, a few conclusions can be drawn for the mechanism of humid aged compression set. It appears the local morphology on the molecular level of the foam has changed due to humid aging. Furthermore, upon compressing the foam many of the water to water hydrogen bonds are broken which allows for chain slippage to take place. In the compressed state, a new equilibrium state is taken on by reforming hydrogen bonds. Therefore, upon release, the foam usually loses 40-50 percent of its original height (43).

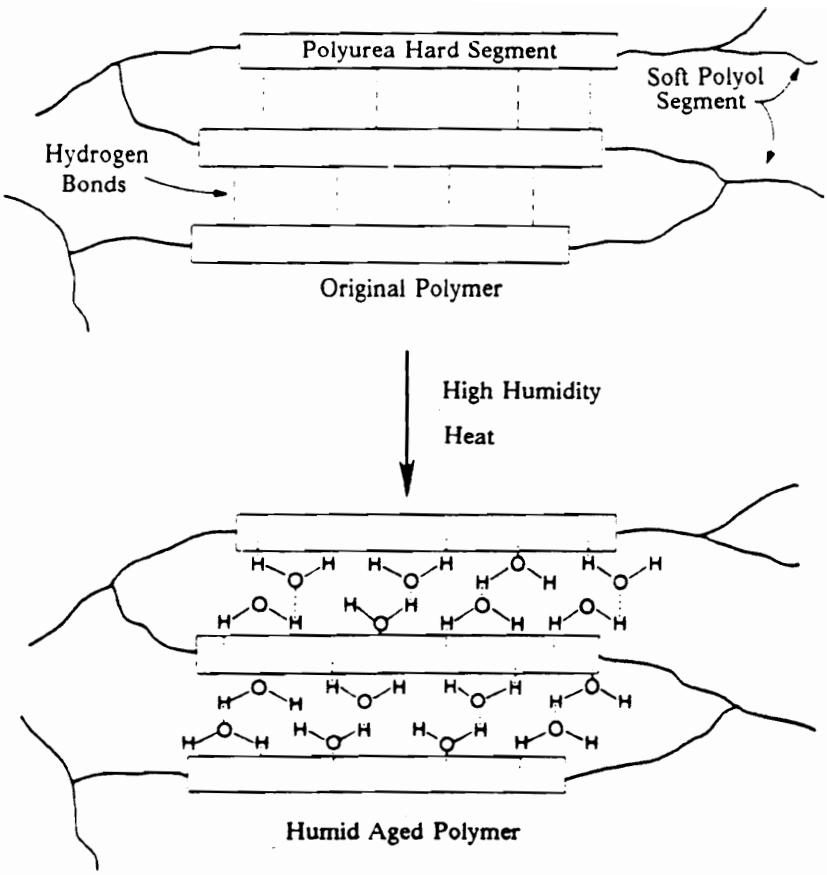

Figure 2.16. Proposed Model for Humid Aged Flexible Foam: taken from ref. 43

Indentation load loss is affected in some similar ways to that of compression set. One way that the two differ is that the isocyanate index has a greater effect on the %ILD loss. Dwyer and Hilyard have shown an increase in fatigue resistance i. e., lower %ILD loss with increasing isocyanate indexes up to 115 (35,47). This could be attributed to the formation of allophanate structures and more likely biuret structures with increasing isocyanate index which allows for less rearrangement of the chemical network. In other words, less stress relaxation occurs with a greater crosslinked polymer system.

Patten and Priest reported the %ILD loss values increase with increasing water content after fatiguing with 60-lb roller shear(HR foams)(38). Kane as well as Dwyer have also reported the same trends for constant deflection static and dynamic tests, respectively (47,49). The increase in fatigue with increasing water content has been attributed to the higher levels of urea content which also corresponds to more hydrogen bonding being present in the foams (38). With more hydrogen bonding present, more hydrogen bonds are disrupted upon deformation which results in lower hardness values upon recovery. A somewhat similar situation was described above for compression set behavior.

In a different study, Lee measured the compression set and the hysteresis loss i.e., the energy loss during the compression set test for an HR foam (51). Lee concluded from his test that the compression set depends heavily on the hysteresis loss (51). Dwyer also observed that the %ILD loss was also related to the hysteresis loss (47). The hysteresis is attributed to the large amount of stress relaxation that takes place during the prolonged compression (22 hrs). Furthermore, the level of stress relaxation is enhanced by increasing the temperature and the relative humidity of the test as several other investigators alluded to in their studies (44,47,51).

Reports on stress relaxation in polyurethane elastomers have shown that below 100°C, the soft segment dominates most of the stress relaxation taking place (52-53). The level of restoring force in the soft segments depends on the polyol functionality and the molecular weight. An elastic soft segment i.e., lower compression set values and %ILD loss in foams are obtained by having a high crosslinking density (up to a limit) and a long chain length between crosslinks. On the other hand, the hard segments exhibit little restoring force upon releasing the load as compared to the soft seg-

ments. Thus, by increasing the hard segment content when at high temperatures and high relative humidities, one would expect greater stress relaxation and likewise higher compression set values and %ILD loss values as mentioned above.

A few investigators have reported on the compression and tensile stress relaxation behavior and compression creep behavior in foams (22,54-58). Ball and Doherty reported on a set of conventional slabstock foams with varying density, isocyanate index, and water levels (54). From the limited data that was obtained intermittently, it could be concluded that the higher water content foams showed greater stress decay and thickness losses with time. This of course is consistent with the results shown above. For a set of urea-urethane cast films, Kane also reported an increase in stress relaxation with increasing urea content (49).

Ball and Doherty also showed that the data for the percent thickness loss and percent hardness loss over time could be described by the following general equation,

$$\Delta L = At^X \qquad [2.3.1]$$

where t is time, ΔL is the percentage loss of either thickness loss or hardness and A and X are constants. The constant X could be thought of as a "relaxation" time or rate of stress decay. Doherty and Ball did report a small increase in X with increasing water content (54).

In a more recent study, Moreland observed the same linear behavior for tensile stress relaxation in a set of variable water-content flexible slabstock foams(20). An increase in the magnitude of the relaxation time(X) was also seen with increasing water content. In addition, upon stretching the foams parallel and perpendicular to the blow axis, the stress decay rates were practically the same. This observation indicates that the tensile stress relaxation in these materials is dependent only on the cellular wall material(22).

Meincke also reported observing the same stress relaxation behavior as defined in Eq. (1) for a rubber-latex foam (flexible but generally denser foam than flexible polyurethane foams) (55). Furthermore, the relaxation rate was independent of the compression level when plotted on a log-log scale. Thus, a master curve was obtained and exhibited a linear relationship between log modulus and log time. This linear behavior has also been observed in 2,4 TDI-ED-PTMO urea-

urethane elastomers (26). Sung et. al. reported observing a greater decay in stress for a lower molecular weight soft segment polyurethane elastomer. The faster rate was attributed to the lower soft segment MW sample having more solubilized hard segments which will lead to greater viscous flow.

Mitz and Raman have studied the stress relaxation behavior for a set of plastic packaging foams (semirigid foams) which consisted of two polyether bonded chip foams, a polystyrene foam, and a polyethylene foam (56). In their study, they have used a model developed by Peleg(57) to evaluate their data. In short, the model is empirical in orgin and the stress was normalized by the following equation,

$$Y(t) = \frac{\sigma(0) - \sigma(t)}{\sigma(0)} \qquad [2.3.2]$$

where $\sigma(t)$ is the stress at a given time and $\sigma(0)$ is the initial stress. A linear relationship was obtained by plotting the inverse of Y(t) against time. The authors do point out that this linearity is satisfied if the modulus is only a function of time; therefore independent of strain. Two parameters evolve from the model by satisfying the above linearity for a given set of experimental data. They are the initial relaxation rate and an estimate of the residual (asymptotic) modulus at equilibrium conditions.

Mitz and Raman showed that the four semirigid foams studied fit the model well. Furthermore, the time required to obtain the data was only 30 minutes. Thus, this model provides a quick and simple method to obtain the initial relaxation rate and be able to predict the long term stress relaxation behavior in compression(56).

For a different viscoelastic test, Campbell measured the compression creep behavior for several HR flexible foams after placing a known load on a foam(58). He found that for the time frame(2 hours) of his tests the creep behavior fit the following equation,

$$y = -m \ln \theta + B \qquad [2.3.3]$$

$$y = \left(\frac{L}{L_0}\right)$$

where y is the displacement(in percent thickness), L_0 is the original thickness, L is thickness at time θ, B is initial deflection and m is the rate of creep. In this study, the rate of creep was observed to be dependent on the initial level of compression. The results showed that the initial creep rate, m, goes through a maximum with the initial displacement at about 20 to 30% strain. This change in creep rate with strain was attributed to the struts buckling and was confirmed through microscopy studies. The buckling effect appeared to begin somewhere after 12% compression and to stop between 60 to 75% compression(of original thickness). Thus, Campbell measured the effects of a few of the formulation variables on the creep behavior at the higher strains where the compression level was independent of the creep rate. He found that the density had little effect on the creep rate, but for increasing water content in a set of two foams the creep rate increased. This observation of course is consistent with the other viscoelastic studies discussed earlier for flexible foams(58).

2.4 FTIR Applications

Structure-property relationships in polymers are evaluated to obtain a better understanding of the resulting morphology and its relationship to the mechanical properties. In the previous two sections of this review, the morphology of the solid state portion of flexible foams has been characterized and the mechanical properties of these foams have also been described. In attempt to obtain a better understanding of the morphological features in the solid portion of flexible foams and their relationship to the important mechanical properties, the segmental orientation behavior has recently, for the first time, been measured on two of the compression molded plaques mentioned in the morphology section (22-23). In this recent study which was a continuation of the earlier morphological study, the technique of linear IR-dichroism was used to measure the orientation behavior of the hard and soft segments in the plaques under unixial extension. In short,

linear IR-dichroism utilizes linearly polarized radiation in characterizing the orientation behavior of specific chromophoric groups of a polymer molecule. By doing so, this rheo-optical technique has the ability to separate the orientation behavior of the different segments in multicomponent or multiphase materials(59-61). Before summarizing the results from this most recent study, some background on the materials and thin film preparation as well as a few details concerning the method of linear IR-dichroism are provided.

2.4.1 Materials

The two foams used in this recent study were the two lowest hard segment content materials of the four flexible slabstock foams mentioned earlier in the morphology section(20-21). These two foams differ in that foam F1 has a 21 wt% hard segment content, while foam F2 has a slightly higher hard segment content of 26 wt%. The compression molded plaques of these foams were used to carry out the IR-dichroism measurements. These plaques were made by compression molding at 204°C for 10 minutes. In most cases, in order to obtain thin enough plaques so that sufficient sample transmittance could be obtained, the foams were subjected to pretreatment process before compression molding. Briefly, this process involved swelling the foam in either DMF or THF overnight and drying the foam thoroughly before compression molding. As discussed earlier in the morphology section, this process does extract a small weight percentage which was thought to consist mostly of a polyurea based species(more so in DMF than THF). The nomenclature that will be used for the plaques is defined below in Table 2.1.

Table 2.1: Nomenclature for Compression Molded Plaques

Foam	DMF	THF	No Solvent	Plaque
F1	-	-	x	P1
F1	-	x	-	1-THF
F1	x	-	-	1-DMF
F2	x	-	-	2-DMF

In evaluating the possible effects of this pretreatment process on the morphology of the the plaques, several structural techniques were used on pretreated plaque 2-DMF and untreated plaque P2. Overall, the results from these techniques revealed that there are some small changes in the morphology of the pretreatment process. These small changes appeared to related to the partial extraction of the polyurea based species as well as the disruption of the hydrogen bonding network which most likely takes place while swelling the foams in the interactive liquid(20-21).

Also, in this recent investigation a urea- urethane thermoplastic elastomer was used for purposes of comparison. The urea-urethane elastomer was made from TDI-80 and a 2000 MW polypropylene oxide diol(P2000) with methylene-bis(2- chloroaniline) (MOCA) as the chain extender. This elastomer was referred to as the "PUU" elastomer and its thin films were solution cast from a DMF solution onto a Teflon® surface. After allowing the solution to stand overnight, the remaining solvent was removed at 50°C in a vacuum oven(22).

2.4.2 Theory and Method of Evaluation

IR-dichroism provides a method to obtain the degree of orientation of polymer films. This is done by measuring the dichroic ratio, D - this ratio being defined as

$$D = \frac{A_{\parallel}}{A_{\perp}} \qquad [2.4.1]$$

where $A_{\parallel}$ and $A_{\perp}$ are the absorbances of linearized polarized radiation with the polarization vector parallel and perpendicular to the deformation axis, z, respectively (see Figure 2.17). The peak heights are normally utilized in measuring the absorbances.

The state of orientation can be expressed by the Herman's orientation function, f, where f is given as

$$f = \frac{3 < \cos^2\beta > - 1}{2} \qquad [2.4.2]$$

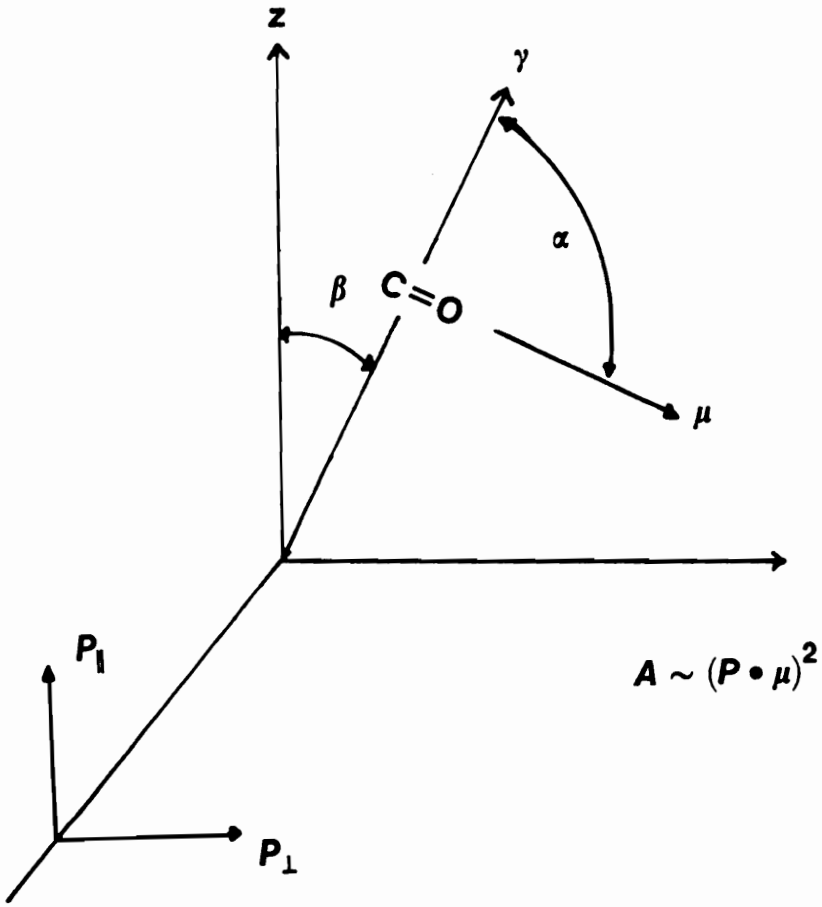

Figure 2.17. Coordinate System for Linear Dichroism

and β is defined in Figure 2.17 as the angle the chain axis makes with the deformation axis. In addition f is related to D and the transition moment angle, α, by the following equation,

$$f = \left(\frac{D_o + 2}{D_o - 1}\right)\left(\frac{D - 1}{D + 2}\right) \qquad [2.4.3]$$

where $D_o = 2cot^2\alpha$ and α is defined in Figure 2.17 as the angle the transition moment of the selected absorbing group makes with the chain axis (61).

The upper and lower limits of Eq. [2.4.3] are defined by Eq. [2.4.2] such that for parallel alignment of the chains, f equals 1 and for perpendicular alignment, f equals -0.5. For D_o equal to 0, the lower limit of Eq. [2.4.3] does approach -2 as D approaches infinity which appears to contradict the last statement. However, Eq. [2.4.2] is defined for uniaxial orientation only and thus the lower limit when assuming uniaxial orientation can be shown to be -0.5. In certain cases of biaxial orientation, it can be shown that the lower limit of the orientation function approaches minus one (62-65).

If specific absorption bands of known α can be selected, Equation [2.4.3] provides a means to obtain the state of orientation for the specific components or phases in a material. The absorbing groups of interest for the plaques and the PUU elastomer are summarized in Table 2.2 along with their absorbing frequencies, transition moment angles and component representation. As an example from Table 2.2, the N-H stretching vibration is mostly representative of the hard segment and to a smaller extent the interface of the hard and soft phases. It has a reported transition moment angle of 90°.

In this most recent study, three different types of deformation experiments were performed at ambient conditions in obtaining the segmental orientation behavior with a simultaneous mechanical response(22). These were stress-strain, cyclic deformation, and stress relaxation. In the paragraphs to follow, a summary of the segmental orientation behavior with mechanical response obtained from this most recent study for the plaques as well as the PUU elastomer are given(22). In addition, comparisons to reports in the literature on similar studies for urethane and urea-urethane

Table 2.2: Absorbing Frequencies for the Plaques and the PUU Elastomer

Frequency (cm^{-1})	Assignment*	Transition Moment Angle (°)**	Component Representation
3300	$\nu(N-H)$	90	Hard Segment Interface
2940	$\nu(CH_2)$	90	Soft Segment
2860	$\nu(CH_2)$	90	Soft Segment
1730	$\nu(C=O)_f$	78	Interface
1640	$\nu(C=O)_{ur}$	78	Hard Segment
1475	$\delta(CH_2)$	90	Soft Segment
1370	$\omega(CH_2)$	0	Soft Segment

* ν - stretching vibration, ω - wagging mode, δ - bending mode

** taken from references 67, 74

elastomers are included. Finally, application of linear IR-dichroism to variable temperature studies on urethane elastomers is also given.

2.4.3 Orientation-Elongation Behavior

The orientation-elongation behavior that was obtained at ambient conditions for plaque 1-DMF of foam F1 and for plaque 2-DMF of foam F2 are shown in Figures 2.18 and 2.19, respectively(20-21). The soft segment orientation behavior which is represented by the $\delta(CH_2)$ group for plaque 2-DMF and the $\omega(CH_2)$ group for plaque 1-DMF display very little change in orientation with elongation. The orientation level with elongation at the interface of the hard and soft components is positive and slightly greater than that of the soft segments as shown by the $(C=O)_f$ absorbing group in Figures 2.18 and 2.19. On the other hand, the hard segments exhibit significant amounts of negative orientation with elongation as shown by the $\nu(N-H)$ group in Figures 2.18 and 2.19 and the $(C=O)_{ur}$ group in Figure 2.19. The orientation behavior for plaques 1-DMF and 2-DMF are very similar, with the exception of the small difference in hard segment orientation level at the higher elongations (to be addressed later). In addition, the orientation behavior observed for plaque 1-DMF showed the same trends and similar orientation levels to that of plaque P1 which was prepared without using the pretreatment process. Thus, it was suggested that the pretreatment process had little if any effect on the orientation behavior in the plaques(23).

The orientation-elongation behavior for plaque 1-DMF(Figure 2.18) and plaque 2-DMF(Figure 2.19) compare well with the orientation- elongation behavior shown in Figure 2.20 for the PUU elastomer up to the range of 75% elongation. The PUU elastomer consists of only linear chains and has a microphase morphology typical of urea-urethane elastomers. The orientation behavior of the plaques and the PUU elastomer furthermore, have the same trends reported in the literature for both diphenylmethane diisocyanate(MDI) and TDI based urea- urethane elastomers that utilized a polytetramethylene oxide(PTMO) soft segment (37, 66-72).

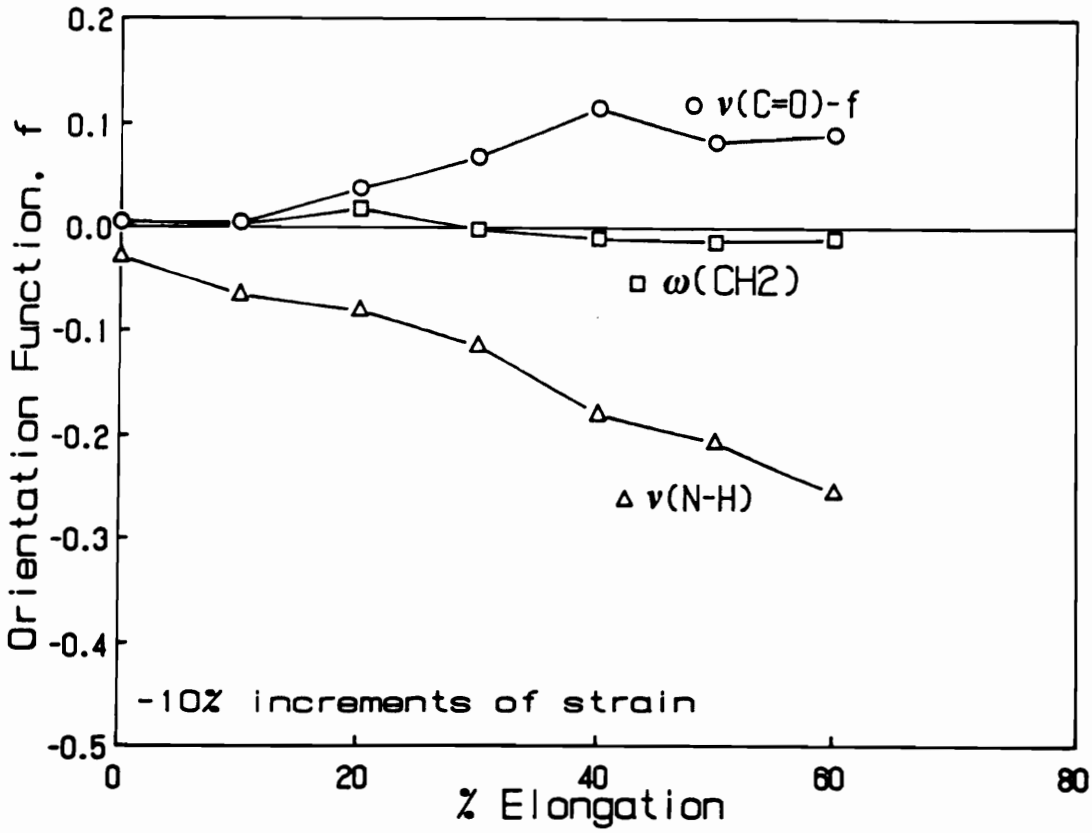

Figure 2.18. Orientation-Elongation Behavior for Plaque 1-DMF: taken from ref. 23

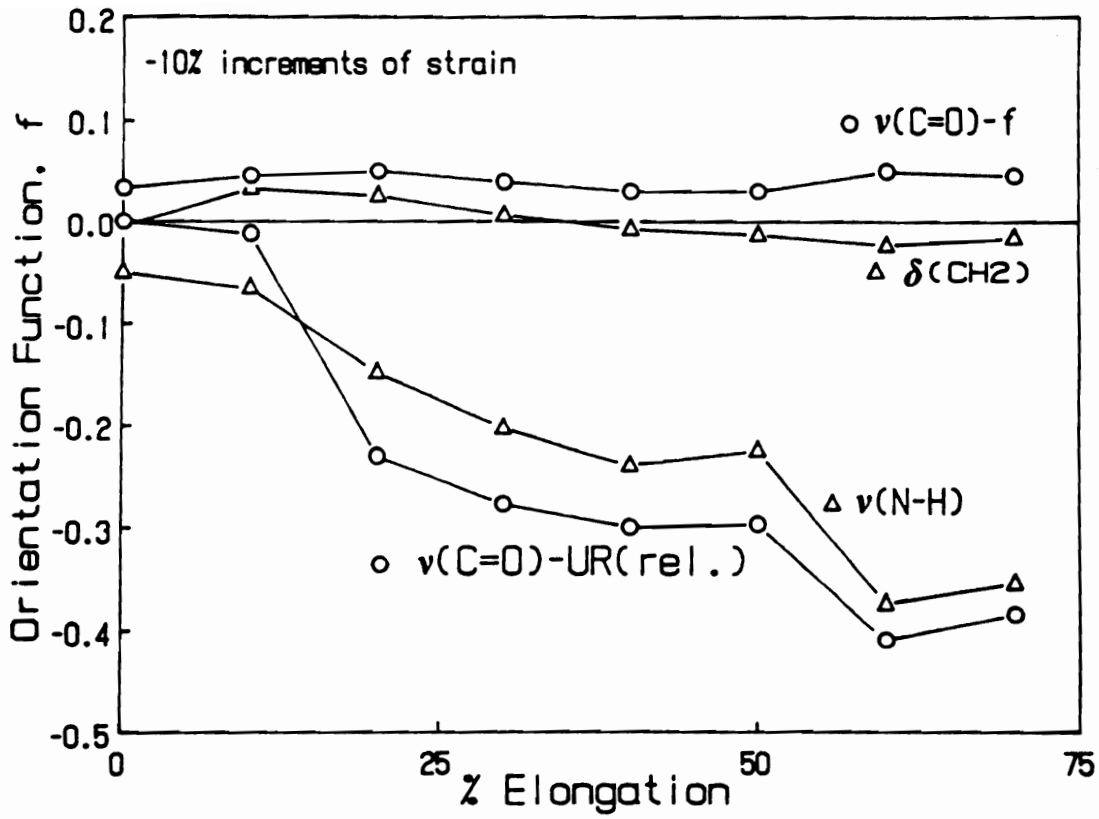

Figure 2.19. Orientation-Elongation Behavior for Plaque 2-DMF: taken from ref. 23

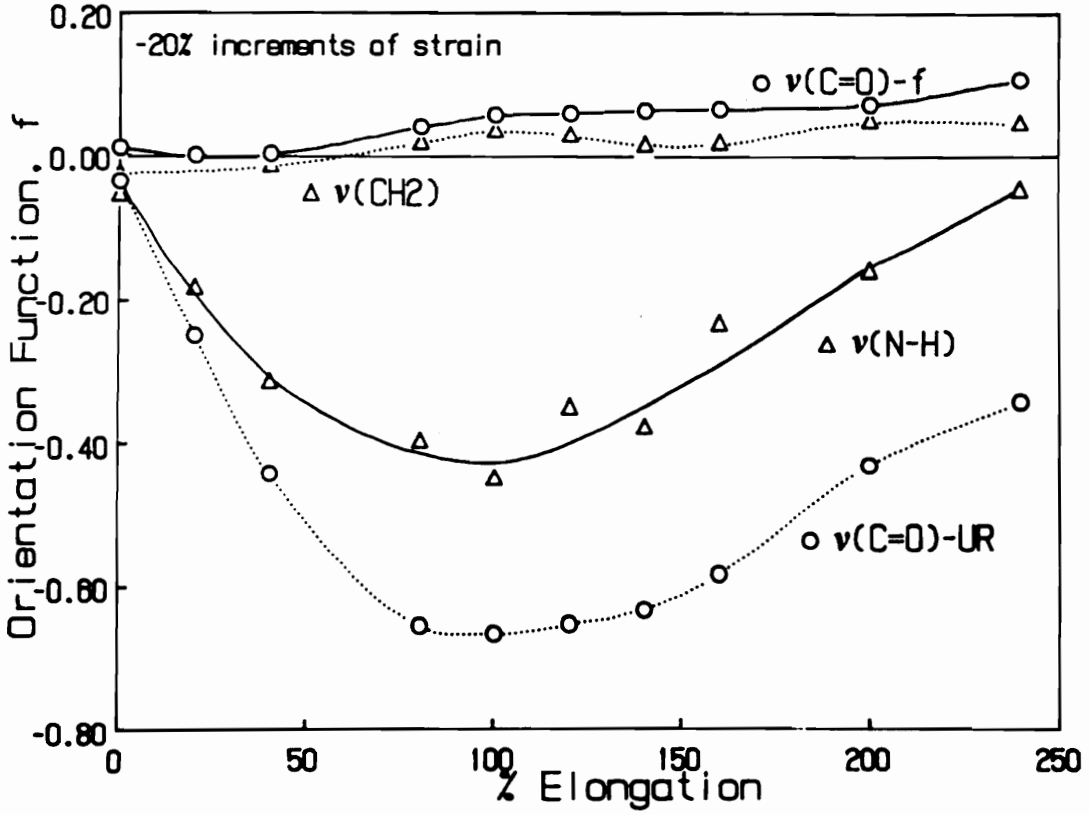

Figure 2.20. Orientation-Elongation Behavior for the PUU Elastomer: taken from ref. 23

The low state of orientation for the soft segments of plaques 1-DMF and 2-DMF as well as the PUU elastomer was attributed to the entropy driven relaxation of the soft segments leading to more disorder. The soft segments in the plaques and the PUU elastomer appeared to have had a greater effect on the orientation at the interface in comparison to the hard segments (see Figures 2.18-2.20). Cooper and Wang have suggested for MDI-PTMO urea-urethane elastomers that the retractive force which accompanies the relaxation of the soft segments could exert a tension on the urethane linkage at the interface; therefore leading to a small amount of a positive orientation for the $(C=O)_f$ group (37). This explanation was also thought to apply to the case at the interface of the hard and soft segments in the plaques and the PUU elastomer.

The orientation level for the $\nu(C=O)_{ur}$ groups is, for the most part, more negative than the $\nu(N-H)$ groups for plaque 2-DMF and the PUU elastomer (see Figures 2.18-2.19). This is expected, since the $N-H$ groups are present in both the urea and urethane linkages. As discussed above, the urethane groups exhibit positive orientation levels which suggests the orientation of the $\nu(N-H)$ groups should be higher than the $(C=O)_{ur}$ groups. Several investigators of urea-urethane elastomers have also reported the same trend for the orientation-elongation behavior up to elongations of 100-200% (37,66-72). In addition, these investigators along with those that have studied segmental urethane elastomers have suggested similar explanations for the negative orientation of the hard segments (37,66-76). For the most part, these investigators suggested that the negative orientation or transverse orientation at the smaller elongations(< 200%) can be attributed to the hard domains possessing lamellar-like textures as shown, for example in Figure 2.21 (37,66,67,70-72). These lamellar-like hard domains have been reported by investigators of urea-urethane and urethane elastomers as being crystalline or paracrystalline in order, but they can also be amorphous (65- 69,73). It is also thought that upon deforming these materials the long axis of the lamellar-like domains initially orients in the stretch direction or the hard segments of these domains orient transverse to the stretch direction which gives rise to the negative orientation (see Figure 2.21)(66-68). Bonart and Hoffman have also suggested for a MDI-PTMO based urethane elastomer there exists both smaller hard segment domains (as in Figure 2.10) and lamellar-like hard domains (76). They predict that the smaller hard segment domains align in the stretch direction -

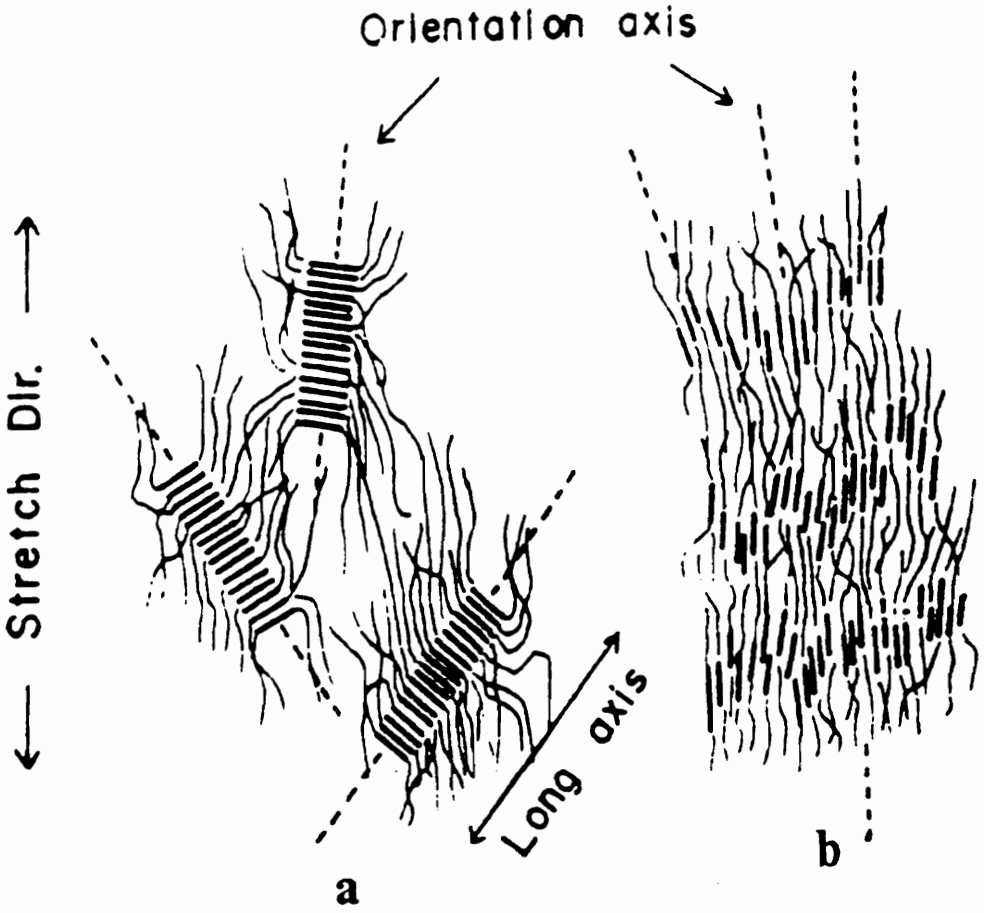

Figure 2.21. Proposed Mechanism for Deformation of Lamellar Hard Domains: taken from ref. 67

giving rise to positive orientation. However, the overall negative orientation behavior which was detected at the lower elongations was attributed to the lamellar-like domains dominating the hard segment orientation behavior (23). In comparing the hard segment orientation behavior of urethanes and urea-urethanes, one usually observes at the lower elongations more transverse orientation in the urea-urethanes (66-76). This difference is most likely due to the stronger hydrogen bonding in the hard domains of the urea-urethanes. The stronger hydrogen bonding suggests there is more resistance to shear stresses disrupting the lamellar-like domains which, if it occurs, leads to a positive orientation result at higher elongations.

Based on the negative orientation of the hard segments in plaques 1 and 2, and the explanations given in the literature, it was speculated that the smaller hard domains and the polyurea aggregates do not necessarily possess the structures exactly portrayed in the earlier morphological model for a urethane foam proposed by Armistead et. al.(18) in Figure 2.10, but they may or at least many may also possess a lamellar-like or rodlike texture as shown in Figure 2.22a. It was also suggested that possibly only one of the two types of hard domains(smaller hard segment domains or polyurea aggregate) has a lamellar-like structure as Bonart and Hoffman suggested in their model for a MDI-PTMO based urethane elastomer. However, due to the significant change in the hard segment orientation behavior with deformation in both plaques P1 and P2, it did not appear that only one of these domains could be contributing to and dominating this behavior (see Figures 2.18 and 2.19). In addition, the TEM micrographs for these plaques showed no evidence of the aggregate structure in plaque P1, but there was an indication of such structures in plaque P2 (20). Thus, it was believed that both the polyurea aggregates and the smaller hard domains possessed a lamellar-like texture and were contributing to the hard segment orientation behavior as shown by the modified, but still oversimplified morphological model in Figure 2.22. In this model, the polyurea aggregates and the smaller domains are thought to align as a whole with their long axis in the stretch direction upon deforming the plaque. This, of course, leads to the negative hard segment orientation behavior shown in Figures 2.18 and 2.19.

As indicated earlier, a possible explanation for the difference in orientation level for the hard segments of plaque 1-DMF and 2- DMF would be provided. It appeared to the authors that the

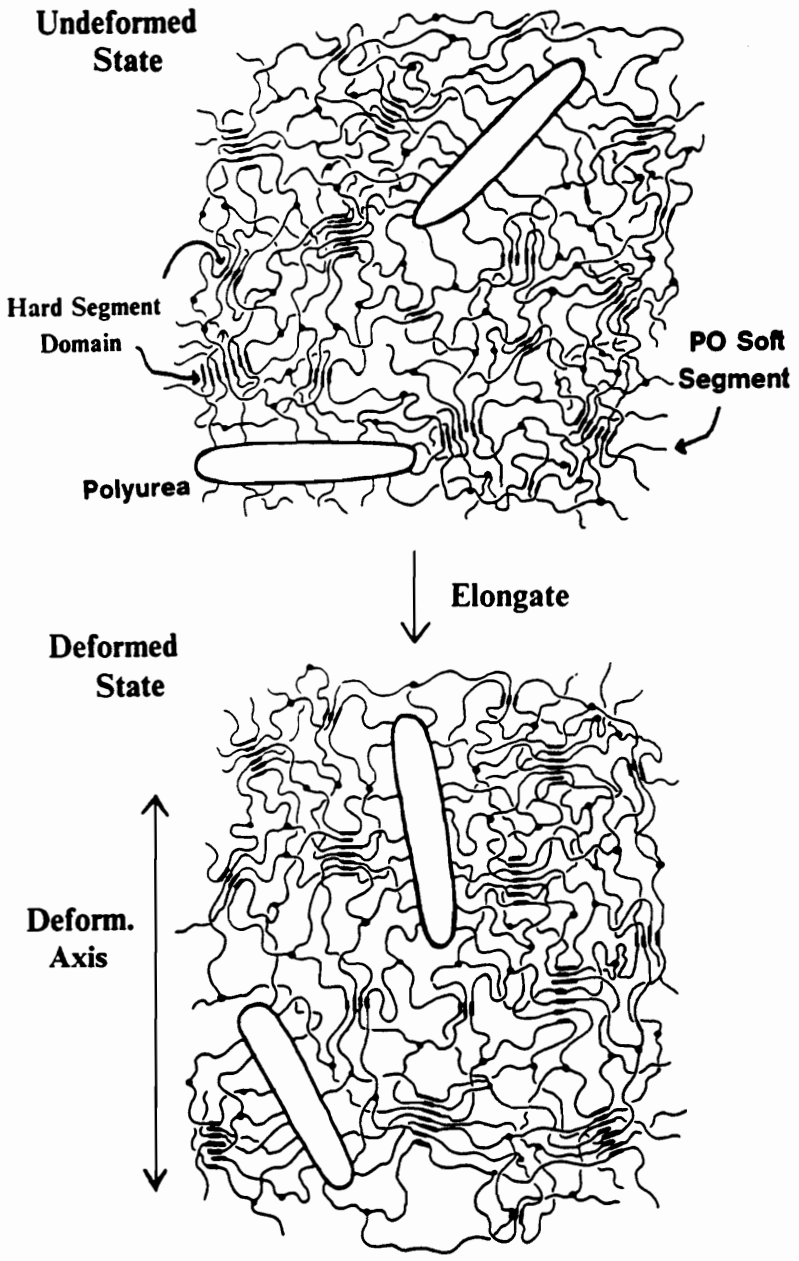

Figure 2.22. Modification of Morphological Model in undeformed(a) and deformed(a) states.: Previous model is shown in Figure 2.10. Modifications suggest the polyurea aggregates possess a more elongated lamellar structure and some of the hard segment domains also possess lamellar-like textures.(taken from ref. 23)

local strain on the hard segments would be greater in plaque P2 than in plaque P1 due to the lower volume content of soft segments in plaque P2. Therefore, upon deforming these materials, this greater local strain in plaque P2 suggested that more hard segment orientation would be observed for plaque P2 than for plaque P1 at the same level of elongation (23). Some differences in the hard segment orientation level for both urethane and urea-urethane elastomers have been observed(37,73). In the case for urethane elastomers, these differences were most pronounced when the level of phase separation was different or structural changes in the hard domains were detected(71). For urea-urethanes the trend of the orientation level with increasing hard segment content is not consistent, but there are noticeable differences in this behavior which have been reported(35).

Lamellar-like hard segment domains were also suspected to be present in the PUU elastomer due to the two-step reaction method used to make this elastomer(21). The formation of these lamellar-like hard domains also appeared to be driven by the symmetrical structure of its chain extender, MOCA. The structure of MOCA which is shown in Figure 2.6 is similar to that of MDI in that its symmetry is thought to promote the formation of partially crystalline and paracrystalline domains in urea- urethane and urethane elastomers. The WAXS patterns of this material also showed some apparent hard segment ordering which suggests at least paracrystalline character. Thus, similarly to the plaques, the distinct transverse orientation shown in Figure 2.20 for the PUU elastomer is thought to be attributed to the lamellar-like hard domains orienting as a whole with their long axis aligned in the stretch direction. Unlike the plaques, the PUU elastomer can be stretched to higher elongations at least partially because of its lack of a covalent network. Therefore, a positive upturn in the hard segment orientation level of the PUU elastomer is observed near elongations of 100%(see Figure 2.20). It was suggested that this change in orientation behavior was due to some of the lamellar-like hard domains being disrupted and possibly forming smaller hard domains. Furthermore, these smaller hard domains were more likely to align with the hard segment axis in the stretch direction; this event would have given rise to positive orientation behavior. Other investigators of MDI- based polyurea-urethane elastomers have also suggested that the positive upturn in the hard segment orientation level is due to some disruption in the lamellar

hard domains (66-72). However, the actual mechanism by which the lamellar hard domains are disrupted and the hard segments of these domains align more in the stretch direction is not fully understood and agreed upon (66-72).

In Figure 2.20, the orientation function of the $\nu(C=O)_{ur}$ group for the PUU elastomer is below the lower limit of -0.5 defined by linear dichroism theory for uniaxial orientation. Bonart and Hoffman have also observed orientation values below -0.5 for a MDI-PTMO urea- urethane elastomer (65). The authors in this case implied that biaxial orientation existed in the hard segments of their polymer upon deformation. It is also thought upon deforming the PUU elastomer, the hard segments are also partially biaxially oriented. In a uniaxially deformed system, the theoretical derivation for the dichroic ratio is based on a random distribution of the chains about the stretch direction and the transition moments for $(C=O)_{ur}$ groups about the chains (recall Figure 2.17). By considering a case of non-random distribution for either situation and reinspecting the derivation of the dichroic ratio, the experimental values obtained for the dichroic ratio giving orientation function values less than -0.5 were calculated. These calculations are shown in some detail elsewhere for the interested reader(23,24). The results of the calculations suggested (a) the lamellar-like (lathe like) hard domains as a whole align preferably at an angle to the surface of the film and/or (b) the rigid nature or the energy barriers for free rotation of the hard segments causes the distribution of the transition moments about the chain axis to be skewed. The former was speculated to be the more probable origin of the observed biaxial orientation.

2.4.4 Orientation Hysteresis

The orientation hysteresis behavior with a simultaneous mechanical response was obtained by subjecting a sample to a cyclic strain test. The orientation measurements and the mechanical response were evaluated in 10% increments of strain. The cyclic stress-strain as well as the orientation behavior for plaque 2-DMF is shown in Figure 2.23. The mechanical hysteresis is small for plaque 2-DMF (see Figure 2.23a) and was slightly larger for the PUU elastomer. This difference

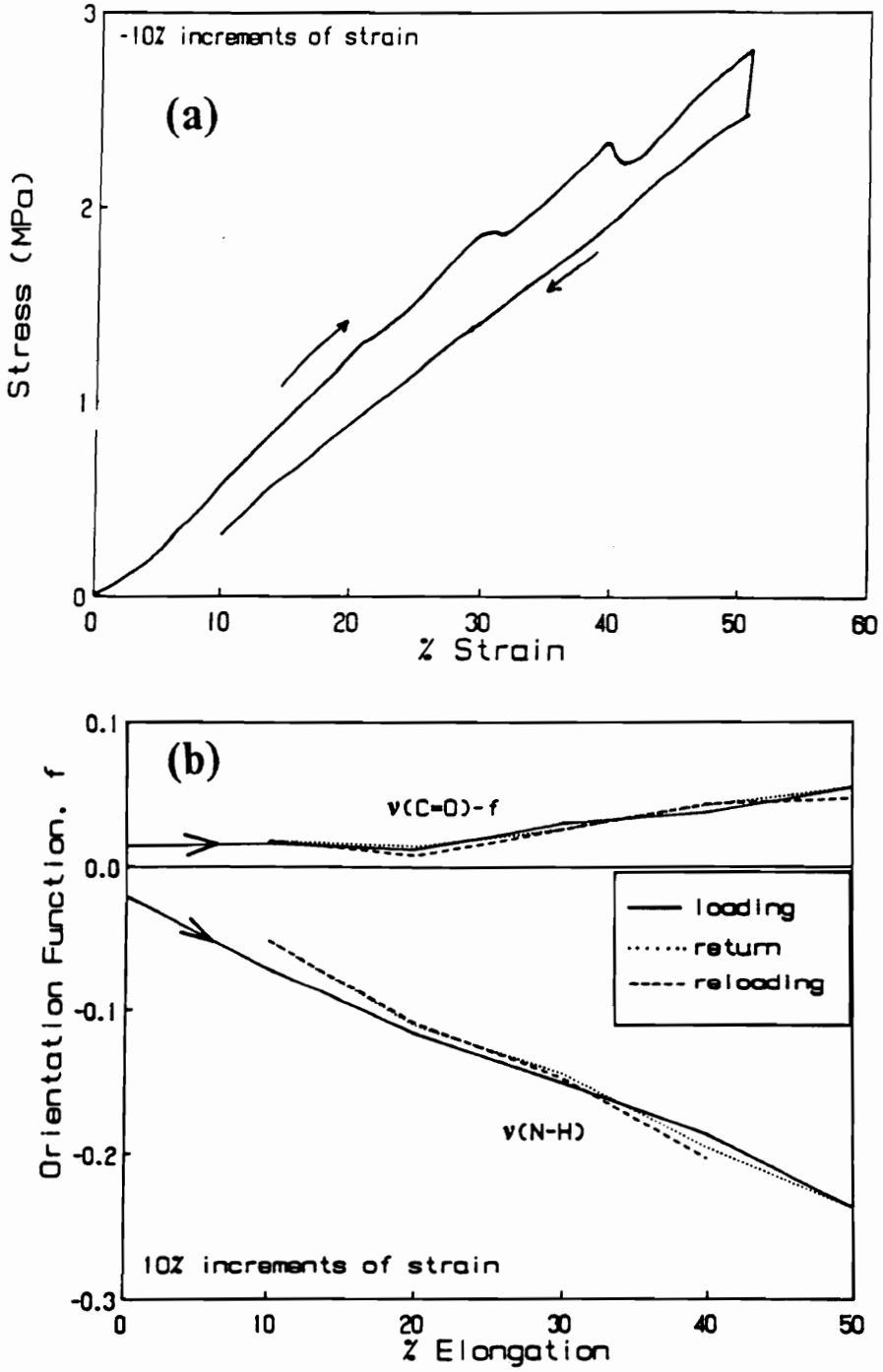

Figure 2.23. **Mechanical(a) and Orientation(b) Behavior for Plaque 2-DMF during Cyclic Deformation:** taken from ref. 23

was attributed to more chain slippage or rearrangement of chains taking place in the PUU elastomer since it consists of only linear chains. On the other hand, the movement of the chains is limited in plaque 2-DMF, since it has a covalent network(22-23).

The simultaneous orientation behavior for plaque 2-DMF (Figure 2.23b) and the PUU elastomer both exhibited near reversible behavior for the hard segments, at the interface and for the soft segments. This orientation behavior is consistent with the small amount of mechanical hysteresis observed for both materials as discussed above. The near reversible orientation of the hard segments suggested that the hard segment domains and the polyurea aggregates of plaque 2 as well as the lamellar-like hard domains of the PUU elastomer were not disrupted up to elongations of 50% (see Figures 2.23b). However, at initial strain levels of 125% in the PUU elastomer, significant irreversible hard segment orientation behavior has been observed, while the soft segments and the interface exhibit practically reversible behavior (21). This irreversibility is attributed to some of the lamellar-like hard domains being disrupted at the higher strains as discussed earlier. Other investigators of urea-urethane elastomers have also observed similar irreversible hard segment orientation at high strain levels and have given a similar explanations (66-67). The irreversible orientation behavior of the hard segments in the PUU elastomer was also believed to be a result of an increase in the mechanical hysteresis at this higher initial elongation level of 125%(22-23).

In another related work to hysteresis in these materials, Shibayama et. al. measured the segmental orientation changes due to fatiguing a MDI-PTMO based urea-urethane elastomer(71-72). The samples were strained to a static strain of 100% as well as dynamically to 20% strain over different time periods. Upon returning to zero elongation after cyclic straining the material, Shibayama et. al. observed only small changes in the hard and soft segment orientation levels with fatigue time. These changes were more significant after fatiguing for 10^5 seconds. The orientation-elongation behavior of the hard segments was also shown to be affected by the fatigue process. After observing significant negative orientation for the hard segments up to strains of 100% for the as-cast sample, the authors reported only observing a small amount of negative orientation after fatiguing the sample for 10^5 seconds. The results reported by Shibayama suggested that the changes in the

segmental orientation behavior due to the fatigue process were caused by disruption taking place in the hard domains as well as some irreversible behavior of both the hard and soft segments(71-72).

2.4.5 Time Dependent-Orientation

As discussed earlier in the review of the mechanical properties, a better understanding of the viscoelastic behavior in polyurethane foams is of importance due to its relation to compression set and fatigue. Some features of viscoelastic behavior were therefore evaluated in plaque 1 and plaque 2 as well as the PUU elastomer after imposing a 30% strain level and then by periodically following the orientation of the different absorbing groups as well as the stress relaxation. Over a 60 minute time period, the majority of the stress relaxation for plaques 1-DMF and 2-DMF as well as the PUU elastomer took place within the first ten minutes and then began to level off (more so in plaques). As one would speculate, more stress decay was observed in the PUU elastomer since it is a linear segmented system. On the other hand, the plaques possess a covalent network which allows for less rearrangement and therefore less relaxation(22-23).

Even though some stress relaxation was observed in these materials, no significant segmental orientation changes with time were detected. No appreciable orientation changes with time were expected to be observed in the soft segments since they are known to relax quickly and most likely before the first experimental point is taken (30 seconds). It was also not surprising to see any significant orientation changes at the interface since the interfacial region between the hard and soft segments is thought to be influenced mostly by the soft segments. On the other hand, some significant orientation changes were anticipated to be observed in the hard segments since they are more rigid and hence are thought to relax slower. However, the results did not show any significant changes in orientation level with time. Therefore, as the authors suggested, the possibility exists that either the average of the orientation of the hard segments was not changing or the hard segments do re-orient with time, but the changes were small and within the accuracy of the experimental measurements of the orientation function ($\pm$ .05 orientation units)(22-23).

2.4.6 Effects of Temperature on Orientation Behavior/ Hydrogen Bonding

In obtaining a better understanding of how temperature effects the properties of polyurethanes, infrared has been an useful probe for detecting structural changes brought about by increasing temperatures. Several reports in the literature have examined these type of effects of temperature on urethane elastomers and to a small extent on urea-urethane elastomers(50,77-84). To the authors knowledge, no reports on such studies for flexible polyurethane foams have been published in the literature. Before reviewing the reported work related to segmental orientation changes in poylurethane elastomers due to temperature, a review of the effects of temperature on the hydrogen bonding in these materials is necessary. Thus, without going into a lot of detail, the hydrogen bonding thermal studies for both MDI and TDI based urethane elastomers have revealed the following general observations and conclusions(77-83);

1. A decrease in hydrogen bonding content is observed with increasing temperature in the bonded (N-H) band as well as the bonded urea and urethane (C=O) bands. In some cases, for the higher hard segment materials or higher molecular weight soft segment materials a transition in this behavior is also observed such that a more significant increase in the hydrogen bond disruption is seen after this transition (transition temperature ranges from 60°C to 120°C depending on the composition of the elastomer).

2. The transition temperature for the change in the fraction of hydrogen bonds has been reported as increasing with hard segment content.

3. Based on other thermal studies (DSC or TMA), the temperature transition in the behavior of hydrogen bonding does not appear to be dependent on structural changes that may take place with increasing temperature. That is, this transition does not necessarily take place at the point of the softening of the hard domains.

4. Based on the results from the IR-thermal study for 2,4 TDI and 2,6 TDI urethane elastomers, it was thought the behavior of the hydrogen bonding with increasing temperature was rather independent of the structural order, i.e. crystalline versus amorphous hard domains.

5. A significant degree of hydrogen bonding was still detected in these materials up to 150°C in TDI based urethane elastomers and 200°C in MDI based urethane elastomers.

6. The hydrogen bonding between the hard and soft segments is thought to be disrupted at lower temperatures (< 100°C) for the most part. On the other hand, at the higher temperatures the hydrogen bonding in the hard domains is believed to be mostly disrupted.

7. The hydrogen bonding content related to the degree of phase separation was found to be mostly dependent on the molecular weight of the soft segment.

In an orientation-temperature study, Cooper et. al. have reported observing the level of orientation for a 5000 MW PTMO- 55 wt% HS polyether urethane and 1000 MW polytetramethylene adipate(PTMA)-46 wt% HS polyester urethane going through maximum(f_{max}) as a function of temperature(74,83). The temperature where f_{max} occurs is above the hard segment T_g (or softening temp. of hard domains) which indicated the hard domains are more easily disrupted near their T_g i.e., the hard segments can align easier in the stretch direction. In addition, at temperatures greater than the temperature at which f_{max} takes place, the transition in the behavior of the hydrogen bonding content occurs(as described above). This observation, of course, suggests the hard segments are able to relax more after being deformed and thus take on a lower orientation state.

For a 2000 MW PTMA-60 wt% HS polyester urethane, Siesler also observed an increase in the orientation function of the hard segments from 25°C to 75°C(below the T_g of the hard segments) (84). The increase in hard segment orientation function at 75°C was so significant that it surpassed the orientation level of the soft segments at strains greater than 80%. This difference was thought to be significant since at ambient conditions the reverse trend was observed at all strain levels. Thus, the increase in the hard segment orientation behavior with temperature was mostly

attributed to the disruption of the hydrogen bonding in the hard domains. This type of disruption was believed to allow for the hard segments to orient more in the stretch direction(84).

2.5 Summary

Flexible water-blown polyurethane foams are made in a "one-shot" continuous process by generally adding five different chemical components. These components are a diisocyanate, a polyether or polyester polyol, water, silicone surfactant, and tin and amine catalysts. A blowing reaction which consist of two primary reactions and a gelling reaction take place during the foam formation. In the early stages, the formation of disubstituted urea via the blowing reaction is the dominant species in the foam mixuture. Towards the end of the foam rise, disubstituted urea has been detected to precipitate out of solution. After the end of foam rise, the gelling reaction becomes more effective and the urethane linkages are for the most part formed at this time.

The morphology of the solid portion of flexible slabstock foams are similar to that of polyurea-urethane elastomers. For example, the SAXS results and the thermomechanical spectrum suggest similar morphologies. Both techniques detect a two-phase morphology. The DMS results exhibit a rubbery plateau and a fairly sharp soft segment glass transition which is independent of the hard segment content. The SAXS results detected scattering centers (hard domains) that were approximately 9 nm apart and contained fairly sharp phase boundaries. Furthermore, both techniques predicted better phase separation in the plaques. The TEM results showed evidence of large polyurea domains that increased in size from approximately 100 nm to 400 nm with increasing hard segment content. Based on the above results, the solid morphology of the flexible slabstock foams on the molecular scale is represented best by Figure 2.10.

The mechanical properties are dependent on the above morphology of the solid portion of the foam as well as the cellular structure. The compressive stress-strain behavior goes through a linear

elastic region (cell bending), a non-linear region (cell wall buckling), and then densification of the foam. The stress-strain behavior depends primarily on the cell regularity and the cell geometry, and secondarily on the cell density and cell size. The tensile strength and hardness of flexible foams increase with the hard segment content for a set of constant density foams. The isocyanate index, the structure of the polyol, and other formulation variables also have an effect on the stress-strain properties of foams.

The viscoelastic properties of flexible foams are also affected by the formulation components and by the cellular structure as well as by temperature and humidity. The water content has the greatest effect on the indentation load loss and the compression set at high temperatures and at high relative humidities. The isocyanate index and the blowing agent levels have secondary effects on these viscoelastic properties. The loss in the properties can be attributed to stress relaxation. The compressive as well as the tensile stress relaxation behavior show a linear relationship in a plot of log stress versus log time. The stress relaxation behavior in tension does appear to be independent of the celluar textures and thus is thought to be dependent only on the solid portion of the foam. The compression creep behavior is linear in the form of compressive strain versus log time. In addition, the initial rate of creep obtained from this relationship is dependent on the initial compression level. This dependency is mostly attributed to the cell walls buckling upon compressing the foam.

At low strain levels(30-50%), the orientation behavior of the plaques compressed from the flexible foams is similar to that of a related polyurea-urethane elastomer. This observation does suggests that similar forces govern the orientation changes with deformation in these materials; despite the fact that the plaques possess a covalent network morphology while the elastomers form a linear segmented system. The orientation-elongation behavaior of the plaques revealed that the small hard domains as well as the polyurea aggregates likely possess a lamellar-like texture with the hard segments perpendicular to the long axis of the lamallae(see Figure 2.22). The low orientation and mechanical hysteresis behavior suggests the plaque(foam) structures do behave reversibly up to elongations of 50%. At a 30% level of strain, no significant segmental orientation changes with time are observed and/or detected in the plaques.

Chapter III

3.0 Experimental

3.1 Materials

The flexible polyurethane foams used in this investigation were conventional slabstock water-blown foams. These foams were made at Dow Chemical in Freeport, Texas in a homemade, boxfoaming operation. This operation consisted of a mixing container, a mechanical stirrer, and a wooden box. The mixing container was a 16 inch diameter carbon steel baffled tank that fits over an 8 inch diameter multiple blade stirrer. The stirrer was being driven by a motor. The wooden box was of 3 cubic feet and lined with a polyethylene bag (3,20).

The formulation components given in Table 3.1 were used to make the foams for this investigation and are also used on a commercial scale. These foams were processed by using the formulation amounts given in Table 3.2. The water, the polyether polyol, the surfactant, and the amine catalyst were first mixed for 30 seconds at 900 revolutions per minute. This was followed by addition of the tin catalyst and mixing for 30 more seconds at the same speed. The diisocyanate was then added and mixing took place for 5 more seconds at 1200 rpms. The mixture was then poured

Table 3.1: Formulation Components for Flexible Water-Blown Foams

Isocyanate	T-80, 80:20 mixture of 2,4- and 2,6- isomers of toluene diisocyanate (Dow Chemical)
Polyol	Voranol 3100, a 3000 MW propylene oxide glycerine initiated polyether polyol; approximately trifunctional (Dow Chemical)
Water/ Blowing Agent	Deionized water - no chemical blowing agent used
Catalysts	T-9, a tin catalysts commonly known as stannous octoate (MET Chemical) DABCO 33LV, an amine catalyst which is triethylenediamine in dipropylene glycol (Air Products)
Surfactant	BF-2370, a silicone surfactant (Goldschmidt)

Table 3.2: Formulation Amounts for Flexible Foams

Component	Foam #						
	F1	F2	F3	F4	44-0	44-4	44-5
Voranol 3100	100	100	100	100	-	-	-
Water	2	3	4	5	5	5	5
T-80	30.79	41.43	52.06	62.70	-	-	-
Surfactant	1.0	1.0	1.0	1.0	-	-	-
Tin Catalyst	0.15	0.15	0.15	0.15	-	-	-
Amine Catalyst	0.3	0.3	0.3	0.3	-	-	-
Lithium Chloride	-	-	-	-	-	0.4	0.5

Comments:
1. Formulations based on 100 parts by weight of polyol.
2. An isocyanate index of 110 was used for Foams F1-F4.
3. In some instances 0.2 pphp tin catalyst was used for recently made Foams F1-F4
4. Compression molded plaques were made by applying pressure for 10 minutes at 204°C.
5. Formulation amounts for all components are not given for foams 44-0, 44-4, and 44-5 due to proprietary reasons.
6. Isocyanate index for foams 44-0, 44-4, and 44-5 was 100.
7. The tin catalyst level for LiCl foams(44-4,44-5) was lower than that of its control(44-0).

in a lined wooden box and allowed to react. After the foams had cured, they were then trimmed. The remaining block was used for various testing analysis. All of the foams investigated were prepared in this manner (20).

Foams F1-F4 are the same foams that were discussed earlier in the morphology section and as well as in the linear IR-dichroism(F1 and F2) study of the literature review. Additional samples of foams F1-F4 were recently made for the tests in compression using the same methods described above and the formulation amounts in Table 3.2. In some cases the tin catalyst level had to be adjusted slightly(0.15 to 0.2pphp), in order to get a better quality foam. However, this adjustment was not believed to affect the cell structure or the solid morphology based on the earlier studies in which the adjustment of the tin catalyst level was studied(20). Foams 44-0, 44-4, and 44-5 were made with similar formulation components to that of F1-F4, but in the case of 44-4 and 44-5 they contain 0.4 parts per hundred polyol(pphp) and 0.5 pphp of lithium chloride, respectively. As will be discussed later on in this dissertation, the LiCl component does bring about a change in the solid morphology of a foam while still maintaining the same hard/soft composition to that of a foam without lithium chloride in its formulation.

Compression molded plaques were also made from each foam by applying pressure for 10 minutes at 204°C. In some cases the foams were subjected to a pretreatment process before compression molding. The pretreatment process consisted of first soaking the foams in DMF or THF overnight. The foams were then patted dry and the excess solvent was taken off by storing the foams in a vacuum oven at 50°C for at least 24 hours. After this solvent removal treatment, the foams were then compression molded using the above conditions. The nomenclature used for the plaques prepared from the pretreated foams was given earlier in Table 2.1 in the linear IR-Dichroism section of the literature review. For a brief reminder, plaque 2-DMF represents plaque P2 (made from foam F2) which was pretreated with DMF before compression molding.

A urea-urethane cast elastomer was used in this investigation for comparison purposes to that of the foams since the foams are also urea-urethane materials. The urea-urethane elastomer was made from T-80 (see Table 3.1) and a 2000 MW polypropylene oxide diol (P2000) with a methylene-bis(2-chloroaniline) (MOCA) curing agent. The elastomer was also prepared at Dow

Chemical by first making a prepolymer. This was done by mixing P2000 and T-80 for 4hrs at 80°C. The prepolymer which contained 5% extra NCO groups was then mixed with MOCA. This mixture was then poured into a mold for 1 hr at 130°C and then allowed to cure for 16 hrs at 70°C. This urea-urethane elastomer contains a 31 wt% hard segment content and is referred to as the PUU elastomer for this investigation(the same elastomer mentioned in the linear dichroism section of the literature review).

3.2 Experimental Techniques

The main objective of this work was to evaluate the viscoelastic behavior of flexible slabstock polyurethane foams as well as the plaques of these same foams under controlled testing conditions. The compression molded plaques were studied because they offer the advantage of analyzing the material comprising the foam independent of its geometry. As discussed earlier, the compression molding process does not alter the morphology of the solid material significantly. The three main techniques utilized in characterizing the viscoelastic nature of these materials were tensile stress relaxation, compression load relaxation, and compressive creep. Additional experimental techniques such as small angle x-ray scattering(SAXS), wide angle x-ray diffraction(WAXD), transmission electron microscopy(TEM), scanning electron microscopy(SEM) and solid state nuclear magnetic resonance(NMR) were used to characterize the morphology of foam 44-0 and the LiCl foams. In continuing earlier work, linear IR dichroism measurements were further utilized to evaluate the effects of temperature on the orientation behavior.

3.2.1 Tensile Stress Relaxation

Stress relaxation in tension was used to follow the stress decay with time at constant temperatures as well as at controlled temperature and relative humidity conditions. The controlled temperature experiments were carried out on an Tensilon/UTM II Tensile Tester that was equipped with a homemade thermal chamber. The temperature was controlled by an OMEGA® miniature micro-processor temperature controller and a type K thermocouple. For ambient conditions(aprrox 25°C), the relative humidity ranged from 30 to 60 percent depending on the time of year. The controlled temperature/relative humidity(RH) tests were carried out on a MTS tensile tester equipped with a Thermitron environmental chamber.

In both experimental set-ups, the same 550 gram load cell was used to monitor the load exerted by the foams, the plaques and the PUU elastomer. The analog signal from the load cell was converted into a digital signal through use of A/D card and a computer. The digital signal was then converted into a load value through use of a linear calibration curve. The stress exerted by the foams, plaques, or elastomer was then calculated using the cross sectional area and the acceleration due to gravity. When calculating the stress for the foams, the differences in density for foams F1-F4 were accounted for. At the completion of an experiment, the stress values as a function of time were stored on to a computer disk.

A typical experiment involved placing a small dogbone specimen with a 10mm gauge length and 1.6mm width in the testing clamps. After reaching the appropriate conditions in the testing chamber, these conditions were maintained for 30 minutes in order to give ample time for the sample to come to equilibrium with its surroundings. Based on moisture weight-up take studies on the plaques of these foams, the 30 minute period was believed to be an adequate amount of time for the foam samples to reach saturation for the high relative humidity tests. After pre-conditioning the samples, they were then stretched at a 40mm/min extension rate to a constant elongation of 25 percent for generally 3 hours and in some cases for 2 to 3 days. During stretching the decay of the

stress was monitored periodically by computer. The experiment was repeated 3 or 4 times for a given sample and set of conditions. A fresh sample was used for each experiment.

Based on previous studies which showed very little difference in the relaxation behavior upon stretching the foams parallel or perpendicular to blow direction, the dogbone samples were only cut so that the samples would be stretched parallel to the blow direction. Before cutting the dogbone specimens, the foams were sliced with a die such that the thickness of samples was always 5mm. Foams F1-F4 were tested in the temperature range of 25°C to 140°C. Foams F1 and F4 were also tested at temperatures of 30, 60, and 90°C where the relative humidity was held constant in the range of 0 to 100 percent.

Once again the compression molded plaques of foams F1 and F4 were tested to further evaluate the anisotropic dependence of the cell geometry on the stress relaxation behavior for the foams. The thicknesses of the plaques were generally in the range of 5 to 8 mils and the testing conditions were carried out in the temperature range of 25°C to 140°C. The PUU elastomer was also tested in order to compare the stress relaxation behavior for chemically similar materials, but different morphologies, i.e. crosslinked network(foams) vs. linear segmented system(elastomer). Its thicknesses ranged from 2 to 4 mils and it was tested at temperatures in the range of 25 to 125°C. At temperatures greater than 125°C the PUU elastomer snapped after applying a strain to it.

3.2.2 Compression Load Relaxation

The load relaxation behavior in compression was utilized to monitor the decay of the load with time under controlled conditions(Temperature, %RH). The experimental procedures followed for these test were not standardized compression tests given in the ASTM standards for flexible foams. However, these experiments were developed by the author based on his reviewal of the literature and the need for a better understanding of the relaxation behavior as a function of time for flexible foams. The compression load relaxation tests were carried out on an Model 1122 Instron equipped with a 10 lb. compression load cell. The conditions of the tests were controlled by a Russells

Technical Products environmental chamber. This chamber has the capability of controlling temperature in the range of -4°C to 315°C and in the temperature range of 4°C to 85°C, relative humidity can be controlled from low humidity (0 to 15 percent) to high humidity (95 to 100). A more detailed description of the environmental chamber and the other equipment used in carrying out the compression load relaxation tests is given in Appendix A. As in the case of the tensile stress relaxation tests, the load exerted by the sample was monitored by computer. A schematic of the overall set-up for the compression load relaxation test is given in Figure 3.1. The other features shown in this schematic are the arm extension from the crosshead[1] with a 2″ diameter indenter[2] and the extension from the load cell with a 5″ x 5″ sample plate[3].

A typical test involved placing a foam specimen on the sample plate and lowering the indenter such that it is just touching the top of foam sample(this was detected by the monitoring the signal from the load cell on the computer). The conditions in the chamber were then allowed to reach equilibrium. In approaching the conditions for the high temperature tests, the indenter had to be raised slightly(0.5 to 2mm) due to expansion of the foam as well as the indenter. In determining the testing parameters, i.e. the compressive strain, the movement of the indenter due to the foam expansion was accounted for. After maintaining the desired conditions for 30 to 45 minutes, the sample was compressed twice at a 350 mm/min crosshead speed in a cyclic fashion to 70% elongation to mimic the indentation load deflection(ILD) tests given in ASTM standards for flexible foams(85). Five minutes later the foam was compressed to the desired strain at a 350 mm/min crosshead speed. Upon approaching the constant strain level, the load-strain behavior was acquired via computer. The constant strain level was generally 65% due to the common ILD test specified by ASTM standards for flexible foams. Other strain levels ranging from 5 to 80% were also used to evaluate the dependence of the relaxation behavior on strain. After reaching the constant strain level, the load was periodically monitored by computer for 3 hours and in a few cases in order to obtain the long term behavior, the testing period was on the order of 12 to 70 hours. At the end of the test, the load-strain behavior was acquired and in some cases the foam was re-compressed to follow the immediate load-strain behavior. Furthermore, at the end of the test the loss in thick-

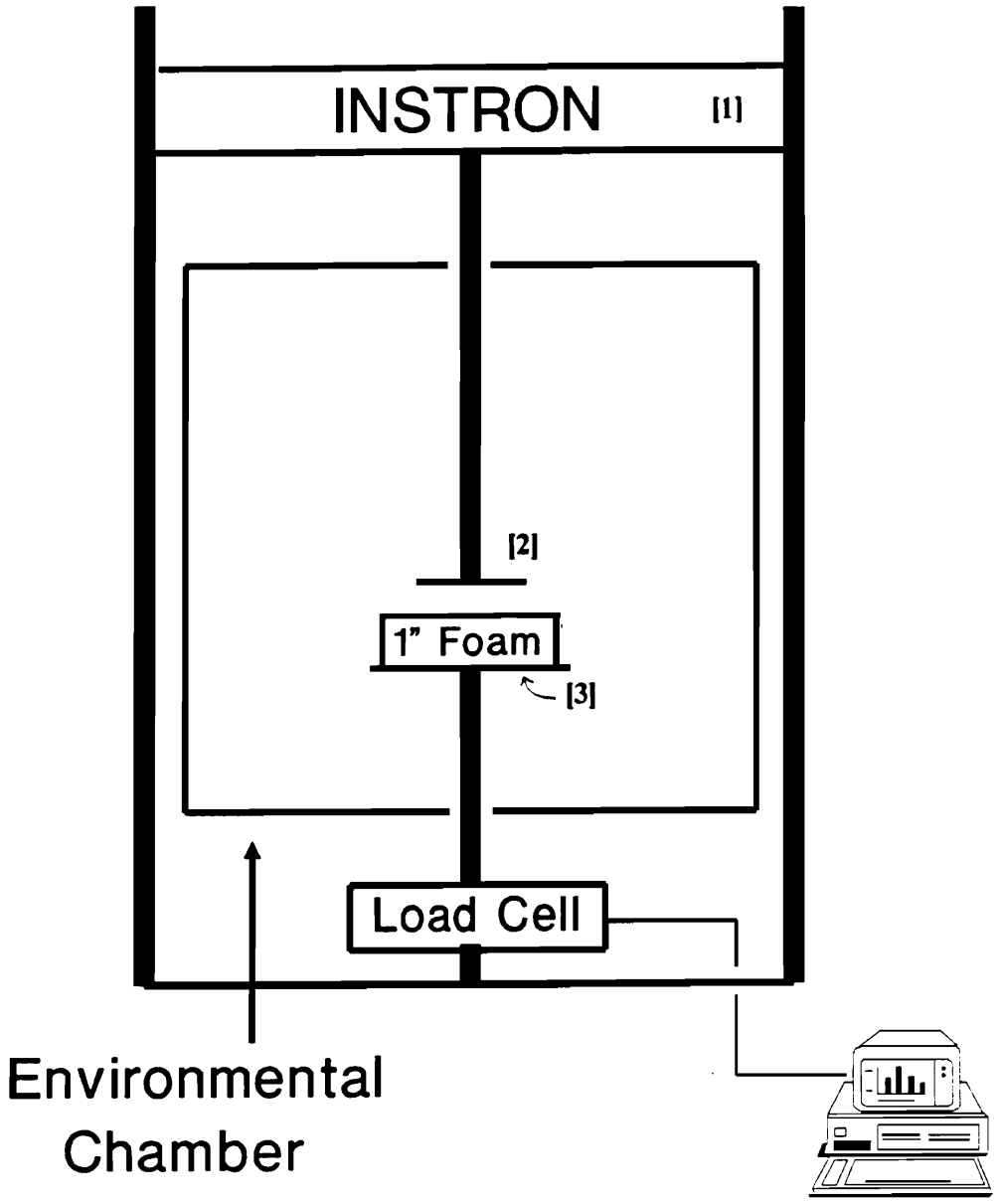

Figure 3.1. Experimental Set-Up For Compression Load Relaxation Tests

ness or compression set in the foam sample was obtained by lowering the crosshead to the top edge of the foam.

The foam samples used in these tests were 4″ x 4″ and had approximately a 1″ thickness which was measured carefully with calibers. The samples were cut so that they would be compressed parallel to the blow direction. Foams 44-0,44-4, and 44-5 were also used and cut in the same manner to that of Foams F1-F4. The testing conditions for the compression load relaxation tests ranged from 30-140°C in temperature. The relative humidity was varied from low(0-15 percent) to very high(95-100 percent) at temperatures of 30, 60, and 85°C. In most cases only one sample was tested for a given foam and condition. However, at some experimental conditions two to three samples for a given foam were tested to obtain a range of error in the measurements.

2.3 Compression Creep

The third viscoelastic test, compression creep, was utilized in order to monitor the change in thickness or strain under a constant load and at controlled testing conditions. The experimental set-up as well as the procedure of these tests were designed after a similar study by Campbell(55). The design criteria in constructing the instrument, a description of the instrument as well as its operation, and the procedures used in carrying out the compressive creep measurements are given below.

In simple terms, an instrument that would be able to monitor the change in thickness of a foam with time in a controlled environment was desired. One of the key features desired in carrying out the creep measurements, was frictionless movement of the arm detecting the change in thickness. This criteria, of course, enables detection of the change in the material thickness only. The creep behavior was desired to be monitored by an on-line computer. In addition, the capability of applying a wide range of constant loads to the foams was desired. Finally, temperature and percent relative humidity were also desired to be controlled during the test.

In meeting the above criteria, a twin shaft web assembly with a moving carriage that was manufactured by Thompson Inc. was used as the base for the compression creep device as well as to minimize friction. As shown schematically in Figure 3.2, the rest of the creep device was machined to fit with this assembly. Displayed in Figure 3.2 is an extension arm[2] which is attached to the moving carriage[1] and furthermore extends down into the testing chamber[3]. The testing chamber utilized for these tests was the same environmental chamber mentioned above in the experimental section for the compression load relaxation tests. A 2″ diameter indenter at the end of the extension arm[2] does come in contact with the foam[4] which rests on 5″ x 5″ plate. Also shown in Figure 3.2, is a linear voltage displacement transducer(LVDT[5]) and its capillary[6] which is attached to the moving carriage(capillary does slides freely inside the outer housing of the LVDT). The LVDT served to detect the movement of the carriage and likewise the creep in the foam. In addition, it sent out a voltage signal relative to the position of the capillary in the outer housing. This signal was then converted to a digital readout on the computer via an analog to digital(A/D) card in the computer. Through use of a calibration curve the digital signal was converted into compressive strain where it was then stored on computer disk. The calibration curve was obtained by using a dial indicator. Finally, the constant load which was applied on the foam is controlled by the pulley system[8] shown in Figure 3.2. The pulley system was incorporated into the design in order to be able to offset the weight of the carriage as well as the arm extension and thus enables one to apply loads as lowest as 100 grams and as high as 5000 grams.

A typical experiment involved placing a 4″ x 4″ foam sample of known thickness onto the 5″ x 5″ plate. The indenter was then lowered and held in place so that it was just touching the top of the foam. Meanwhile the desired testing conditions were approached and during this approach, adjustments for thermal expansion of the foam and the indenter were made by raising the extension arm. After maintaining the conditions for 30-45 minutes, a constant load was manually applied to the foam by releasing the extension arm into a freefalling motion. Upon releasing the arm, the compressive strain as a function of time was monitored via computer.

The samples used for the compression creep tests were the same in size and foam series to those used in the compression load relaxation studies(see Table 3.2). The loads that were applied

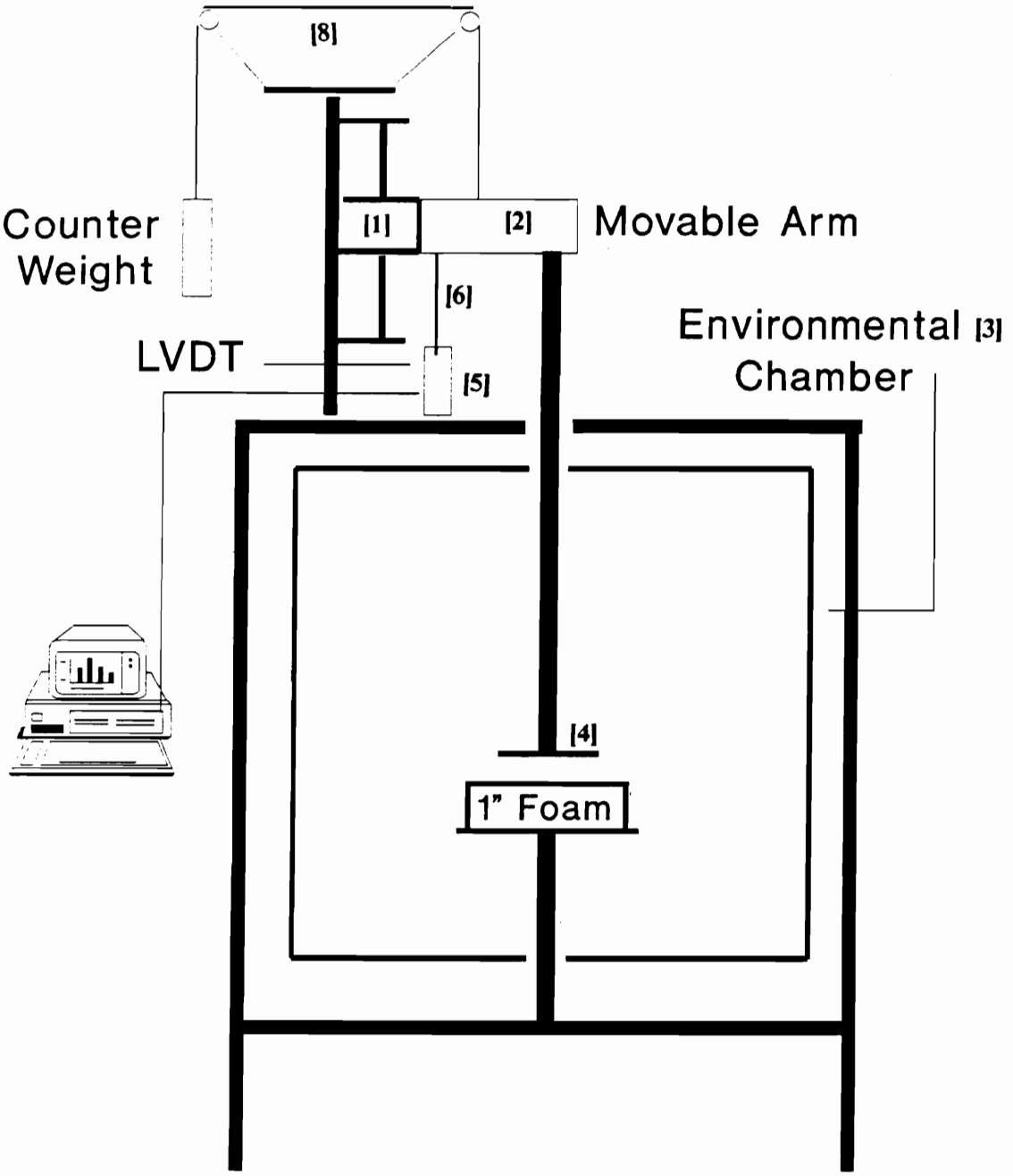

Figure 3.2. Schematic for Compression Creep Device

varied from 750 grams to 3.5 kilograms. The tests were generally run for 3 hours and in some cases over longer time periods. The testing conditions were carried out at low humidity(0-15 percent) at 30, 85, and 125°C and at high humidity(95-100 percent) at 30 and 85°C. As in the case of the compression relaxation tests, only one sample for a given foam and testing condition was normally used, except in a few instances in order to obtain a range of error in the measurements.

3.2.4 Additional Experimental Techniques

X-Ray Analyses

Wide angle x-ray diffraction(WAXS) patterns and small angle x-ray scattering(SAXS) behavior in general were obtained to help characterize the foams with(foam 44-5) and without(foam 44-0) lithium chloride. The WAXS setup consists of a Phillips Table-Top X-Ray Generator PW 1720 with a standard vacuum-sealed Statton Camera. The foam samples tested were 10mm in thickness and were compressed to approximately 3mm. The exposure times were in the range of 22 to 24 hours. The sample to film distance was 7.8 cm. Small angle x-ray scattering was carried out with a Siemans Kratky camera system. The x-ray source was a Siemens Cu-W tube powered by a Siemans Model 1726 Generator. A Braun position sensitive detector was utilized to monitor the angular dependence of the scattering intensity. A package developed with ASYST by Dinesh Tyagi and modified by H.H. Huang was used to convert and analyze the data.

SEM

Scanning electron microscopy was utilized to distinguish if there were any major differences in the bulk morphology of foams 44-0 and 44-5. A Cambridge Instruments Streoscan electron microscope was used to obtain the micrographs for these foams. Foam samples of approximately 2 mm in thickness were cut both parallel and perpendicular to the blow axis. The samples were placed on aluminum stubs which had been coated with silver conducting paint. This was followed by a gold coating of approximately 200 angstroms with a Biorad Polaron sputter coater.

TEM

Transmission electron microscopy was utilized to determine the effect on the morphology of the solid portion of the foam by adding LiCl to the foam formulation. The micrographs were obtained at Dow Chemical by using a JEOL 2000FX Analytical TEM which was operated at an accelerating voltage of 100kv. The foam samples were prepared by first embedding small pieces of foam with D.E.R. 331 epoxy. Ulttathin sections(ca. 100nm) were then cut at room temperature from these sample utilizing a diamond knige on a Riechert-Jung Ultracut E microtome and were mounted on a carbon-coated copper grid. The foam samples characterized in this manner were foams 44-0, 44-4 and 44-5.

Linear IR-Dichroism

As discussed in the literature review, IR-dichroism is an useful technique to obtain the molecular orientation for segmented polymers. In continuing earlier work, the effects of temperature on the orientation behavior in the plaques of the flexible water-blown polyurethane foams was measured utilizing this technique.

The equipment utilized to obtain the molecular orientation by IR dichroism as well as the simultaneous mechanical response were an infrared source, a suitable polarizer, and an appropriate mechanical apparatus equipped with a thermal chamber. A Nicolet 5DXB FTIR Spectrometer with $4cm^{-1}$ resolution was used as the infrared source. An IR-grid polarizer with KRS-5 substrate material with 70% maximum efficiency was utilized to polarize the infrared beam parallel and perpendicular to the deformation axis. An automated rheo-optical stretching apparatus equipped with a thermal chamber was utilized to deform thin film samples at a constant temperature. The apparatus along with the thermal chamber fits inside the FTIR sample chamber where the experiment took place. For the interested reader, more detail on the design and the operation of the mechanical apparatus and its thermal chamber can be found in the author's Masters Thesis(22).

In utilizing the above rheo-optical system, two different types of deformation experiments were performed at temperatures ranging from 25 to 125°C in obtaining the orientation behavior simultaneously with determining the mechanical response - these were stress-strain and stress relaxation.

The stress strain tests involved stretching a thin film sample at an initial extension rate of 400%/min in 10% increments of elongation. At the end of each increment the dichroism measurements were made after "stress equilibration" was approached. This usually took 1 to 5 minutes depending on the sample and the strain level. The measurements involved taking two IR spectra(32 scans each) with the polarizer parallel and perpendicular to the stretch direction. The IR spectra for the plaques as well as the PUU elastomer contained no band overlap in the regions of interest(see Table 3.3). In determining the dichroic ratio for the chromophoric groups of interest, the peak heights were then measured using a peak- picker routine which was part of a Nicolet software package. During the stress-strain tests, the mechanical behavior was monitored for each increment of strain to give the "stress-strain" behavior.

The stress relaxation experiment was used to provide an indirect measure of the "general" orientation behavior with time. The test involved stepping to a 30% strain level and then following dichroism measurements with time. Only 10 scans for each polarization direction were used which took 30 seconds to obtain the absorption values. The stress relaxation behavior was also obtained simultaneously.

The orientation behavior as well as the simultaneously measured mechanical data that will be presented later are not an average over many experimental tests. However, in some cases the experiments were repeated and the same general behavior was reproduced. In addition, based on earlier experiments with this same rheo-optical system, the maximum range of error in the orientation function was ± 0.05 orientation units.

The samples that were tested using the above technique were plaque 1 and plaque 2-DMF as well as the PUU elastomer. Recall that plaque 2-DMF was prepared by pretreating the foam sample in DMF and followed by a thorough drying before compression molding. This pretreatment procedure was used in order to obtain plaques with thicknesses in the range of 1 to 1.5 mils. Thin films in this thickness range were necessary so that sufficient energy could be transmitted through the sample to be analyzed by the IR detector.

Solid State NMR

Solid state NMR has been utilized to better understand the localized motions of the hard and soft segments in the foams as well as to aid in further understanding the morphology of the solid portion of the foams. Two different NMR relaxation measurements were made at the North Carolina State University Chemistry Department by S.S. Sankar on a Chemagnetics CMC 200S NMR spectrometer equipped with a cross polariztion(CP)-magic angle spinning(MAS) probe. Two rotating frame relaxation times, $T_{1\rho}(^1H)$ and $T_{1\rho}(^{13}C)$, were measured. The pulse sequences used for these measurements are given in Figure 3.3. The solid state (^{13}C) NMR spectra were obtained under Hartman-Hann conditions near 50kHz. In addition, 2000 transients(block- averaged in groups of 200) were collected for each τ value over a spectral width of 15kHz using 2k data points, 5.2 μsec 90° pulse, a 3 msec contact time, and with a spinning rate of approximately 4kHz. A second pulse delay was utilized to allow the spins to return to equilibrium. The majority of relaxation measurements were made at ambient conditions and in a few instances at 75°C. The relaxation times were determined by fitting the experimental data to several model distributions of first order relaxation behavior by means of a PC-XT program, RELAX(ation), written by Robert Skarjune of 3M Corporation. All foam samples listed in Table 3.2 were characterized using solid state NMR.

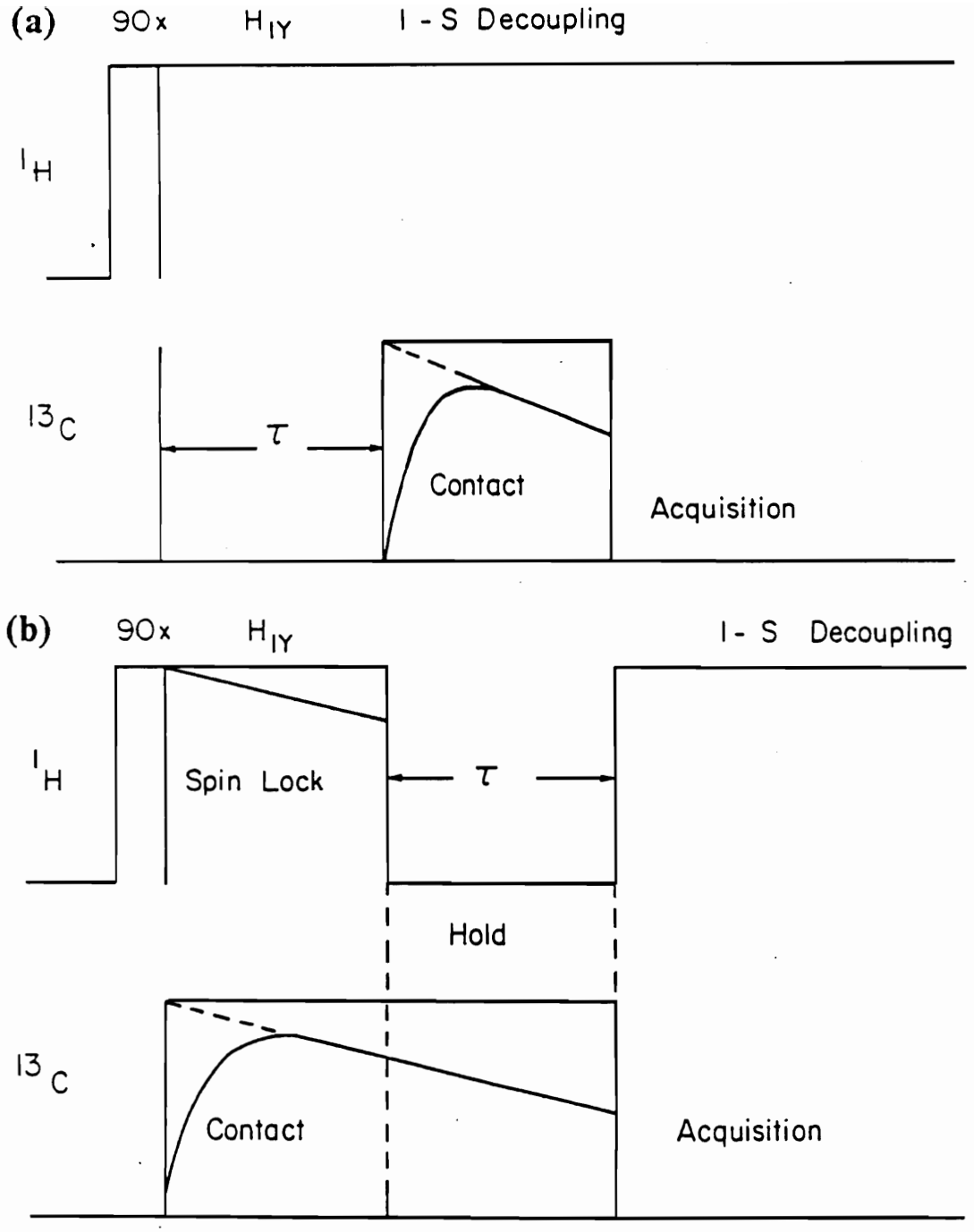

Figure 3.3. Pulse Sequences for (a)$T_{1\rho}(^1H)$ and (b)$T_{1\rho}(^{13}C)$ Relaxation Times

Chapter IV

4.0 FTIR Thermal Analysis

In continuation of the earlier FTIR work presented in the author's Masters thesis, the following chapter will concentrate on utilizing FTIR to evaluate the effect of temperature on the stability and orientation behavior for the plaques of the compression molded foams and a polyurea-urethane(PUU) elastomer. Although, the work presented in this chapter is not the main emphasis of this dissertation, it does provide insight for understanding the thermal effects on the viscoelastic behavior of polyurethane foams. Thus, the main objective of this study is to obtain a better understanding how temperature may alter the morphology of the foams, i.e hydrogen bond disruption, chemical changes, etc.. In meeting this objective two different types of experiments have been performed. The first is an evaluation of the thermal dependence of the absorbance for various chromophoric groups in the range of 25°C to 150°C. Also, linear IR-dichroism with a simultaneous mechanical evaluation was utilized to measure the orientation-time and orientation- elongation behavior at temperatures in the range of 25 to 140°C.

4.1 Thermal Effects on the Solid Morphology

As mentioned in the literature review, a considerable amount of work in this area has been performed on polyurethane elastomers, but very little on the polyurea-urethanes in general(50, 78-84). From FTIR-thermal studies on urethanes, the main emphasis has been on understanding the changes that take place in hydrogen bonding upon increasing temperature. For well phase separated urethane elastomers, the hydrogen bonding is thought to exist mostly within the hard domains between the urethane carbonyl and that of the $N-H$ group(50, 78-84). As discussed in the literature review, the plaques(foams) and the PUU elastomer studied in this dissertation are also believed to be quite well phase separated systems with hydrogen bond formation in the urea hard domains as well as to a smaller extent to the urethane linkages which are at the interface of the hard and soft segments. Thus, for the thermal analyses of the plaques as well as the PUU elastomer, it was desired to obtain a better understanding of the change in hydrogen bonding to the urea and urethane groups. In addition, other structural changes that may occur as a result of increasing temperature were of interest; for example, chain scission within weak or unstable chemical groups. Before reviewing these results, some comments concerning the absorbance levels determined for the plaques and the method utilized for analyzing the data are made.

The FTIR measurements were carried out in the transmission mode on thin plaques compressed from flexible foams and thin films cast from solution for the PUU elastomer. The nomenclature and the composition of these materials are summarized in Table 4.1. When making measurements in the transmission mode, it is desirable to have very thin films so that the intensity level is less than 0.7 absorbance units(AU) in order to keep within the sensitivity of the detector. In the case of the PUU elastomer this does not present a problem since thin films can be cast from solution. On the other hand, it is much more difficult to obtain thin films for the plaques, since they are partial network materials and thus have to be thermally compression molded at 204°C in order to form a film - much less a thin film. Thus, the absorbance levels utilized in analyzing the results for the plaques were usually higher than 0.7 AU and in some cases as high as 2.0(e.g. urea

Table 4.1: Materials Used for FTIR Thermal Analysis

Material	Wt% Hard Segment	Study Utilized
Plaque P1	21	Thermal Analysis
Plaque P2	26	Thermal Analysis
Plaque P4	34	Thermal Analysis
Plaque 2-DMF	26	Orientation
PUU Elastomer	31	Both

-Plaques compression molded from foams at 204°C for 10 minutes
-Plaque 2-DMF was made by pretreating foam in DMF and followed by thorough drying before compression molding
-PUU elastomer was cast from DMF-solution

carbonyl and the $\omega(CH_2)$). However, the results which are presented later for the plaques are believed to be reproducible based on results obtained for several tests on plaque P1. Due to the high absorbance levels that were obtained in analyzing the data for the plaques, the results for the plaques are discussed on a relative basis.

Method for Analyzing IR Spectra

As reported in the literature for FTIR-thermal analysis of urethane elastomers, the evaluation of some regions of the IR spectra can be rather difficult to interpret(78-84, 86). These difficulties arise due to shifts in peak intensities, band broadening, and considerable band overlap. In overcoming these difficulties, techniques such as deconvolution of peaks and curve fitting have been used so that absorbance levels can be measured for different bands. Within this study, such techniques were not available and thus in evaluating the spectra other methods were utilized. Before reviewing these methods, the different absorbance bands of interest are discussed below.

In Figure 4.1, a typical IR spectrum for the foams and the PUU elastomer is shown with its different regions and bands labeled. The three regions or bands of interest for this study are the $N-H$ region from 3500 to $3200cm^{-1}$, the carbonyl region from 1800 to $1600cm^{-1}$, and the free isocyanate band at $2270cm^{-1}$. As discussed in the literature review, the $N-H$ and the carbonyl regions are believed to give the most useful information with regard to hydrogen bonding in urethane and urea-urethane materials. One of the more recent by investigations by Coleman et. al. on a urethane elastomer, however, has indicated that the absorbtivity coefficient for the hydrogen bonded $N-H$,$(N-H)_b$, group at $3300cm^{-1}$ does decrease with temperature due to a weakening effect in its hydrogen bonding(86). With this in mind, the discussion concerning the effects of hydrogen bonding will concentrate on the results obtained from the carbonyl region. The carbonyl region contains several bands between 1800 to $1600cm^{-1}$ as listed in Table 4.2. The bands that are of most importance for this study are the hydrogen bonded carbonyl urea($(C=O)_{ur}$) at $1640cm^{-1}$, the free carbonyl urea which is thought to exist at $1715cm^{-1}$, the hydrogen bonded urethane(

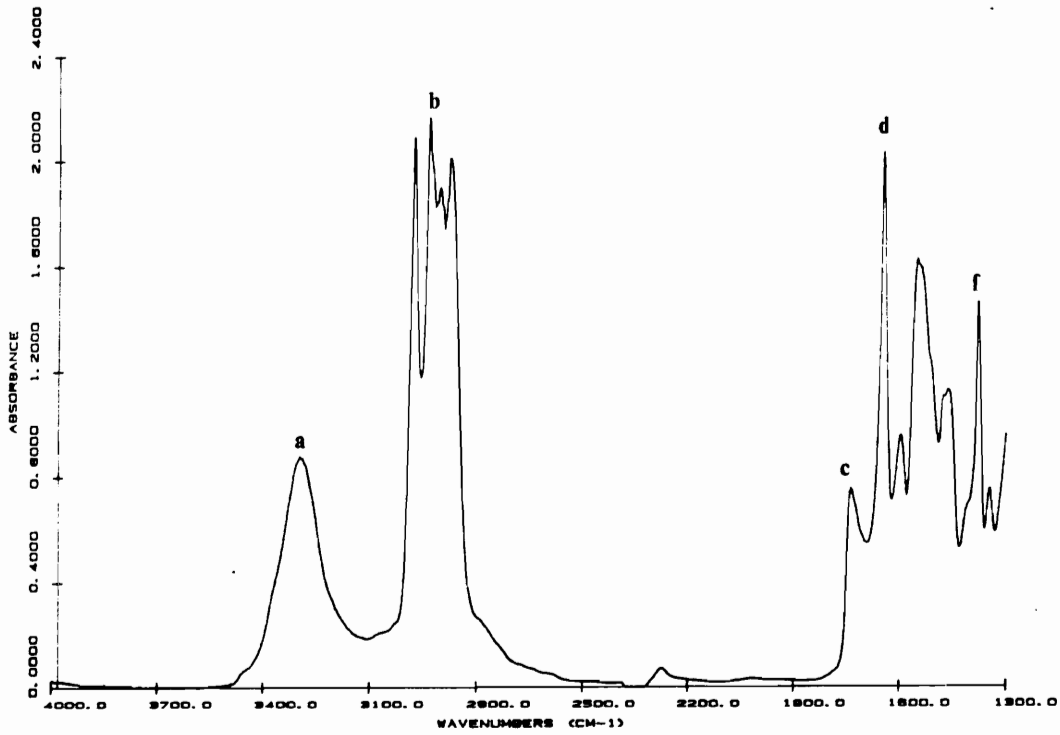

Figure 4.1. Infrared Spectrum of a Polyurea-urethane: (a) $N-H$ region, (b) $\nu(CH_2)$, (c) $(C=O)_f$, (d) $(C=O)_{ur}$ and (f) $\omega(CH_2)$. For further details, see Table 4.2

Table 4.2: Absorbing Frequencies for the Plaques and the PUU Elastomer

Frequency (cm^{-1})	Assignment*	Transition Moment Angle (°)**	Component Representation
3300	$\nu(N-H)$	90	Hard Segment Interface
2940	$\nu(CH_2)$	90	Soft Segment
2860	$\nu(CH_2)$	90	Soft Segment
1730	$\nu(C=O)_f$	78	Interface
1720	$\nu(C=O)_b$	78	Interface***
1715	$\nu(C=O)_{ur-f}$	78	Hard segment****
1700	$\nu(C=O)_b$	78	Interface***
1640	$\nu(C=O)_{ur}$	78	Hard Segment
1475	$\delta(CH_2)$	90	Soft Segment
1370	$\omega(CH_2)$	0	Soft Segment

* ν - stretching vibration, ω - wagging mode, δ - bending mode

** taken from references 67, 74

*** $1700cm^{-1}$ and $1720cm^{-1}$ bands are for urethane links with 2,6 and 2,4 TDI isomers, respectively

**** $1715cm^{-1}$ band is for "free" urea

$(C=O)_b$) at $1700cm^{-1}$ and $1720cm^{-1}$, and the non-hydrogen bonded(free) urethane($(C=O)_f$) at $1730cm^{-1}$(64,70,87). As one can see from Figure 4.1, all of these bands are not easily resolved and thus presents some problems that will be addressed in more detail in the discussion.

The preferred, but less common by far, method for determining the true absorbance level for FTIR thermal studies is by measuring the area under the peak. However, due to limitations in being able to resolve some of the peaks, peak intensities were utilized as is often done. This latter method, for example, was used for measuring the absorbance for the hydrogen bonded $N-H$ group, the $(C=O)_f$ band at $1730cm^{-1}$, and the free isocyanate at $2270cm^{-1}$. Since the $(C=O)_{ur}$ and $\omega(CH_2)$ bands were resolved and not hindered by band overlap, peak areas were measured for these bands. The absorbance for the $\omega(CH_2)$ group was utilized to normalize the spectra, since temperature has been reported to have very little effect on the soft segments in urethane and urea-urethanes up to 150°C. For both the plaques and the PUU elastomer a small increase in the $\omega(CH_2)$ absorbance level is observed with increasing temperature which is believed to be related to an overall increase in the intensity of the entire spectrum. Therefore, this increase was accounted for by normalizing the absorbance levels on the area of the $\omega(CH_2)$ band.

4.1.1 Thermal Analysis of Plaques

In Figures 4.2-4.4 the thermal dependence on the absorbance level for the $(C=O)_{ur}$, $(N-H)_b$, and the $(C=O)_f$ bands are presented for plaques P1, P2, and P4, respectively. As shown in Figures 4.2-4.4, there is a steady decrease in the three absorbance bands with increasing temperature for all of the plaques. The decrease in the $(C=O)_{ur}$ and the $(N-H)_b$ groups do indicate the hydrogen bonding to these groups are being disrupted or weakened to some extent to the $(N-H)_b$ groups with increasing temperature. In addition, this increase does appear to be greater for the $(N-H)_b$ group than that of the $(C=O)_{ur}$ group. Thus, one might predict from this difference, the amount of hydrogen bond disruption within the urethane linkages since the $(N-H)_b$ group is contained in both urethane and urea linkages. However, as mentioned earlier, the

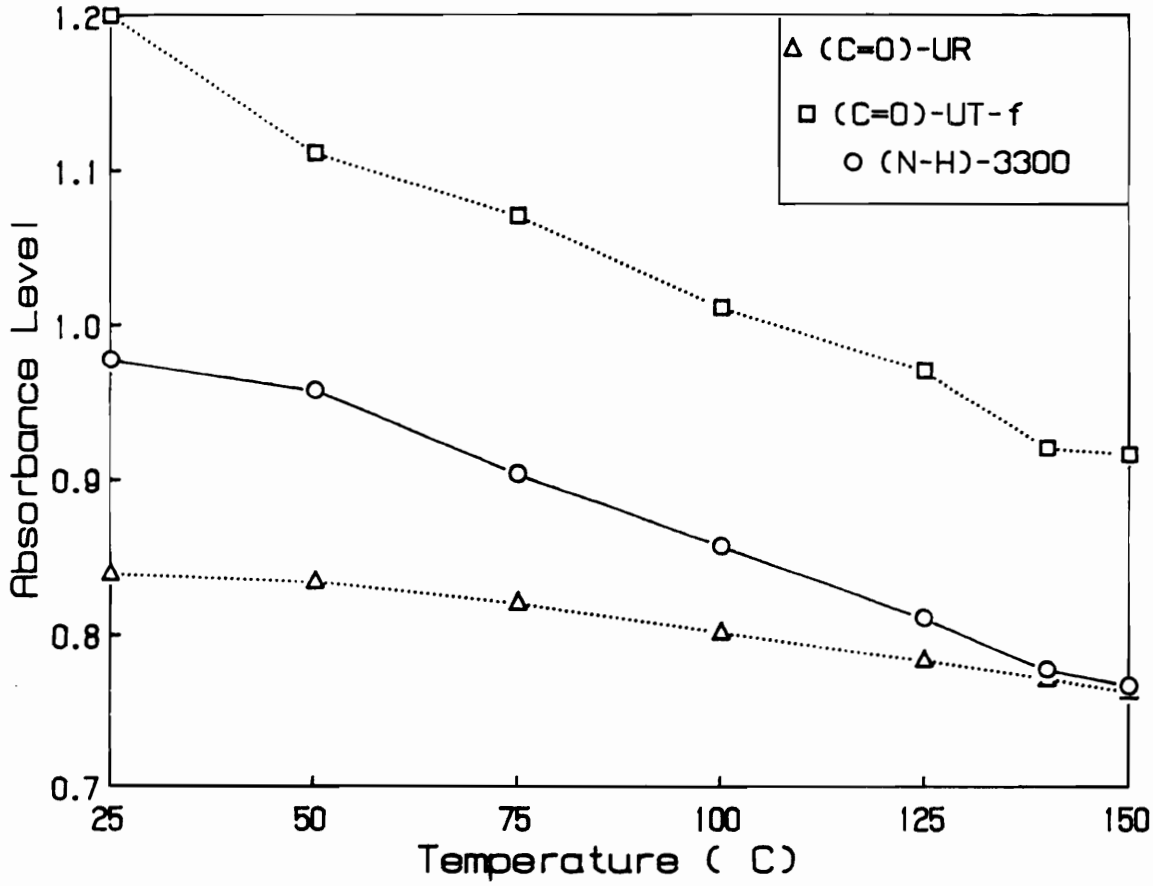

Figure 4.2. FTIR Thermal Behavior for P1: Data normalized by the absorbance of $\omega(CH_2)$

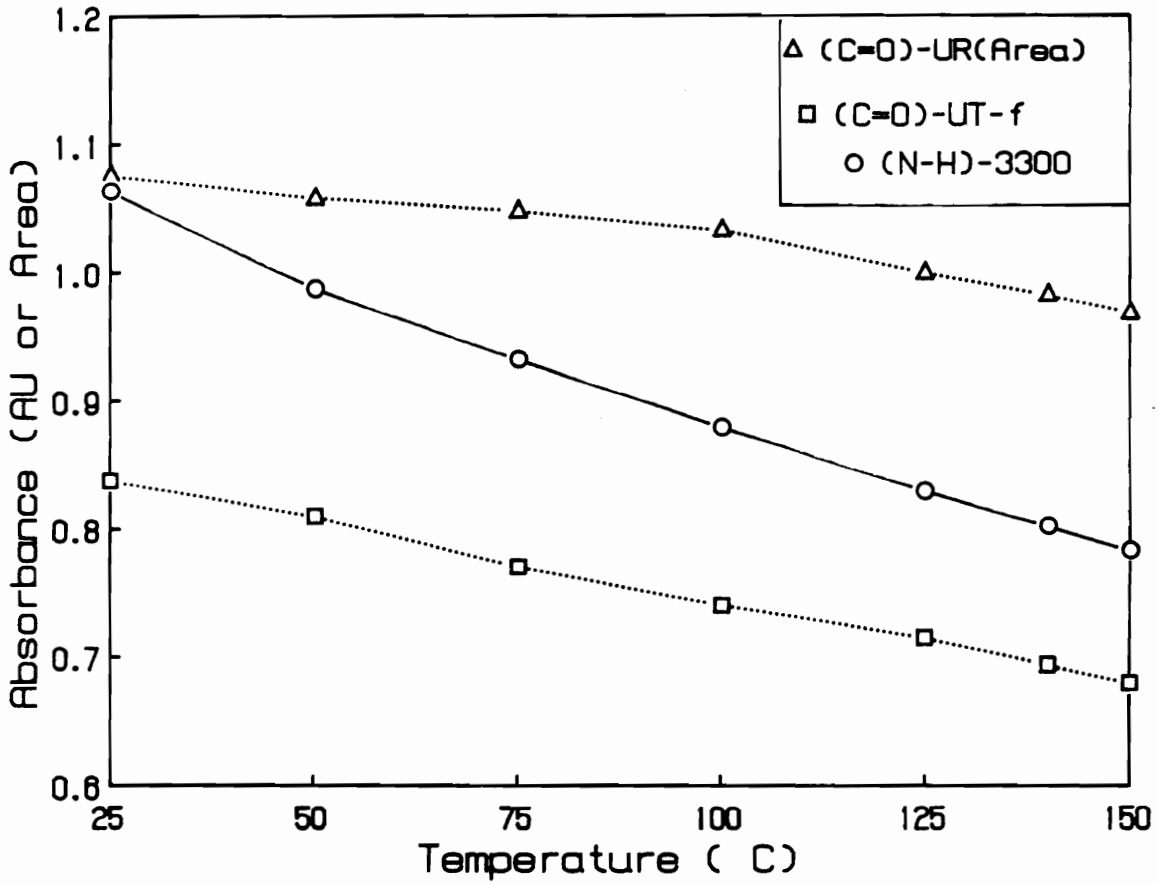

Figure 4.3. FTIR Thermal Behavior for P2: Data normalized by the absorbance of $\omega(CH_2)$

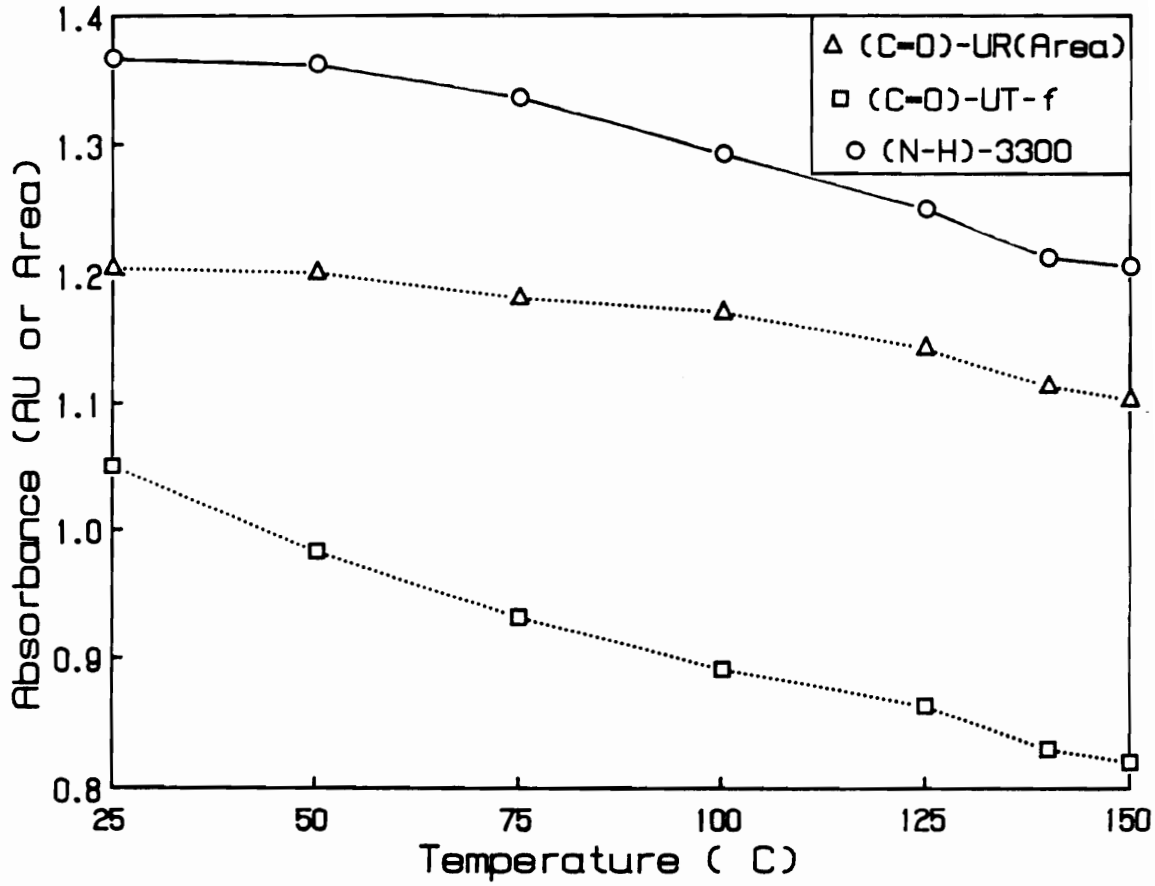

Figure 4.4. FTIR Thermal Behavior for P4: Data normalized by the absorbance of $\omega(CH_2)$

absorptivity coefficient for the hydrogen bonded $(N-H)_b$ group has been reported to change with increasing temperature which makes it difficult and impractical to compare the behavior for these two bands(86).

The decrease in the absorbance level for the the non-hydrogen bonded urethane carbonyl with increasing temperature in Figures 4.2-4.4 is surprising since reports in the literature on urethane elastomers show the exact opposite behavior for the $(C=O)_f$ group. Generally for urethane elastomers, an increase in the absorbance level for the $(C=O)_f$ group is observed along with a decrease in the hydrogen bonded urethane carbonyl absorbance; thus, indicating that hydrogen bonds are being disrupted with increasing temperature. In addressing the unusual behavior for the non-hydrogen bonded urethane carbonyl in Figures 4.2-4.4, further analysis of the data in the carbonyl region was performed by using spectral subtraction. This method involved subtracting the various spectra obtained above ambient by the spectrum obtained at 25°C. Before subtracting the spectra, they were zeroed and the high temperature spectra were normalized based on the ratio of the absorbance level for the $\omega(CH_2)$ band. An example of the data used for this process is shown in Figure 4.5, for the 2 spectra and the resulting difference spectrum. In looking at the two spectra which were subtracted, one will notice that the 125°C spectrum is much broader than the 25°C spectrum in the urethane carbonyl region. The broader spectrum at 125°C does explain why the peak intensity level in Figures 4.2-4.4 decreases with temperature. Also, this observation suggests a shift to higher frequencies(wavenumbers) for the absorbing groups in this region is taking place. In addition, this type of shift indicates a weakening of bonds within or to the urethane carbonyl groups in this region. As shown in Figure 4.5b, the shift to higher frequencies with increasing temperature is clearly seen by the negative absorption band at approximately $1745cm^{-1}$ in Figure 4.5b.

In further analyzing the urethane carbonyl region, the change in the peak intensities at approximately $1730cm^{-1}$ and $1745cm^{-1}$ as well as the shoulder intensity at $1715cm^{-1}$ have been measured from the difference spectra. The results for these intensities of the difference bands are given in Figures 4.6 and 4.7 for plaques P1 and P4, respectively. As shown for both plaques, there is an increase in the magnitude of all difference bands with increasing temperature. First, the difference band near $1715cm^{-1}$ is thought to give an indication of the disruption of hydrogen bonds

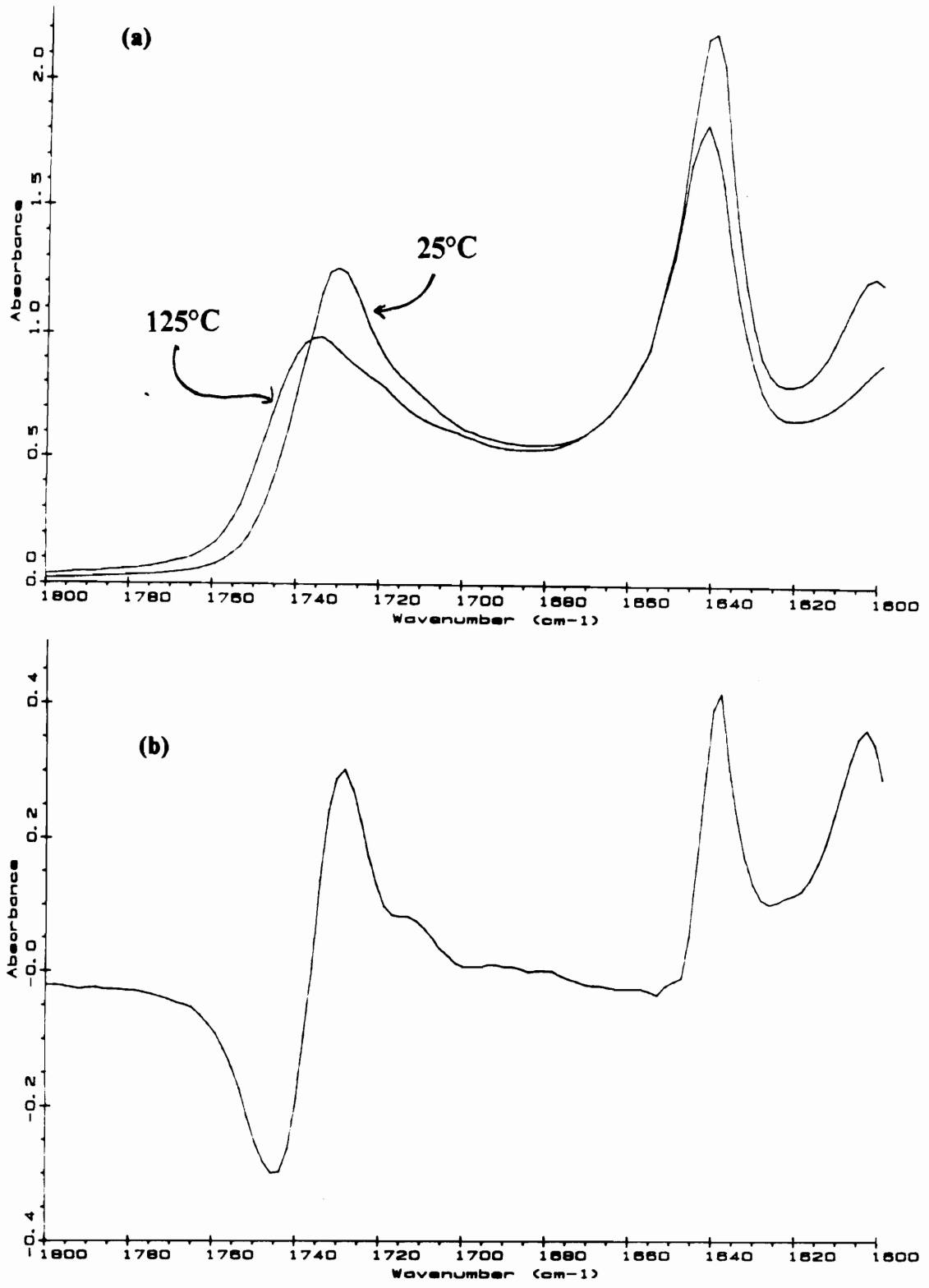

Figure 4.5. Spectral Subtraction for the Urethane Carbonyl Region of Plaque P1: (a) IR Spectra obtained at 25°C and 125°C and (b) Difference Spectrum

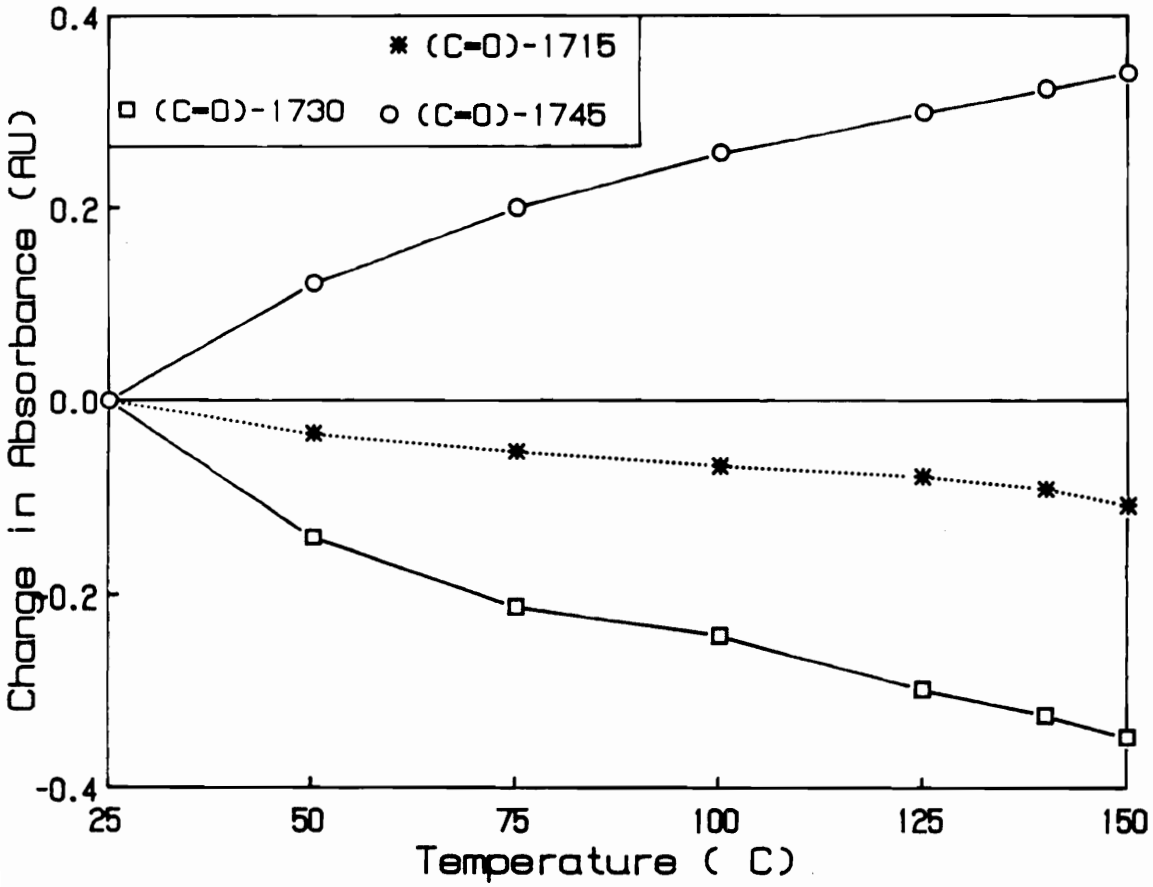

Figure 4.6. FTIR Thermal Behavior from Spectral Subtraction for Plaque P1

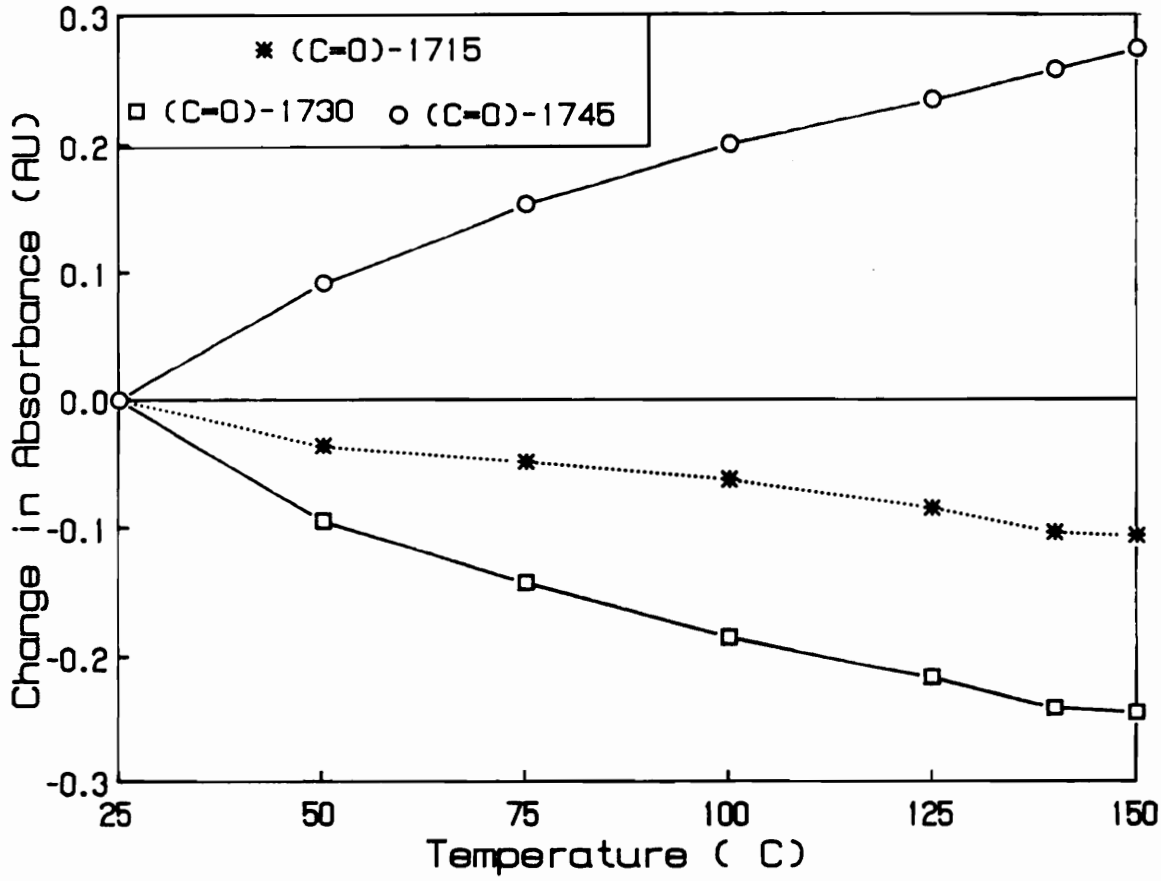

Figure 4.7. FTIR Thermal Behavior from Spectral Subtraction for Plaque P4

to the urethane carbonyl. As reported in the literature for TDI based urethanes as well as urea-urethanes, the hydrogen bonded carbonyl for 2,6 TDI is near $1700cm^{-1}$ and that of 2,4 is thought to be near $1720cm^{-1}$(78-79). However, another possible contribution at $1715cm^{-1}$ is "free urea"(non-hydrogen bonded urea) which has been reported by investigators of flexible polyurethane foams(10-11,14,87). It is likely that "free urea" is being formed as shown by the loss in the absorbance level of the $(C=O)_{ur}$ band in Figure 4.2-4.4 which in turn would add a negative contribution to the difference band at $1715cm^{-1}$ with increasing temperature. In fact, through personal communication it has been learned that there can be as much as a 15 to 25 percent increase in the "free urea" at $1715cm^{-1}$ in flexible polyurethane foams over a temperature range from 25°C to 150°C(87). Thus, the change observed in Figures 4.5 and 4.6 does indicate that there is an increase in the disruption of hydrogen bonds with increasing temperature, but to what extent is not known due to the possible band overlap by the "free urea" groups.

The difference bands shown in Figures 4.6-4.7 at $1730cm^{-1}$ and $1745cm^{-1}$ are reportedly in the range for non-hydrogen bonded carbonyl urethane bands The change in the absorbance levels for these bands is rather symmetrical for both plaques and slightly more symmetrical in the case for P1. This observation suggests that the loss in the absorbance near $1730cm^{-1}$ is likely shifted to the higher frequency of $1745cm^{-1}$. There are several factors which could cause this shift and broadening effect with increasing temperature. The most likely cause for the shift to higher frequencies as well as the broadening is a weakening of the free urethane carbonyl bonds. This factor is better known as the Doppler shift or broadening which results in a larger distribution of vibrational energies with increasing temperature. Another factor is that the disruption of hydrogen bonds to the urethane groups could also lead to a shift to higher frequencies. Also, a disruption in the structural ordering of the urethane carbonyls could contribute to a shift to a higher vibrational frequency. Such changes in ordering are thought to be related to additional phase mixing at or near the interface of the hard and soft segments and furthermore they are likely to occur at the higher temperatures.

One of the objectives of this study was to determine the difference in the thermal effects on the hydrogen bonding to the urethane and urea groups. However, due to difficulties in analyzing the data which were related mostly to resolving the different peaks in the urethane carbonyl region, this

objective can only be qualitatively addressed. As discussed above and exhibited in Figures 4.6-4.7, increasing temperature does disrupt the hydrogen bonding and is believed to cause a weakening of the bond strength in the urethane carbonyls. On the other hand, the thermal effects on the urea carbonyl appear only to lead to the disruption of hydrogen bonds. As shown in Figure 4.5, there is only a small shift in the 1640 cm^{-1} urea carbonyl band at 125°C in comparison to that of 25°C which, of course, indicates very little weakening in the bond strength of the urea carbonyl. Thus, from an overall standpoint the thermal effects on the two carbonyls does appear to be greater on the urethane groups. This observation has been confirmed by unpublished results obtained on similar materials to those of the plaques, but more importantly the FTIR-thermal studies were carried out on the foams instead of the plaques(87).

Further comments on the FTIR thermal analysis are necessary upon comparing the behavior between the plaques. As shown in Figure 4.8, the behavior for the change in urea carbonyl absorbance does not change that much with increasing hard segment content or in other words from P1 to P4. This does, however, indicate that the amount of hydrogen bonds disrupted does increase with increasing hard segment content since there are more urea groups in P4 than in P1 and P2. Overall, the amount of hydrogen bond disruption that takes place involving the urea carbonyl is not that particularly significant for all of the plaques.

Predictions for the relative change in the urethane carbonyl group with increasing temperature have also been made for the three plaques by utilizing the peak heights from the 1730cm^{-1} difference bands (values given in Figures 4.6 and 4.7). The results for these predictions were normalized by the absorbance level of the $\omega(CH_2)$ at 25°C for the respective plaques. As shown in Figure 4.9, the relative change is the greatest for P1 in comparison to P2 and P4; thus indicating that temperature has a more significant effect on the urethane carbonyls for plaque P1.

A comparison of the isocyanate absorbance levels for the three plaques is given in Figure 4.10. As shown, the isocyanate levels remain rather constant up to 100°C for all three plaques. As somewhat of a surprise, these levels begin to increase at 100°C and continue to increase quite rapidly with increasing temperature. Although the absorbance levels at 150°C are similar for all three plaques, the changes due to increasing temperature are more significant in P1 versus P2 and P4.

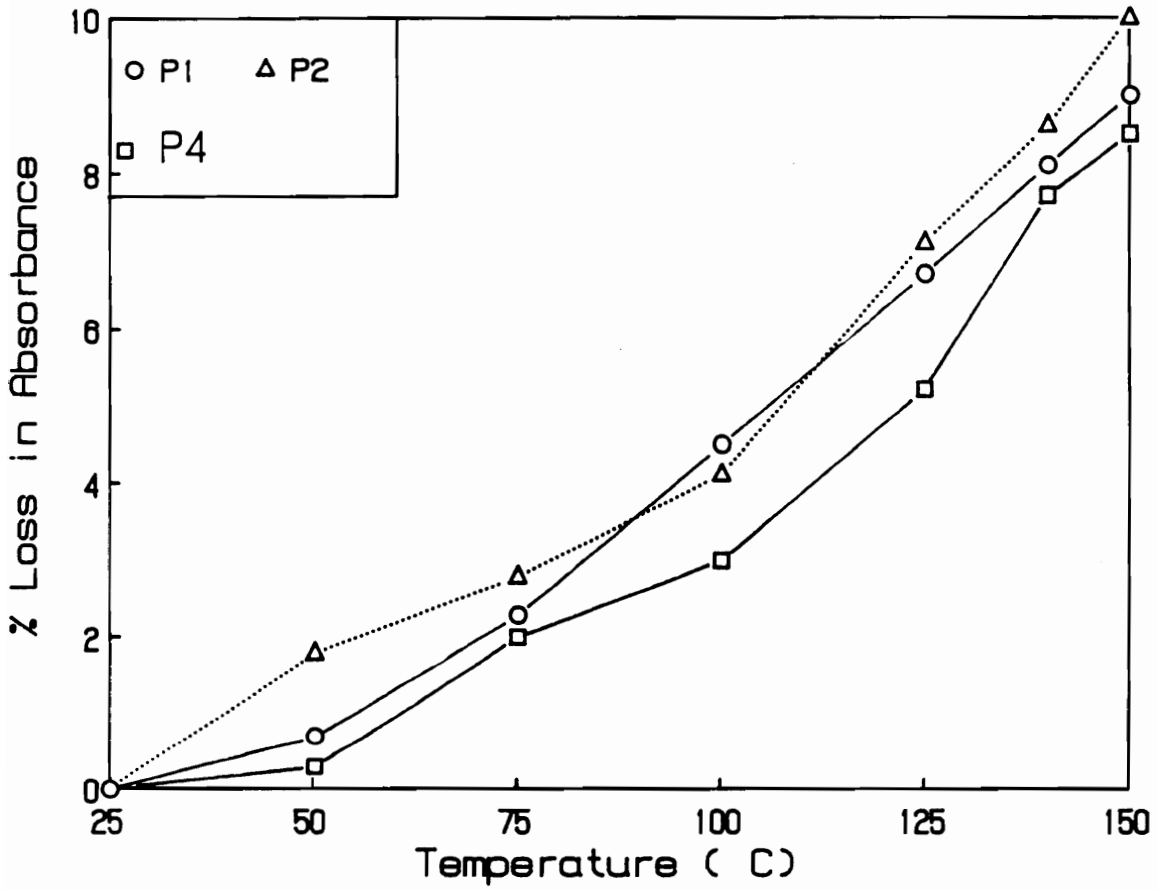

Figure 4.8. Summary of Thermal Effects on Urea Carbonyl for Plaque P1, P2, and P4:

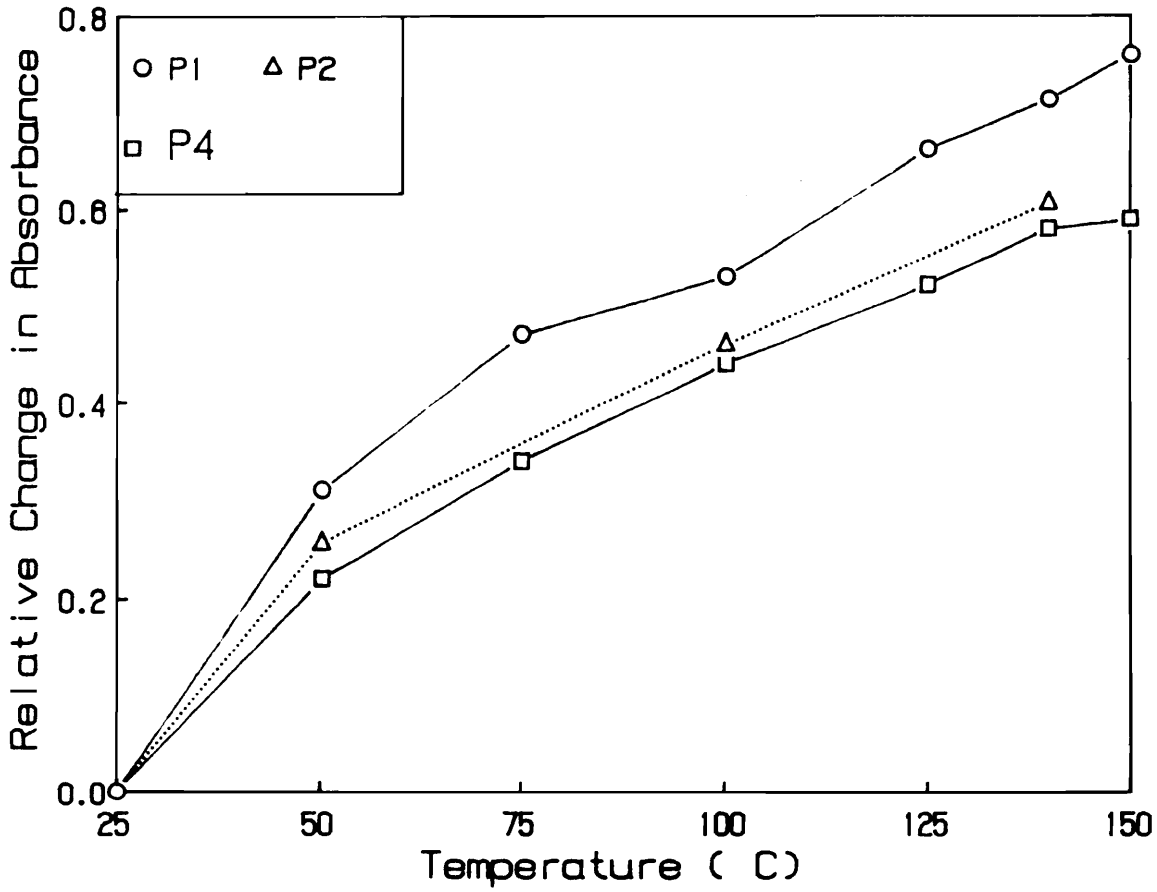

Figure 4.9. Summary of Thermal Effects on Urethane Carbonyl for Plaques P1, P2, and P4:

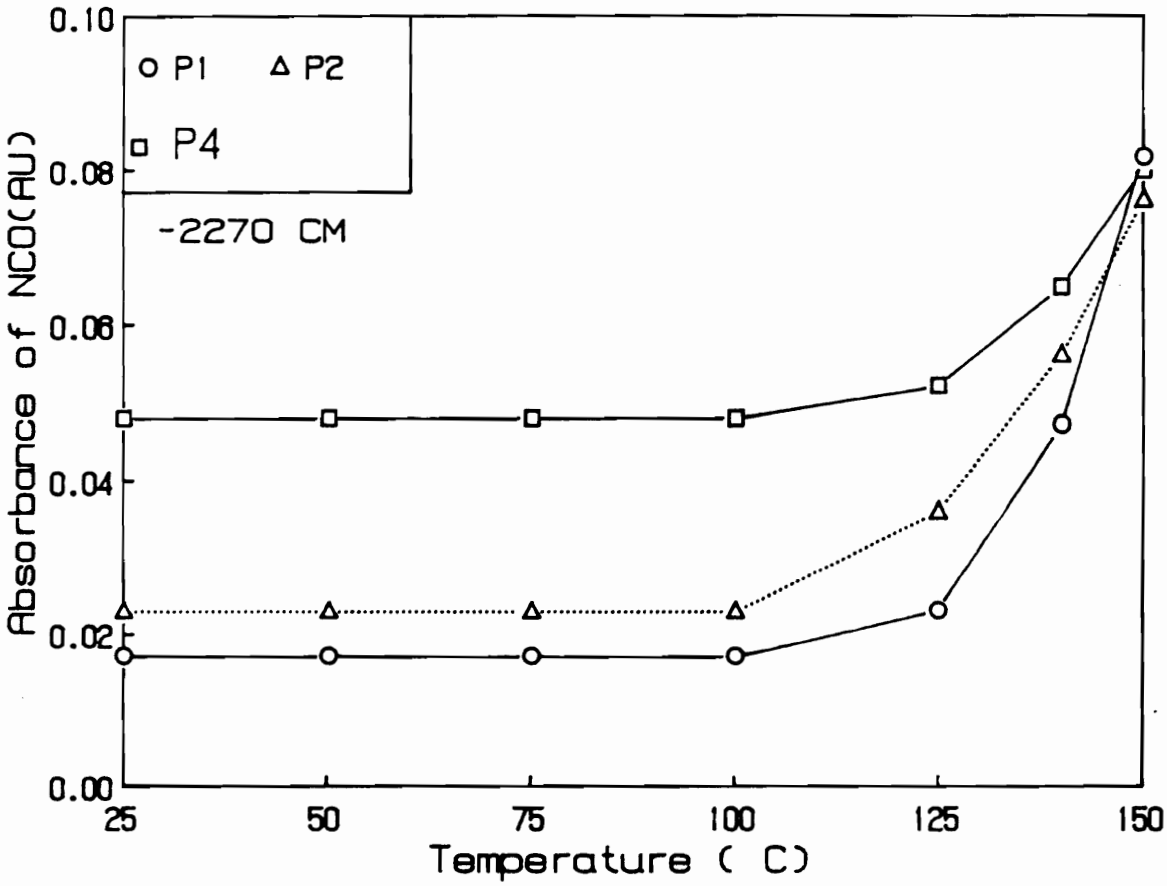

Figure 4.10. Thermal Evolution of Free Isocyanate for Plaques P1, P2, and P4:

For all three plaques, the observance of free isocyanate at the higher temperatures suggests that chain scission is taking place and to a greater extent in plaque P1. Based on results discussed above, this may suggests that the chain scission is occurring more so in the urethane linkages instead of the urea linkages. In contrast, others authors who have carried out similar studies on the flexible foams have suggested that the chain scission is taking place to a greater extent in the urea linkages(87). These authors have based their arguments on thermal studies performed on model urea compounds(from reports in the literature) which show signs of degradation at temperatures greater than 100°C. With this in mind, these authors believed that by increasing temperature the thermal stability of the hydrogen bonding to the urea groups is weakened; thus allowing for some of the urea groups to undergo chain scission(87). This speculation does seem to be in agreement with the lower hard segment plaque, P1, having a greater change in its free isocyanate band. That is, plaque P1 and likewise foam F1 are believed to have a lower structural order and less hydrogen bonding to the urea based hard segments in comparison to the other plaques of foams F2-F4. While, the above hypothesis does seem to account for free isocyanate evolution, there is still the question of which linkage is involved in promoting this evolution to a greater extent. For now, based on the results shown in this chapter and the information provided from outside sources, it is assumed that both of the linkages are being degraded at temperatures greater than 100°C(87).

4.1.2 Thermal Analysis of PUU Elastomer

A summary of some of the results obtained from the FTIR thermal analysis of the PUU elastomer are shown for the $(N-H)_b$, and the $(C=O)_{ur}$ and the $(C=O)_f$ bands in Figure 4.11. Basically a decrease is observed with increasing temperature for these three bands. In the case of the $N-H$ and the $(C=O)_{ur}$ it indicates an increase in the disruption of hydrogen bonds and/or weakening of the hydrogen bonding in the case of the $(N-H)_b$ groups with increasing temperature. Although, the behavior for the $(N-H)_b$ and $(C=O)_{ur}$ do look similar, the actual change is greater for the $(N-H)_b$ band. As explained earlier, due to the change in the extinction coefficient of the

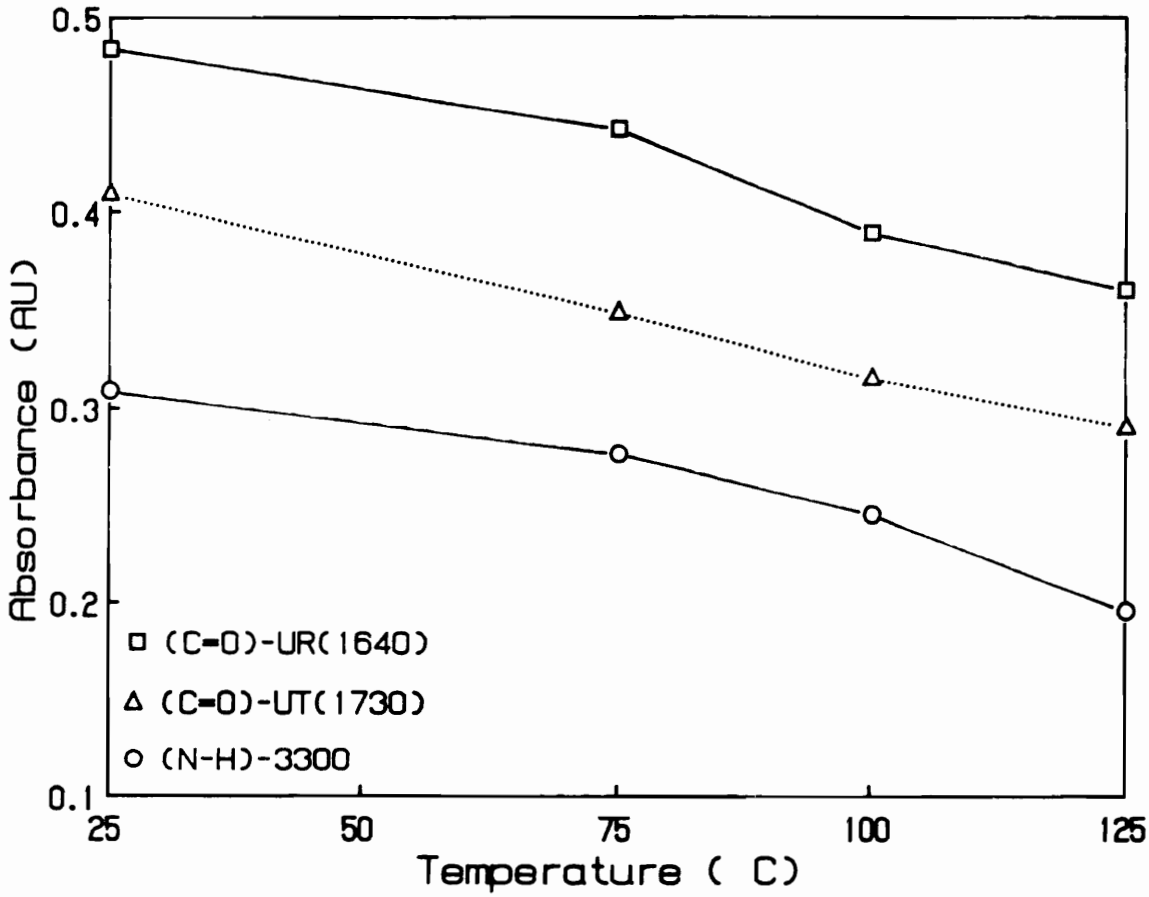

Figure 4.11. FTIR Thermal Behavior for the PUU Elastomer: Absorbance levels were normalized on $\omega(CH_2)$

$(N-H)_b$ group with increasing temperature, this band is not believed to be reliable for determining the extent of disruption of hydrogen bonds as well as the difference in this disruption between the urethane and urea linkages. Thus, the evaluation of the effects of temperature on the PUU elastomer are concentrated on the urea and urethane carbonyl regions.

Like the plaques, the decrease in the peak height absorbance level for the free urethane carbonyl with increasing temperature is believed to be related to the shift and broadening effect that occurs in the urethane carbonyl region. Similar behavior to that shown earlier in Figure 4.5a has also been observed for the PUU elastomer upon comparing the urethane carbonyl region from a high temperature spectrum to one obtained at ambient conditions. Thus, spectral subtraction was utilized to obtain a better understanding of the thermal effects within this region. The results of the peak intensity for the difference bands at $1715cm^{-1}$, $1730cm^{-1}$ and $1745cm^{-1}$ are given in Figure 4.12. As shown, there is a decrease in the absorbance level for the $1715cm^{-1}$ difference band with increasing temperature. As discussed earlier, this band or region of the spectrum is believed to have two main contributions, i.e. the hydrogen bonded carbonyl and the "free urea". It does appear that this contribution is greater for the loss in the hydrogen bonding to the urethane linkage. However, as also stated earlier, the actual extent of this loss cannot be determined due to band overlap.

Figure 4.12 shows rather symmetrical behavior for the absorbance change in the $1730cm^{-1}$ and $1745cm^{-1}$ difference bands, but the absolute change is somewhat greater for the $1730cm^{-1}$ band. Similar but more symmetrical behavior was shown earlier for these same difference bands in Figures 4.6 and 4.7 for plaques P1 and P4, respectively. Thus, some of the same factors, i.e. weakening of urethane carbonyl bonds and disruption of hydrogen bonds, that were mentioned earlier are also thought to bring about the loss in the absorbance in the $1730cm^{-1}$ difference band and the shift to higher frequencies near $1745cm^{-1}$. One additional factor that was not mentioned earlier is the absorptivity coefficient for the hydrogen bonded carbonyl are reportedly greater by a factor of 1.3 to 1.4 than that for the free urethane carbonyl(87). This difference might help explain why there is greater loss in the $1730cm^{-1}$ band in comparison to the gain for the $1745cm^{-1}$(see Figure 4.12).

As in the case of the plaques, a quantitative comparison for the PUU elastomer could not be made between the changes in the urethane and urea carbonyl groups- in particularly the hydrogen

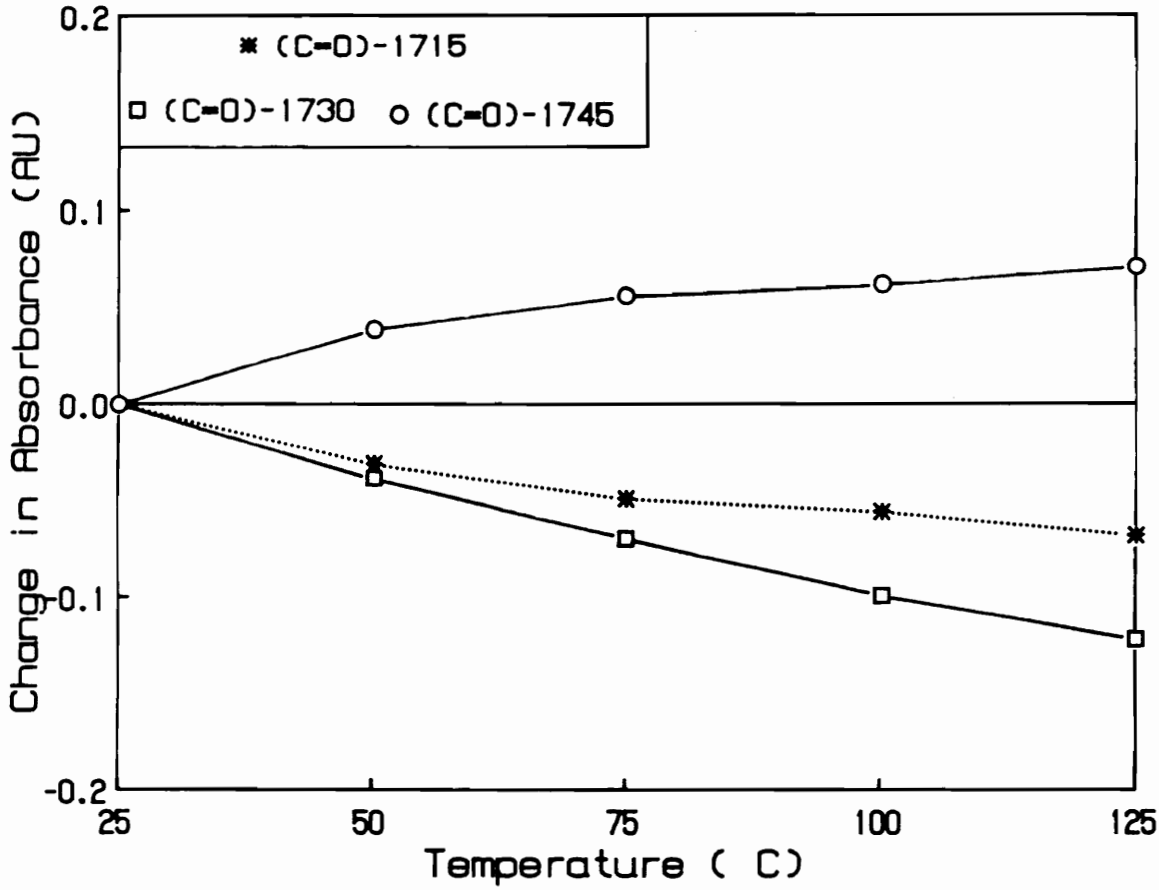

Figure 4.12. FTIR Thermal Behavior from Spectral Subtraction for the PUU Elastomer

bond disruption. However, from a qualitative point of view it does appear that the temperature does have a greater overall effect on the urethane carbonyl versus the urea carbonyl. This observation is based on fact that there appears to be a loss in hydrogen bonding as well as weakening of bonds in the urethane carbonyl region whereas the hydrogen bonding of the urea only appears to be affected significantly.

The structural changes that are taking place with increasing temperature in the PUU elastomer do seem to be greater than that of the plaques. For example, the percent change in the urea carbonyl absorbance is 22 percent at 125°C whereas for the plaques it ranges from 7 to 10 percent. In addition, on a relative basis the thermal effects appear to be greater on the urethane carbonyl region for the PUU elastomer than that of the plaques. Also, while the behavior of the evolution of free isocyanate with increasing temperature is similar between the PUU elastomer and the plaques, the percent increase at temperatures greater than 100°C is more significant. At 115°C, an increase of 150 percent in the free isocyanate has been observed for the PUU elastomer. On the other hand, this increase is on the order of 25 to 100 percent for the plaques at 125°C. Overall, these differences in behavior for the elastomer and the plaques are thought to be mostly related to the chemcial differences between these two materials. That is, the PUU elastomer contains a MOCA chain extender in its hard segment where as the plaques do not(recall Figure 2.6 for structure of MOCA). Another factor which may contribute to these thermal differences, is the presence of a covalent network in the plaques which is believed to provide some additional thermal stability.

4.2 Effects of Temperature on Segmental Orientation Behavior

Within this section, the effects of temperature on the orientation-elongation behavior and orientation-time behavior for plaque 2-DMF and the PUU elastomer are discussed. A few com-

ments are also made on the simultaneous stress relaxation behavior obtained with orientation time evaluation. However, these comments will be limited since in the following chapter in depth discussion is given on the viscoelastic behavior of flexible polyurethane foams. Before, discussing the results, a few reminders concerning the nomenclature and the significance of important chromophoric groups are given below.

The main chromophoric groups utilized were hydrogen bonded $(N-H)_b$, the hydrogen bonded urea carbonyl($(C=O)_{ur}$), and the non-hydrogen bonded carbonyl($(C=O)_f$). As discussed earlier in this chapter, the $\nu(N-H)$ group is contained in both the urea and urethane groups, but is mostly contained within the urea group. Thus, it is believed to principally characterize the orientation behavior of the (urea based)hard segments in both the smaller microdomains and the urea aggregates for plaque 2-DMF or the lamellar like domains in the case of the PUU elastomer. The $(C=O)_{ur}$, on the other hand, does fully represent the hard segment orientation behavior. However, since it is a strong absorbing group its behavior was not evaluated for plaque 2-DMF due to very high absorbance levels. The $(C=O)_f$ group is at the interface of the hard and soft segments and is believed to be mostly representative of the soft segment orientation behavior since it is a non-hydrogen bonding group. As a reminder, the reader is referred to the experimental section for the data analysis performed in obtaining the orientation values as well as preparation of the thin films utilized to measure the orientation behavior. Also, recall that this study is a continuation of earlier work which was summarized in the literature review; thus, the focus of the following discussion is on the effects of temperature on the orientation behavior and not on re-explaining the orientation behavior.

4.2.1 Orientation-Elongation Behavior

The orientation-elongation behavior at three different temperatures is presented in Figure 4.13 for plaque 2-DMF for the $\nu(N-H)$ and the $(C=O)_f$ bands. As shown in Figure 4.13, the general trend of the results at the three different temperatures is the same for the $(N-H)_b$ and $(C=O)_f$

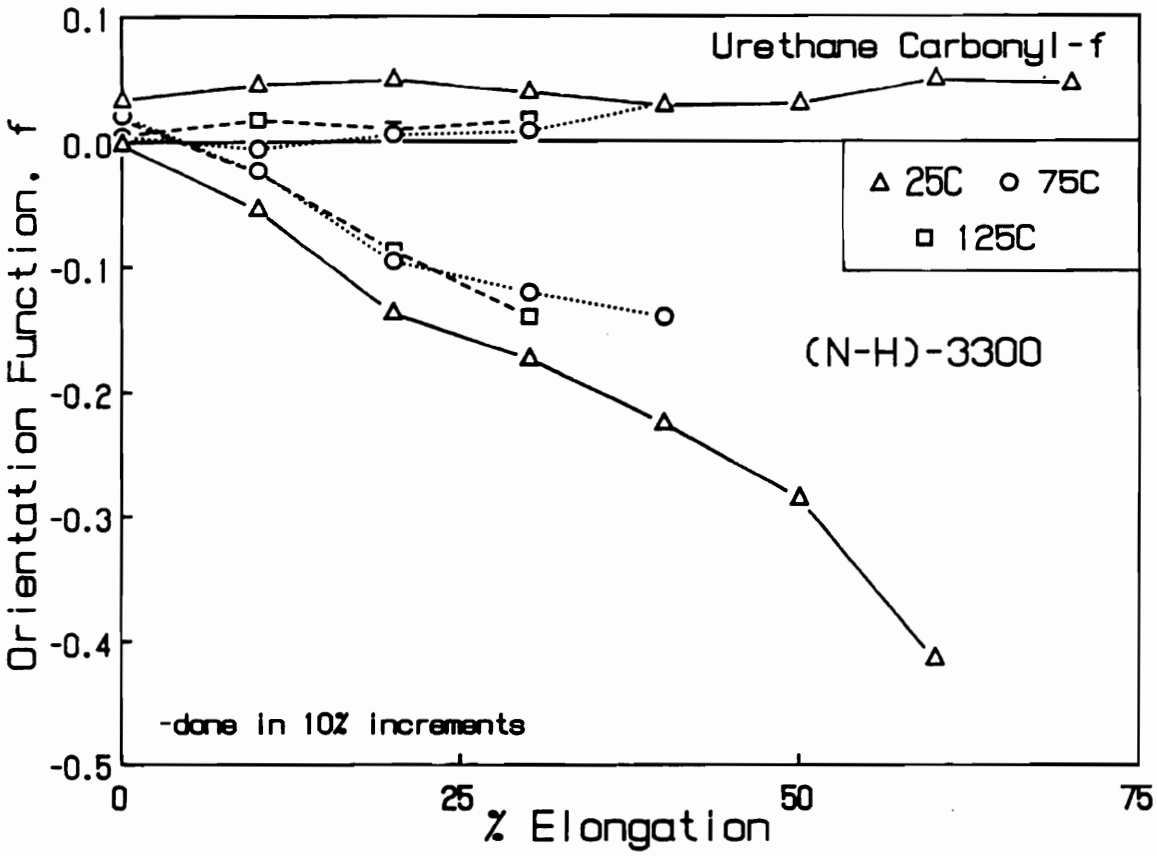

Figure 4.13. Variable Temperature Orientation-Elongation Behavior for Plaque 2-DMF: Extension rate equal to 400%/min

groups. In the case of the $(C=O)_f$ orientation behavior, there appears to be very little effect of increasing temperature on its orientation level as denoted by the Herman's orientation function, *f*. On the other hand, the hard segment orientation behavior does appear to increase or approach a somewhat more random state up to 75°C. However, in increasing the temperature from 75°C to 125°C there appears to very little difference in the results.

As a whole, the changes in the results with increasing temperature for plaque 2- DMF *at similar elongation levels* appear to be rather consistent with those shown for the PUU elastomer in Figure 4.14. For the PUU elastomer, there does seem to be little change in the orientation behavior with increasing temperature for the $(C=O)_f$ group. On the other hand at an 80 percent elongation, there is an approach towards a more random oriented state for the hard segment orientation behavior up to 75°C. However, at 100°C, the orientation level at 80 percent elongation is at a higher orientation state than at 75°C.

Based on both sets of results given above, some general observations and conclusions can be made about the effect of temperature on the orientation behavior as well as possible relation to structural changes that may be occurring. First, temperature does not appear to have a significant effect on the orientation-elongation behavior for temperatures ranging from 25°C to 125°C for both plaque 2-DMF and the PUU elastomer. This conclusion was unexpected, especially for the hard segment orientation behavior at temperatures greater than 100°C. With regards to the structural organization in plaque 2-DMF and the PUU elastomer, it does indicate that the different types of hard domains in these materials are not disrupted to a great extent. The FTIR-thermal analysis of the plaques and the PUU elastomer also support this conclusion by indicating only small amounts of disruption in the hydrogen bonding to the urea carbonyl. Before adding to this discussion, other results for the orientation time behavior are shown below.

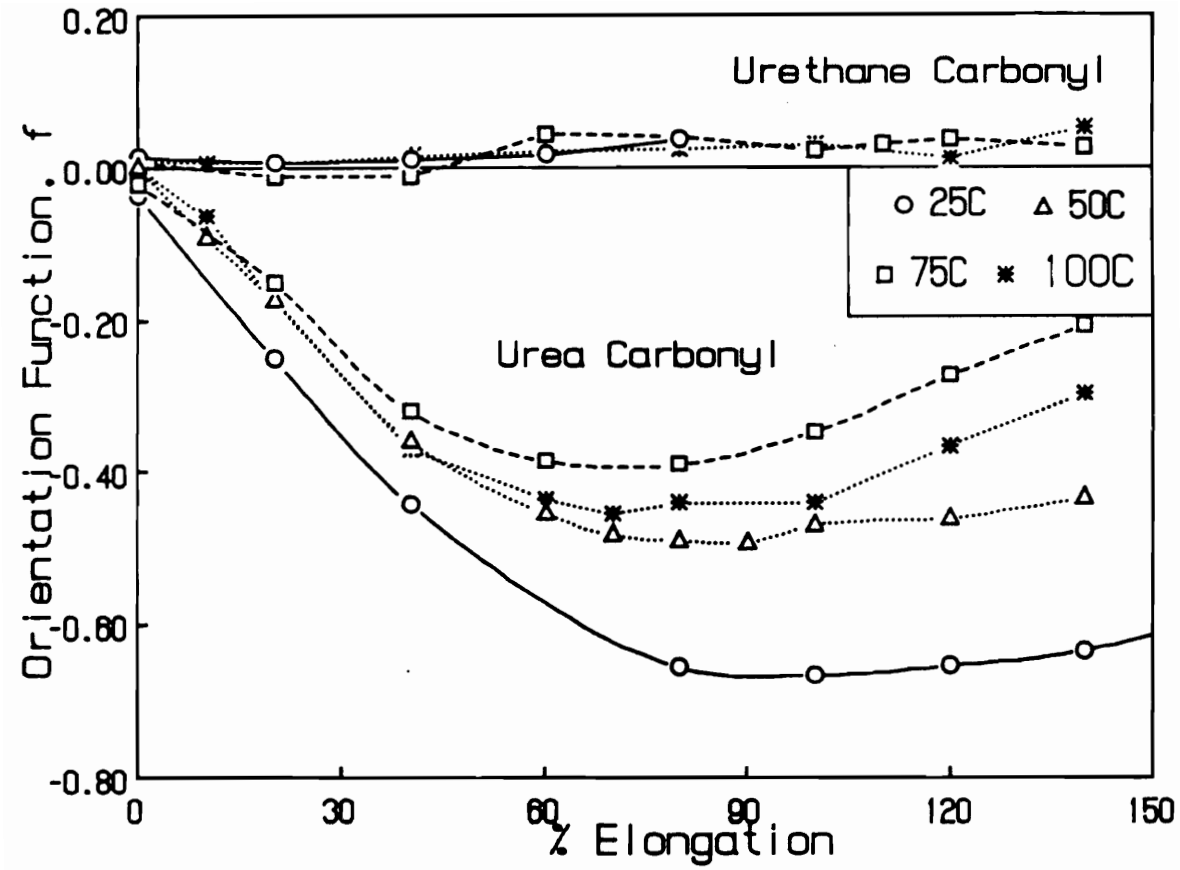

Figure 4.14. Variable Temperature Orientation-Elongation Behavior for the PUU Elastomer: Extension rate equal to 400%/min

4.2.2 Orientation-Time Behavior

The hard segment orientation-time behavior at ambient conditions for a 30 percent strain level and at 125°C for a 25 percent strain level is shown in Figure 4.15a. The simultaneous stress relaxation behavior at the two conditions is displayed in Figure 4.15b. As exhibited in Figure 4.15a, the orientation changes over time in the hard segment are not major for either condition. However, in comparing the behavior at the two conditions, there clearly appears to be a greater trend towards a more transversely oriented state at 125°C due to a steady, but small, decrease in the orientation function with time. This difference in the hard segment orientation behavior does correspond to the greater amount of relaxation observed at 125°C in comparison to that at 25°C(see Figure 4.15b). Although, one would expect to see greater changes over time in the hard segment orientation level due to the significant increase in the amount of stress relaxation from 25°C to 125°C. Thus, it appears that re-orientation of the hard segments or its domains is not a major factor leading to this increase in the stress relaxation at 125°C. On the other hand, the rather small orientation change at 125°C does indicate that the hard domains are not disrupted over long time periods.

An additional relaxation experiment was carried out on plaque 2-DMF, in order to evaluate the orientation level at 25 percent elongation while increasing the temperature periodically from 25°C up to 140°C. The thermal dependence of the average orientation function along with the stress relaxation response is shown in Figure 4.16. First, there is a small, but noticeable, decrease in the orientation level for the $(C=O)_f$ band with increasing temperature. As shown in Figure 4.16a, there is also a small increase in the hard segment orientation level up to 100°C which is believed to be within experimental error and then a drop in this orientation level thereafter. In looking at the simultaneous stress relaxation response in Figure 4.16b, one will notice that the more significant changes do occur at the higher temperatures which do again correspond with the orientation behavior exhibited in Figure 4.16a. As discussed in the previous paragraph, the changes in the orientation level seem small in comparison to the changes in the stress relaxation behavior. However,

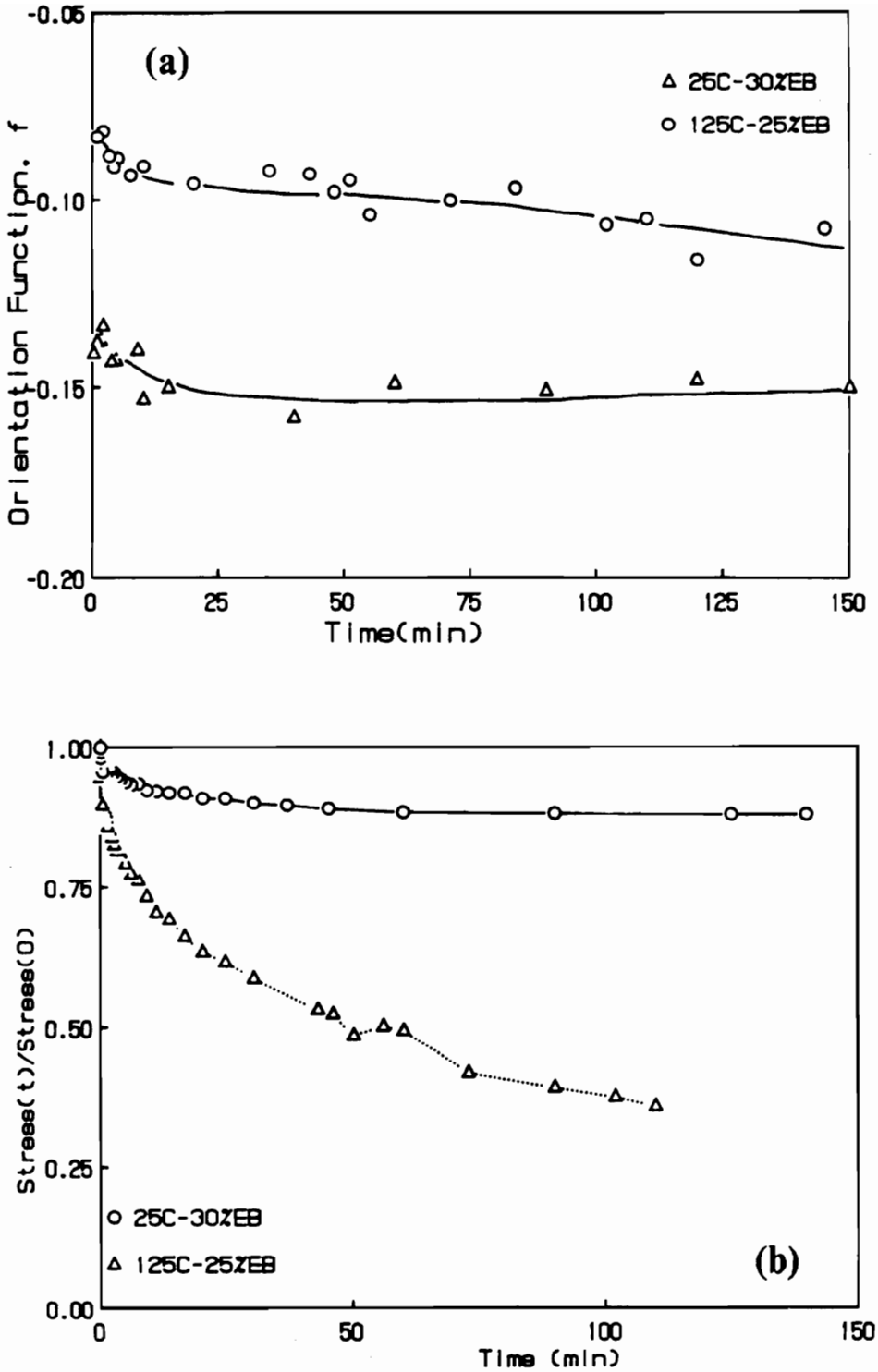

Figure 4.15. Variable Temperature (a)Orientation-Time Behavior with (b)Simultaneous Stress Relaxation Behavior for Plaque 2-DMF: Elongation level was 30% at 25°C and 25% at 125°C

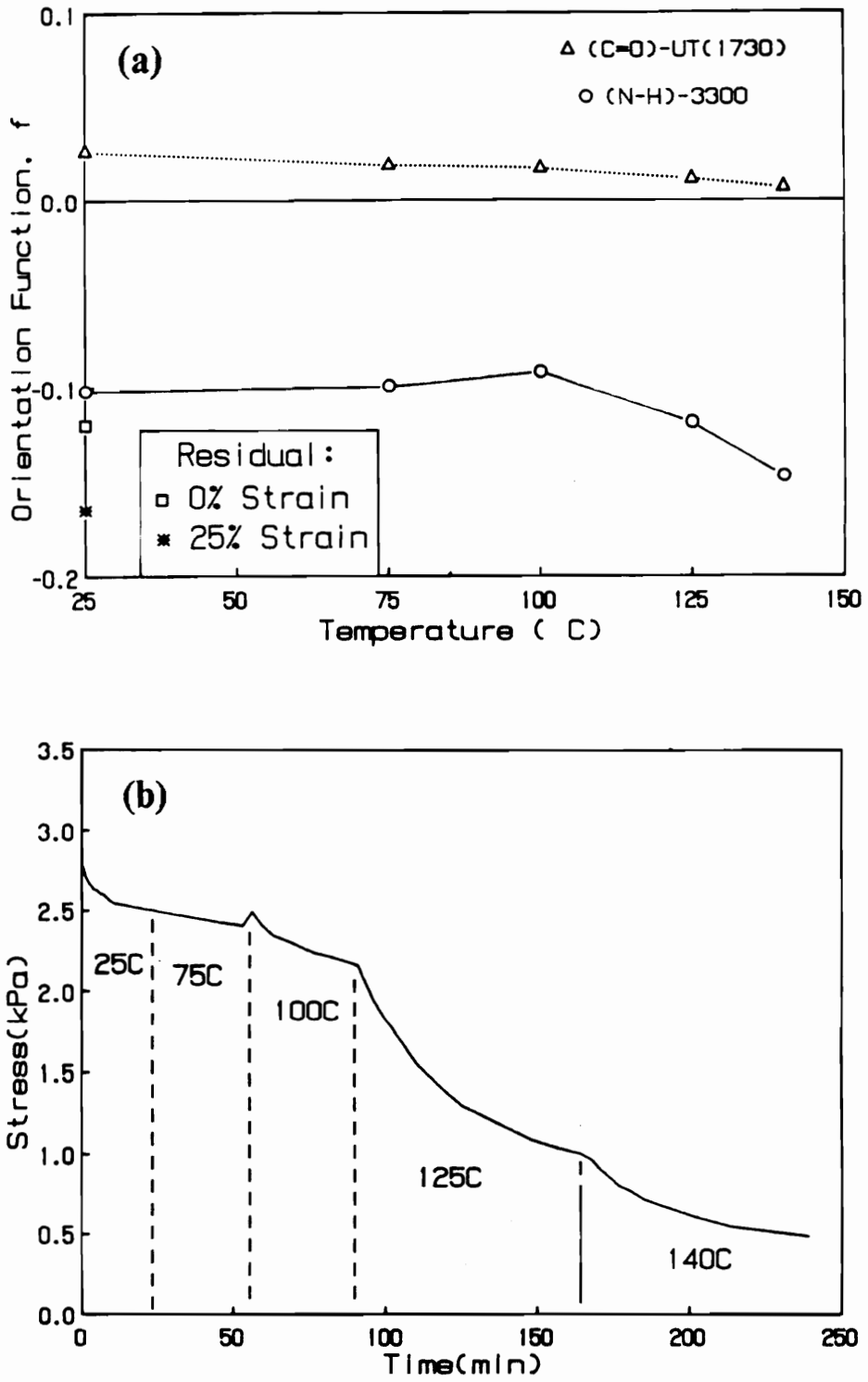

Figure 4.16. Variable Temperature (a)Orientation-Time Behavior with (b)Simultaneous Stress Relaxation Behavior for Plaque 2-DMF: Elongation level was 25% over entire temperature sweep; Residual orientation levels are also given and commented on in section 4.2.3

they are believed to be real and related to some of the thermal effects on the solid morphology mentioned earlier in this chapter - especially at the higher temperatures.

As discussed earlier, chain scission is believed to take place in both the urethane and urea linkages at temperatures greater than 100°C. Thus, it is possible, that the decrease observed in the hard segment orientation level at 125°C is caused by disruption of some of the urea linkages which are a part of the smaller microdomains that possess a lower structural order (Recall model in Figure 2.16). As explained earlier in the literature review, these smaller microdomains which contain only a few hard segments are likely to orient in the positive direction; therefore, some contribution to the positive orientation level is lost which will, of course, lead to more negative orientation as shown in Figure 4.16a at 125°C. The above speculation is also thought to address the gradual change in the hard segment orientation function over time at 125°C shown in Figure 4.15a.

Another possible explanation for the decrease in the hard segment orientation, is that the lamellar textured domains(microdomain and aggregates) may begin to orient more transversely at the higher temperatures. The mechanism for this decrease is thought to be a result of chain scission within the urea as well as the urethane linkages. As explained above the degradation in the urea linkages is thought to be more related to smaller hard domains and furthermore, but not mentioned above, to the "free" urea linkages. The urethane linkages that undergo chain scission are most likely connected to these same types of structures. In addition, there is also the possibility that some of the free urethane linkages that are linked to the large urea aggregate structures may be broken since they are at the interface of the soft and hard segments and are not as thermally stabile. With the above possible locations for chain scission in mind, it is speculated that a reduction in the localized strain on the lamellar textured domains in plaque 2-DMF is brought about at temperatures greater than 100°C. This reduction is not only thought to occur due to degradation at the interface of the hard and soft segments in the lamellar textured domains, but also as a result of neighboring structures undergoing chain scission. By reducing the localized strain on these larger domains, they are thought to be able to rotate and begin to orient more transverse to the stretch direction. This type of rotation will lead to more negative orientation as shown in Figures 4.15a and 4.16a.

Chain scission within the non-hydrogen bonded urethane linkages is also thought to promote the small decrease in the non-hydrogen bonded urethane orientation level(see Figure 4.16a) As mentioned above, the urethane linkages that are most susceptible to chain scission are likely those at the interface of the soft and hard segments which are not apart of the large lamellar like domains. These particular linkages do orient more in the positive direction than a free urethane linkage connected to a lamellar-like domain which is thought to orient transversely.

In Figure 4.17, the results for the orientation-time behavior at 115°C are shown for the PUU elastomer along with its mechanical response. As shown in Figure 4.17, there are some changes in the orientation level over time within the urethane linkage as well as the hard segments. However, these changes do appear to be rather insignificant in comparison to the large amount of stress relaxation that takes place (see Figure 4.17b). Once again, the orientation results for plaque 2-DMF and the PUU elastomer are comparable as exhibited by the hard segment orientation behavior in Figures 4.15a and 4.17a. As stated in the literature review, this further emphasizes that similar forces are governing the orientation changes with deformation as well as temperature in these materials; despite the fact that the plaques possess a covalent network morphology while the elastomer forms a linear segmented system.

4.2.3 Residual Hard Segment Orientation in Plaque 2-DMF

As discussed in the literature review, there is very little hysteresis observed in the hard segment orientation-elongation behavior at ambient conditions. This particular behavior has not been monitored at the higher temperatures, but the orientation state after completing some of the orientation-time studies has been evaluated. One of the results is shown in Figure 4.16a for which the hard segment orientation level was measured at a 25 percent strain after cooling the sample back to ambient conditions and after releasing the strain on the material at ambient conditions. Both of the results do indicate that there is a significant amount of residual orientation retained after testing at the higher temperatures. In addition, this orientation state has been maintained at the level shown

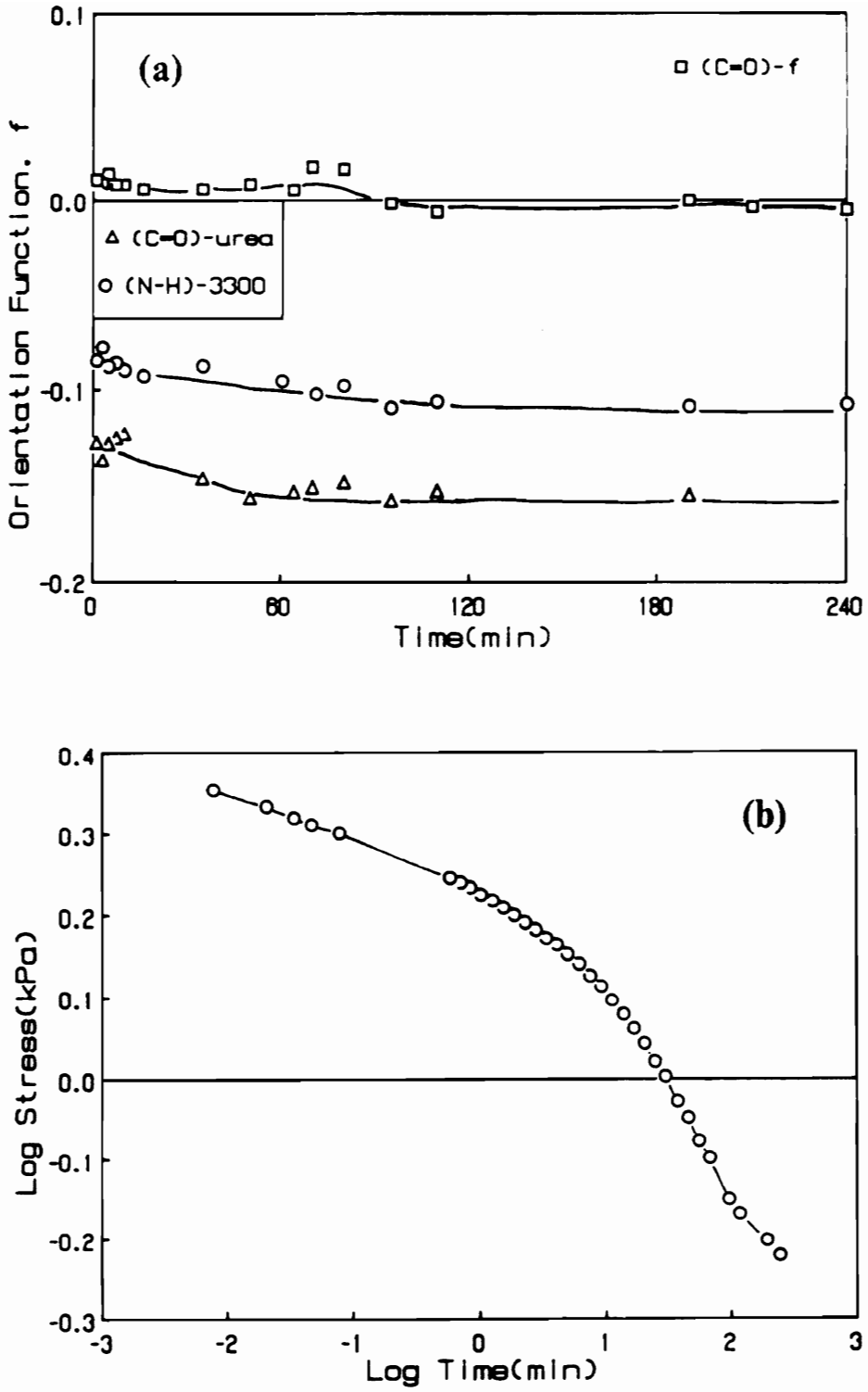

Figure 4.17. Variable Temperature (a)Orientation-Time Behavior with (b)Simultaneous Stress Relaxation for the PUU Elastomer

for no-strain state in Figure 4.16a. Also, similar residual orientation behavior has been observed after testing at 125°C. However, up to temperatures of 75°C, no significant amount of residual orientation has been observed(was not measured at 100°C). Thus, at the higher temperatures there appears to be some irreversible changes occurring in the hard segment orientation level which are believed to be mostly related to chain scission within the urea and urethane linkages.

4.3 Summary

In summary, for all three plaques(P1, P2, and P4), an increase in hydrogen bond disruption to the urea and urethane links with increasing temperature was indicated by the absorbance levels of the $(N-H)_b$ and $(C=O)_{ur}$ bands as well as the urethane difference band at $1715cm^{-1}$. From a qualitative standpoint, the effects of temperature for all three plaques were greater on the urethane carbonyl in comparison to the urea carbonyl. The percentage change in the hydrogen bond disruption to the urea carbonyl up to 150°C was on the order of 8 to 10 percent for the three plaques. The relative change in the urethane carbonyl group(difference band at $1730cm^{-1}$) with increasing temperature was greater for plaque P1 than P2 and P4. Based on the detection of free isocyanate band($2270cm^{-1}$) at temperatures greater than 100°C, chain scission was believed to be taking place in the urea and urethane linkages. The changes in the free isocyanate evolution with increasing temperature were more significant for P1 versus P2 and P4. Overall, the changes observed by the FTIR thermal analysis indicated that temperature has a greater effect on the lower hard segment content plaque, P1, in comparison to P2 and P4 - especially at temperatures greater than 100°C. This greater effect was attributed to the lower structural order as well as lower hydrogen bonding content in plaque P1 and likewise foam F1.

Similar results to those of the plaques were also obtained for the PUU elastomer. The changes which were observed in the PUU elastomer were greater than those of the plaques. This difference

was thought to be mostly related to the PUU elastomer containing the MOCA chain extender within its chemical structure while the plaques do not.

The effects of temperature(25-140°C) on the orientation behavior were not that significant for plaque 2-DMF as well as the PUU elastomer. The changes, but rather small, were most noticeable in the hard segment orientation-elongation and orientation-time behavior. For instance, up to temperatures of 75°C a somewhat more randomly oriented state was observed for the hard segment orientation-elongation behavior of both plaque 2-DMF and the PUU elastotmer. At temperatures greater than 100°C, plaque 2-DMF and the PUU elastomer exhibited signs of small changes to a more transversely oriented state over time for the hard segments. Overall, the rather small changes observed for the hard segment orientation behavior at the higher temperatures indicated that the hard domains(microdomain and urea aggregates) were not disrupted to any great extent. A significant amount of residual orientation was observed for the hard segments of plaque 2-DMF at temperatures greater than 100°C. These changes were thought to be related to the degradation of the urethane and urea linkages.

In short, the results shown in this chapter do indicate that temperature does alter the morphology and more than likely causes degradation in some of the chemical links - mainly those of urea and urethane. These changes do appear to be most significant at temperatures greater than 100°C. In the next chapter on the viscoelastic behavior of flexible slabstock foams F1-F4, the importance of the results shown here will become evident.

Chapter V

5.0 Viscoelastic Behavior

The viscoelastic behavior of flexible polyurethane foams is of importance due to its relation to the recoverability in the foam's shape and strength as well as influencing deformation response. With the objective of obtaining a better understanding of this behavior, tests in both the tension and compression modes of deformation have been carried out on a series of flexible foams which systematically increase in hard segment content and are designated F1-F4, respectively. The hard segment content along with other important variables for these foams are given in Table 5.1. The viscoelastic tests which were carried out under controlled conditions(temperature and/or relative humidity) were tensile stress relaxation, compression load relaxation and compression creep. The results and discussion on the viscoelastic behavior of foams F1-F4 and the compression molded plaques of these foams are now presented.

Table 5.1: Materials for Viscoelastic Tests

Foam\ Plaque	pph H_2O	pph TDI	Density (lb/ft^3)	wt% HS
F1	2	30.79	2.85	21.1
F2	3	41.43	1.92	25.8
F3	4	52.06	1.43	30.1
F4	5	62.70	1.24	33.8
P1	2	30.79	-	21.1
P4	5	62.70	-	33.8

- Plaques were compression molded at 204°C for 10 minutes

5.1 Tensile Stress Relaxation

When testing flexible polyurethane foams, the tests are often carried out in the compression mode since these materials are generally utilized in this manner. However, in order to give additional understanding to the viscoelastic nature of flexible foams and in particular, better probe the response of the cellular wall material(struts), the stress relaxation in tension has also been evaluated. In addition, it allows direct comparison to the compression molded plaques of the foams (which cannot be easily measured in compression) as well as to the orientation studies on the plaques. As mentioned earlier in the literature review, previous work on the same series of materials given in Table 5.1 suggested that the cellular wall material is governing the viscoelastic decay in tension(22). This conclusion was based on the similar relaxation behavior observed upon deforming the foam samples parallel and perpendicular to the blow direction; thus, indicating that the anisotropic cellular textures do not significantly influence the rate of stress relaxation in tension. Therefore, the results presented in this section on the tensile stress relaxation for foams F1-F4 were obtained by only stretching the foams parallel to the blow direction. Within this section, the effect of temperature on the stress relaxation behavior for foams F1-F4, compression plaques P1 and P4, and the chemically similar PUU elastomer are presented. In addition the effect of relative humidity on the viscoelastic behavior for foams F1 and F4 is also given.

5.1.1 Variable Temperature Relaxation Behavior for Foams F1-F4

The stress relaxation results presented in this first part have been obtained at a constant strain level of 25 percent and under controlled temperature conditions, but not relative humidity. The relative humidity was not controlled due to the sample chamber that was utilized. During these tests, the relative humidity at temperatures near 25°C was 50% to 60% and decreased as the tem-

perature was increased. As will be discussed later in section 5.1.5, the influence of relative humudity will be addressed in conjunction with temperature.

The stress relaxation behavior over a three hour time period for foam F1 at 25, 75 and 125°C is shown in Figure 5.1. At 25°C and 75°C about 80 percent of the relaxation over 3 hours appears to occur in the first 10 minutes and then begins to approach an equilibrium value although true equilibrium is never reached. However, at 125°C the stress continues to decay over the three hour time period and does not appear to be approaching equilibrium on this same time scale. Before further discussing the results in Figure 5.1, the same stress relaxation curves are shown in a three-dimensional plot(Figure 5.2) in order to give a better overall perspective of how temperature effects the stress relaxation behavior for F1. The surface in Figure 5.2 was generated by applying a 3- dimensional grid conversion developed by Cohort Software to the stress-time data obtained at various temperatures in the range of 25 to 140°C(88). The irregularities in this surface which are most noticeable at 125°C(near 120 minutes and greater) are due to data averaging which at some temperatures caused the decay of the stress not to be as smooth over time; furthermore, these irregularities have been amplified to some extent by the formation of the 3-dimensional grid.

As shown in Figure 5.2, the initial and 3-hr stress levels go through a maximum with temperature at 100°C. The increase in the stress level up to 100°C is believed to be rather consistent with the theory of rubber elasticity which predicts an increase in the level of stress with temperature at "pseudo equilibrium" conditions. In confirming this hypothesis, "equilibrium" stress values were calculated from the three hour stress level at 25°C and compared to the values that were obtained experimentally. As displayed in Table 5.2, a small negative deviation from predictions obtained by rubber elasticity theory exists up to 100°C which is not surprising since true equilibrium is not manifested in the results. Furthermore and more importantly, classical theory is not expected to directly apply to these micro-phase separated systems, even though they do contain a covalent network structure through the glycerine extended propylene oxide soft segment. Thus, the small deviations from predictions are thought to be mostly related to disruption and reformation of secondary bonding which has been indicated by the FT-IR-thermal analysis discussed earlier - partic-

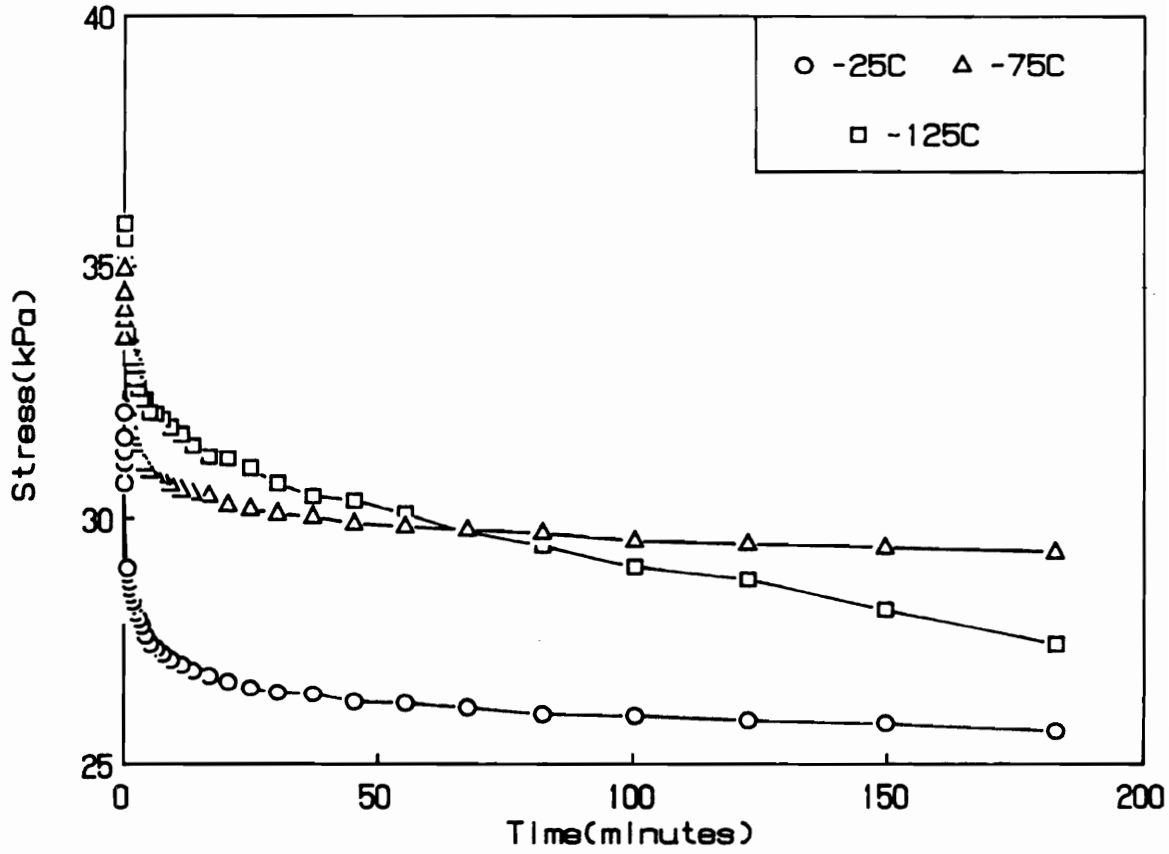

Figure 5.1. Variable Temperature Stress Relaxation Behavior for F1 at 25, 75 and 125°C: Performed at 25% strain level and stretched parallel to blow axis

Table 5.2: Summary of Variable Temperature Stress Relaxation Results for Foam F1

Temp(°C)	σ_o(kPa)	Slope(x-10²)*	% Stress Decay**	% Deviation***
25	32.1	2.2	20	-
50	34.6	1.8	17	0
75	35.0	1.7	16	-2
100	36.6	1.7	16	-4
125	35.8	2.3	23	-20
140	31.8	4.2	40	-45

* Correlation funtion was in the range of 0.995 to 0.999 except at 125°C and 140°C.
** The percent error in the % stress decay results varied from 1 to 5%.
***%Deviation from predictions given by rubber elasticity;
predictions based on the stress level at 25°C and 180 min.

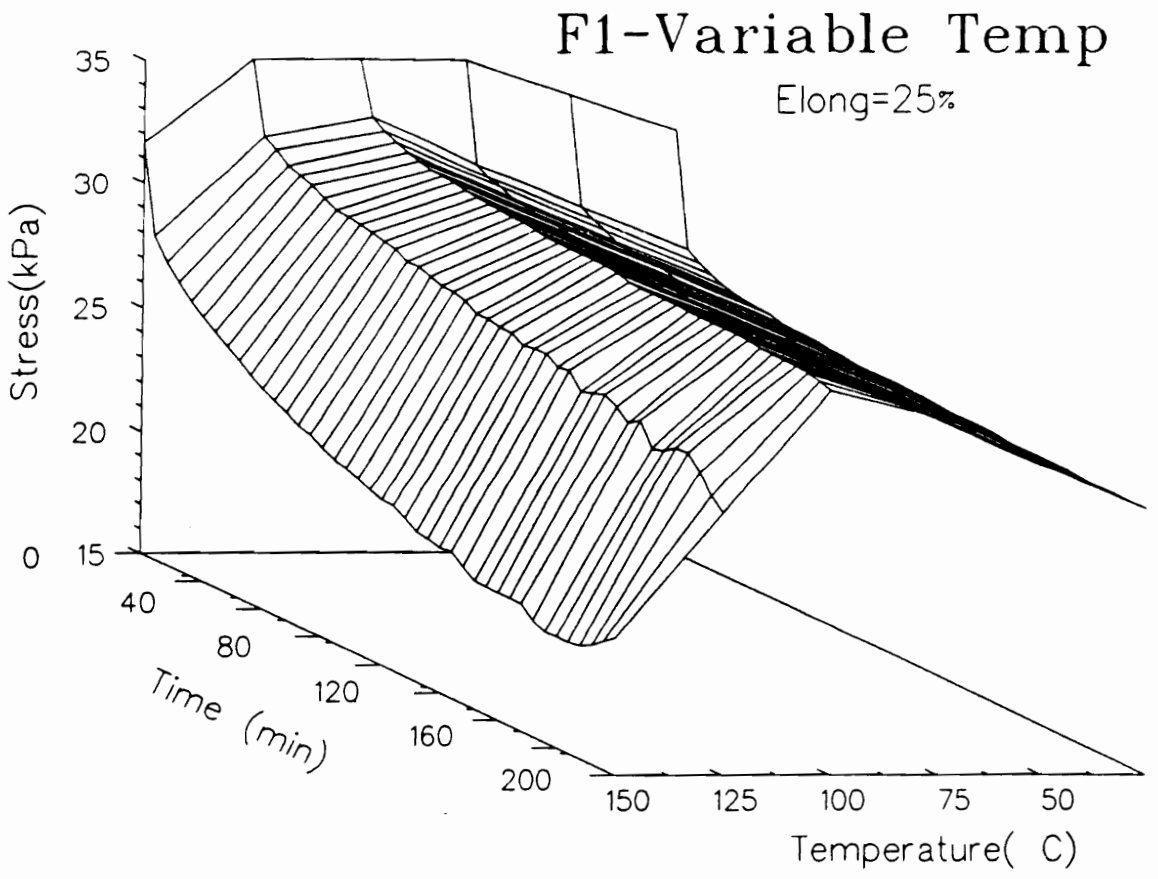

Figure 5.2. Variable Temperature Stress Relaxation Behavior for F1: Performed at 25% strain level and stretched parallel to blow axis

ularly in the range of 25-100°C. Further comments on the behavior at temperatures greater than 100°C are given later in this chapter.

As discussed in the literature review, quite linear behavior is obtained upon plotting the log $\sigma(t)$ versus the log t as demonstrated in Figure 5.3 for temperatures ranging from 25 to 100°C(20). Although this particular relationship between stress and time has no molecular or theoretical basis, it does provide a means of obtaining a comparative stress decay rate(σ_d) by calculating the slope over the 3 hour time period using linear least squares. As mentioned in the literature review, this approach has been applied to stress relaxation data for polyurethanes as well as other crosslinked polymeric materials. The values for σ_d which were obtained from the data in Figure 5.3 are given in Table 5.2 and do decrease slightly in magnitude with increasing temperature up to 100°C. Also shown in Table 5.2, are the percent stress decay values which decrease slightly from 25°C to 100°C and then begin to increase with temperature thereafter. Possible reasons for the decrease in the stress decay rates as well as the percent stress decay values are given below.

The values for σ_d and the percent stress decay values within the temperature range of 25°C to 100°C indicate that stress relaxation is approaching equilibrium conditions faster with increasing temperature. Several factors are thought to contribute to this acceleration of stress relaxation with increasing temperature. First, the relative humidity has not been controlled for these tests and it is believed that the humidity level as well as the effect of humidity on the stress relaxation behavior decreases with increasing temperature. Recall that the time these tests were carried out, the relative humidity at ambient conditions(25°C results) was in the range of 50 to 60 percent. Another factor is the amount of stress relaxation that takes place upon reaching the constant strain level is thought to increase with temperature and can be attributed to several processes. One thermally activated process is the soft segments relax much faster or on a shorter time scale due to more mobility in their chains. Another mechanism is hydrogen bond disruption which leads to chain slippage between molecular chains including the hard segment units. This type of disruption during stretching or even during the time period taken to reach equilibrium testing conditions has been indicated by the FTIR-thermal studies presented in the previous chapter. Basically, the results obtained from

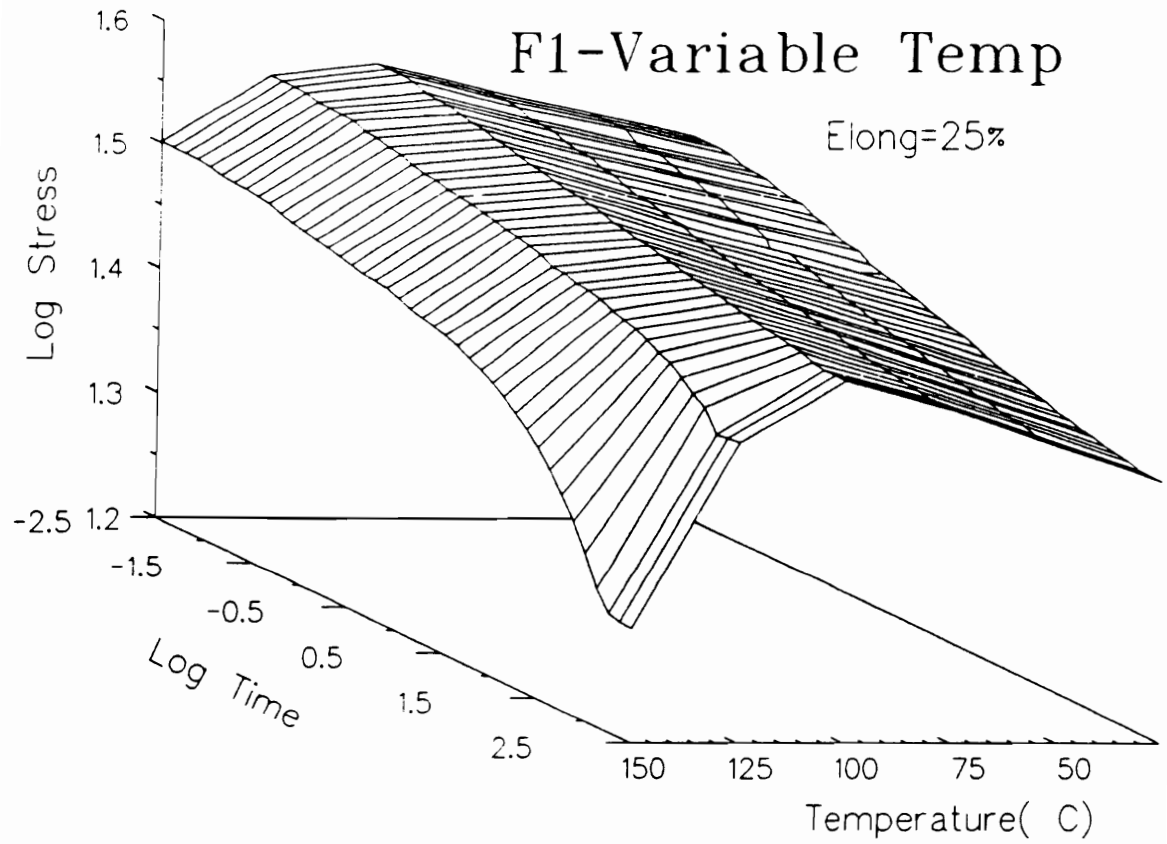

Figure 5.3. Log σ(t)-Log t Variable Temperature Stress Relaxation Behavior for F1

FTIR demonstrate that there is a weakening of hydrogen bonds which is thought to be mostly related to the urethane groups in the temperature range of 25°C to 100°C.

At temperatures greater than 100°C, a more significant increase in the amount of stress relaxation is observed in Foam F1 as shown in Figures 5.1-5.3. This increase is not only indicated by the higher percent stress decay values and the non-linear behavior in the $\log\sigma(t)$ versus the log t plots, but also in the larger negative deviation from predictions by rubber elasticity theory(see Table 5.2). One reason for these more rapid changes in the stress relaxation rate at higher temperatures is due to an increase in the disruption of hydrogen bonds with increasing temperature as indicated earlier in the FTIR-thermal behavior for plaque P1 compressed from foam F1(recall Figure 4.2). Another reason suggested by the FTIR-thermal studies, is possible chain scission that is thought to be taking place in the urethane and urea linkages. In a stress relaxation study at 120°C on a set of polyurethane rubbers, Tobolsky has also indicated that chemical changes are taking place in the urea and urethane linkages(89). In addition, Tobolsky suggested that the weakest linkages were the urea and biuret linkages upon observing that the stress decay was greater for a polyurethane rubber containing urethane, urea, and biuret linkages in comparison to one that only contained urethane linkages(89). Both of the above changes, i.e. hydrogen bond disruption and chemical degradation in the structure of the foam will lead to further local chain slippage which in turn causes more stress relaxation to occur.

The variable temperature stress relaxation behavior for $\log\sigma(t)$ vs log t is shown in Figure 5.4 for the highest hard segment containing material, foam F4. The initial stress level as well as the three hour stress level decrease with increasing temperature. This decrease in the stress levels and in particular the three hour stress level is not consistent with rubber elasticity theory as shown in Table 5.3. As stated earlier, this theory does not account for changes in secondary bonding which are thought to be fairly significant in F4(at least in comparison to F1). Thus, it is believed that the disruption and reformation of hydrogen bonding in F4 is strongly contributing to the decrease in the initial as well as the final stress levels with increasing temperature. Such changes in hydrogen bonding with increasing temperature have been indicated by the FTIR thermal analysis for plaque P4(recall Figure 4.4).

Table 5.3: Variable Temperature Stress Relaxation Results for Foam F4

Temp(°C)	σ_e(kPa)	Slope(x-10²)*	% Stress Decay**	% Deviation***
25	98.7	2.9	27	-
50	93.7	3.0	26	-11
75	88.2	2.6	23	-19
100	82.7	2.4	22	-26
125	76.9	2.9	27	-42
140	78.2	3.9	36	-50

* Correlation funtion was in the range of 0.995 to 0.999 except at 125°C and 140°C.

** The percent error in the % stress decay results varied from 1 to 5%.

*** %Deviation from predictions given by rubber elasticity;
predictions based on the stress level at 25°C and 180 min.

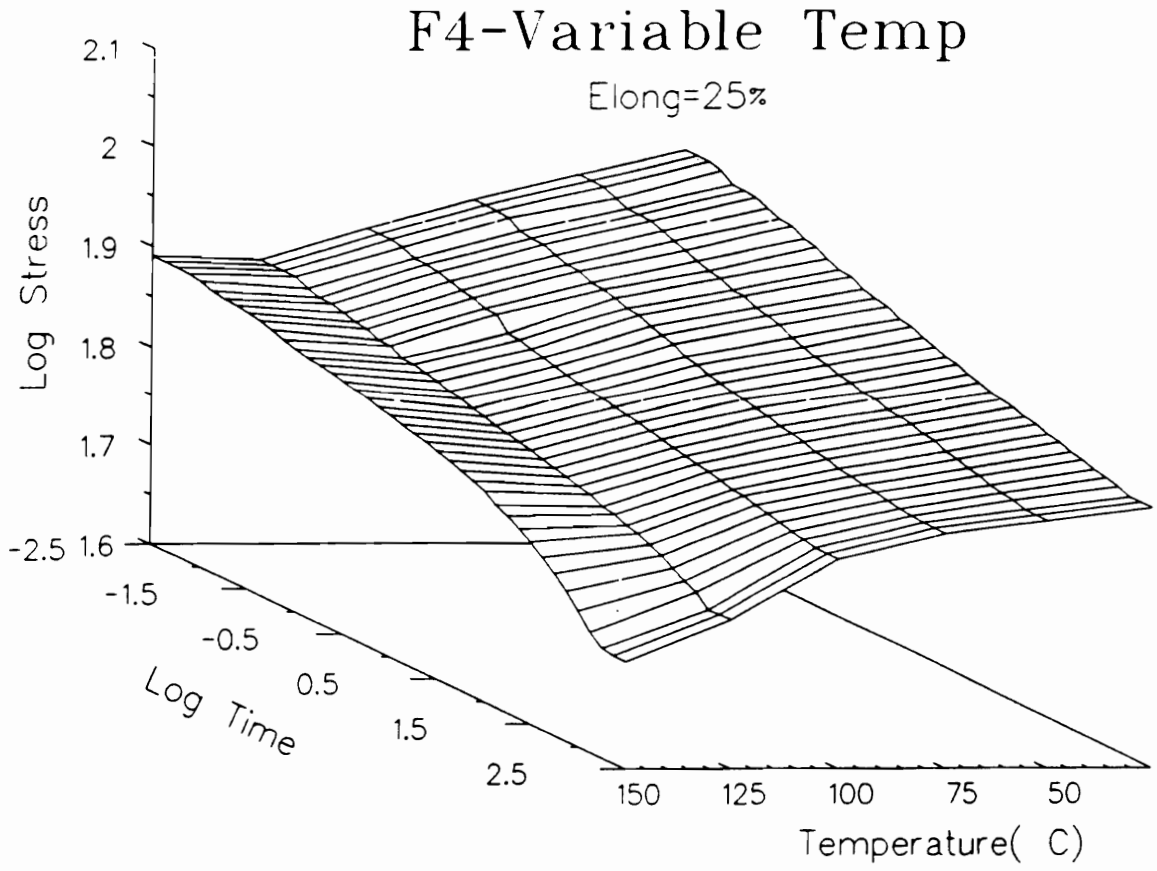

Figure 5.4. Log σ(t)-Log t Variable Temperature Stress Relaxation Behavior for F4

Figure 5.4, as well as in Table 5.3 for foam F4, shows that there is a slight decrease in the amount of stress decay and in the absolute values for σ_d up to 100°C. This decrease indicates that the stress relaxation is approaching equilibrium conditions faster by increasing temperature. Two factors that were mentioned above, i.e. relative humidity and stress relaxation occurring while reaching the constant strain level are also thought to promote this shift in the relaxation behavior for F4. Further evidence for this argument will be given in a later section for both foams F1 and F4.

At temperatures from 100°C to 125°C, an increase in the percent stress decay as well as in the deviation from predictions from rubber elasticity is observed for foam F4(see Table 5.3). In addition, non-linear behavior is observed for the $\log\sigma(t)$-log t behavior at 125°C. These results indicate that there is a significant increase in the stress relaxation behavior at temperatures near 125°C which is thought to be principally related to hydrogen bond disruption as well as some thermally induced chain scission.

Some additional comments are necessary upon comparing the stress relaxation behavior of foams F1 and F4. Also, in evaluating the effect of hard segment content on these materials, some of the results obtained for foams F2 and F3 will be utilized to assist in this comparison. As shown in Figure 5.5, the amount of stress relaxation as a function of temperature is higher for foam F4 than for foam F1, except at 413°K(140°C). Also, the stress decay rates are higher in magnitude for foam F4 than F1 at a given temperature. Finally, the negative deviation from rubber elasticity predictions increase systematically with increasing temperature for both foams F1 and F4, but to a greater extent for F4(see Figure 5.6). Also, in Figure 5.6 there is a constant, but small decrease in this behavior up to 100°C for both foams and thereafter there is significant change in this behavior. Furthermore, the initial slope in this behavior up to 100°C is greater for F4 than F1, but at the higher temperatures this slope appears to be greater for F1 than F4. Most of these differences can be related to the higher hard segment content of foam F4 and thus more available hydrogen bonds to undergo disruption. The specific effect of hard segment content can be seen in Figure 5.7 for foams F1-F4 where a systematic increase in the amount of stress decay is observed with increasing hard segment content up to temperatures of 125°C. However, at 140°C there is a minimum

Table 5.4: Constants for Thermal Dependence of Stress Decay for Foams F1 and F4

Foam	$\tau_1(1/°K)$	C_1	$\tau_2(1/°K)$	C_2	$T_o(°K)$
F1	258	60	14.9	1.19	373
F4	252	90	18.3	2.33	375

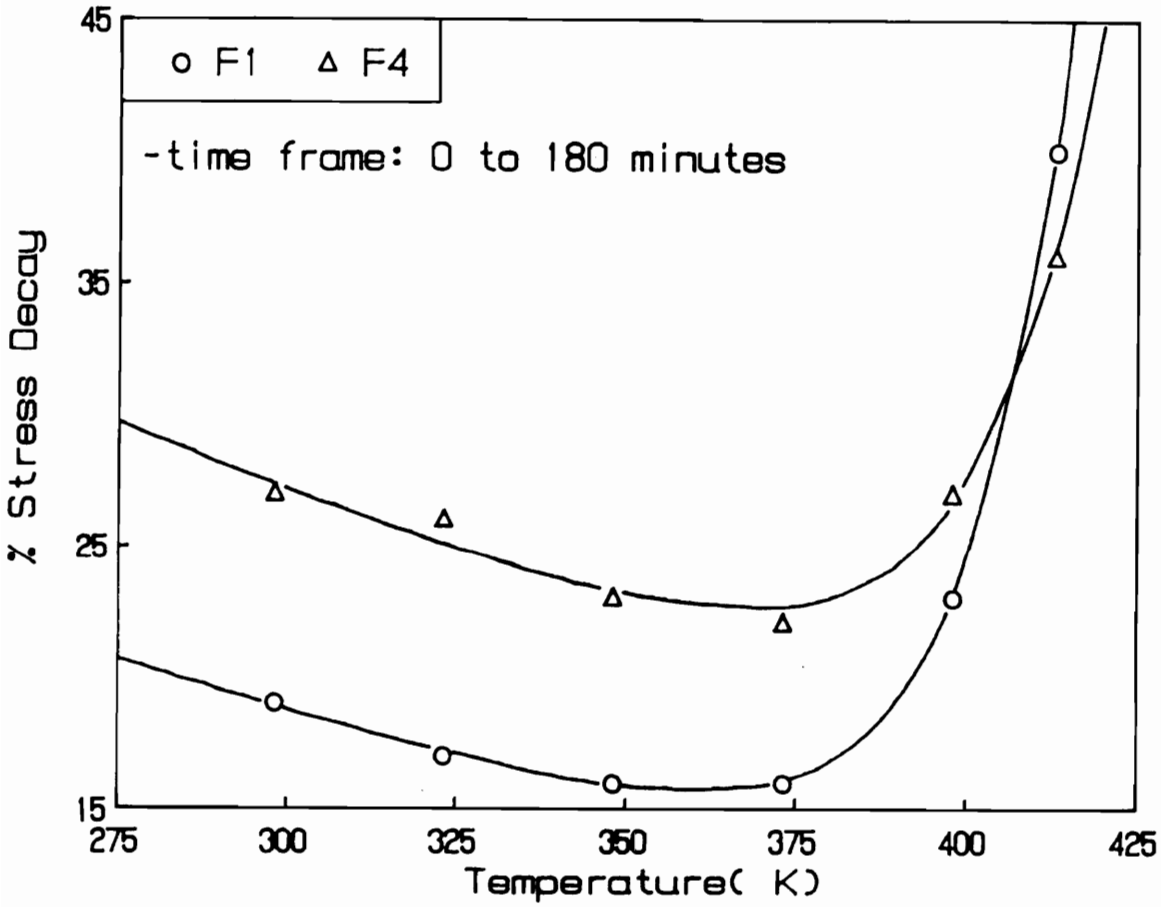

Figure 5.5. Percent Stress Decay at Different Temperatures for Foams F1 and F4: Curve shown through data is based on model described in text by Equation [5.1];

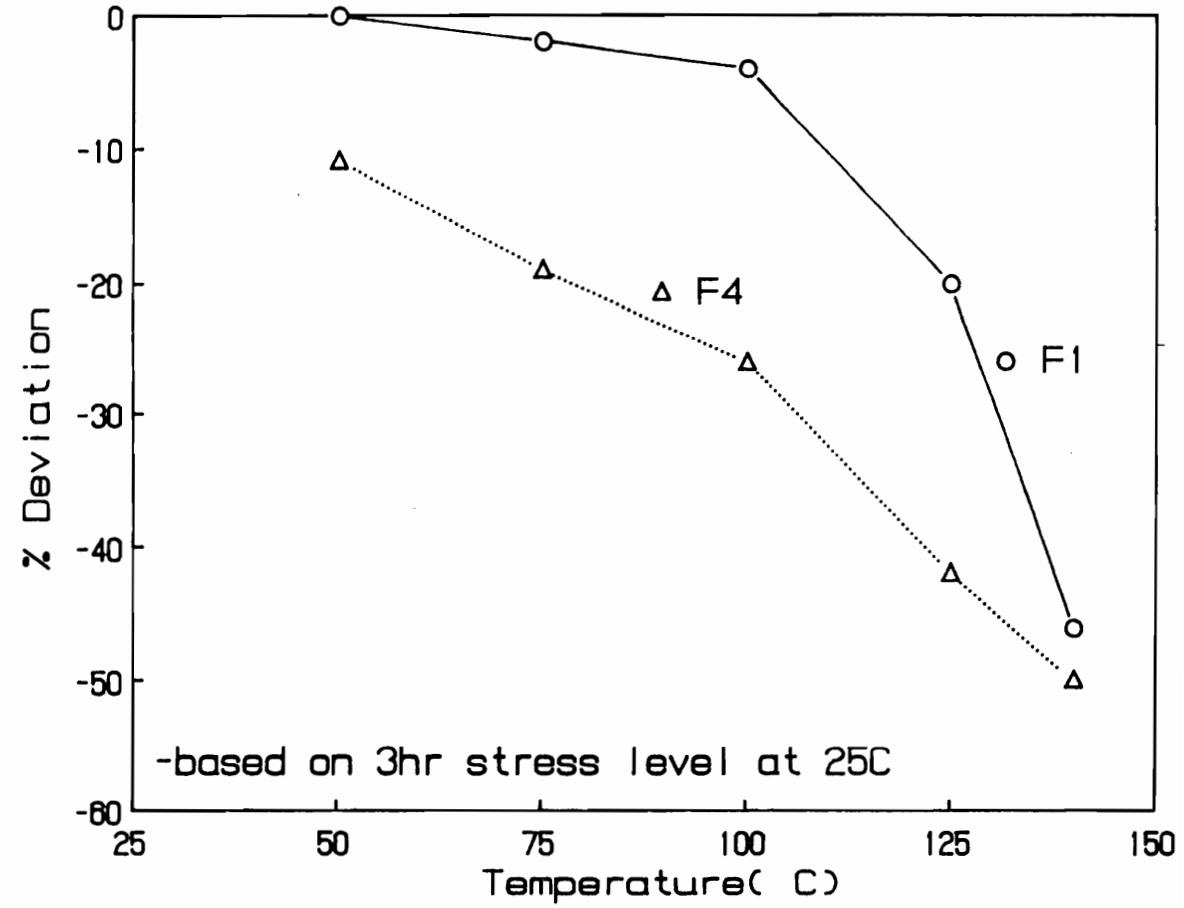

Figure 5.6. Deviation From Rubber Elasticity Theory Predictions for Foams F1 and F4: Predictions based on 3 hour stress level at 25°C

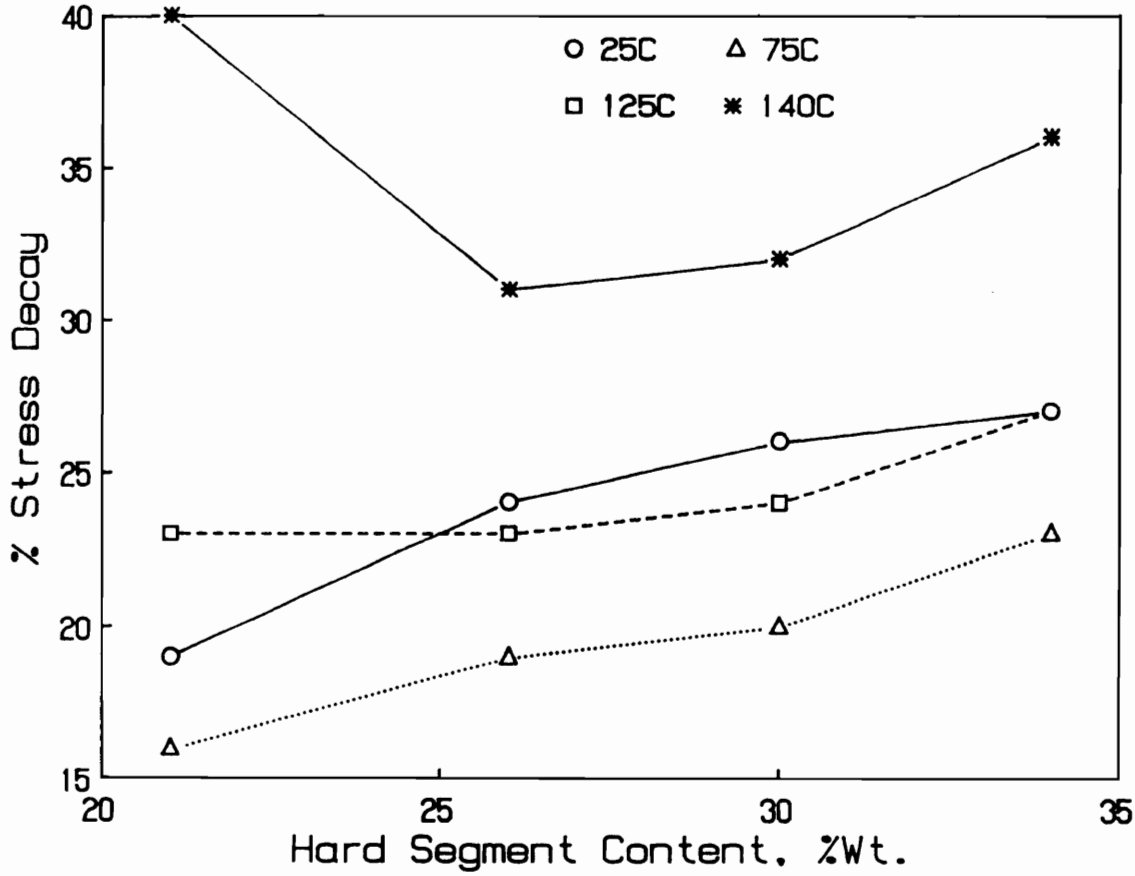

Figure 5.7. Effect of Hard Segment Content on Stress Relaxation Behavior: Results obtained from foams F1-F4

in this behavior at 26 wt% hard segment content. Interestingly, the highest amount of stress decay at 140°C occurred in foam F1 which has a 21 wt% hard segment content - the lowest of the 4 foams tested. This behavior at 140°C suggests that additional causes for stress relaxation are taking place in foam F1 and certainly in the other foams as well. As indicated by the FTIR-thermal studies for the plaques of the foams, the hydrogen bonding to the urethane group is thought to be weakened significantly and furthermore, chain scission is also speculated to be taking place in the urethane linkages as well as in the urea linkages. In addition, based on the results from the FTIR thermal analysis, these structural changes are believed to be greater in foam F1 in comparison to the other foams; thus giving reason for the larger amount of relaxation observed at 140°C for F1(recall Figures 4.9-4.10).

In further evaluating the stress relaxation behavior for foams F1 and F4, the results of the thermal dependence of stress decay have been fit using a two parameter model. As shown in Figure 5.5, there are two distinct portions of the response for foams F1 and F4. Thus, one requirement of the model is to account for the slight decrease in the stress decay values up to 100°C. The second is to account for the significant increase in the amount of stress relaxation at temperatures greater than 100°C. The two parameter model developed, though empirical, does somewhat resemble a generalized two component Maxwell-Wiechert model, and is as follows,

$$Stress\ Decay = C_1 \exp[\frac{-T}{\tau_1}] + C_2 \exp[\frac{T - T_o}{\tau_2}] \qquad [5.1]$$

where C_1 and C_2 are constants(front factors), τ_1 and τ_2 are temperature relaxation constants with units of reciprocal °K, and T_o(°K) is a constant which takes on a value(ca. 370°K) near the up-turn in the stress decay-temperature behavior(see Figure 5.5). In equation [5.1], the first term on the right hand side governs the thermal dependence of percent stress decay up to 100°C and the second term accounts for the significant changes in stress decay thereafter. The first temperature relaxation constant, τ_1, is thought to indicate the extent to which temperature accelerates the approach to near equilibrium conditions. On the other hand, the value for τ_2 suggests how extensive the thermal effects are on a foam at the higher temperatures.

Equation [5.1] was fit using a BASIC program developed by R.W. Ramette at Carleton College(90). The program involved setting two(T_o and C_1) of the five variables to constant values and then calculating the best fit of the data by changing the other variables. The process usually involved 5 to 10 iterations depending on how good the first estimate was for the other three variables. The values of the data constants used are given in Table 5.4.

As shown in Figure 5.5, the two parameter model fits the data very well and does account for the two different parts of the curve. In looking closer at the constants, one will notice that the temperature relaxation constant, τ_1, for F4 is slightly lower than τ_1 for F1(see Table 5.4). This behavior indicates that increasing temperature in the range of 25°C to 100°C results in a greater acceleration of the stress relaxation process for F4 in comparison to that of F1. On the other hand, τ_2 is greater for F1 than F4, which signifies a more significant thermal effect on the stress relaxation of foam F1 at the highest temperatures. In addition to understanding the stress relaxation behavior through the values of τ_1 and τ_2, equation [5.1] can be utilized to predict percent stress decay up to a 3 hour period at a given temperature. The temperature range over which the constants are thought to best fit Equation [5.1], is between 25°C to 140°C. However, it may be feasible to utilize the constants for temperatures somewhat outside of this range if no additional causes for stress relaxation occur other than the ones are already mentioned.

5.1.2 Variable Temperature Behavior for Plaques P1 and P4

As mentioned earlier, the compression molded plaques of the foams were also utilized to characterize the relaxation behavior of the solid portion of the foam independent of its cellular nature. Recall, for example, that plaque P1 is compression molded from foam F1. In Figure 5.8, the variable temperature stress $\log\sigma(t)$ - log t. relaxation behavior for P1 is shown in the 3-dimensional form. As noted, the initial stress increases very systematically with increasing temperature and as in the case of F1, the 3 hour stress level goes through a maximum near 100°C(compare Figures 5.3 and 5.8). The stress relaxation behavior is nearly linear for the $\log\sigma(t)$ versus log t plot up to tem-

Table 5.5: Variable Temperature Stress Relaxation Results for Plaque P1

Temp(°C)	σ_o(kPa)	-Slope(x10²)*	% Stress Decay**
25	1410	2.0	18
75	1480	1.9	17
100	1520	1.9	18
125	1570	2.3	25
140	1640	3.9	37

* Correlation function was in the range of 0.995 to 0.999 except at 125°C and 140°C.

** The percent error in the % stress decay results varied from 1 to 5%

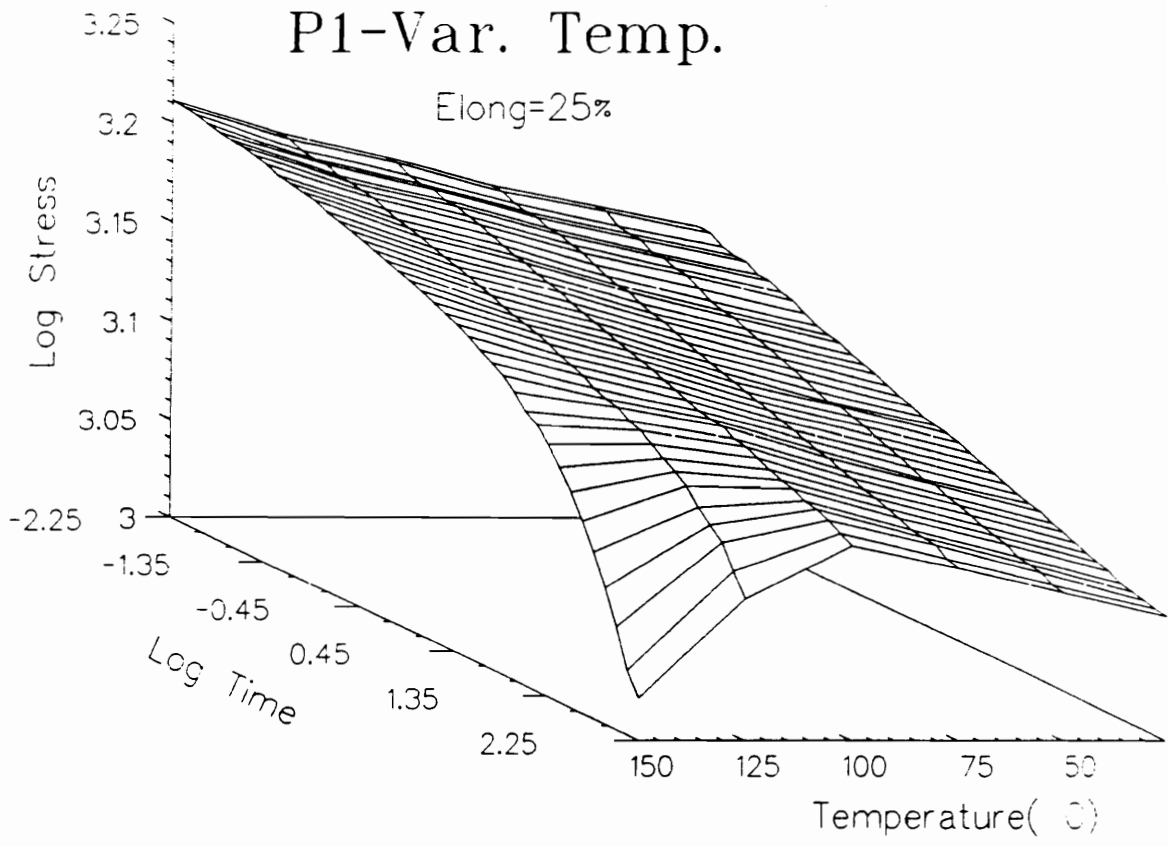

Figure 5.8. Log σ(t)-Log t Variable Temperature Stress Relaxation Behavior for P1: Tests performed at 25 percent strain level for 3 hours

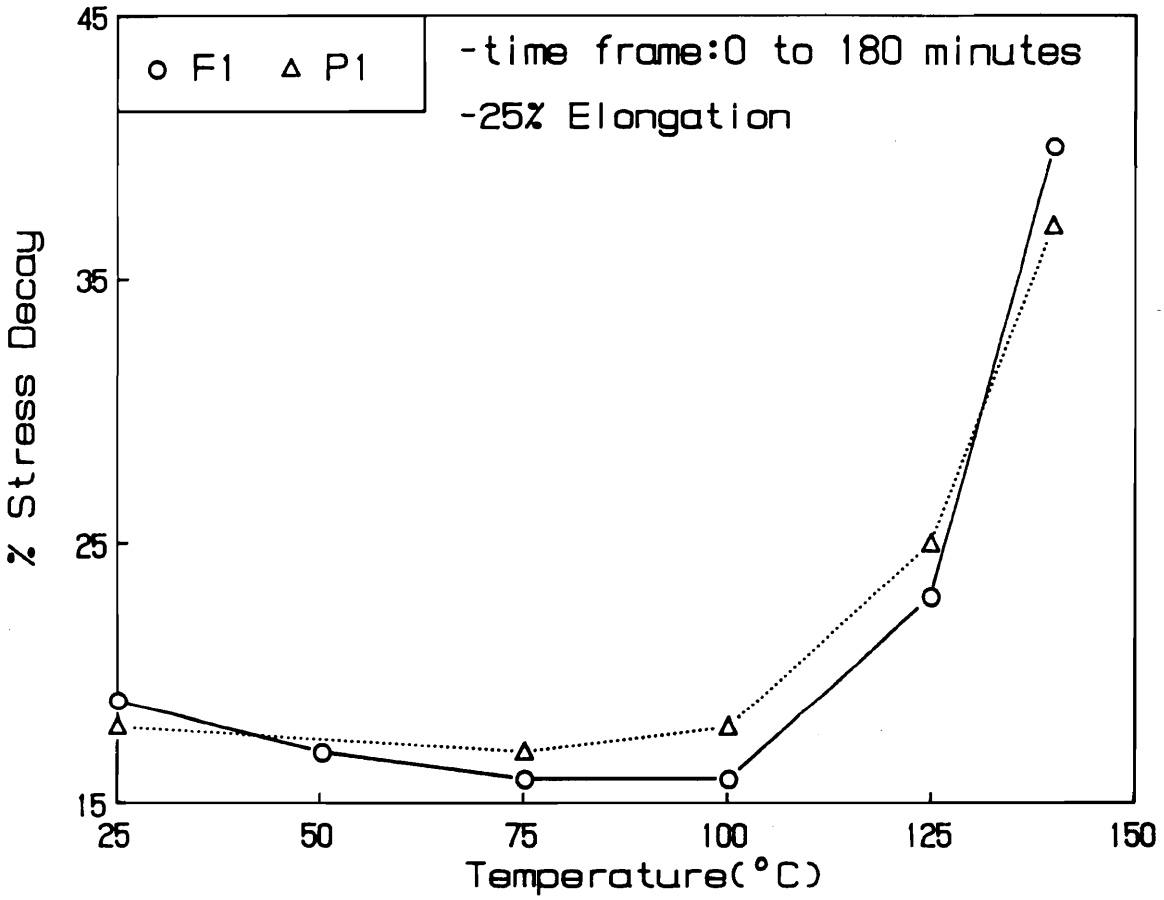

Figure 5.9. Percent Stress Decay as a Function of Temperature for Foam F1 and Plaque P1: Values calculated over 3 hour time period

peratures of 100°C and thereafter exhibits non-linear behavior(see Figure 5.8). For the "linear" behavior, the stress decay rates of P1 are very analogous to those of F1 as given in Tables 5.2 and 5.5, respectively. In addition, as shown in Figure 5.9 the stress decay values as a function of temperature are also very similar for F1 and P1, except that P1 shows a slightly greater decay rate 25°C and 140°C. Overall, the stress relaxation behavior for the compression molded plaque, P1, is very comparable to that of its respective foam. Before, drawing further conclusions concerning the plaques, the results of the higher hard segment plaque, P4, will be addressed.

The $\log\sigma(t)$ - log t variable temperature stress relaxation behavior for plaque P4 is shown in Figure 5.10 and the key results are summarized in Table 5.6. The initial stress level and the final(3 hr) stress level increase slightly up to 75°C and thereafter decrease with increasing temperature. In this respect, the stress relaxation behavior for P4 is somewhat different to that of its respective foam as seen by comparing Figures 5.4 and 5.10. On the other hand, as shown in Figure 5.10 nearly linear behavior is observed for P4 up to 100°C and non- linear behavior is seen thereafter. Like foam F1, this behavior is again consistent with that of its foam F4 presented earlier in Figure 5.4. In addition, the stress decay rates given in Tables 5.3 and 5.6 are similar for F4 and P4, respectively. Also, as shown in Figure 5.12, the thermal dependence of the percent stress decay values is comparable for plaque P4 and its respective foam.

In summary, *the stress relaxation behavior for plaques P1 and P4 are quite similar to that of their respective foams*. The differences in the behavior between the plaques and their respective foams are mostly related to the behavior of the initial and final stress levels with increasing temperature. These small differences are not fully understood, but are thought to be related to the compression molding process which is believed to bring about slight changes in the morphology; for example, better phase separation and possibly further crosslinking. Most importantly, regardless of these differences, the relaxation behavior and the rate of relaxation for the foams and their respective plaques are very similar(see Figures 5.9 and 5.11). *This observation gives further indication that the solid portion of the foams is governing the relaxation behavior in tension for these materials and is not dominated by cell structure.*

Table 5.6: Variable Temperature Stress Relaxation Results for Plaque P4

Temp(°C)	σ_o(kPa)	-Slope(x10²)*	% Stress Decay**
25	6720	3.2	29
75	6850	2.7	24
100	6300	2.7	24
125	6150	3.2	29
140	5600	3.9	35

* Correlation function was in the range of 0.995 to 0.999 except at 125°C aand 140°C.

** The percent error in the % stress decay results varied from 1 to 5%.

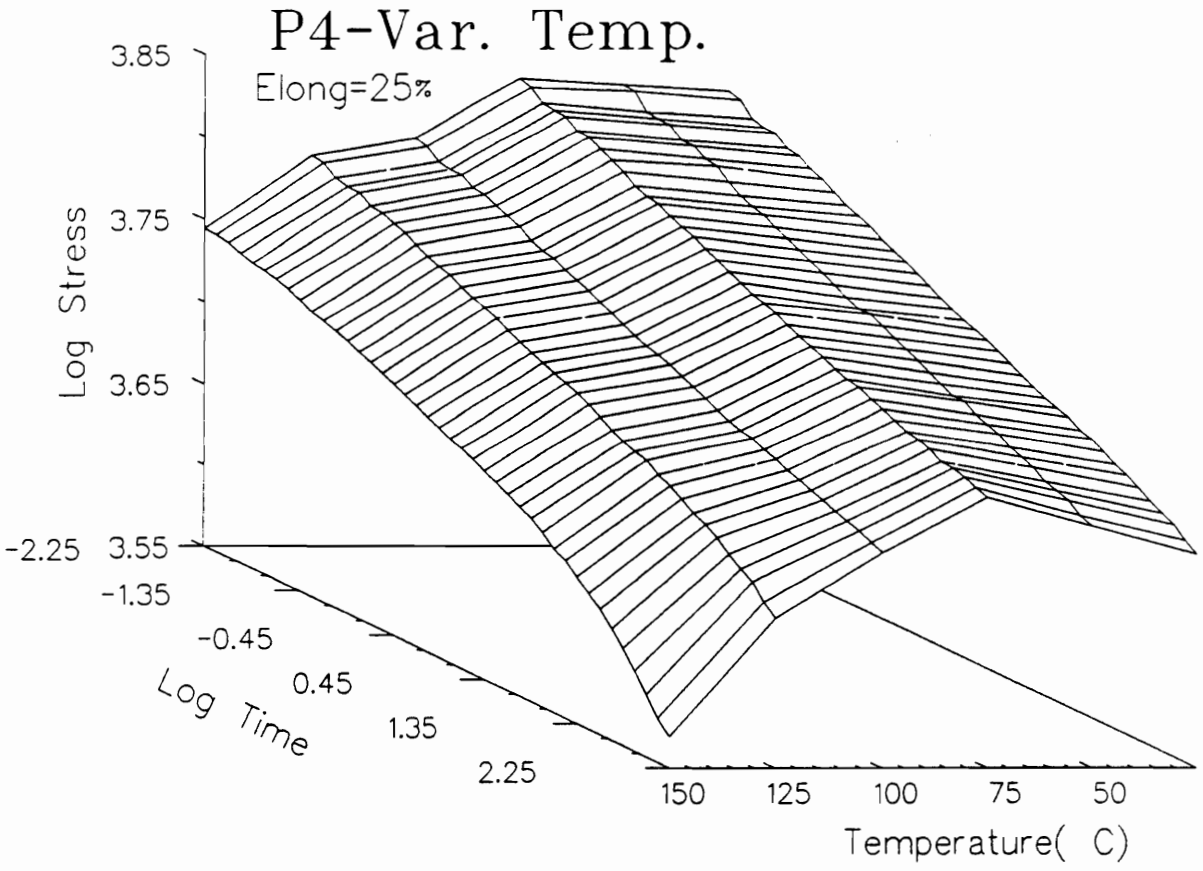

Figure 5.10. Log σ(t)-Log t Variable Stress Relaxation Behavior for Plaque P4: Tests performed at 25 percent strain level for 3 hours

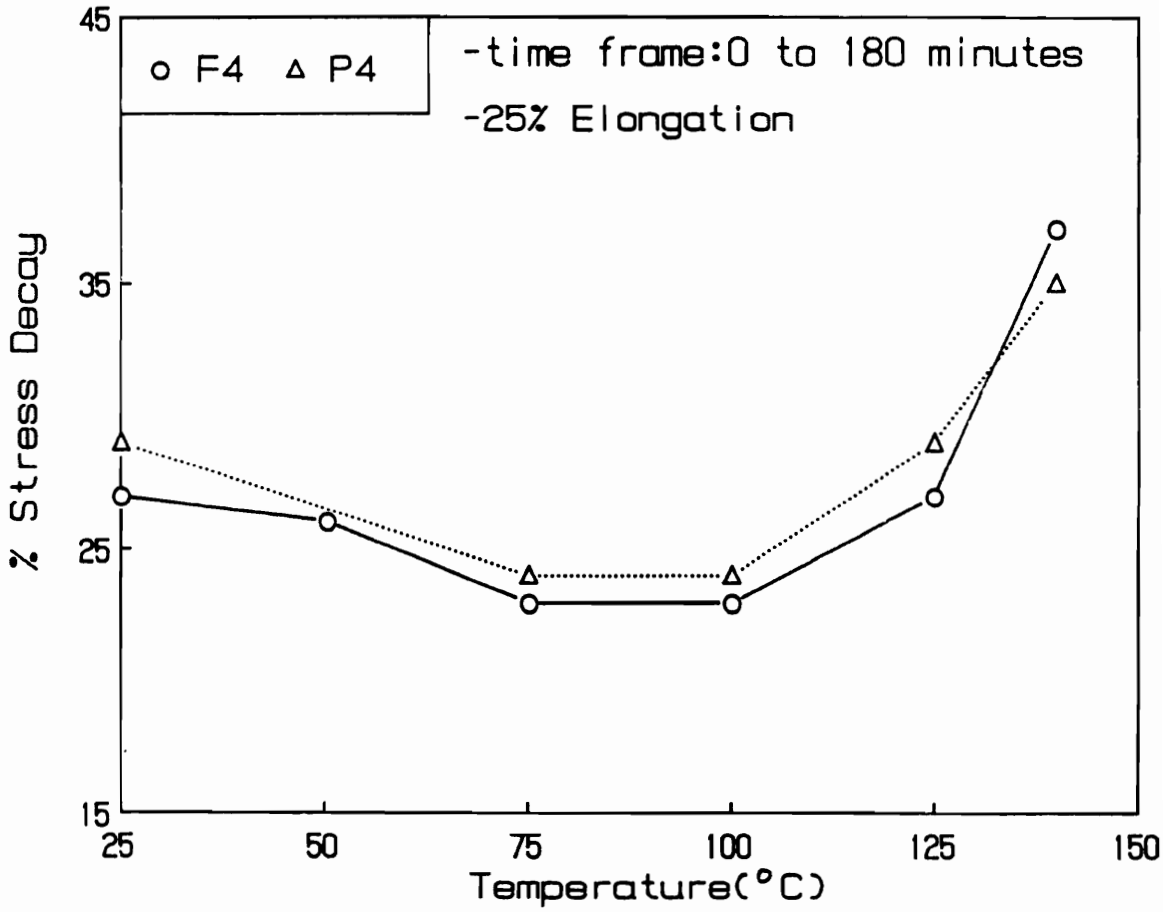

Figure 5.11. Percent Stress Decay as a Function of Temperature for Foam F4 and Plaque P4: Values calculated over 3 hour time period

5.1.3 Variable Temperature Behavior for the PUU Elastomer

In further evaluating the effect of temperature on the stress relaxation behavior for a micro-phase separated segmented material, a thermoplastic elastomer, the PUU elastomer, was utilized. It is recalled that the PUU elastomer was made with many chemically similar components to those in preparing the foams. However, the noteworthy point is that the linear TPU elastomer has a segmented morphology whereas the foams also possess a covalent network structure in addition to a two phase hard/soft domain texture with large urea aggregates.

The $\log\sigma(t)$ - log t stress relaxation behavior at temperatures ranging from 25°C to 125°C is shown for the PUU elastomer in Figure 5.12 as determined at a constant elongation of 25%. The stress decay rates along with the initial stress levels and percent stress decay values are given in Table 5.7. As shown in Figure 5.12, the behavior again is rather linear up to temperatures of 100°C and then begins to exhibit negative deviation at 125°C. The linear behavior is quite similar to that displayed earlier in Figures 5.3 and 5.4 for foams F1 and F4. However, there is a more significant increase in the amount of stress relaxation taking place from 100°C to 125°C for the PUU elastomer than in the case for F1 and F4(see Tables 5.2, 5.3, and 5.7). A similar transition in the same temperature region has also been reported for stress relaxation results obtained at a 25 percent elongation for another segmented polyether polyurethane elastomer by Seymour et. al.(53). Based on both the FTIR-thermal and orientation studies, this significant increase in the amount of stress relaxation for the PUU elastomer is attributed to the disruption of hydrogen bonds and to possible chain scission taking place in the urea and urethane linkages. This conclusion is also consistent with and gives support to the above arguments presented for the foams in explaining the large changes in the stress relaxation behavior at temperatures greater than 100°C. It is clearly noted that the rates of relaxation as well as the stress decay values are higher for the PUU elastomer in comparison to the foams. This type of behavior is certainly expected since the elastomer has a linear segmented morphology while the foams also possess a covalent network. Also, these materials are chemically different since the PUU elastomer contains a MOCA chain extender where as the foams do not.

Table 5.7: Variable Temperature Stress Relaxation Results for the PUU Elastomer

Temp(°C)	σ_o(MPa)	-Slope(x10²)*	%Stress Decay**
25	2.8	4.4	37
75	2.85	4.6	37
100	2.7	5.4	43
125	2.45	8.1	59

* Correlation funtion was in the range of 0.995 to 0.999 except at 25°C and 125°C

** The percent error in the % stress decay results varied from 2 to 5%.

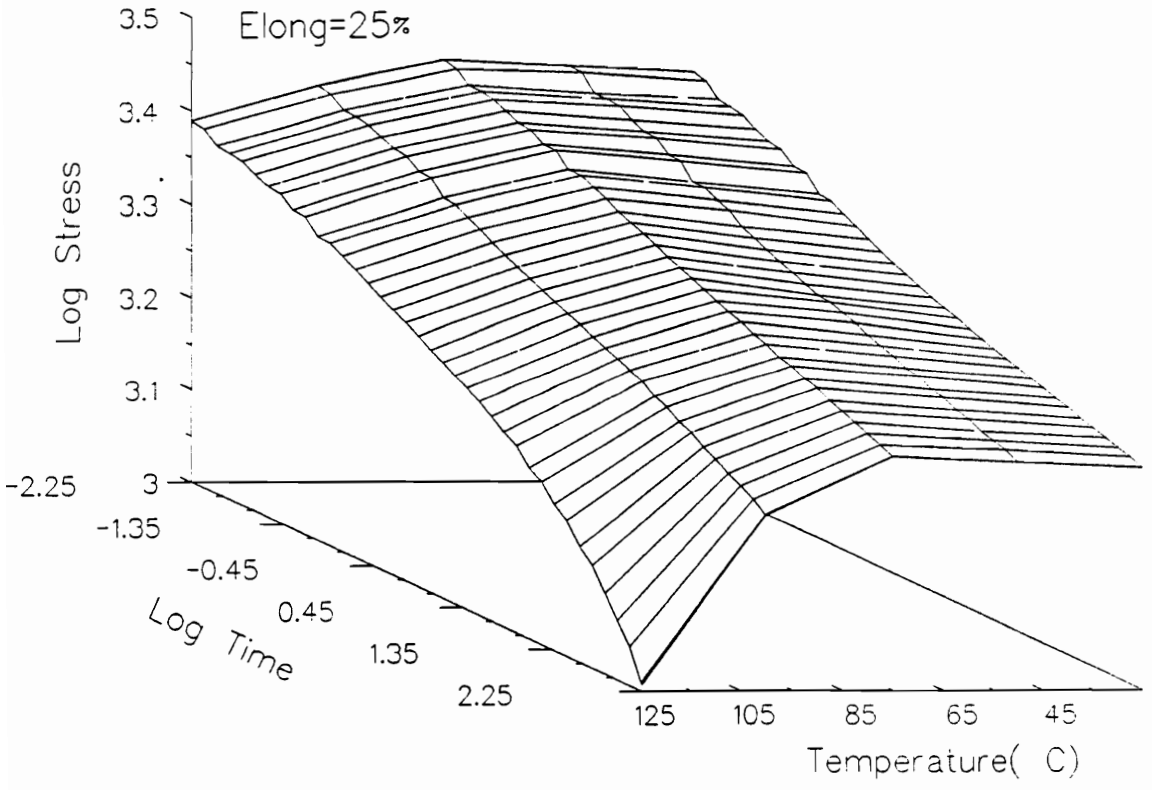

Figure 5.12. Log σ(t)-Log t Variable Temperature Stress Relaxation Behavior for the PUU Elastomer: Tests performed at 25 percent strain level for 3 hours

5.1.4 Long Term Stress Relaxation Behavior for Foams F1 and F4

Unlike the PUU elastomer or thermoplastic elastomers in general, foams F1 and F4 are expected to reach some type of equilibrium stress level over time since they contain a covalent network structure. Thus, the longer term relaxation behavior was measured for foams F1 and F4 over 2 to 3 days at 25°C. These results are presented for F1 and F4 in Figure 5.14. Both foams demonstrate nearly linear behavior for the log $\sigma(t)$- log t over long time periods. In the case of F1, the stress level appears to begin to level off after 46 hours(log time = 3.45) of stress decay. On the other hand for the higher hard segment foam, F4, does not exhibit any sign of reaching an equilibrium stress level until over the full testing time of 66 hours(log time = 3.6). Thus, for both foams no equilibrium stress level is reached over a 3 day time period - even for foam F1. Although, this result is somewhat surprising since these materials possess a covalent network, it is most likely that the continued stress relaxation is observed due to the slow relaxation response of the hard domains. In comparing the behavior for the two foams, it appears that the approach to an equilibrium stress level will take longer for F4 than F1 at 25°C. This difference is thought to be related to a higher hard segment content as well as a higher hydrogen bonding content in foam F4. That is, both of these factors are believed to allow for additional rearrangement at the molecular level which is thought to prolong the relaxation period.

In addition to monitoring the long term relaxation behavior at 25°C, the stress decay was also followed for a 24 hour time period at 100°C. This behavior for both foams F1 and F4 is shown in Figure 5.14a. As exhibited in Figure 5.14a, the relaxation behavior does deviate from linearity for both foams during the testing time period. This onset of an increased relaxation rate takes place on a shorter time scale for F1(3.3 hours-log t = 2.3) than for F4(7.4 hrs-log time = 2.65). Thus, this indicates at temperatures near 100°C and higher, the effect of temperature on the relaxation behavior in F1 is greater than that of F4. In addition, these results at 100°C also demonstrate that the predictions for stress relaxation by the stress decay rate may not be as reliable over long time periods; for example, if equilibrium has been reached or if there is an increase in the rate of relax-

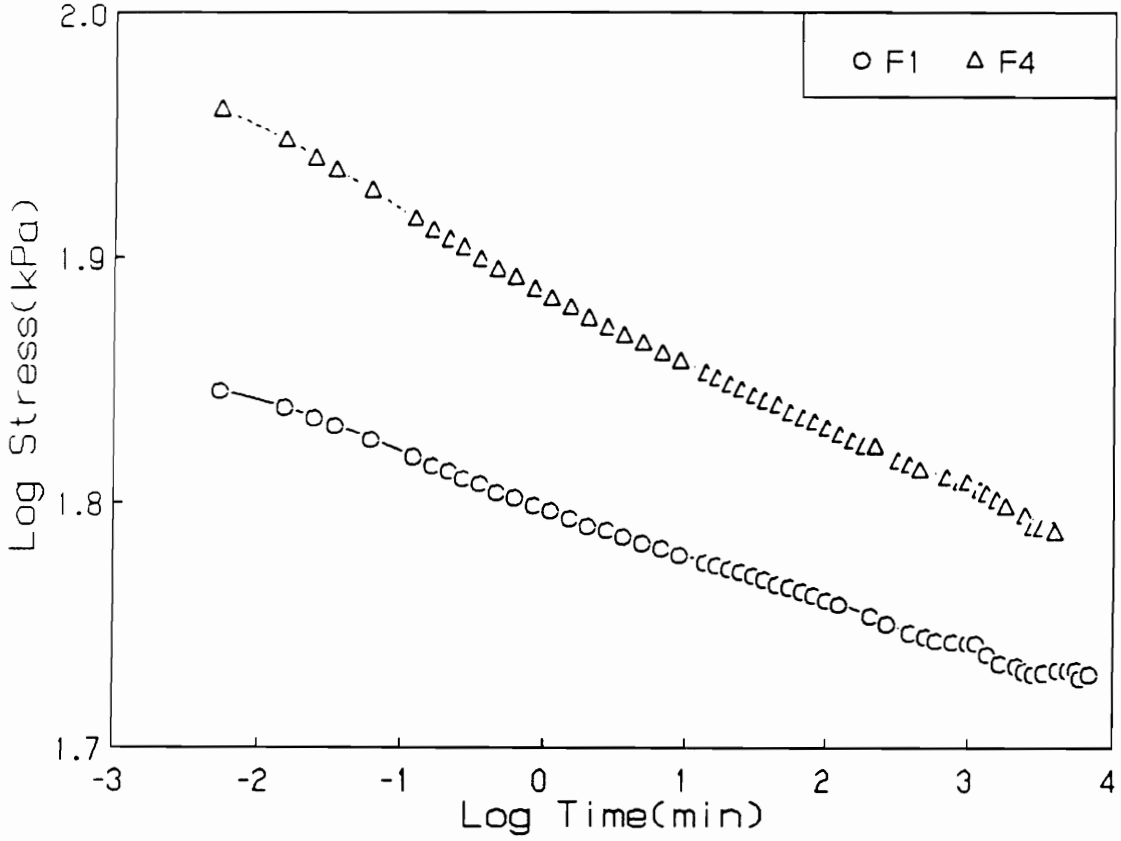

Figure 5.13. Long Term Relaxation Behavior for Foams F1 and F4 at 25°C

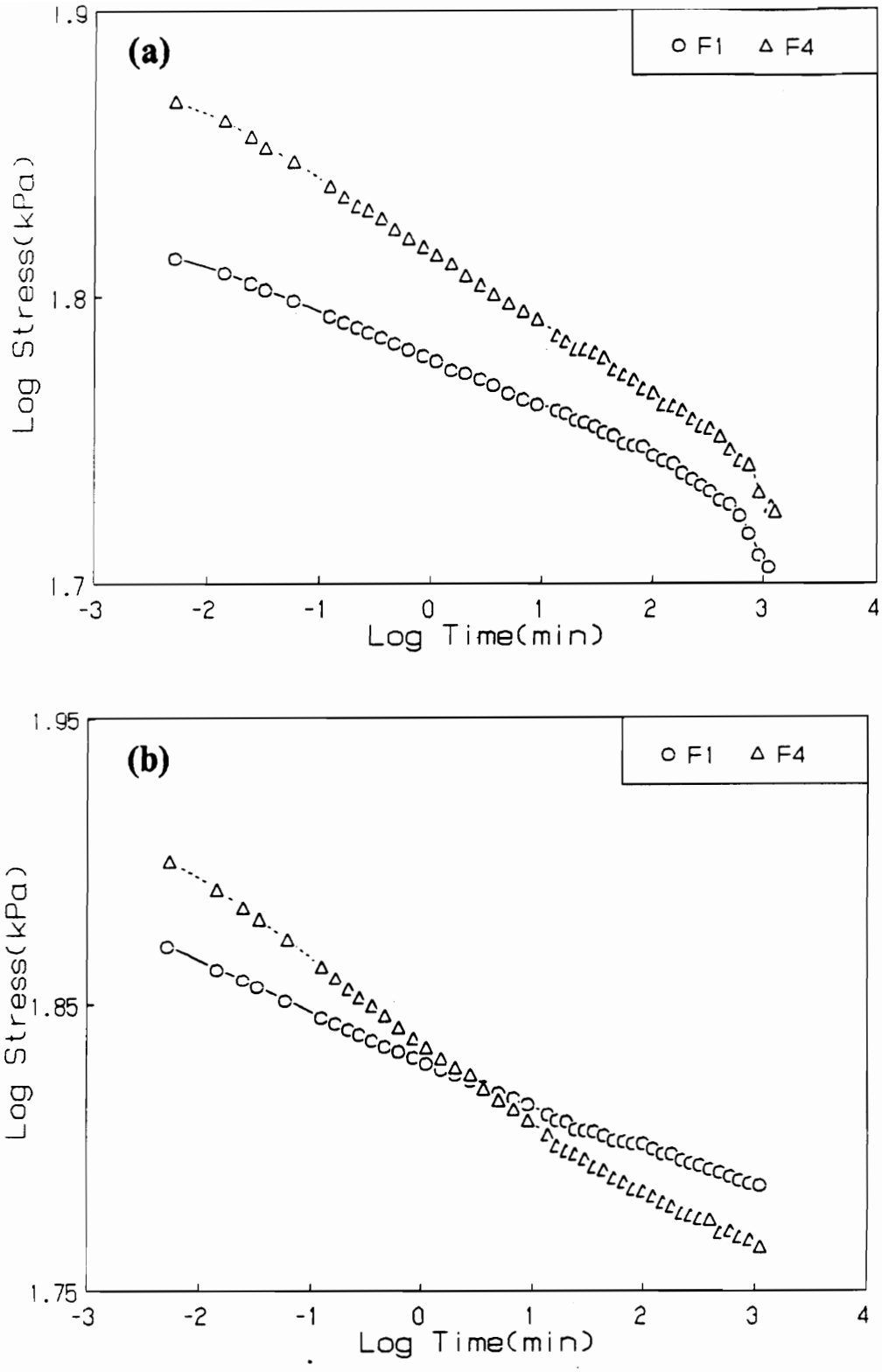

Figure 5.14. Long Term Relaxation Behavior for Foams F1 and F4 at (a)100°C and (b) 75°C

ation as in the case at 100°C. However, the stress decay rates are believed to be of very practical use in predicting the initial shorter term stress relaxation behavior for these foams.

An additional concern based on the relaxation data obtained at 100°C, is at what temperature or in what time range does the relaxation behavior begin to deviate from linearity for the $\log\sigma(t)$-log t behavior. In addressing this concern, the long term behavior at 75°C has also been monitored over an extended time period of 24 hours for both F1 and F4. As shown in Figure 5.14b, both foams do not show a transition in the rate of relaxation, but do begin to exhibit signs of approaching equilibrium conditions. Thus, it is believed that between 75°C and 100°C, temperature(thermal effects) does begin to have a significant effect on promoting additional relaxation in foams F1-F4 that causes nonlinear $\log\sigma(t)$-log t response.

As mentioned earlier, additional experiments were carried out to further substantiate that temperature does accelerate the approach to equilibrium conditions in foams F1 and F4. This experiment involved measuring the stress relaxation behavior in the usual manner at 75°C, except 15 minutes into the test, the conditions of the experiment were then changed and allowed to approach ambient conditions(near 25°C). This took approximately 1 hour for the sample to reach ambient conditions, and during this time and following, the stress relaxation behavior was monitored. The results obtained after the sample reached ambient conditions are shown in Figure 5.15 for both foams along with those obtained for a test performed only at 25°C. As shown in Figure 5.15 for both foams, the the stress decay rate for the test begun at 75°C is much slower than the rate obtained for the test maintained at 25°C. Thus, this difference indicates that equilibrium conditions are approached faster at higher temperatures or in other words the test(one begun at 75°C) has been accelerated with respect to time. In further support of these results, Smith and Dickie have shown for a $\log\sigma(t)$-log t fit of their stress relaxation results obtained over a 100 minute time period that the rate of relaxation for an SBR rubber vulcanizate decreases with increasing temperature in the range of - 45°C to 35°C (91). Smith and Dickie also were able to superpose their results and obtain shift factors that could be used to predict stress behavior over longer or shorter time scales. This approach was applied to the data for F1 as well as in the case for F4, but due to the need for ad-

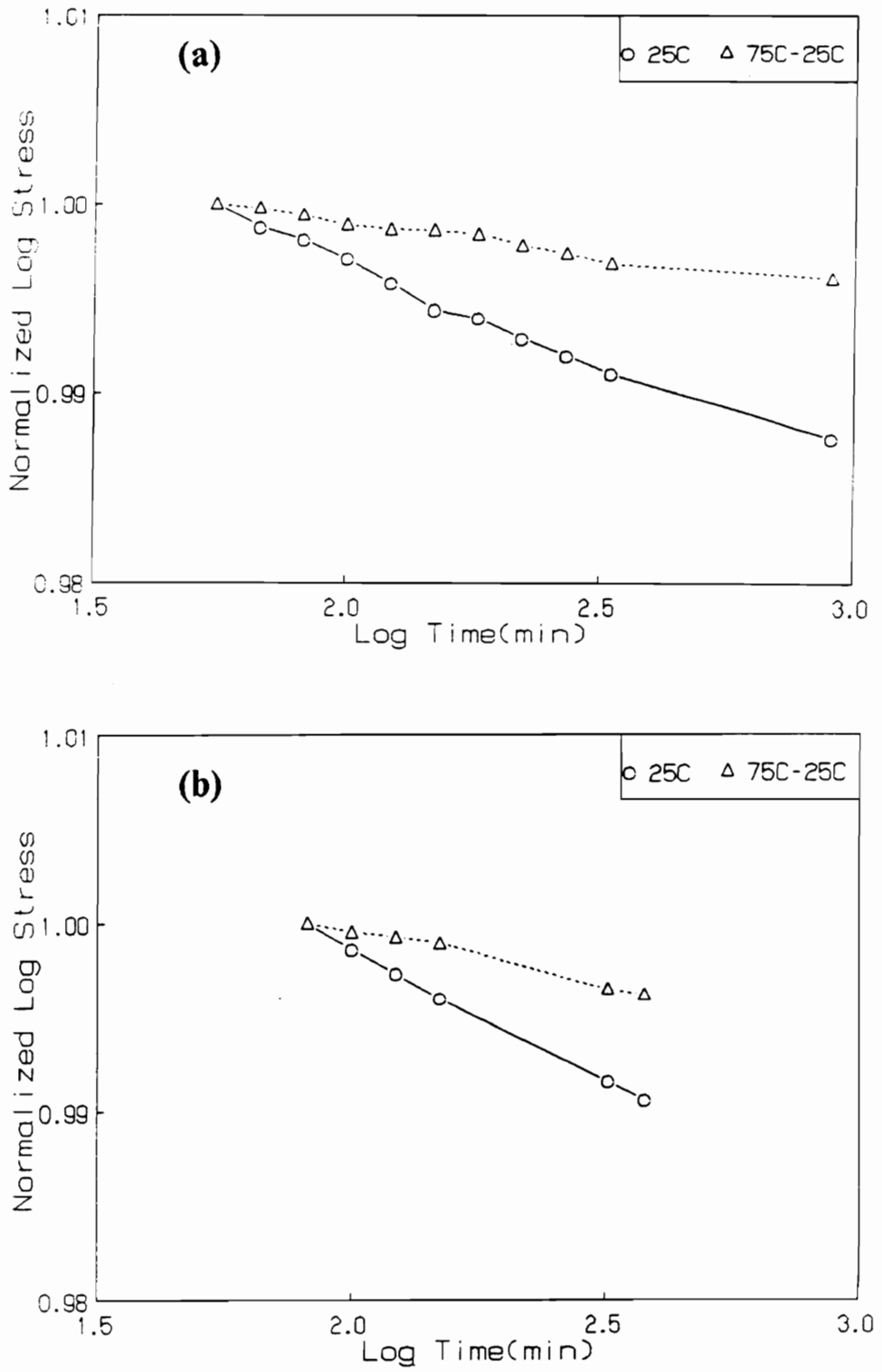

Figure 5.15. Accelerated Stress Relaxation Behavior at 25°C: (a)Foam F1 and (b)Foam F4

ditional, but different vertical shifts for the various temperatures in order to superpose the results, this method did not seem applicable to the present data.

5.1.5 Effects of Temperature and Humidity on the Relaxation Behavior

As mentioned in the discussion for the variable temperature studies, the percent relative humidity was not controlled or monitored. Since humidity is known to effect the properties of flexible polyurethane foams, results are presented in this section from tests where both temperature and relative humidity have been controlled. Before discussing these results, it is of importance to have some idea of how water may interact with the foams and potentially how it might effect the physical properties of these materials. Some potential sites for water to interact to the chemical structure of the foam are schematically shown in Figure 5.16a for both the hard and soft segments. At this level, water is thought to interact more with that of the hard segment due to more possible sites and a greater affinity. On the other hand for the chain structure(see Figure 5.16b), the extent of water interaction with the different morphological units(hard vs. soft) is not known and furthermore it is not known how the extent of this interaction changes with temperature and relative humidity. In an attempt to answer some of these questions, weight uptake studies were carried out at 23°C and at 38°C. It was also desired to quantify the weight uptake at higher temperatures, i.e. 90°C, but due to experimental difficulties this was not possible. The measurements at 23°C and 38°C were made on the plaques since earlier experiments using the foams led to problems with surface water and thus the absorption of water to the solid structure could not be found independent of the cellular structure. The details of the water uptake experiments as well as the results have been written up separately in Appendix B. In short, the weight uptake is 0.5 percent at 23°C for the plaques of foams F1 and F4. At 38°C, the percent weight uptake is 1.3 for F1 and 1.6 for F4. Although the results do indicate that there is an increase in the weight uptake with temperature, the actual extent of this increase is not known due to using different experimental apparatuses for the two temperatures (see Appendix B for more detail). While the weight uptake is similar at 23°C for P1 and P4,

Chemical Single Chain

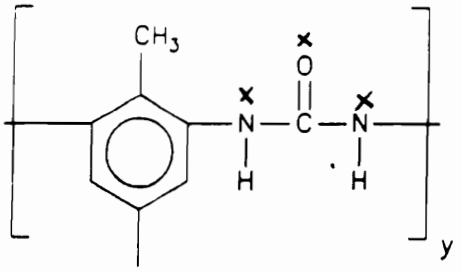

Polyurea repeat unit – hard segment

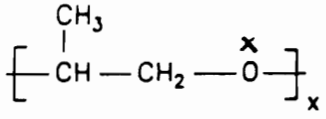

PPO repeat unit – soft segment

Larger Scale

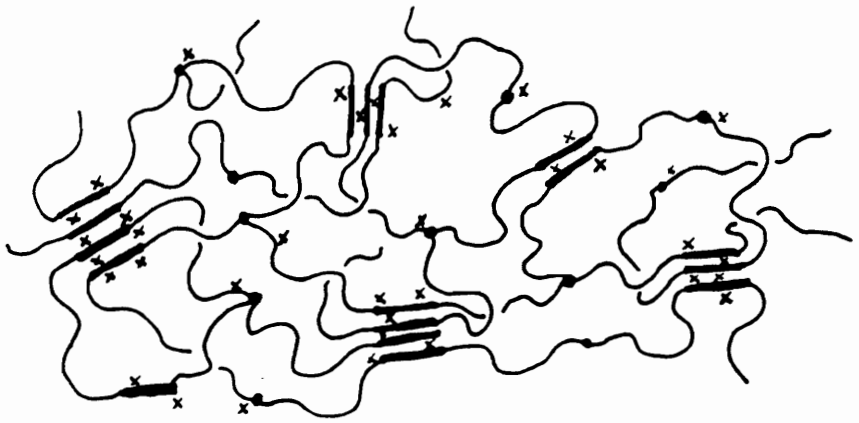

$x = H_2O$

Figure 5.16. Potential Sites for Water to Interact with Polyurethane Foams: (a)Ideal chemical structure and (b)simplified microphase separated molecular model

the higher hard segment plaque, P4, adsorbs about 20 percent more moisture than that of P1 at 38°C. This rather significant increase is to be expected since there are four times as many urea linkages available in P4 versus P1. As discussed above, the urea based hard segments are thought to have a greater affinity for water than that of the soft segments. In an attempt to further answer the above questions on the affinity of water for these materials and how humidity effects the viscoelastic behavior, the stress relaxation results for the two foams possessing the extremes in hard segment content, F1 and F4, are now presented.

The log $\sigma(t)$-log t stress relaxation behavior at 30°C and 90°C from low to high humidity is shown in Figures 5.17 and 5.18, respectively, for foams F1 and F4. The percent stress decay values at 30°C, 60°C, and 90°C are summarized in Table 5.8. At these three temperatures, the stress level at a given time does decrease systematically with increasing relative humidity as shown in Figures 5.17 and 5.18. This behavior is consistent with reports in the literature for studies performed in compression under controlled humidity and temperature(40,47,49). In addition, it also indicates that water is acting as a plasticizing agent by causing increased chain slippage.

Interestingly, the effect of humidity on the stress relaxation behavior is not that significant at 30 and 60°C for both F1 and F4 as indicated by the numbers in the Table 5.8. The change in the amount of stress decay for F1(15%) is actually slightly greater than that of F4(10%) at 30°C and about the same at 60°C. Thus, this indicates the effect of humidity on the relaxation behavior at 30°C is greater for F1 than F4 and hence suggests that the influence of water with F1 is greater than that for F4. However, at 60°C, foams F1 and F4 behave quite similarly. At 90°C, the effect of humidity on the stress relaxation behavior is more significant for both foams F1 and F4(see Table 5.8 and Figure 5.18). Interestingly, this effect is now greater for F4 than F1 as shown by comparing the response surfaces in Figure 5.18. In addition, the change in the percent stress decay for F4(54%) is higher than that of F1(35%). Also, the relaxation behavior at 90°C- 100%RH for F4 does exhibit rather non-linear results for the log $\sigma(t)$-log t while that of F1 is rather linear at all conditions at 90°C(see Figure 5.18). These differences in relaxation behavior for both foams F1 and F4 indicate that water is interacting more with F4 due to its higher hard segment content. It also appears from the change in the amount of relaxation occurring at 30°C and 90°C that the weight uptake of water

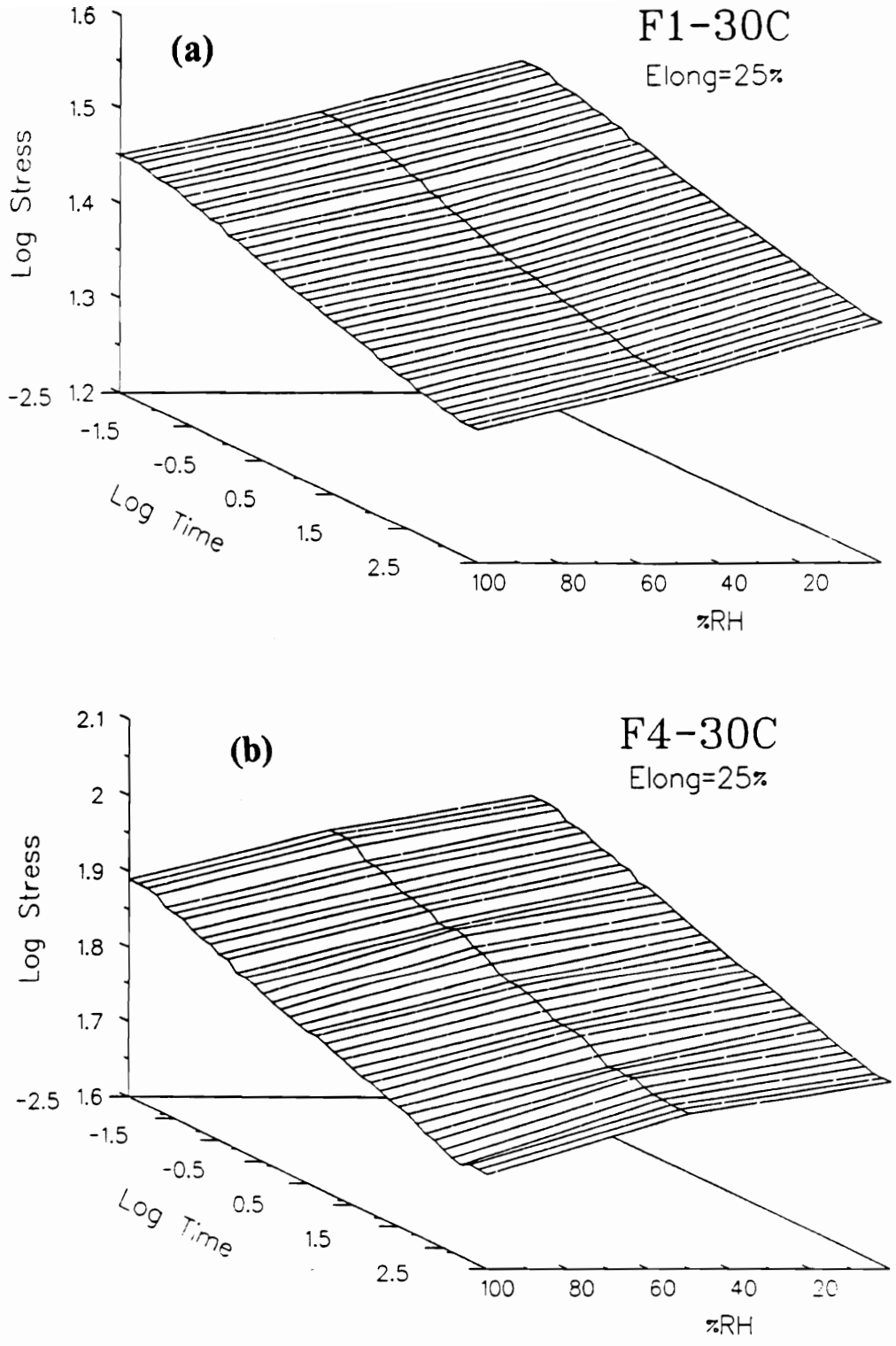

Figure 5.17. Effect of Humidity on the Stress Relaxation Behavior at 30°C for Foams F1(a) and F4(b)

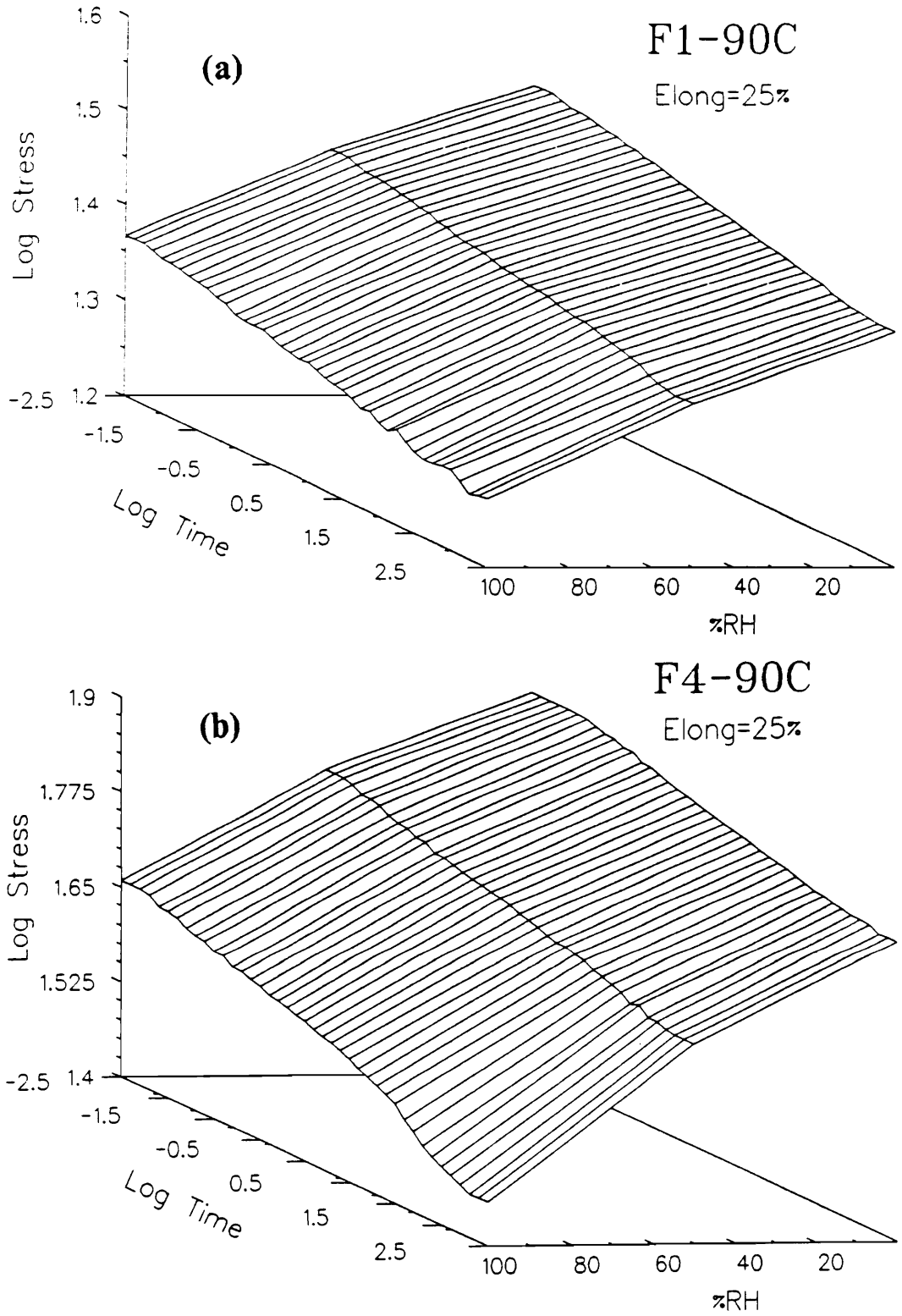

Figure 5.18. Effect of Humidity on the Stress Relaxation Behavior at 90°C on Foams F1(a) and F4(b)

Table 5.8: Percent Stress Decay at Different Temperature/Humidity Conditions

Foam	Temperature(°C)	% Stress Decay(from 0 to 180 min.'s)		
	|%RH=	0-15	50	95-100
F1	30	20	21	22
F4	30	30	31	32
F1	60	20	22	23
F4	60	28	29	32
F1	90	17	19	23
F4	90	24	28	37

increases to a greater extent with temperature for F4 in comparison to F1. This trend is also consistent with the few results obtained from the weight up-take studies at 23°C and 38°C. One possible reason for this increased effect of humidity on the stress relaxation behavior of F4 at the higher temperatures, is the ability of water to enter into the hard domains is more facilitated by the weakening of the hydrogen bonding with increasing temperature.

In summarizing the results for the effect of humidity as well as temperature(up to 90°C) on the stress relaxation behavior for the three hour time period, the 3-dimensional response surfaces are shown in Figures 5.19 and 5.20 for foams F1 and F4, respectively. Both F1 as well as F4 show that as one increases temperature, the rate of relaxation for the most part is lower, except at the highest relative humidities and especially for F4 at 90°C. At low relative humidities, the thermal dependence of the stress decay rates indicate that the approach to an equilibrium stress level is faster and has been accelerated by increasing the temperature. However, this is not the case at the higher temperatures of 125°C and 140°C as displayed in Figures 5.3 and 5.4. Finally, as shown in Figures 5.19 and 5.20, the effect of increasing relative humidity at 30 and 60°C is small, but is much greater at 90°C. In short, based on results presented and discussed for the stress relaxation behavior of these materials, it is concluded at this point that temperature has a more significant effect than relative humidity on the viscoelastic nature of flexible polyurethane foams. In continuation of the understanding of these effects as well as others on the viscoelastic behavior of flexible foams, results from a more applications oriented test, i.e. compression load relaxation, are presented in the following section.

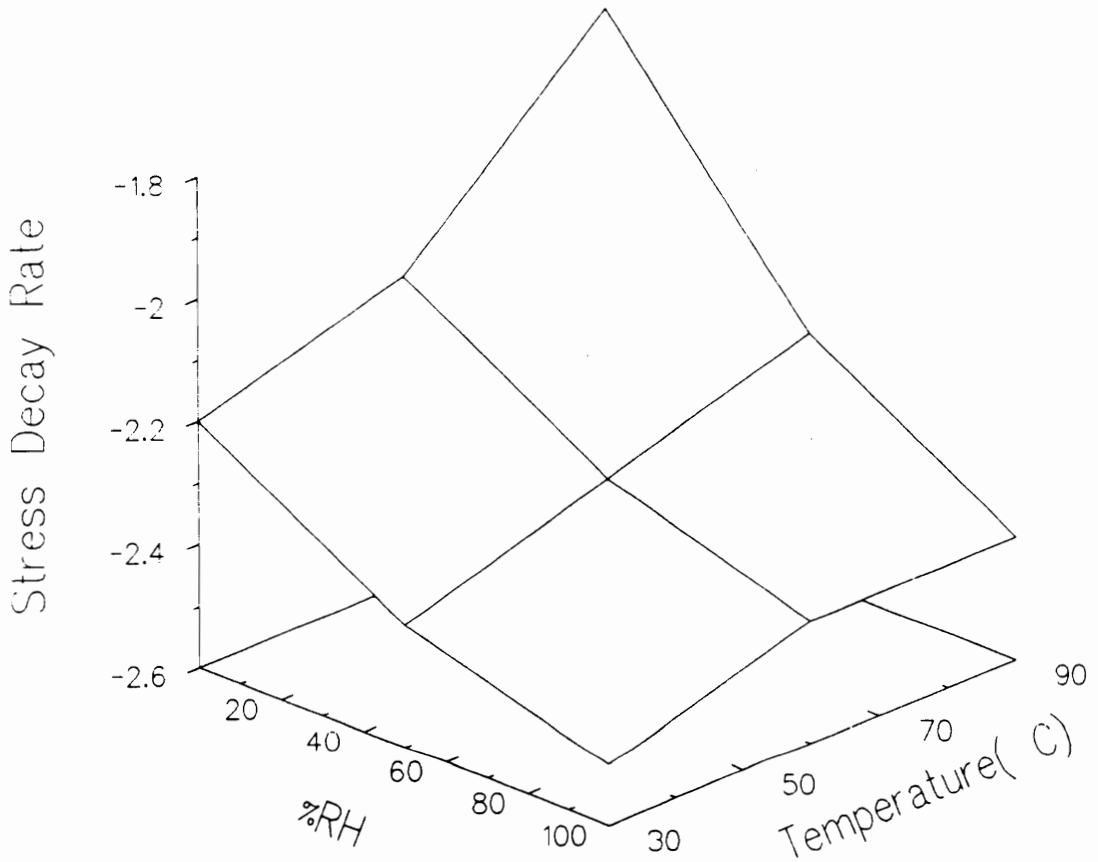

Figure 5.19. Effects of Temperature and Humidity on the Stress Relaxation Behavior for Foam F1

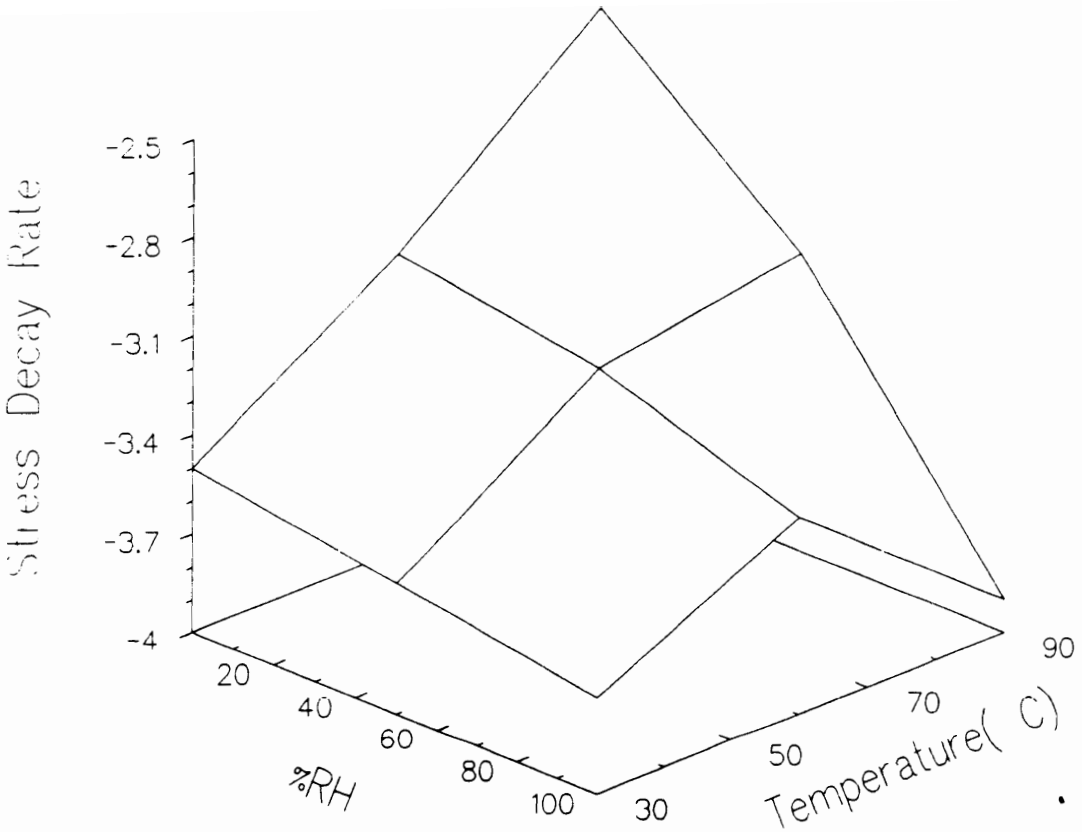

Figure 5.20. Effects of Temperature and Humidity on the Stress Relaxation Behavior for Foam F4

5.2 Compression Load Relaxation

Upon reviewing the literature, it became clear that the studies evaluating the compressive load in flexible foams were mostly limited to single viscoelastic property measurements and also were few in number from the standpoint of exposing foams to various conditions while carrying out the viscoelastic measurements. Thus, in this section, results are presented that were obtained for the compressive load relaxation behavior at a constant strain level under controlled conditions for foams F1-F4. Before discussing these results, some background information is given concerning: (a) the compressive load-strain behavior for these foams, (b) the approach taken to evaluate the load-time data, and (c) the effect of strain on the load relaxation behavior.

The compressive load-strain behavior along with the different "regimes" for this behavior are presented in Figure 5.21 using the response for F3. Generally speaking, the shape of the load-strain behavior for the other foams tested is very similar. As noted, a linear elastic region takes place up to a ca. 10 percent strain level at which point elastic buckling of the struts is believed to begin and to continue up to 60-70 percent strain. In the last region, the cellular walls begin to densify near a 60 percent strain level. As discussed in the literature review, other investigators of flexible polyurethane foams have also observed and attributed the different "regimes" for the compressive load- strain behavior to similar ranges of strain level as shown in Figure 5.21(33-35). Based on the non-linear behavior observed in Figure 5.21, it is expected that the changes in the cellular textures with strain are likely to influence the viscoelastic behavior of the load and/or the thickness of the foam. Before addressing this point, the general load relaxation behavior is discussed. An example of this behavior is shown in Figure 5.22 for F4 at 30°C-50%RH and at a constant strain level of 65 percent. In attempt to quantify the relaxation rate of these materials, the load relaxation has also been plotted in the form of log load(t) vs log t in Figure 5.22b. From the slope of this rather linear relationship, the rate of relaxation or the load decay rate is obtained. As discussed earlier, a similar power law fit has also been observed for the tensile stress relaxation data of these same foams. A

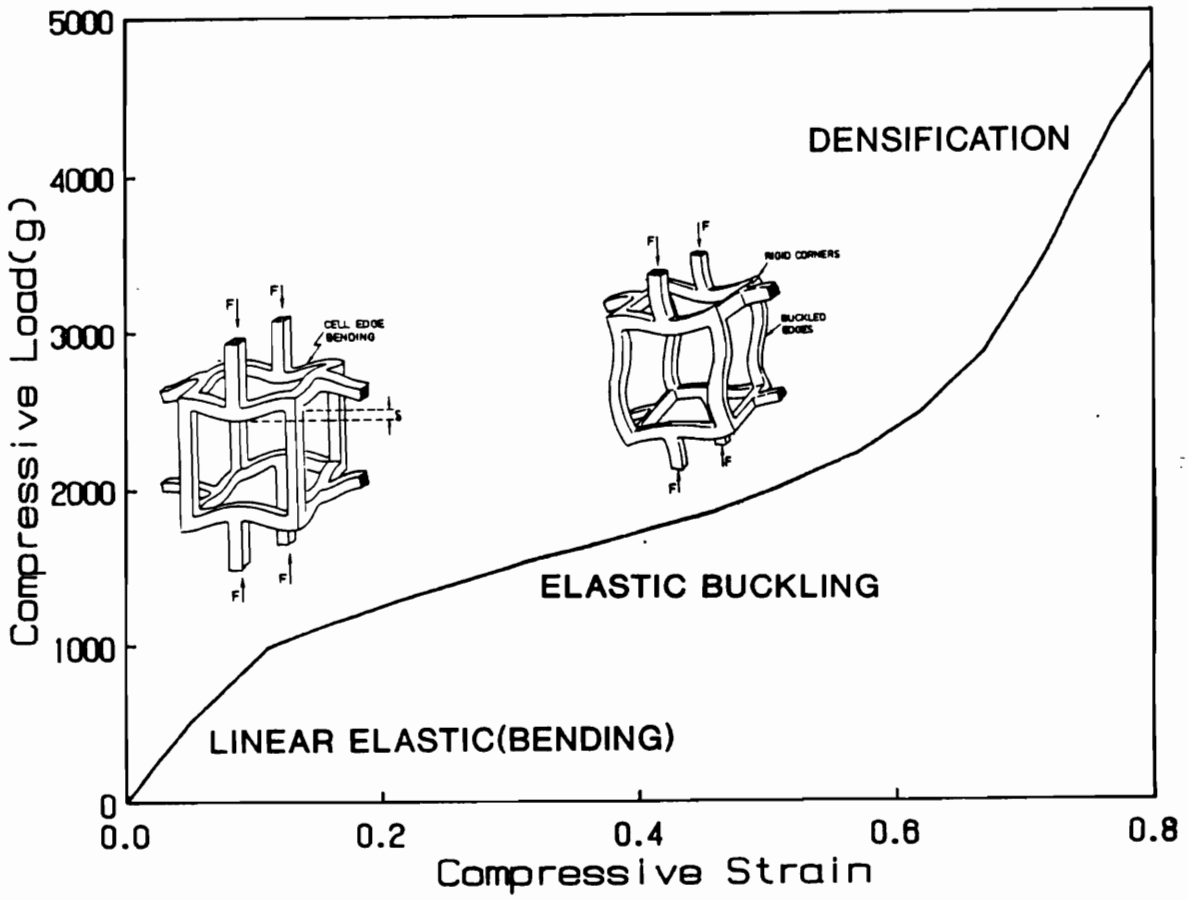

Figure 5.21. Compressive Load Strain Behavior for Foam F3

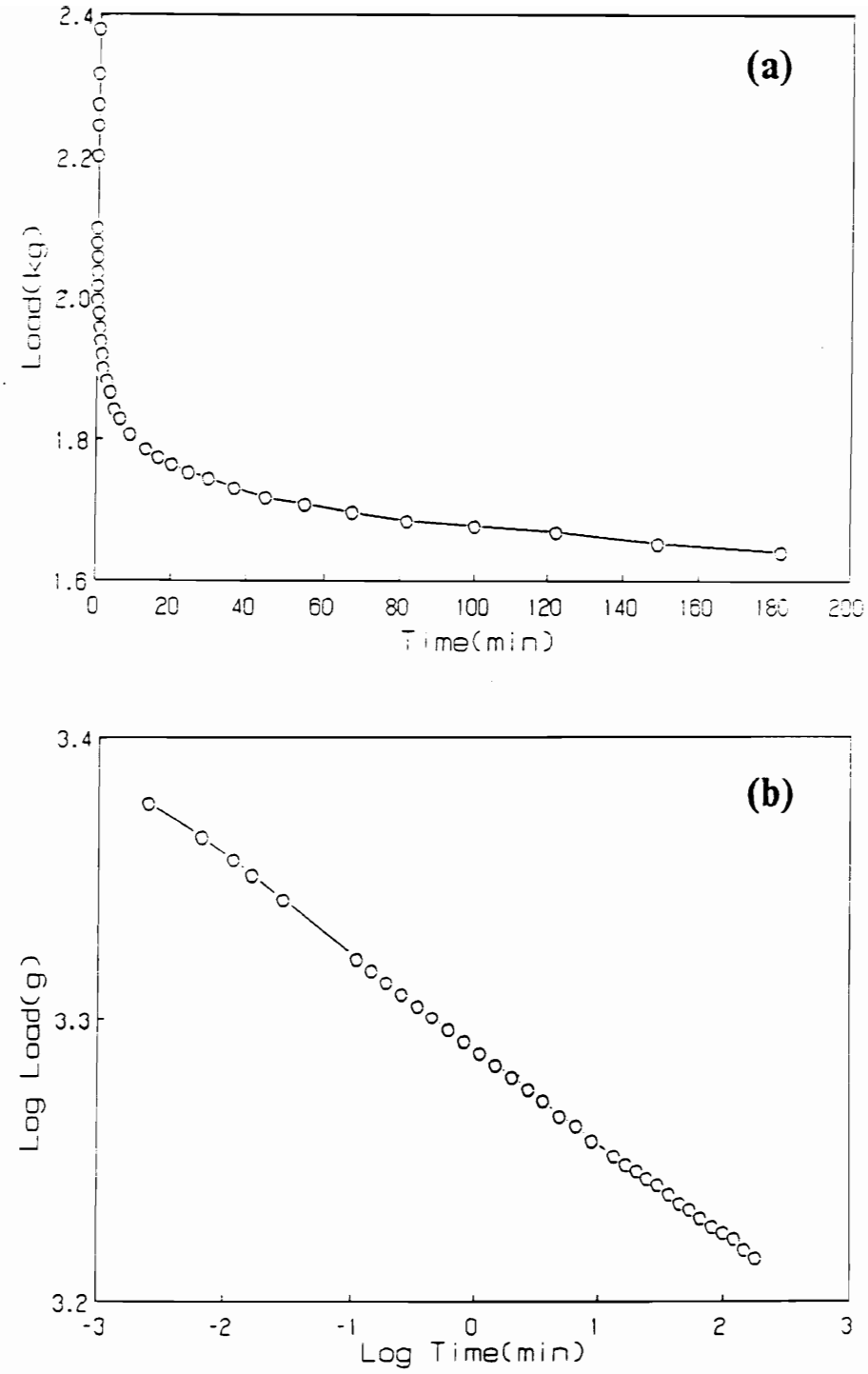

Figure 5.22. Load Relaxation Behavior of Foam F4 at 30°C-50%RH: (a) Load-time curve and (b) log load-log time behavior

similar fit of the data has also been reported by a few investigators of flexible polyurethane foams, polyurethane elastomers, and other polymeric network materials (2,53,54,91)

By utilizing the above method of evaluation for the load relaxation data, the load decay rate as a function of strain level was obtained and is displayed in Figure 5.23 for Foam F3 at 30°C and 50%RH. As shown in Figure 5.23, the rate of relaxation is fairly constant up to a strain level of 65 percent or right at the verge of where densification is thought to begin to take place. At strains greater than 65% the load decay rate increases and reaches a maximum near 75 percent. Similar behavior in this same region is observed for foams F1 and F4 as displayed in Figure 5.24 and summarized in Table 5.9. The increase in the rate of relaxation at the higher strain near 65 percent and greater is thought to be related to an intensification of the local strain of the cellular wall material. This local strain on the solid material is likely caused by the densification of the foam as exhibited in Figure 5.21 for the compressive load-strain curve. The maximum in the load decay rate-strain behavior for foams F3 and F4 at 75 percent is thought to be related to the point where complete densification of the foam occurs. In evaluating this hypothesis, estimates of the densification strain for foams F1-F4 were made using the following empirical equation developed by Ashby,

$$\varepsilon = 1 - 1.4(\frac{\rho}{\rho_s}) \qquad [5.2]$$

where ε is the densification strain, ρ is the density of the foam, and ρ_s is the density of the cellular wall material(33). The values for ε varied from 0.93 to 0.97 for foams F1- F4, respectively; thus, indicating that this maximum is not related to complete densification. However, it does suggests that upon complete densification the rate of decay is thought to approach the rates which were rather independent of strain level.

Based on the above results for the effect of strain level on the load decay rate and the common indentation load deflection(ILD) ASTM test used in testing flexible foams, the majority of the results presented in the paragraphs to follow were obtained at a 65 percent strain level(85). The results that are discussed will consider the effects of temperature as well as humidity on the load relaxation

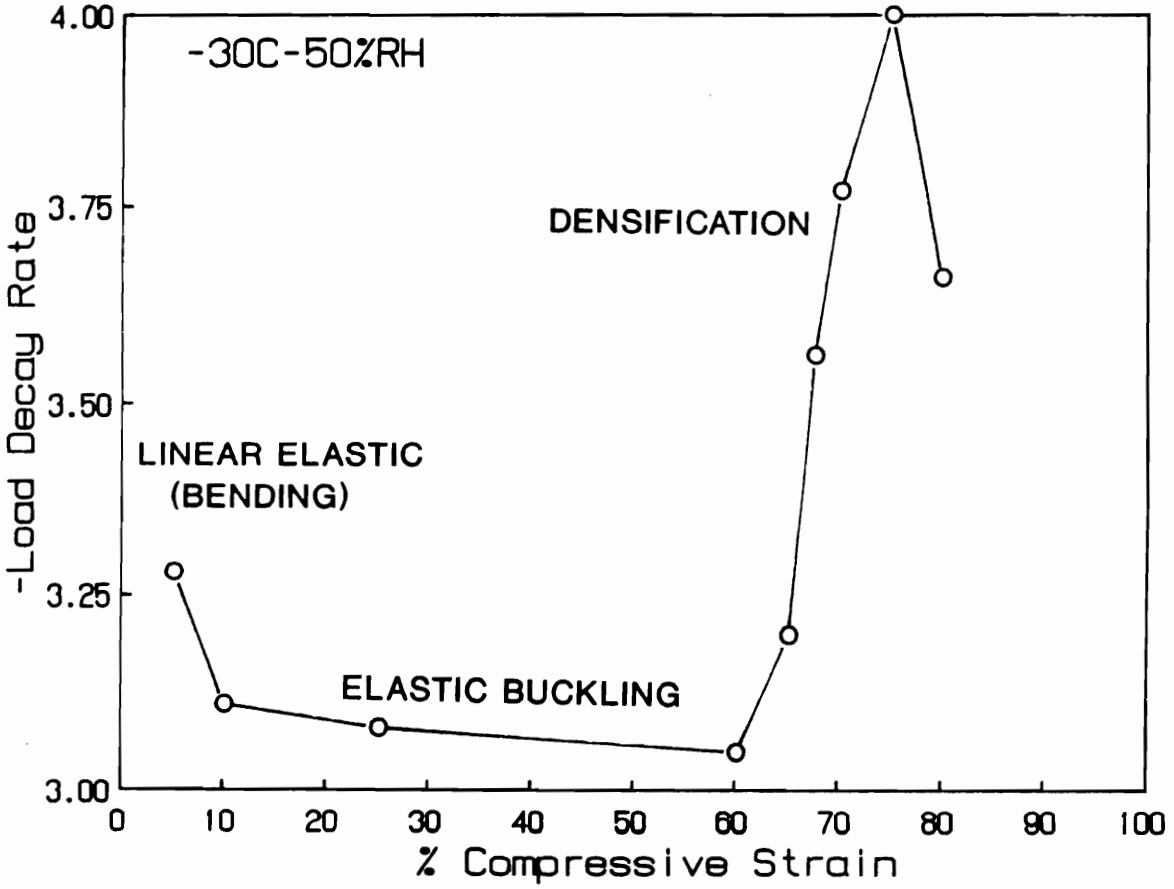

Figure 5.23. Effect of Strain Level on Load Relaxation Behavior for F3: Rates measured over a three hour time period

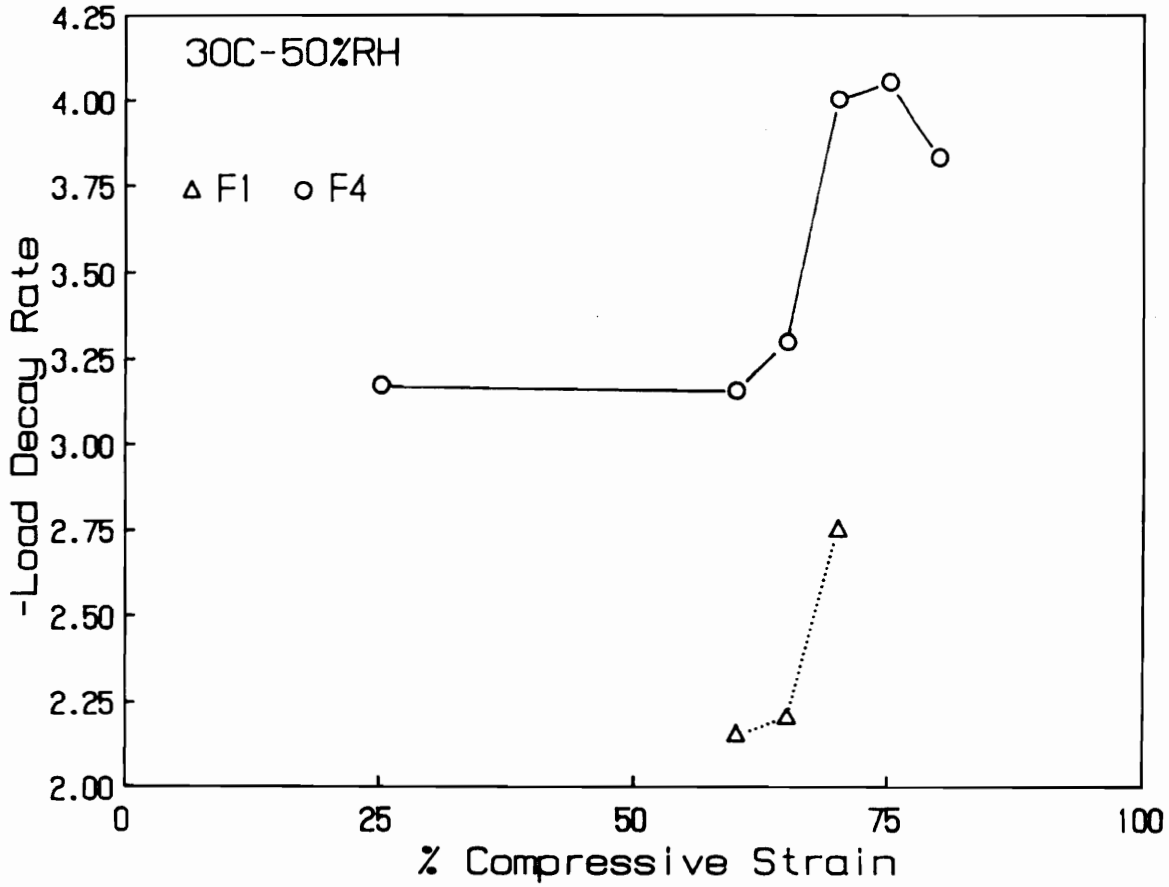

Figure 5.24. Effect of Strain Level on Load Relaxation Behavior for Foams F1 and F4: Rates measured over a three hour time period

Table 5.9: Summary of Load Relaxation Behavior at Variable Strain Levels

Strain Level(%)	-Load Decay Rate x 10^{-2}(% Load Decay)			
Foam =	F1	F2	F3	F4
5			3.3*(30)	
10			3.1(29)	
25			3.1*(30)	3.15(32.5)
60	2.15(22)	3.0(29)	3.05(30)	3.2(31)
65	2.2(22)	3.1(30)	3.2(30.5)	3.3(31)
67.5			3.55(34)	
70	2.75*(27)	3.5(33)	3.75(35)	4.0(36)
75		3.6*(33)	3.95(36.5)	4.05(37.5)
80			3.65*(36)	3.8*(37)

1. Time frame is from 0 to 180 minutes;
2. Correlation coefficient is within 0.995-0.999 except where * appears
3. Error in load decay rates is a maximum of 4 percent and error in load decay values is a maximum of 3 percent; these values are based on results obtained from testing several samples of a given foam at one condition

behavior, long term relaxation behavior and the effects of thermal annealing the foams prior to testing. In addition, the effect of hard segment content on the load relaxation behavior, the hysteresis behavior, compression set, and finally, a comparison between relaxation data obtained in compression and tension will be discussed. Also, the majority of the results presented are from data collected using foams F1 and F4 which provide the extremes in hard segment content.

5.2.1 Effects of Temperature on Load Relaxation

The 3-dimensional surfaces for the log load(t)-log t variable temperature compression load relaxation curves for foams F1 and F4 are presented in Figures 5.25 and 5.26, respectively. In addition, the initial load levels, the stress decay rates, and the percent load decay values at the different temperatures are summarized for F1 and F4 in Tables 5.10 and 5.11, respectively. The initial load for F1 increases for the most part up to temperatures near 100°C to 125°C, while the initial load for F4 changes very little with increasing temperature except for the decrease in this level near 85 to 100°C(see Tables 5.10-5.11). The 3-hr stress level for both foams behave similarly with increasing temperature as exhibited in Figures 5.25 and 5.26. As shown in Figures 5.25 and 5.26, fairly linear behavior for the log load(t) vs log time over the three hour testing period is exhibited up to temperatures of 100°C. In addition, the rates of relaxation and percent load decay values both decrease(even more so in F4) with increasing temperature in the range of 25°C to 100°C. This decrease in the amount of relaxation indicates, as suggested earlier for the tensile stress relaxation studies of these same foams, that the approach to an equilibrium load level appears to be accelerated with increasing temperature.

At temperatures near 125°C and greater, the relaxation rates and the percent load decay values for foams F1 and F4 reveal that there is a significant change in the relaxation behavior from 100°C to 125°C (see Tables 5.9- 5.10). Also, this change can be observed in the non-linear behavior exhibited in Figures 5.25 and 5.26 for foams F1 and F4, respectively. As explained earlier for the variable temperature tensile stress relaxation behavior of these same foams, this significant increase

Table 5.10: Variable Temperature Load Relaxation Results for Foam F1

Temp(°C)	L_o(kg)	-Slope(x10²)*	% Load Decay**
30	3.09	2.2	22
60	3.21	2.0	20
85	3.34	2.0	20
100	3.51	1.9	20
125	3.42	2.4	26
140	3.11	4.2	44

* Correlation function was in the range of 0.995 to 0.999 except at 125°C and 140°C. Maximum error is 4 percent

** Based on data obtained for several samples at same condition, the maximum error in the % load decay is 3 percent; time frame is 180 minutes

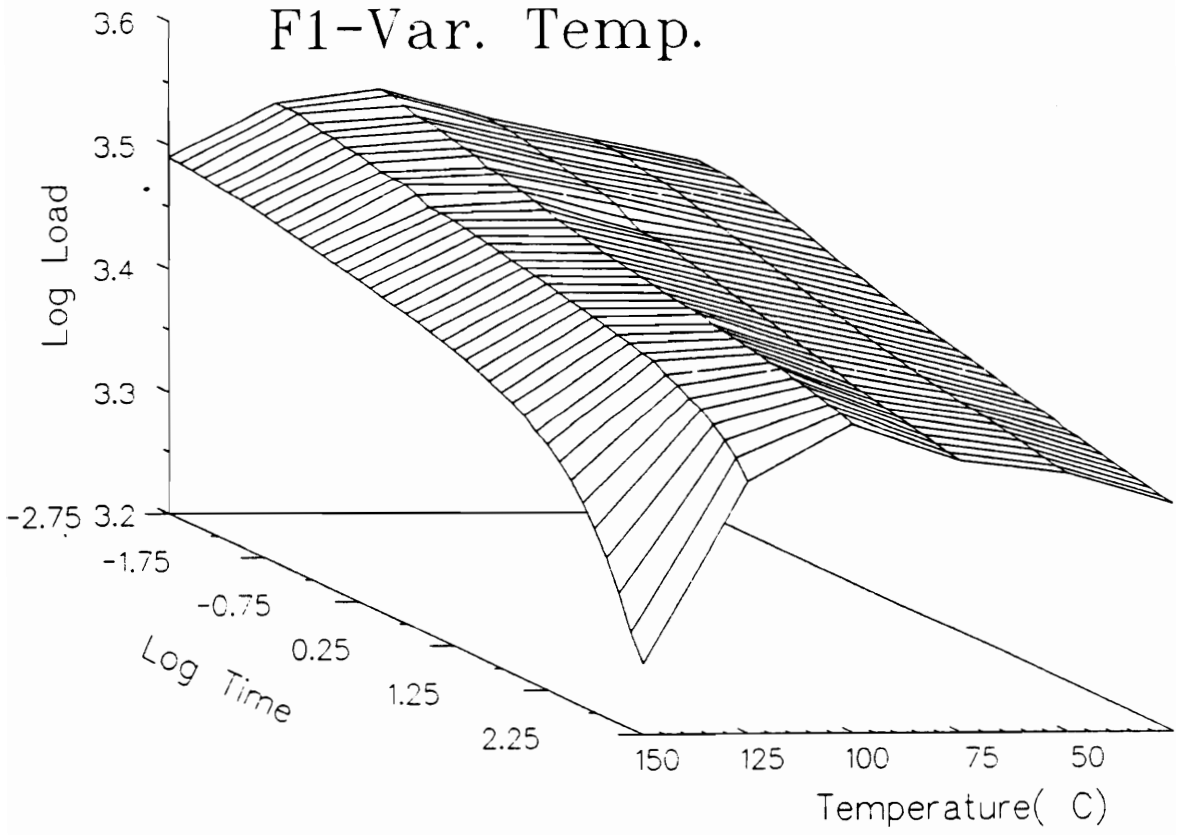

Figure 5.25. Log Load-Log Time Variable Temperature Load Relaxation Behavior for F1: Measured at a 65% constant strain level

Table 5.11 Variable Temperature Load Relaxation Results for Foam F4

Temp(°C)	L_o(kg)	-Slope(x10²)*	% Load Decay**
30	2.72	3.2	30
60	2.71	2.9	27
85	2.72	2.7	26
100	2.70	2.6	26
125	2.64	2.8	30
140	2.59	3.6	37

* Correlation function was in the range of 0.995 to 0.999 except at 125°C and 140°C.; maximum error is 4 percent

** Values obtained over 180 minutes; Maximum error is 3 percent

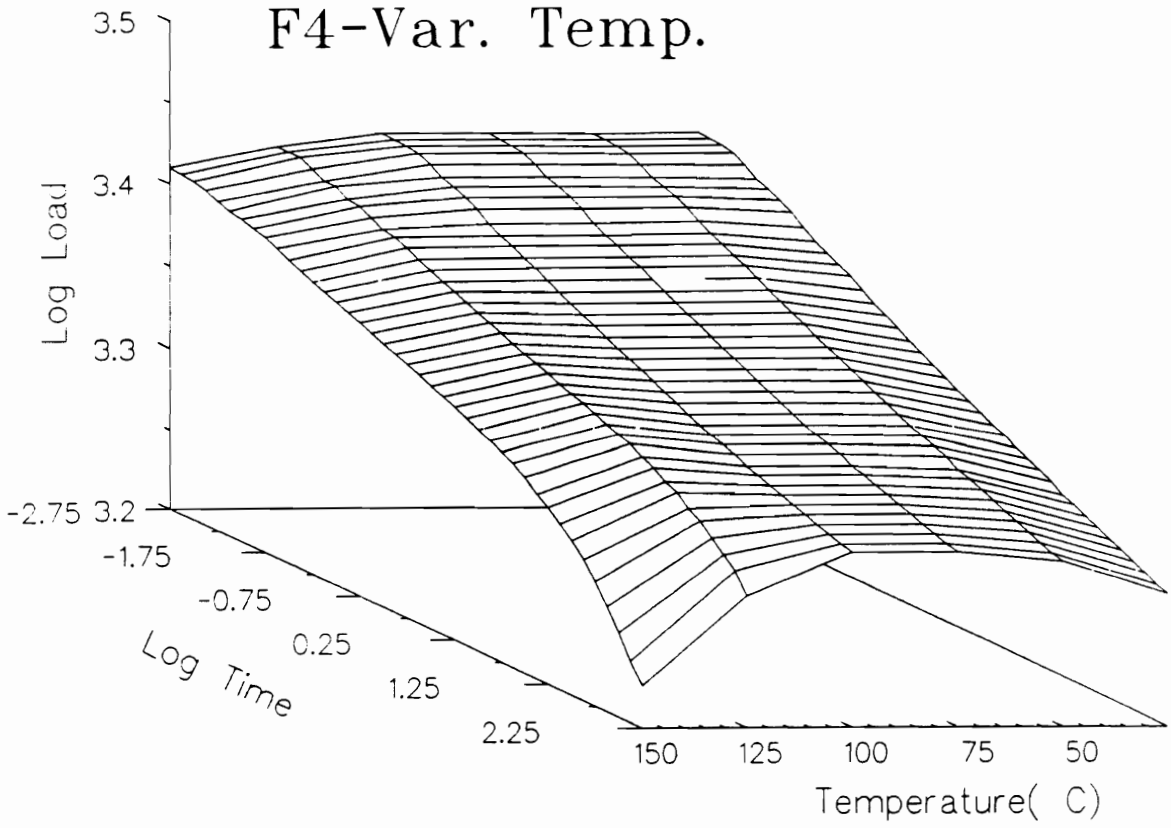

Figure 5.26. Log Load-Log Time Variable Temperature Load Relaxation Behavior for F4: Measured at a 65% constant strain level

in the amount of relaxation is attributed to an increase in the amount of hydrogen bonds that are being disrupted with increasing temperature as well as chain scission that is thought to take place within the urea and urethane linkages. Both of these changes in the microstructure of the foams which have been indicated by the FTIR-thermal studies will, of course, lead to further load decay(Recall Figures 4.2- 4.10).

Additional comments on the load relaxation behavior can be made upon further comparing the results for F1 and F4. First, the behavior of the percent load decay with temperature does fit the empirical model given earlier in equation [5.1] as demonstrated in Figure 5.27 for F1 and F4. The constants for the front factors(C_1 and C_2), the relaxation temperature constants(τ_1 and τ_2), and the transition temperature, T_o are given in the Table 5.12. As discussed earlier in the tensile stress relaxation studies, τ_1 does give insight to the thermal effects on these foams up to 100°C, while τ_2 provides additional understanding of the thermal effects at the temperatures greater than 100°C. The values of τ_1 for foams F1 and F4 indicate as found for tensile stress relaxation temperature is accelerating the compressive stress relaxation to a greater extent in F4. On the other hand, the lower value for τ_2 for F1 indicates that a greater amount of stress decay is taking place in F1 than for F4 at higher temperatures. This signifies that the additional factors for load decay which were mentioned in the previous paragraph have a greater impact on the morphological features in foam F1.

As also shown in Figure 5.27, the load decay is greater for F4 than F1 up to temperatures of 125°C. This difference is thought to be related to F4 having the higher hard segment content of the two foams. By possessing a higher hard segment content, this provides more available hydrogen bonds for disruption which will lead to further relaxation. At 140°C, on the other hand, the reverse behavior is observed which is thought to be related to degradation that occurs at temperatures greater than 100°C for both the urethane and urea linkages in foams F1 and F4. As discussed in the previous chapter for the FTIR thermal behavior of the plaques of these foams, chain scission is believed to be more significant effect in foam F1 than F4 and thus is thought to promote more load relaxation in F1 at the higher temperatures. A similar explanation was also given earlier for comparable tensile stress relaxation results presented for foams F1 and F4.

Table 5.12: Constants for Thermal Dependence of Load Decay for Foams F1 and F4

Foam	$\tau_1(1/°K)$	C_1	$\tau_2(1/°K)$	C_2	$T_o(°K)$
F1	494	40	12.5	1.09	373
F4	272	90	21.5	3.71	375

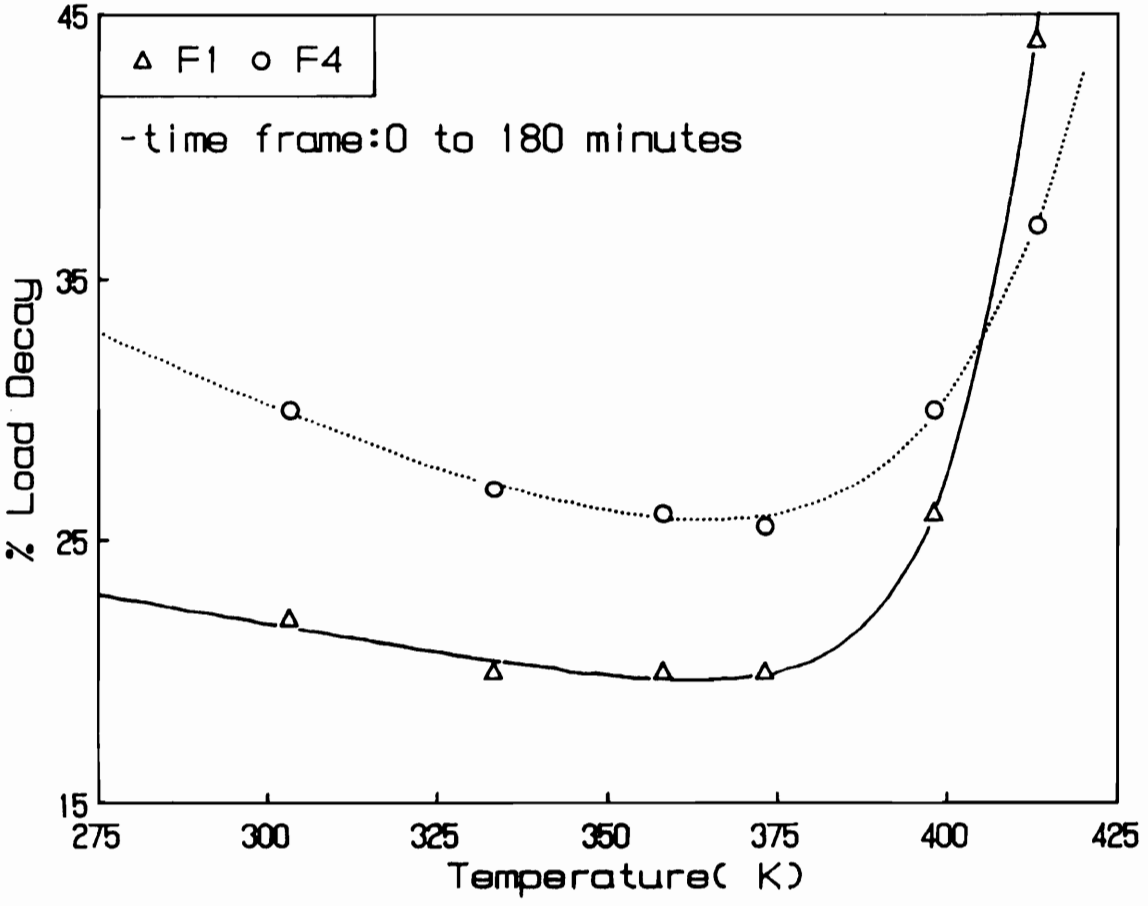

Figure 5.27. Effect of Temperature on Load Relaxation Behavior for Foams F1 and F4

5.2.2 Effect of Prior Thermal Annealing on Relaxation Behavior

In this section, the effect of thermal annealing the foams prior to testing at 30°C and 15%RH is addressed. Furthermore, the long term relaxation behavior at low relative humidity for 30°C and 100°C is discussed. First, the effect of thermal annealing foams F1-F4 has been evaluated since the foams to be investigated were recently manufactured. Also, the relaxation behavior of these foams has been characterized at high temperatures. Thus, if any additional crosslinking occurs during testing at high temperatures this may have an effect on the results. Such additional crosslinking might be expected to occur due to excess TDI used in manufacturing these foams(recall that a 110 index applied to all foams).

As shown earlier in Figures 5.25 to 5.27, a decrease in the amount of load relaxation is observed up to temperatures of 100°C. Therefore, in determining if further crosslinking is taking place and in turn influencing the load relaxation response, a thermal annealing temperature of 100°C was used. As shown, however, in Figure 5.28 for both F1 and F4, the thermal annealing at 100°C for approximately one week has little effect on the relaxation behavior at 30°C-15%RH. In comparing the behavior for the two foams, it does appear that the effect of annealing(what little there is) is more noticeable for F1 as seen by the slight upturn in the load near log time equal to 2.0(ca. 100 minutes) in Figure 5.28a. Similar behavior, to foam F1 has also been obtained upon thermal annealing F2 and F3 for 3 to 4 hrs at 100°C(data not shown here). Thus, the effect of thermal annealing the foams at 100°C over short and long time periods is believed to have very little effect on the load relaxation behavior; thereby, giving further credibility to the data presented in Figures 5.25 and 5.26.

As exhibited in Figure 5.28 for the long term relaxation behavior at 30°C and 15%RH, foams F1 and F4 do not demonstrate any significant signs of reaching equilibrium conditions. However, in comparing the behavior for the two, it does appear that foam F1 would likely reach an equilibrium load on a shorter time scale than F4. This trend is somewhat expected since F1 is of lower hard segment content and furthermore contains less hydrogen bonding which is again thought to

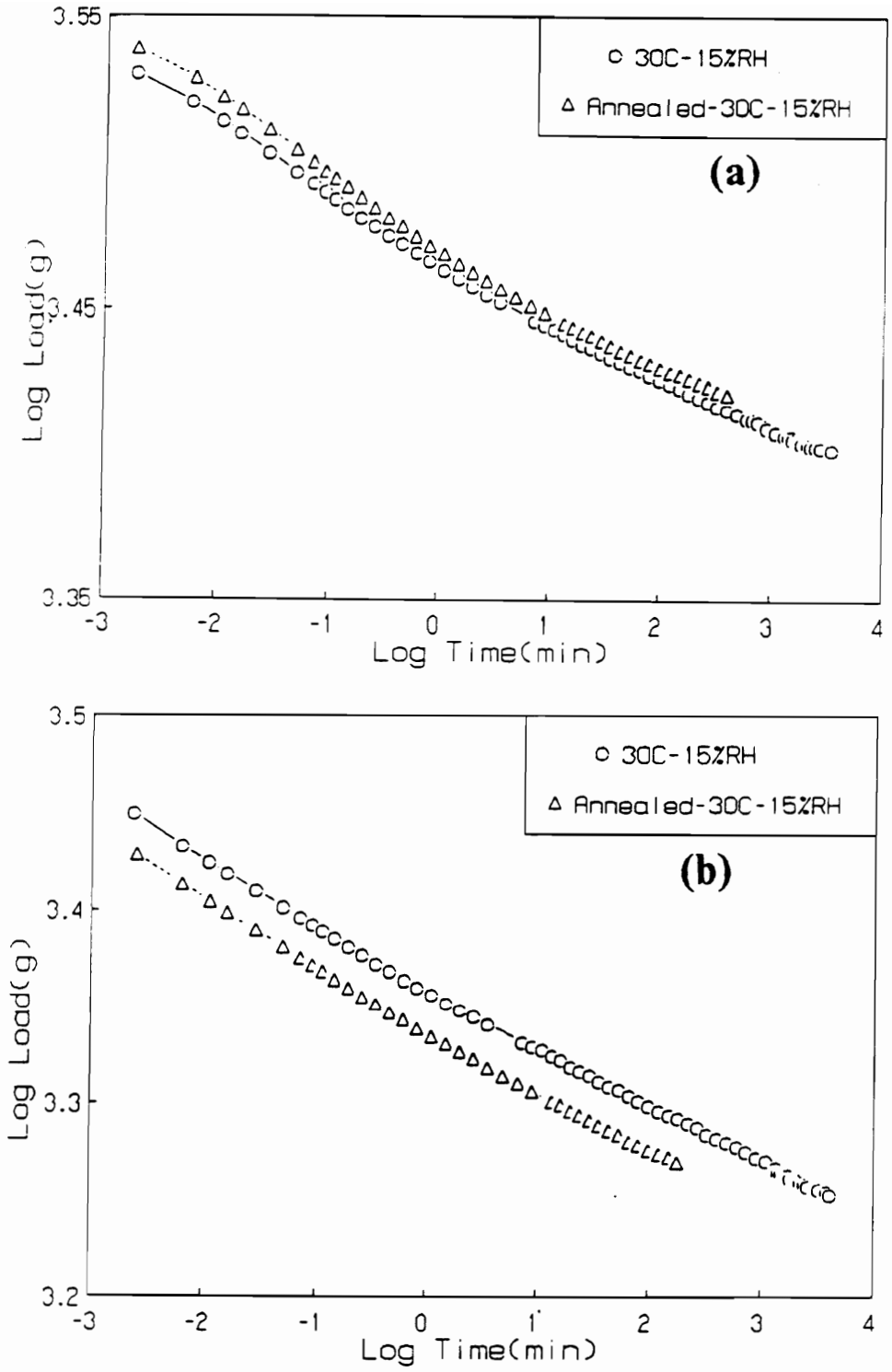

Figure 5.28. Effect of Thermal Annealing on the Load Relaxation Behavior for (a)F1 and (b)F4: Results obtained at 30°C-15%RH; prior annealing done at 100°C

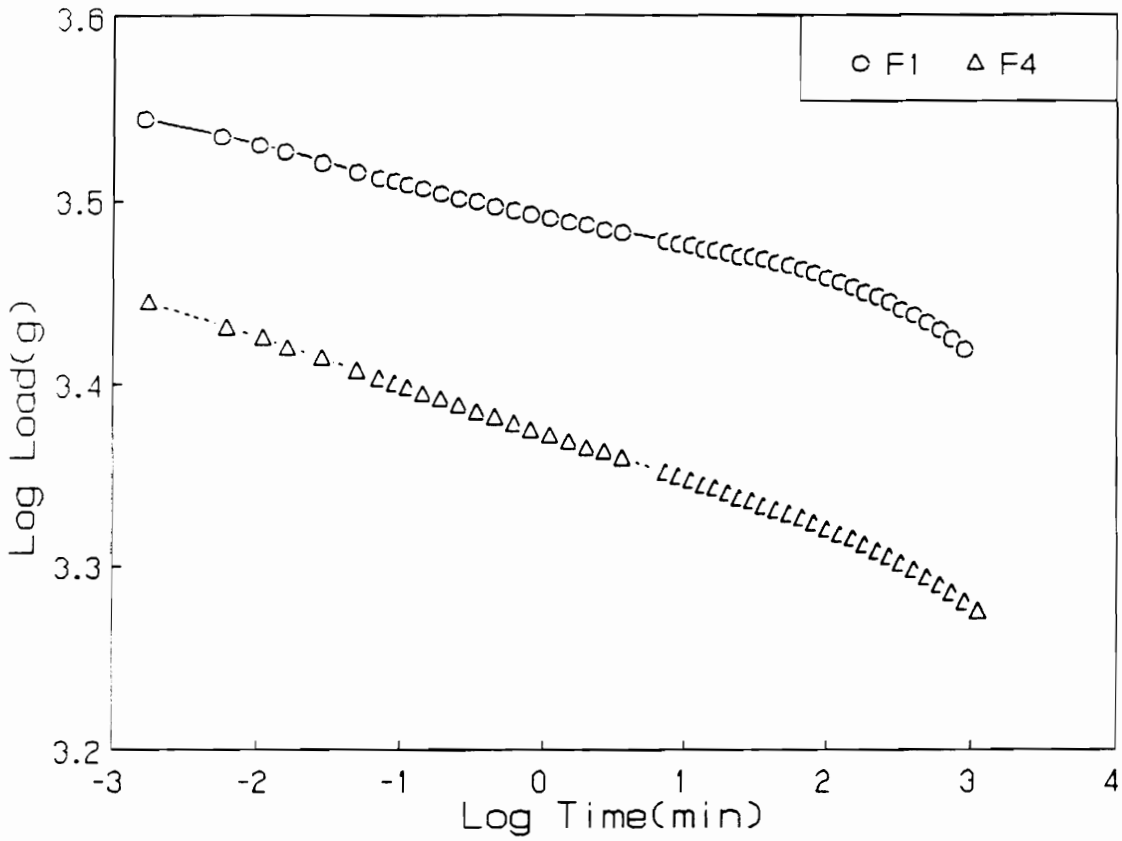

Figure 5.29. Long Term Load Relaxation Behavior at 100°C for Foams F1 and F4: Tests performed at a 65% constant strain level

be an important factor in the difference between the relaxation behavior for F1 and F4 at 30°C-15%RH. On the other hand, as shown in Figure 5.29, the relaxation behavior at 100°C over a 12 hour testing time period does exhibit deviation from linearity for both F1 and F4. This deviation from linearity begins at about 3 hours for both F1 and F4 and is believed to be related to additional hydrogen bond disruption and possibly some chain scission in the urea and urethane groups. Although, such additional changes as chain scission were not implicated by the FTIR-thermal analysis at 100°C, it is possible that this change as well as others are strain activated (recall Figures 4.5-4.9).

5.2.3 Effect of Humidity on the Load Relaxation Behavior

The log load-log t load relaxation behavior at 30°C and 85°C from low to high humidity is shown in Figures 5.30 and 5.31 respectively for foams F1 and F4. The load level at a given time does decrease rather systematically with increasing relative humidity for both foams at 30°C and more so at 85°C. As suggested earlier in the tensile relaxation studies, this decrease is attributed to water acting as a plasticizer.

At 30°C, the relaxation behavior for the 3 hour testing period is near linear when log load is plotted as a function of log t. This rather linear relationship also appears to hold over a 24 hour time period at 30°C-100%RH as shown in Figure 5.32 for both F1 and F4. It is possible in the case of F1 that the relaxation behavior at times greater than 24 hours will begin to deviate from linearity as shown in the slight downturn in the log load behavior near 24 hours(log time = 3.1)- see Figure 5.32. In comparing the results of F1 with F4(at 30°C), the percentage change in the relaxation behavior is slightly greater for F1 as shown by the results summarized for the load decay values and the load decay rates in Table 5.13. At 60°C, however, the percentage change in the rates of decay are the same for F1 and F4(see Table 5.13). The results obtained at 30°C therefore imply that water interacts more with F1 in comparison to F4, while at 60°C, this interaction is similar for the two

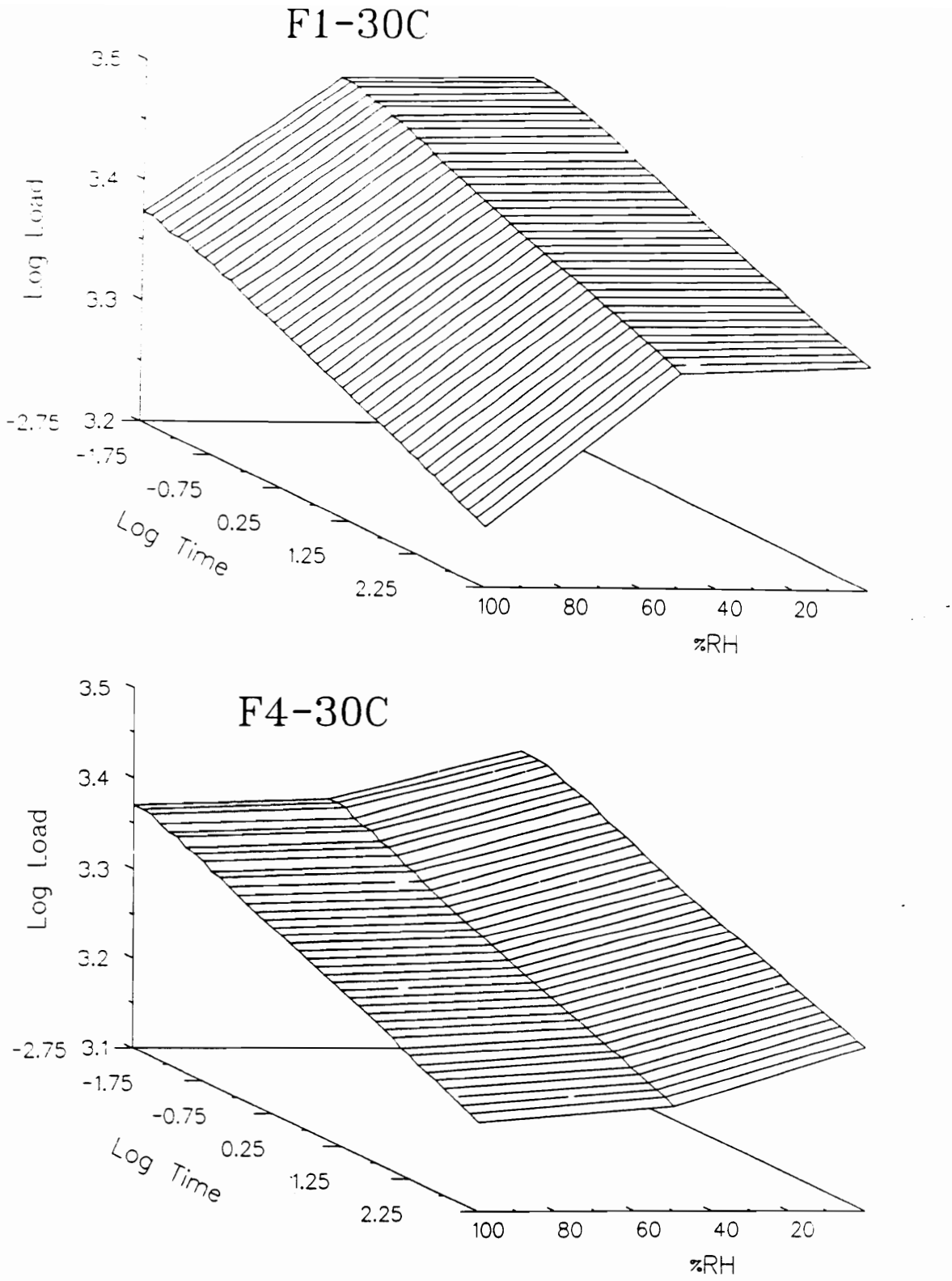

Figure 5.30. Effect of Humidity on the Load Relaxation Behavior at 30°C for Foams F1 and F4: Tests performed at a 65% constant strain level

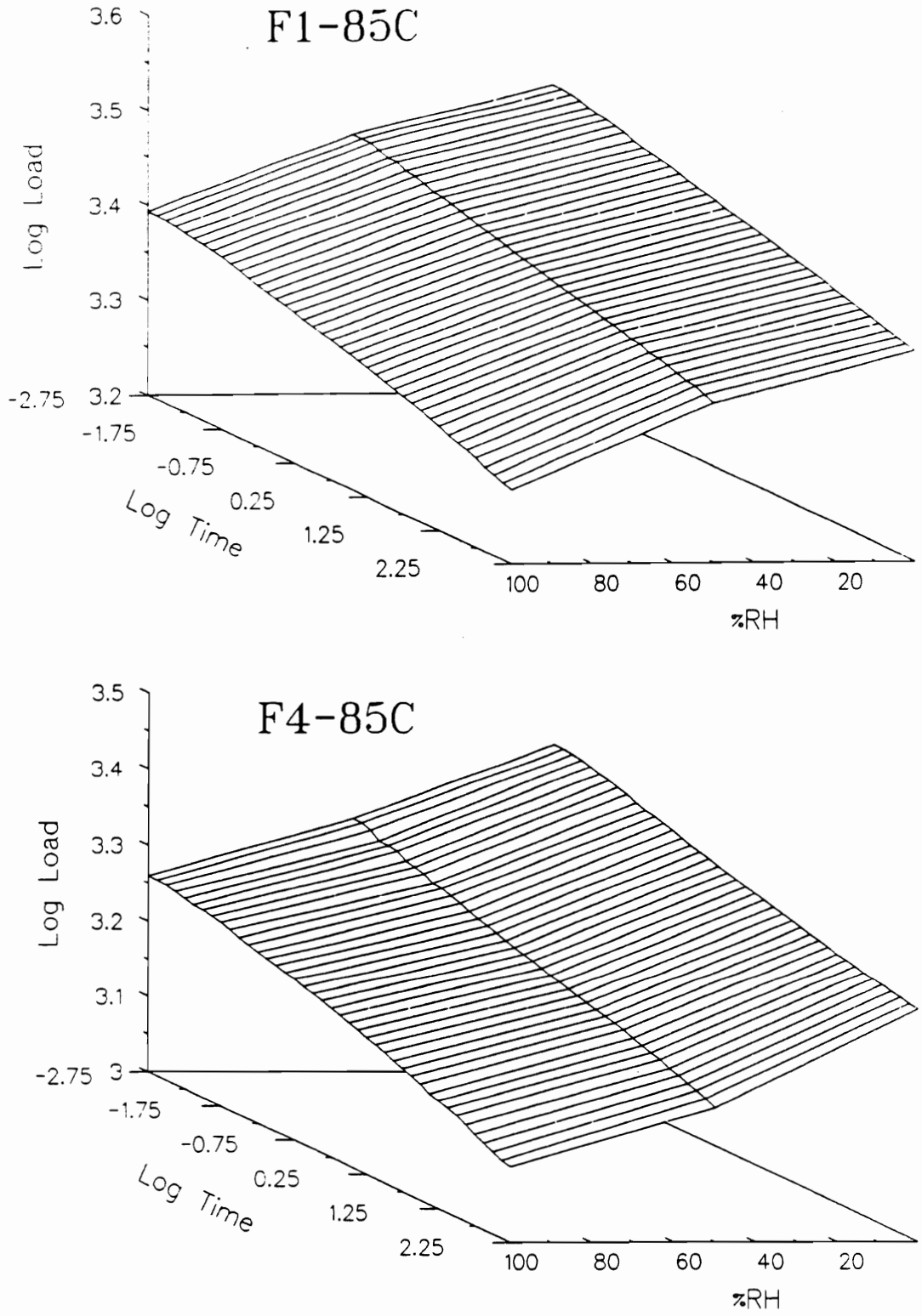

Figure 5.31. Effect of Humidity on the Load Relaxation Behavior at 85°C for Foams F1 and F4: Tests performed at a 65% constant strain level

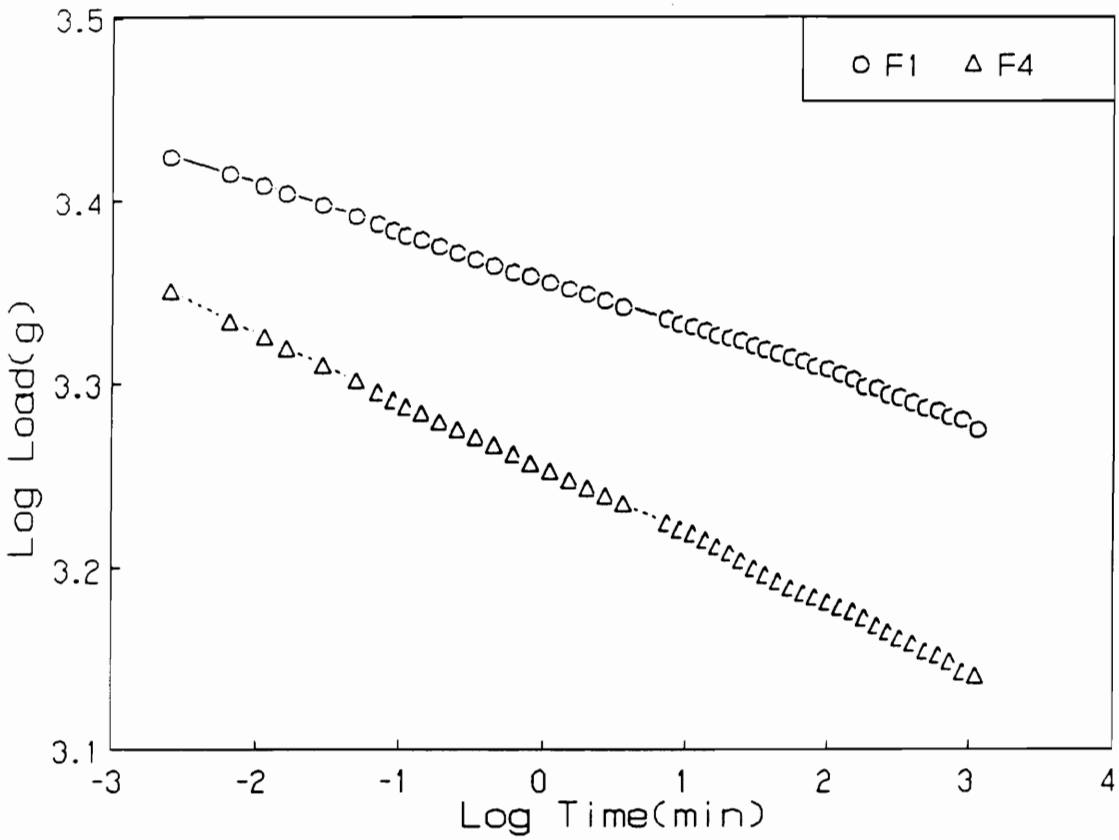

Figure 5.32. Long Term Load Relaxation Behavior at 30°C-100%RH for Foams F1 and F4: Tests performed at a 65% constant strain level

Table 5.13: Percent Load Decay at Different Temperature/Humidity Conditions

Foam	Temperature(°C)	% Load Decay(-Load Decay Rate x 10^{-2})		
	|%RH=	0-15	50	95-100
F1	30	22(2.2)	22(2.3)	25(2.6)
F4	30	30(3.2)	31(3.3)	33(3.6)
F1	60	20(2.0)	21(2.1)	25.5(2.5)
F4	60	28(2.8)	30(3.25)	32(3.5)
F1	85	20(2.0)	22(2.2)	24(2.4)
F4	85	26(2.7)	30(3.1)	32(3.5)

* Time frame is from 0 to 180 minutes;

** correlation coefficient is within 0.995-0.999 except at 85°C-95%RH

*** Maximum error for % load decay is 3 percent and that of the load decay rates is 4 percent; these values are based on several samples of a given foam that were tested at one condition

foams. Another interesting comparison for the results obtained at 30°C and 60°C, is the values of load decay rates are about the same at these two temperatures and for the most part slightly greater in magnitude at 30°C for both foams F1 and F4. This behavior is exhibited by the response surfaces in Figures 5.33 and 5.34 for F1 and F4, respectively.

As shown in Figure 5.31 at 85°C, the relaxation behavior is also rather linear for the log load(t)-log t for the 3 hour time period, except at 85°C-95%RH. The deviation from linearity in both F1 and F4 which occurs after 30 to 60 minutes of testing is demonstrated in Figure 5.35. At 85°C, the percentage change in the relaxation behavior is greater for F4 than F1 which suggests the influence of water is greater for F4 at higher temperatures. The load decay rates for the three hour testing period at 85°C, on the other hand, are similar to those at 30°C for both foams F1 and F4 as shown in the response surfaces in Figures 5.33 and 5.34. However, if one compares the decay behavior at 30°C-100%RH(Figure 5.32) and 85°C- 95%RH(Figure 5.35), it is apparent that over long time periods the amount of load decay becomes greater at 85°C. For example, the increase in the load decay values from 3 to 12 hours of testing for foam F4 is 12 percent at 30°C-100%RH and 19 percent at 85°C-95%RH, thus confirming the last statement. The long term behavior at 85°C-95%RH was not measured for F1, but similar results to F4 are expected upon comparing the increase in the load decay values at 30°C-100%RH to 85°C-95%RH. This suggestion is based on the deviation from non- linearity observed at 85°C-95%RH in Figure 5.35 for F1.

5.2.4 Effect of Hard Segment Content

As discussed above, the variation in hard segment content is believed to be a contributing factor to the differences in the load relaxation behavior for foams F1 and F4. The effect of the full range of hard segment content on the load relaxation behavior are presented in Figure 5.36 for foams F1-F4 at three different temperatures. In addition the load decay rates for the conditions of 30°C- 100%RH and 85°C-95%RH as a function of hard segment content are given in Figure 5.37. In both Figures 5.36 and 5.37, it clear that the load relaxation is greater for the higher hard segment

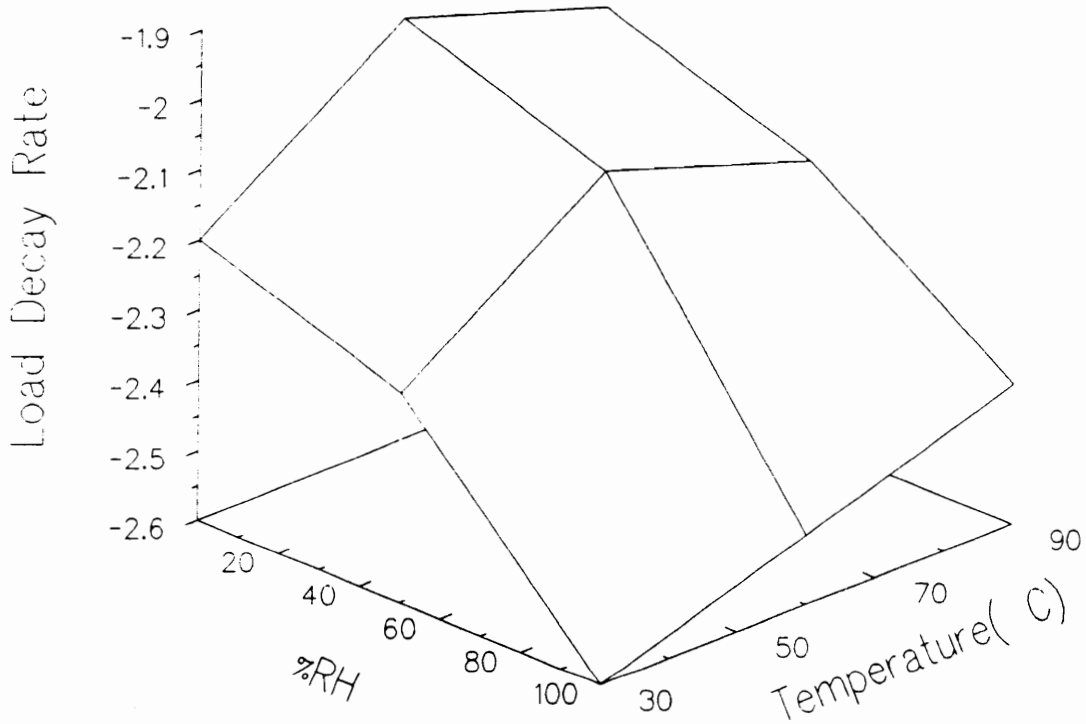

Figure 5.33. Effects of Temperature and Humidity on Load Relaxation Behavior for Foam F1

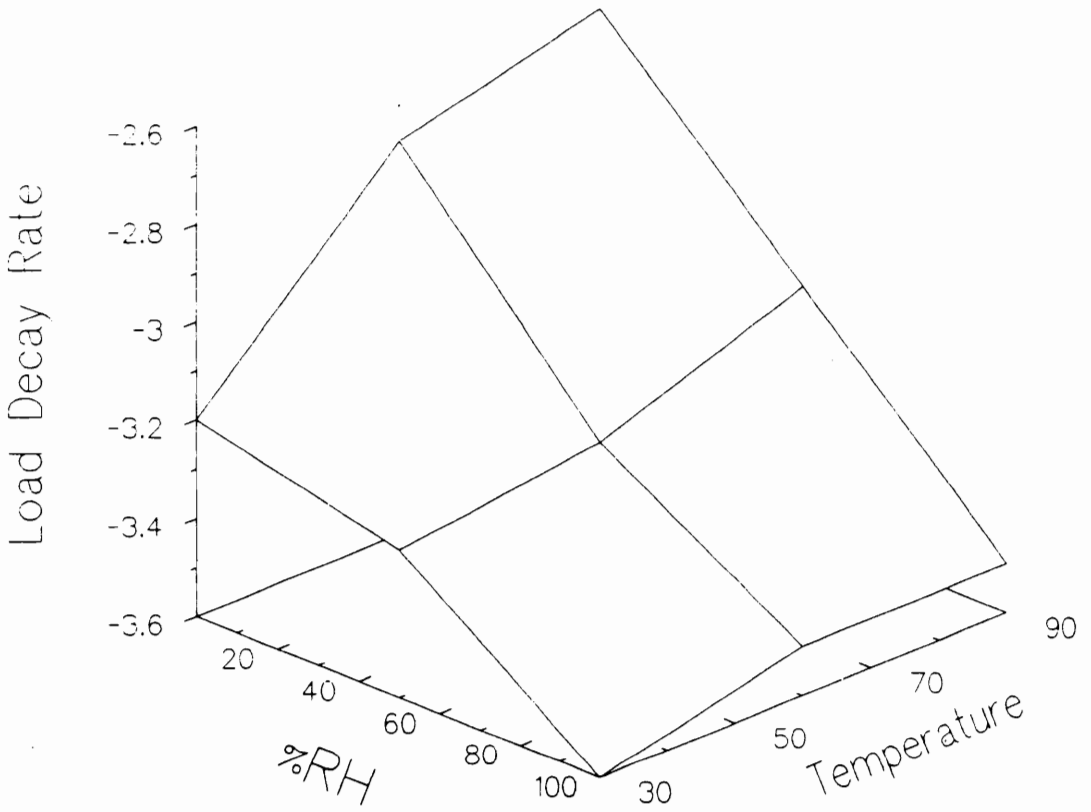

Figure 5.34. Effects of Temperature and Humidity on Load Relaxation Behavior for Foam F4

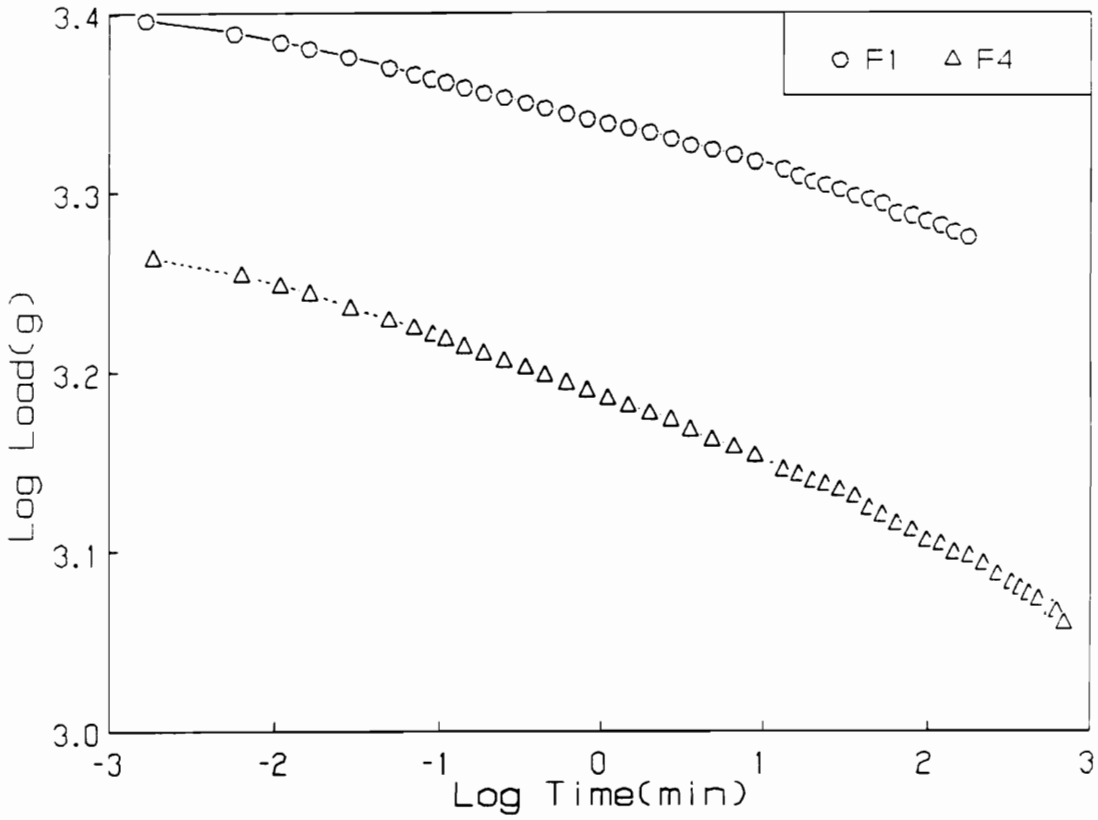

Figure 5.35. Load Relaxation Behavior at 85°C-95%RH for Foams F1 and F4: Tests performed at a 65% constant strain level over a 3 hour period for F1 and 12 hour period for F4

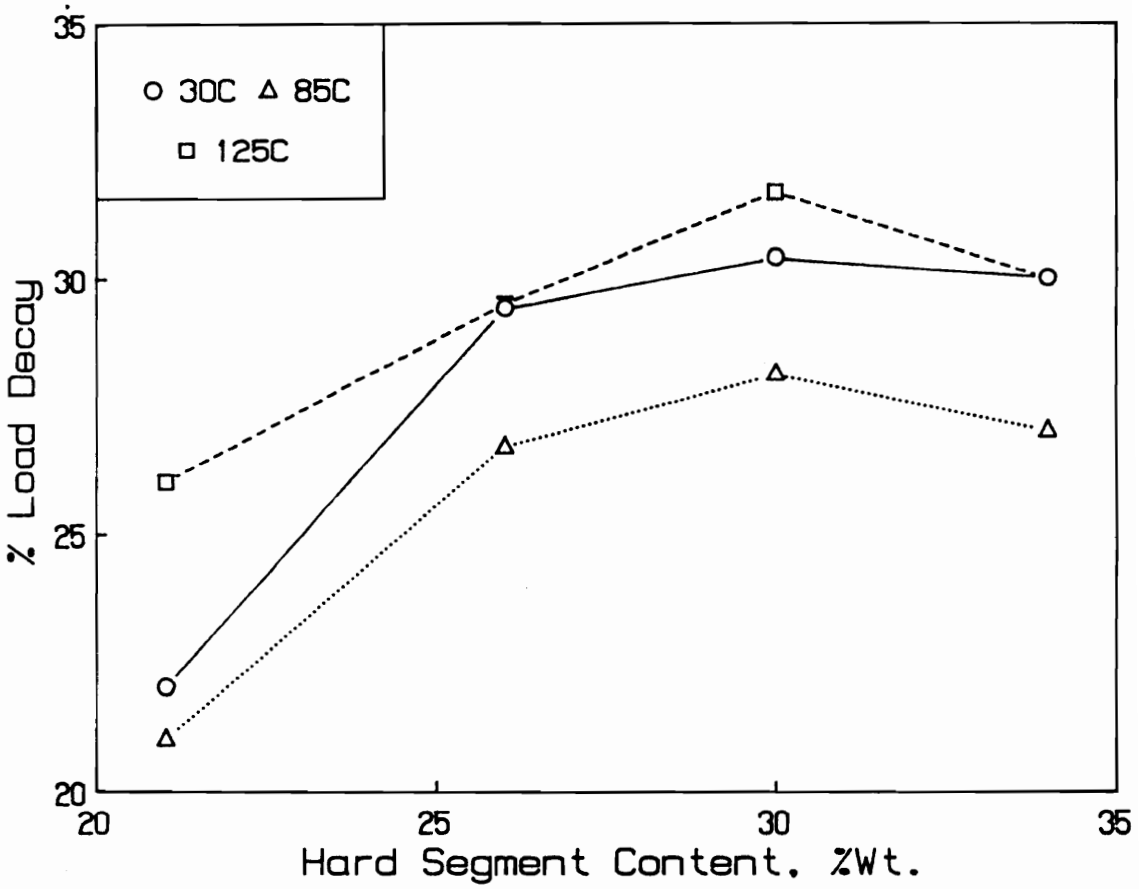

Figure 5.36. Effect of Hard Segment Content on Load Relaxation Behavior at Temperatures of 30, 85 and 125°C: Tests performed at 65% strain level over a three hour period

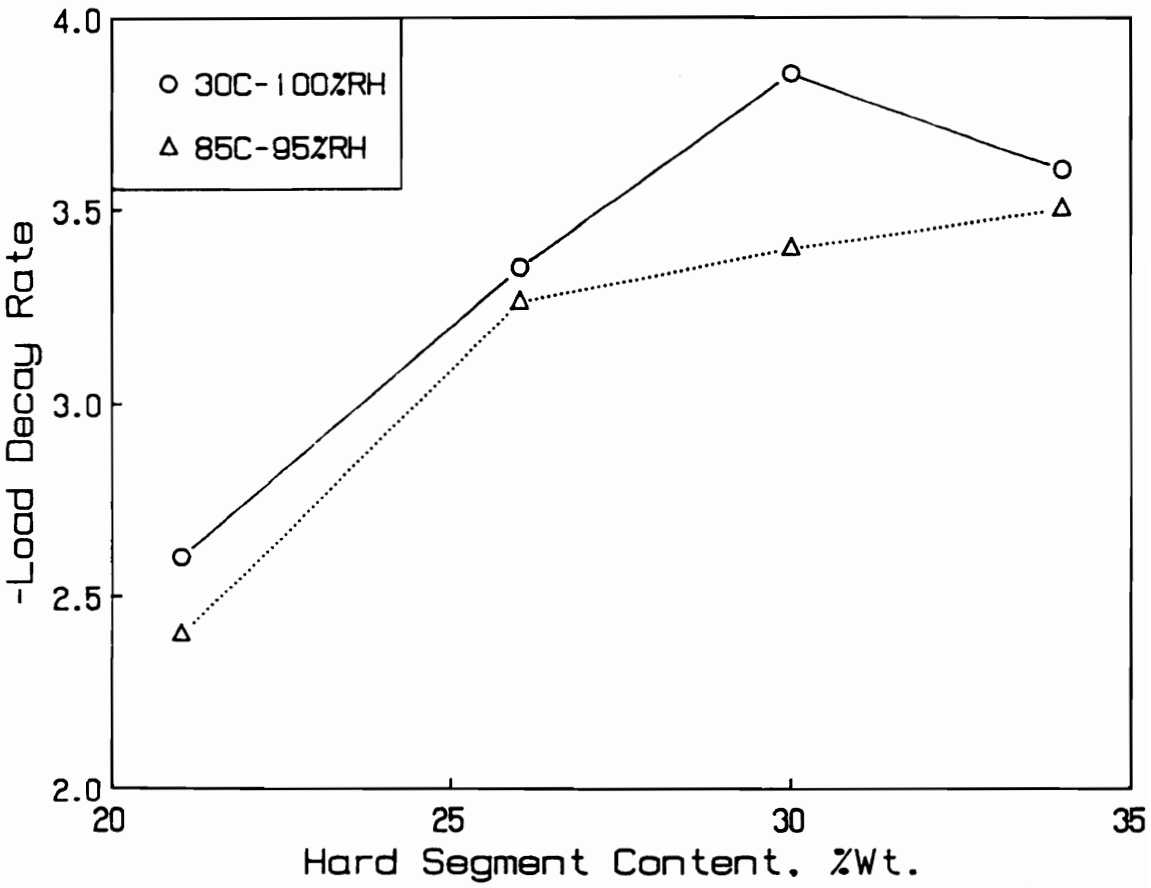

Figure 5.37. Effect of Hard Segment Content on the Load Relaxation Behavior at High Relative Humidities: Tests performed at 65% strain level over a three hour period

foams F2-F4 in comparison to the lowest hard segment foam F1. On the other hand, and somewhat of a surprise, the relaxation behavior does not consistently change in a systematic manner with increasing hard segment content in the range of 26 to 34 percent- see Figures 5.36 and 5.37. Although, the behavior does seem inconsistent especially from 30 to 34 percent hard segment content, the behavior at 30°C in Figure 5.36 and at 30°C- 100%RH have been re-produced for foams F3 and F4(for other conditions only one sample tested for F3). These observations may suggest that the load relaxation behavior is influenced to some extent by the cellular textures of these materials or the difference in density of these foams. The influence of the cellular textures is thought to be small based on earlier results presented for the effect of strain on the load relaxation behavior in Figure 5.23 and 5.24. As discussed earlier, this effect is not that significant up to strain levels of 65 percent. On the other hand, there is a decrease in density with increasing hard segment content for foams F1-F4 - recall Table 5.1. If density is a factor, it is likely to have a greater influence on a higher density foam, i.e F1, since more material per unit volume is compressed. However, as discussed above F1 has the lowest amount of relaxation of the four foams. In addition, several investigators have shown that density does not appear to affect the viscoelastic nature in HR flexible polyurethane foams similar to those of F1 and F2 in hard segment content(38,39). Thus, it appears that density is also not influencing the relaxation behavior in foams F1-F4. In short, there does not appear to be a good explanation for why hard segment content causes very little difference in the load relaxation behavior for foams F3 and F4.

5.2.5 Mechanical Hysteresis and Compression Set

In addition, to measuring the load relaxation behavior for the foams at the different conditions, the mechanical hysteresis, the recovery of the load-strain behavior as well as the immediate loss in thickness(compression set) after testing were measured. Before compressing a foam to a constant strain level and monitoring the relaxation behavior, the foam is cycled twice to a 70% strain level and then there is a 5 minute delay before compression. In Figure 5.39 and 5.40, the cyclic load-

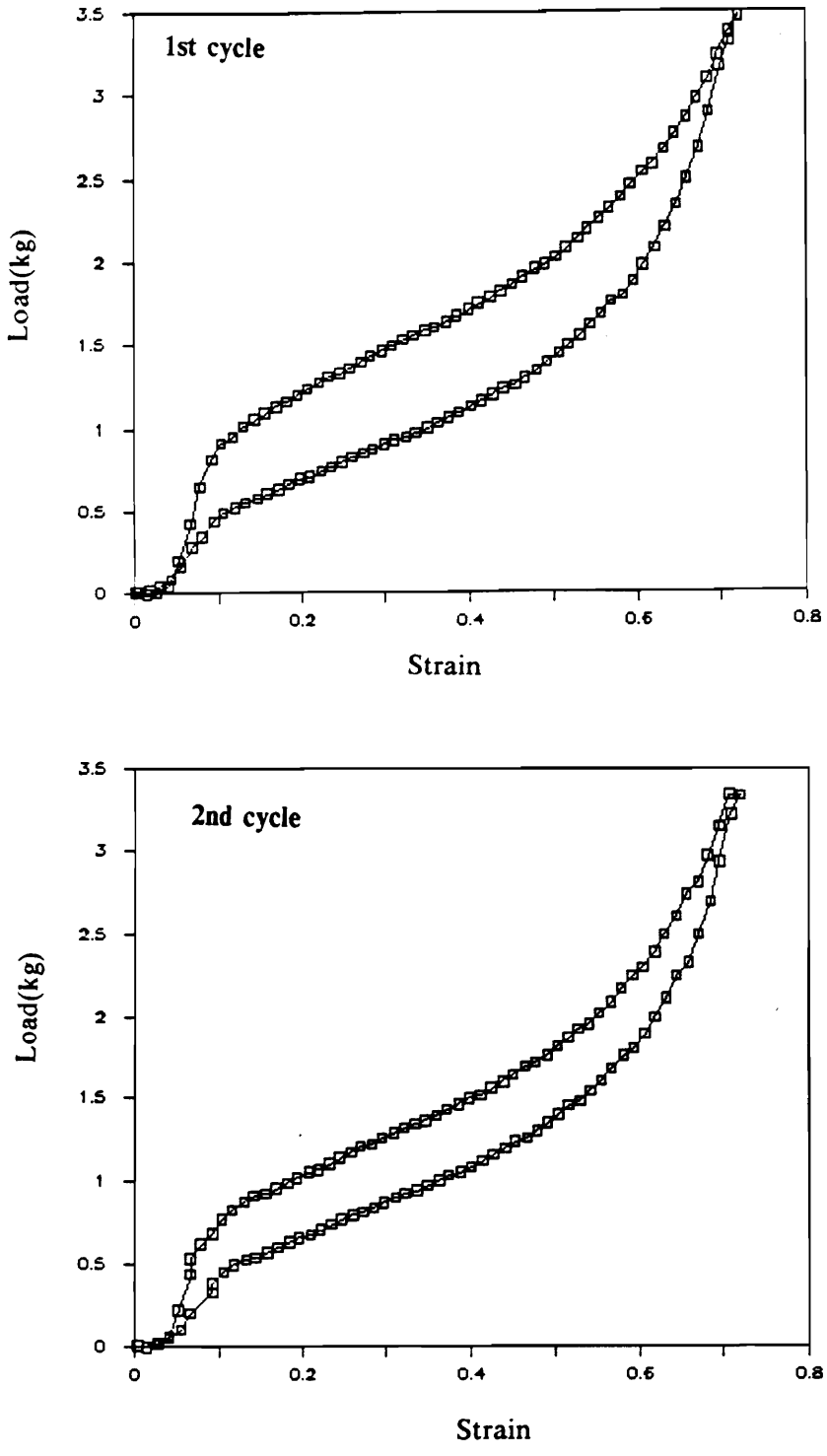

Figure 5.39. Cyclic Load Strain Behavior for Foam F1 at 30°C: Cycled to 70% strain level at 350 mm/min crosshead speed

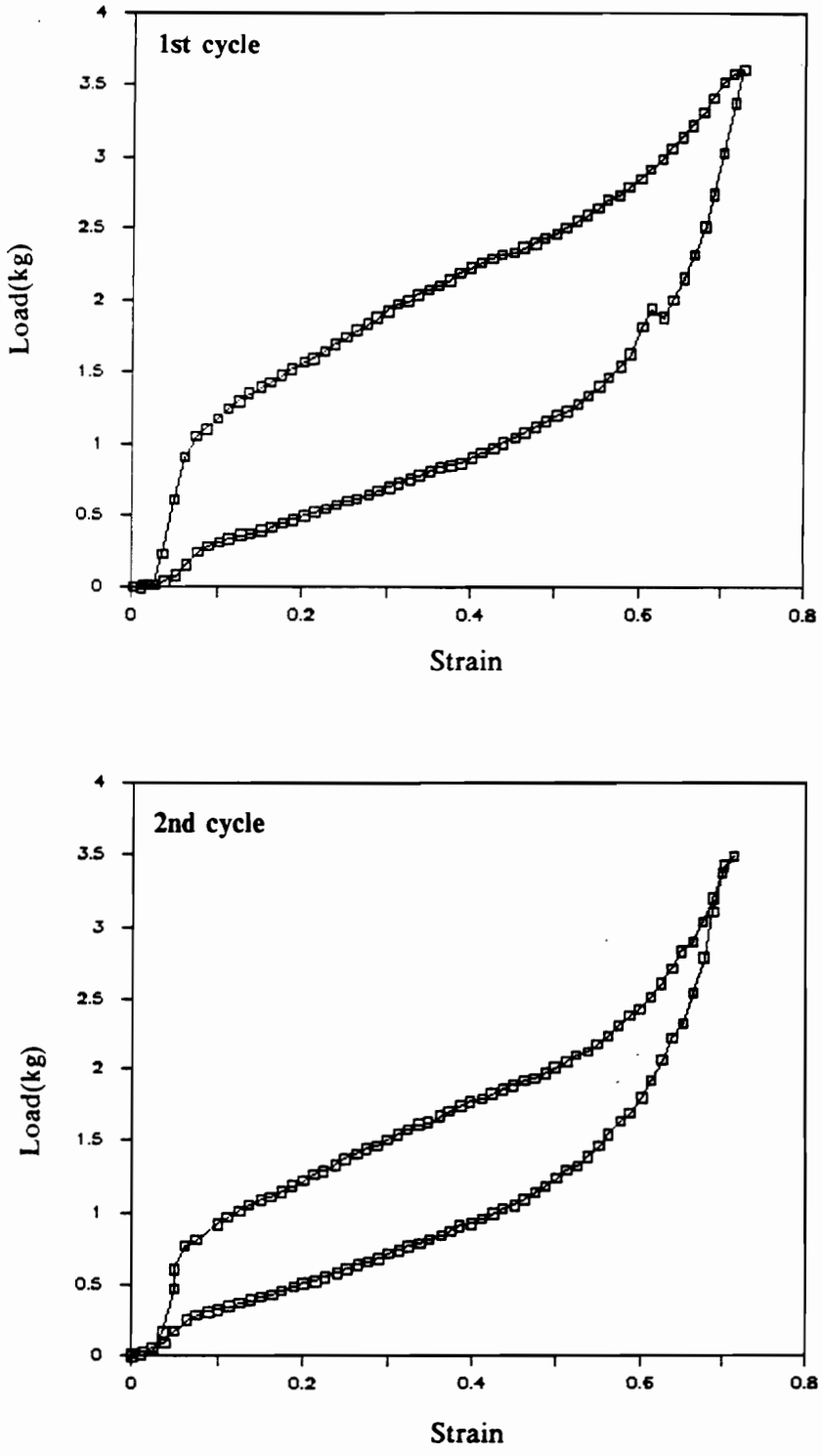

Figure 5.40. Cyclic Load Strain Behavior for Foam F4 at 30°C: Cycled to 70% strain level at 350 mm/min crosshead speed

strain behavior obtained at 30°C-15%RH is shown for foams F1 and F4, respectively. The shape of the cyclic load-strain curves are similar for the two foams. In addition, for both foams the amount of hysteresis is greater in the first cycle and furthermore, the hysteresis is greater for F4 than that of F1 for both cycles. The hysteresis is expected to be more significant in the first cycle, due to weak secondary bonds being disrupted, loose chains becoming unentangled, and crushing of any remaining closed cell windows. In comparing the load levels at 70% strain for the two cycles, there is a 6 percent loss in load for F1 and a 7 percent loss for that of F4. The greater amount of hysteresis for F4 as well as the larger loss in load at 70% strain from the first cycle to the second can be attributed to several factors. One likely factor is the amount of residual orientation for the hard segments is thought to be higher in foam F4 than F1, since foam F4 has the higher hard segment content of the two. This type of recovery for the hard segments is believed to take place since they are rigid and thus do not retain their original orientation state as quickly in comparison to the more flexible soft PO units. Another factor is the disruption of hydrogen bonds which has a greater effect on F4 than F1 due to the higher hydrogen bond content in F4. Hydrogen bond disruption is believed to take place during compression due to increased localized strains on the hard segments which will in turn result in further chain slippage. Chain slippage will, of course, lead to additional load decay which also results in more cyclic hysteresis. In short, during cyclic loading, the hysteresis loss which is also commonly referred to as fatigue in foam terminology, is thought to be mostly a result of stress relaxation or load relaxation taking place in the solid portion of the foam.

An indication of mechanical hysteresis was obtained by monitoring the load behavior for the following steps shown in Figure 5.41; (1) the load-strain behavior up to a constant strain level of 65 percent strain, (2) the load decay for 70 hours of compression at 65 percent strain and (3) the return load-strain behavior from 65 percent to 0 percent strain. Thus, the envelope made by following the path from 1 to 2 to 3 in Figure 5.41(a,b) signifies the mechanical hysteresis for foams F1 and F4. From a qualitative point of view, it is obvious that the amount of cyclic hysteresis is more significant for F4 than F1. This observation is consistent with the data shown in the previous paragraph as well as with the amount of load decay that occurs over time in these foams. Also shown in Figure 5.41 for F1 and F4, is the immediate recovery of the load-strain behavior(step 4)

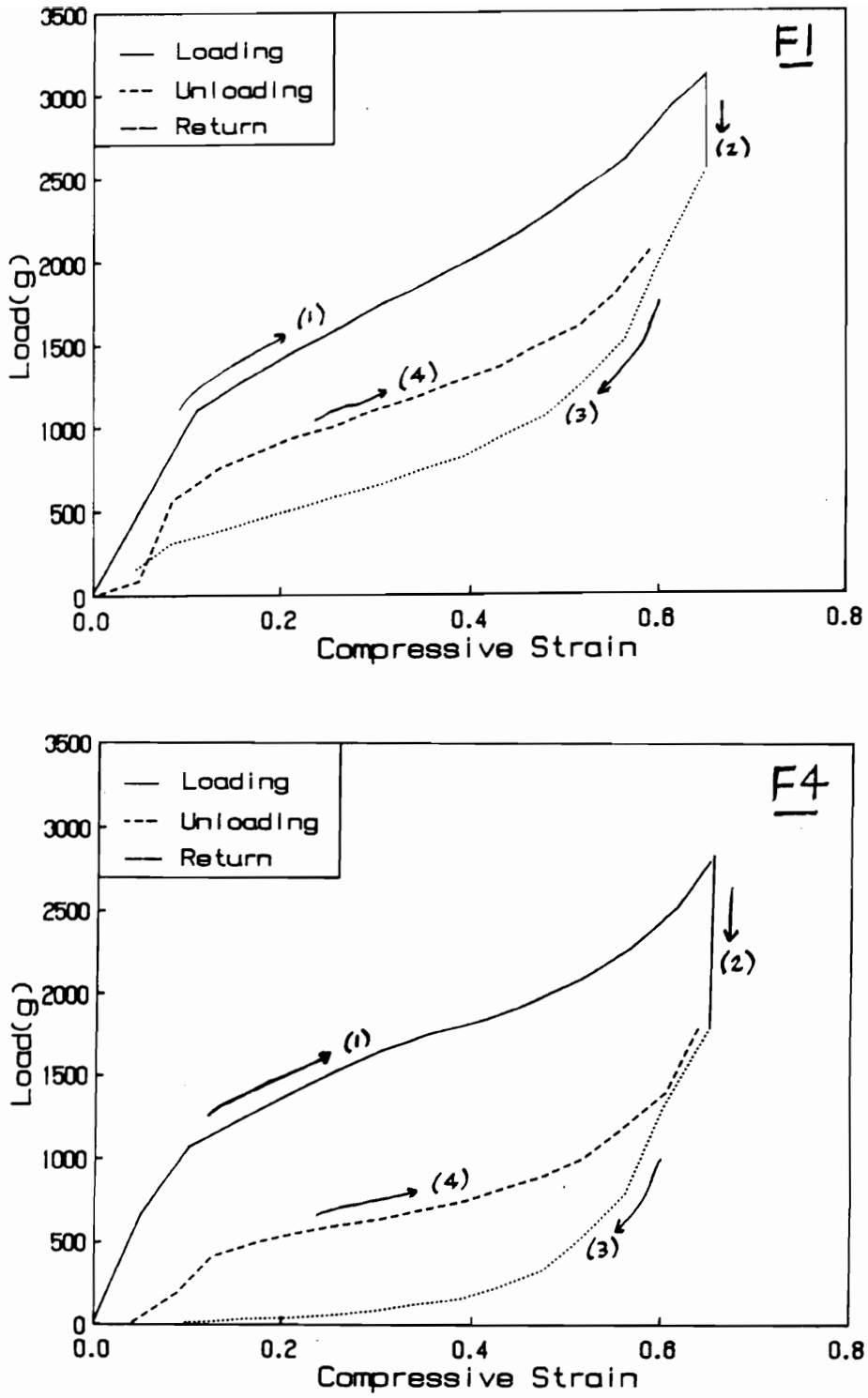

Figure 5.41. Cyclic Hysteresis Behavior for Load Relaxation Tests: Performed at 30°C-15%RH on both foams F1 and F4 at a 65% strain level for approximately 70 hours

after maintaining the foam at a constant strain for a 70 hour period period. Though the shape of the load-strain recovery curve is similar to the initial curve, the immediate loss in the load after testing is fairly significant for both F1 and F4. The recovery of the load that is observed for both F1 and F4 in Figure 5.41 is comparable and this point is especially noticeable by the load levels at 65 percent strain. For other samples and at most conditions(temperatures less than 100°C), the recovery behavior was found to be similar to the results shown in Figure 5.41.

The recovery of the shape of the foam was also evaluated after completing the load relaxation tests by measuring the immediate loss in thickness of the foam and then calculating the compression set. As discussed in the literature review, compression set is a common property measured in flexible foams(ASTM D 1564-81) after compressing the foam for 22 hours at either a 75 or 90 percent compressive strain level and at 25°C and 50%RH to predict the viscoelastic behavior of the foam(38,43-47,85). Also within these compression set studies, different investigators have reported higher compression set values upon exposing the foams to high temperature and high relative humidities prior to the standard compression test described above(43,45). Although, in most cases the foams used in this investigation were only compressed for three hours, the effects of conditions during compression or while applying a stress to the foam have been determined.

For the temperature range of 30°C to 60°C as well as for the high humidities at these temperatures, the results of the compression set (over 3 hours) are only in the range of 1 to 2 percent with the higher values observed for F4 and the lower for F1. In addition, at 85°C-2%RH and at 85°C-50%RH the 3 hour compression set values are in the same range. Over longer time periods at these same conditions, the compression set values are slightly higher. For example at 30°C-100%RH and for an approximately 22 hours of compression, the compression set is 2 percent for F1 and 2.3 for F4.

At the other testing conditions the compression set values for the most part are more significant as summarized in Table 5.14. At 85°C-95%RH, the values ranged from 2.7 percent for F1 to 5 percent for F4. At 125°C, the compression set is much higher for F1 and F2 in comparison to F3 and F4. This difference in behavior is somewhat surprising since the amount and rate of load relaxation at 125°C for F1 and F2 is less than that of F3 and F4. However, as shown by the

Table 5.14: Summary of Compression Set Values for Foams F1-F4

Condition	% Compression Set			
Foam =	F1	F2	F3	F4
85°C-95%RH	2.7	3	3	5.0*
100°C	3**			3**
125°C	22	28	8.7	2
140°C	49			20

* behavior obtained after 12 hours of testing

** behavior obtained after 20 hours of testing

-Other compression set values were obtained after 3 hours of testing

-At other testing conditions (not shown above), the compression set values ranged from 1 to 2 percent for foams F1-F4, respectively

FTIR-thermal studies at temperatures greater than 100°C, there is likely some additional hydrogen bond disruption with the urethane groups and some chain scission in the urea and urethane links is also thought to be taking place. These types of changes, as discussed earlier, are believed to have a greater effect on the lower hard segment materials, that is, foams F1 and F2. At 125°C, based on the loss in thickness which appears to be permanent in all 4 foams, some chain scission is believed to have occurred. Saotome et. al. has reported observing unrecoverable losses of thickness for HR flexible foams exposed under stress at 70°C-95%RH condition and a 75 percent deflection for 22 hrs(44). In attempt to accelerate the recovery of the foam thickness, the authors annealed the foams at high temperatures, but observed only small amounts of further recovery(44). Similar attempts have been made to recover the loss in thickness of foam F1 after testing at 125°C, but no additional recovery is observed. In looking further at the results in Table 5.14, the compression set is higher at 140°C for F1 than F4 and furthermore, the loss of thickness was not recovered. This difference between F1 and F4 is consistent with the load relaxation results as shown in Figure 5.27. In addition, these results at 140°C suggest for both foams that some primary bonds may have been disrupted under stress. This suggestion is also supported by the orientation studies presented in the previous chapter which showed that after deforming plaque 2-DMF at 125°C and 140°C there is a significant amount of residual orientation induced. However, as discussed earlier there is very little residual orientation after deforming plaque 2-DMF at ambient conditions.

5.2.6 Comparison of Viscoelastic Behavior in Compression and Tension

In comparing the viscoelastic decay in compression with that in tension, one must first consider the general stress/load-strain behavior in compression versus tension. The behavior for the tensile stress strain curve is given in Figure 5.42 for foam F4 along with its compressive load-strain response. As shown in Figure 5.42a, the behavior in tension is rather linear at the 25 percent level where the stress relaxation behavior was monitored. On the other hand, the compression load-strain behavior is in a non-linear portion of the curve at the 65 percent level where a majority of the load

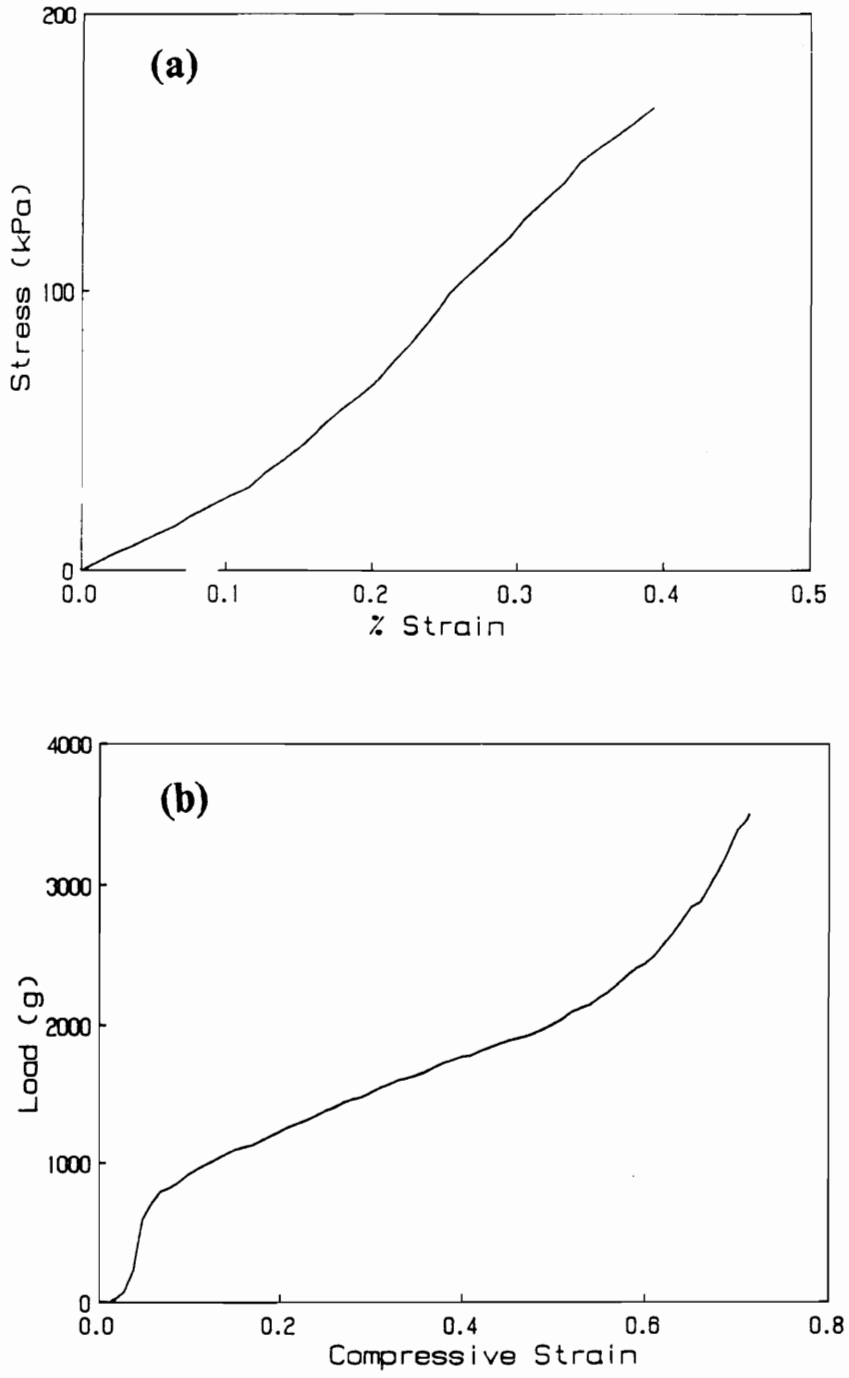

Figure 5.42. Comparison of (a)Tensile Stress-Strain and (b)Compressive Load Strain Curves: 40mm/min and 350 mm/min crosshead speeds for tension and compression tests were used, respectively

relaxation tests were performed. Even though the strain regions that the compression and tensile testing were carried out at are not equal, it is still possible to compare the relaxation behavior for the two modes of deformation. Also, this comparison which is given below evaluates the effect of strain on the relaxation behavior in compression and tension.

The effects of temperature on foam F1 in compression as well as in tension are given in 5.43 and furthermore, the load/stress decay values for the two tests are compared in Figure 5.44. It is important to note that the values given in Figure 5.42 for the compression studies are slightly lower than the ones reported in Table 5.10, since the first point acquired in the data collection for the compression studies was somewhat faster than that in tension. In Figure 5.43, the two response surfaces are noted to be very comparable and the load or stress at a given time behaves similar with increasing temperature. As shown in Figure 5.44, the load/stress decay values are also quite analogous for results obtained in compression and tension. Although, the values are often slightly higher in the compression mode. In addition, the constants obtained upon fitting the results in Figure 5.42 by utilizing Eq. 5.1 are comparable for τ_2 in the tension and compression mode, but differ to some extent for that of τ_1(see figure caption of Figure 5.44 for τ_1 and τ_2 values). This difference in τ_1 basically signifies that the effect of increasing temperature up to 100°C in compression has only a small effect on the amount of load decay for F1 whereas in tension this effect is greater.

The effects of temperature on F4 in compression and tension are shown in Figures 5.45, respectively. In addition, the percent load/stress decay values have been summarized in Figure 5.46 for results obtained in compression and tension. The two surfaces shown in Figures 5.45 are again similar with some slight differences in the load and stress values at a given time with increasing temperature. However, the percent load/stress decay values are very similar for the two modes of deformation with the values being slightly higher in compression up to temperatures of 125°C and the same at 140°C. Also, the values for τ_1 and τ_2 obtained from fitting the data in Figure 5.45 with Eq. 5.1 are comparable for F4 in compression and tension(see figure caption of Figure 5.46 for τ_1 and $\tau_2$values).

The effects of relative humidity on the relaxation behavior are also rather similar for the results obtained in compression and tension for F1 and F4. These results are best summarized by Table

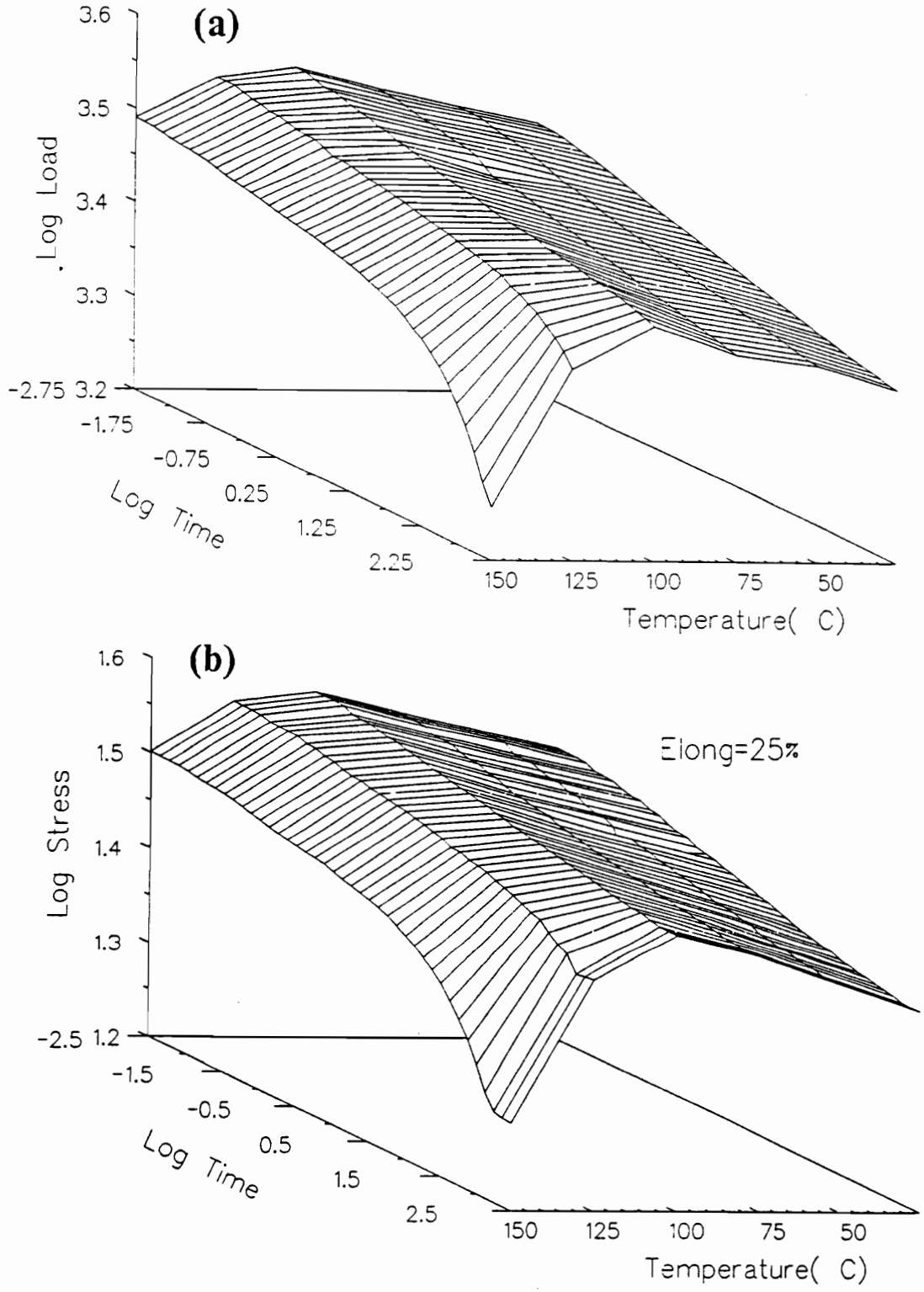

Figure 5.43. Comparison of Variable Temperature Relaxation Behavior in (a)Compression and (b)Tension Modes of Deformation for Foam F1: Behavior in compression obtained at a 65% strain level and that in tension at 25%.

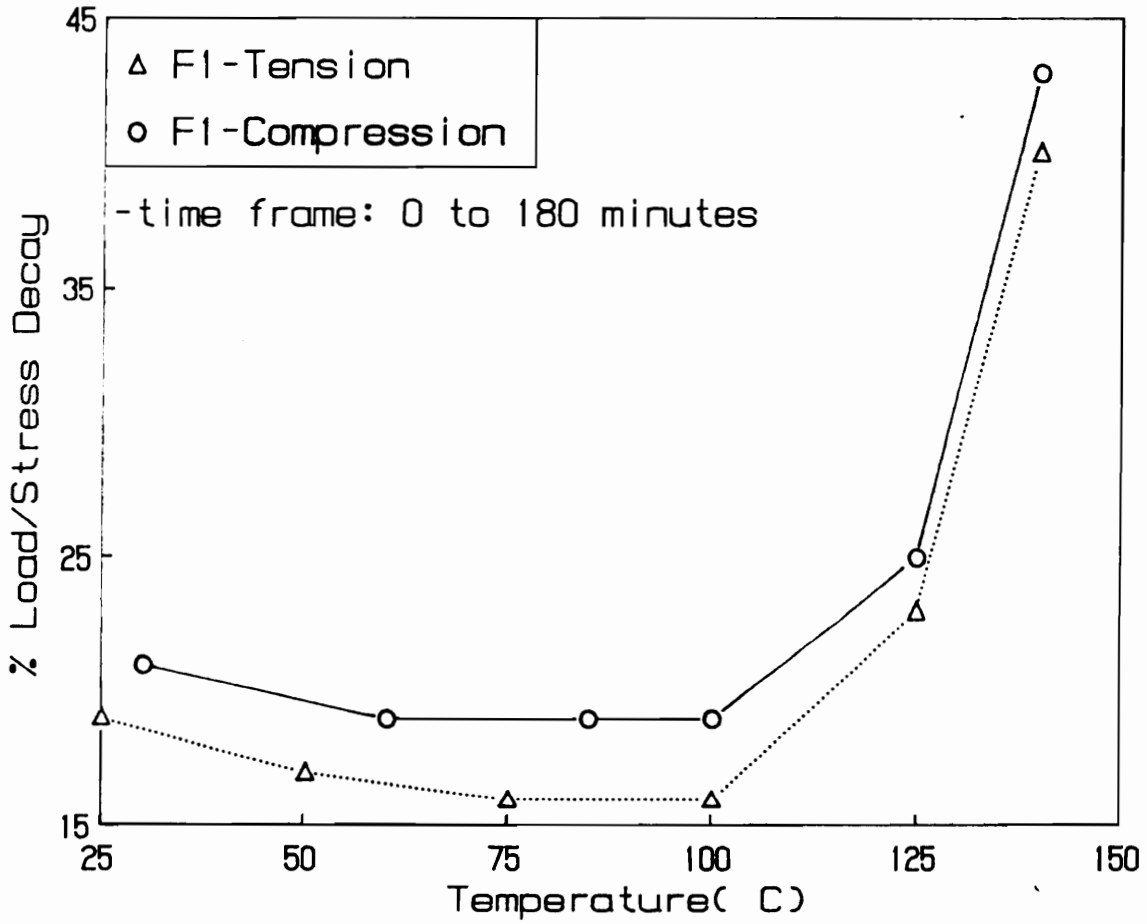

Figure 5.44. Comparison of Load/Stress Decay Values for Foam F1: Compression: $\tau_1 = 494$ and $\tau_2 = 12.5$; Tension: $\tau_1 = 258$ and $\tau_2 = 14.9$.

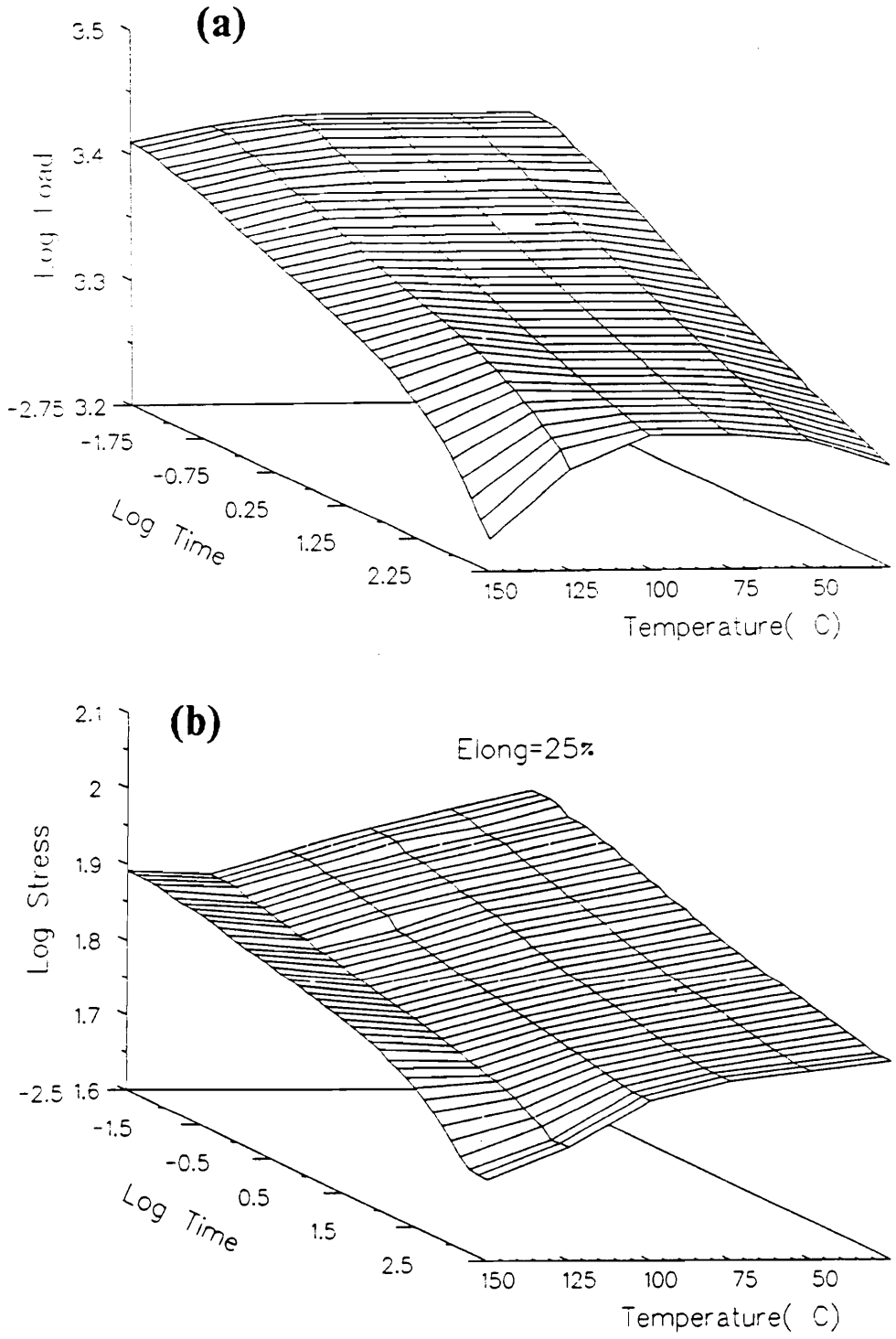

Figure 5.45. Comparison of Variable Temperature Relaxation Behavior in (a)Compression and (b)Tension Modes of Deformation for Foam F4: Behavior in compression obtained at a 65% strain level and that in tension at 25%.

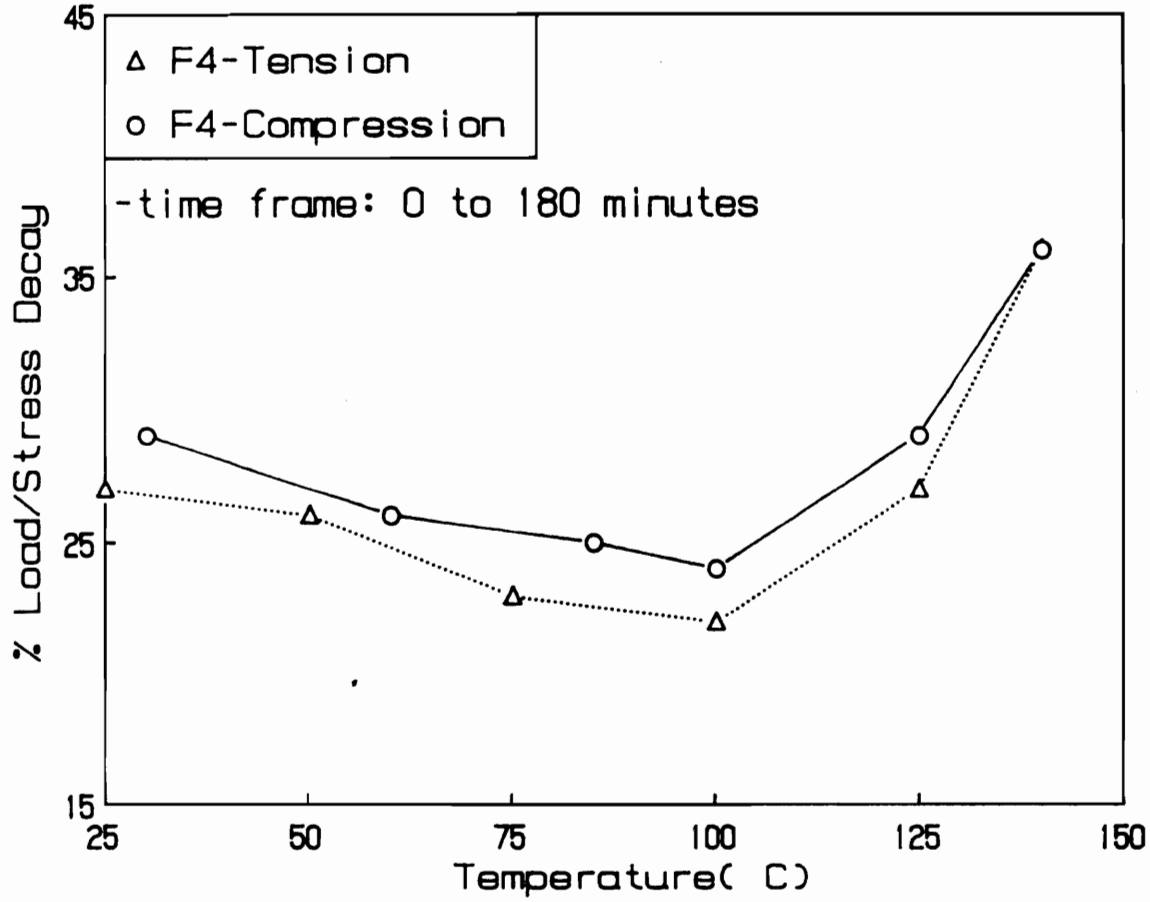

Figure 5.46. Comparison of Load/Stress Decay Values for Foam F4: Compression: $\tau_1 = 274$ and $\tau_2 = 21.5$; Tension: $\tau_1 = 252$ and $\tau_2 = 18.3$.

5.15 as well as by the response surfaces in Figures 5.47-50. As shown in Table 5.15, the results for the percent load/stress decay values are slightly higher in compression. The only significant exception to the last statement, is that the amount of decay is higher at 90°C-100%RH in tension for F4 than in compression at 85°C-95%RH(see Figure 5.50). The reason for this difference is not fully understood, but is believed to real based on reproducability of both results.

A comparison of the effect of the hard segment content on the relaxation behavior in tension and compression at various temperatures is found in Figure 5.51. The results in tension and in compression are comparable as shown in Figure 5.51, but are somewhat different in behavior at the higher hard segment content. In the temperature range from 25°C to 125°C, the amount of decay in tension increases in a more systematic manner than it does in compression. As indicated earlier, the effect of hard segment content on foams F3 and F4 is not well understood in the compression mode.

Overall, the results in compression and tension exhibit many similarities in the relaxation behavior, even though the constant level of strain utilized was higher in compression as well as nonlinear. While there are some differences in the relaxation behavior which are mostly related to the effect of hard segment content on foams F3 and F4, the resemblance exemplified by the corresponding response surfaces and furthermore by the comparable load and stress decay rates as well as the load and stress decay values are much more noteworthy than these differences. It is also important to recall that the studies in tension revealed that the stress relaxation behavior for the foams is governed by the solid portion of the foam. Thus, based on the many similarities in the relaxation behavior in tension and compression as well as the conclusions drawn from the results in tension, it is believed that the relaxation behavior in compression(at a 65 percent strain) is also mostly dependent on the solid portion of the foam material.

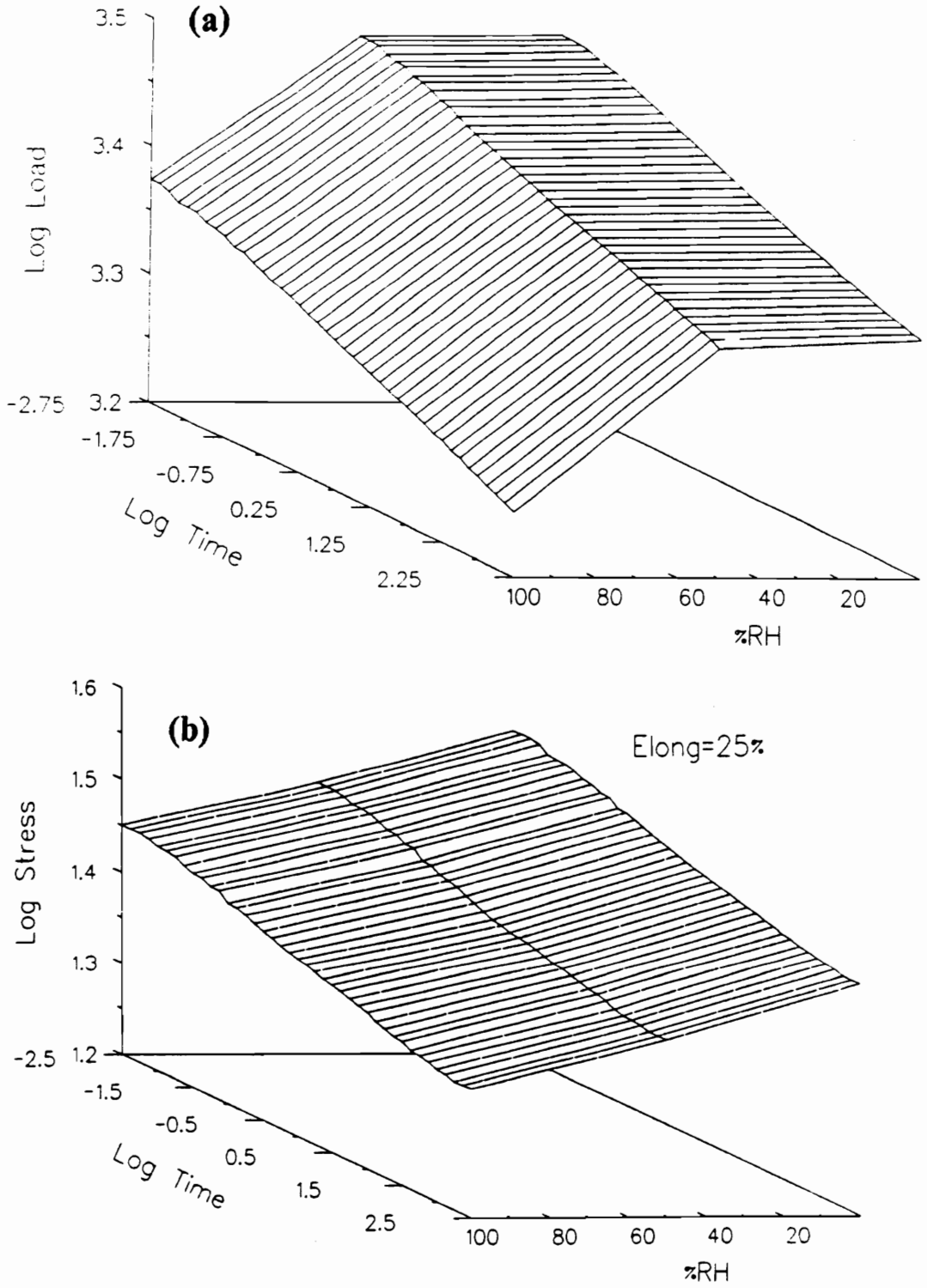

Figure 5.47. Comparison of Effects of Relative Humidity at 30°C on the Relaxation Behavior in (a)Compression and (b)Tension Modes of Deformation for Foam F1: Behavior in compression obtained at a 65% strain level and that in tension at 25%.

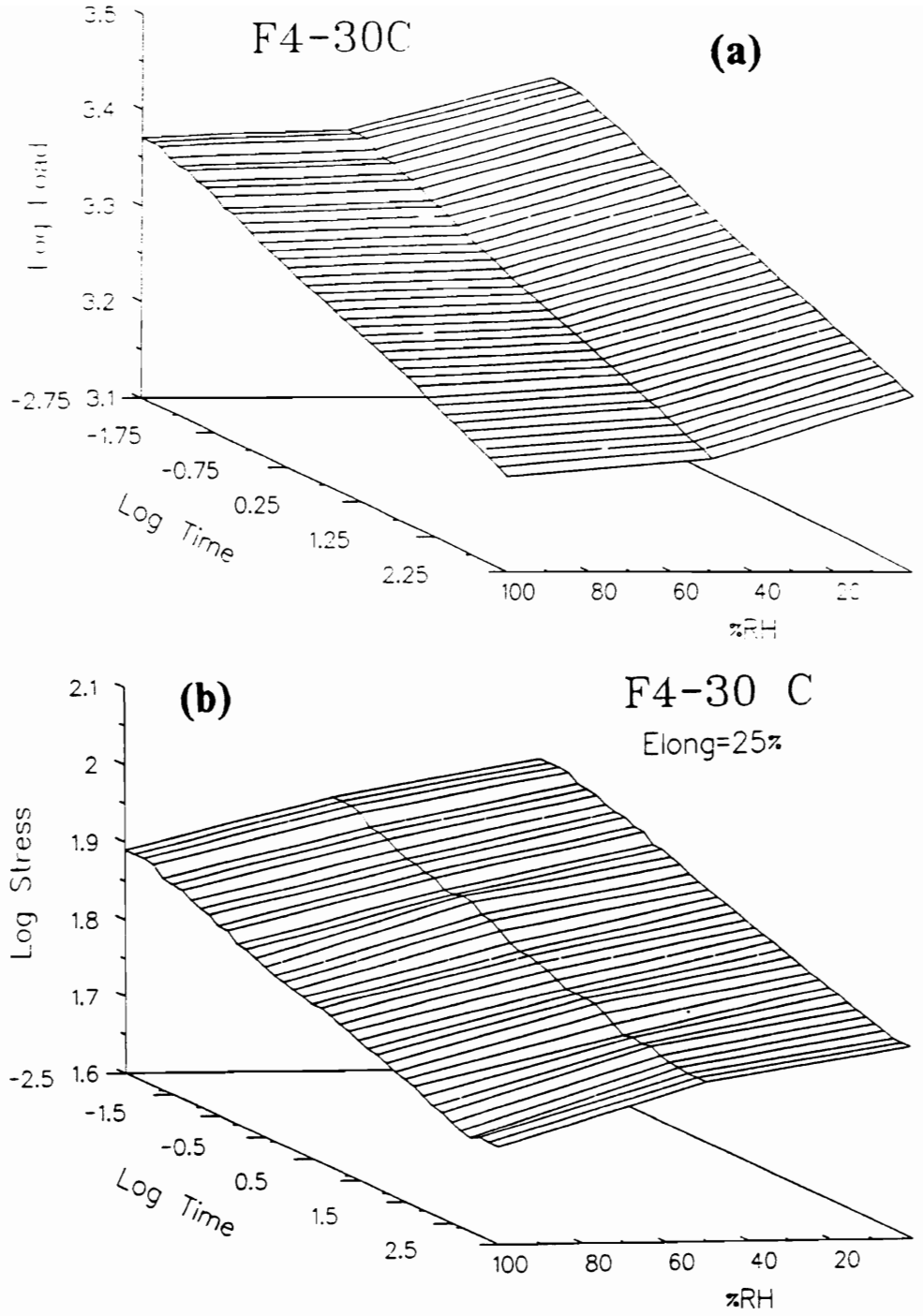

Figure 5.48. Comparison of Effects of Relative Humidity at 30°C on the Relaxation Behavior in (a)Compression and (b)Tension Modes of Deformation for Foam F4: Behavior in compression obtained at a 65% strain level and that in tension at 25%.

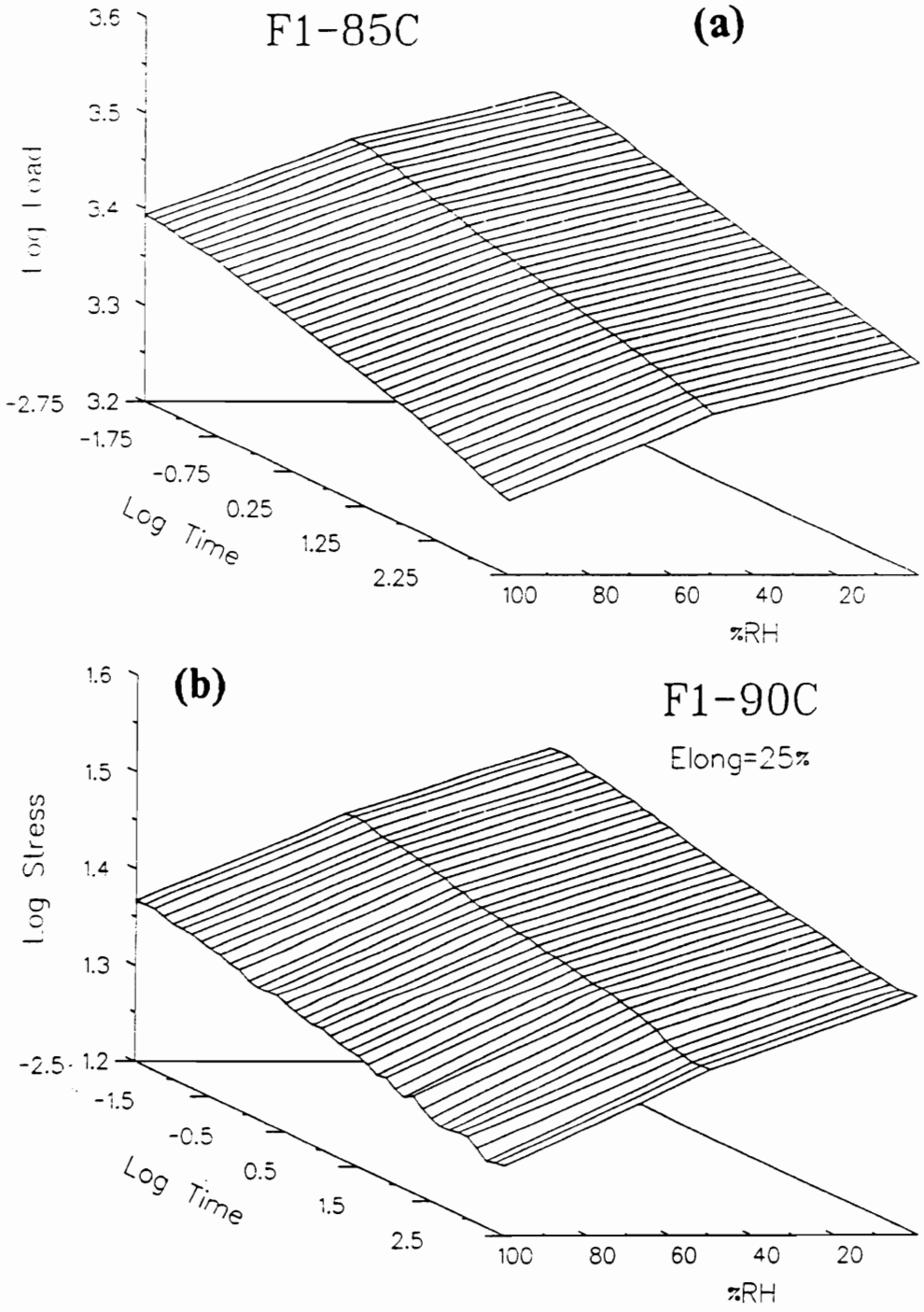

Figure 5.49. Comparison of Effects of Relative Humidity on the Relaxation Behavior in (a)Compression(85°C) and (b)Tension(90°C) Modes of Deformation for Foam F1: Behavior in compression obtained at a 65% strain level and that in tension at 25%.

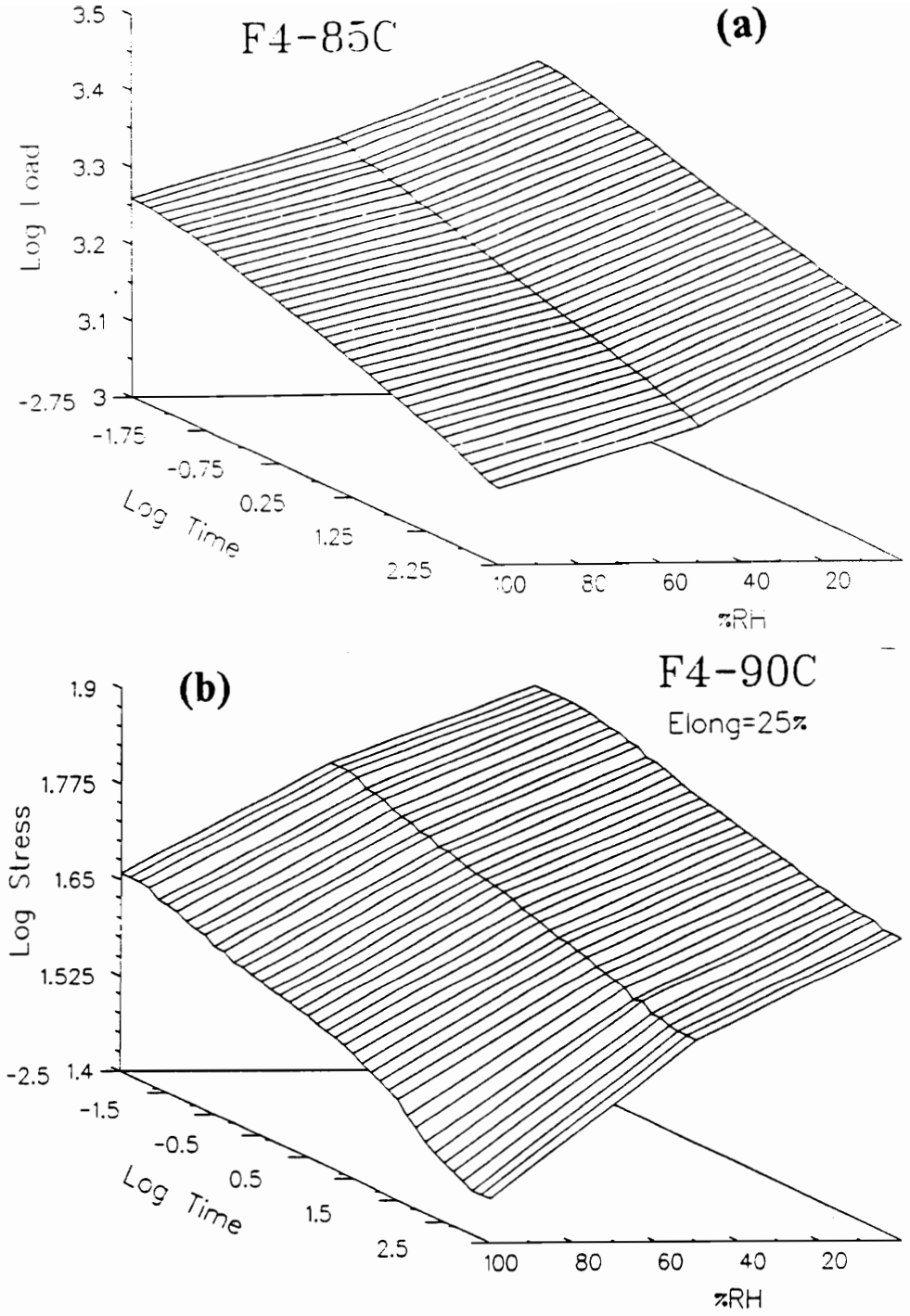

Figure 5.50. Comparison of Effects of Relative Humidity on the Relaxation Behavior in (a)Compression(85°C) and (b)Tension(90°C) Modes of Deformation for Foam F4: Behavior in compression obtained at a 65% strain level and that in tension at 25%.

Table 5.15: Percent Stress and Load Decay Values at Different Temperature/Humidity Conditions

Foam	Temperature(°C)	% Decay(from 0 to 180 min.'s)		
		%RH = 0-15	50	95-100
F1(T)	30	20	21	22
F1(C)	30	22(21)	22(21)	25(24)
F4(T)	30	30	31	32
F4(C)	30	30(29)	31(29)	33(31)
F1(T)	90	17	19	23
F1(C)	85	20(19)	22(21)	24(23)
F4(T)	90	24	28	37
F4(C)	85	26(24)	30(29)	32(31)

(T)-Tension mode; (C)-Compression mode

Results in ( ) are modified values which were calculated over same time scale as that in tension

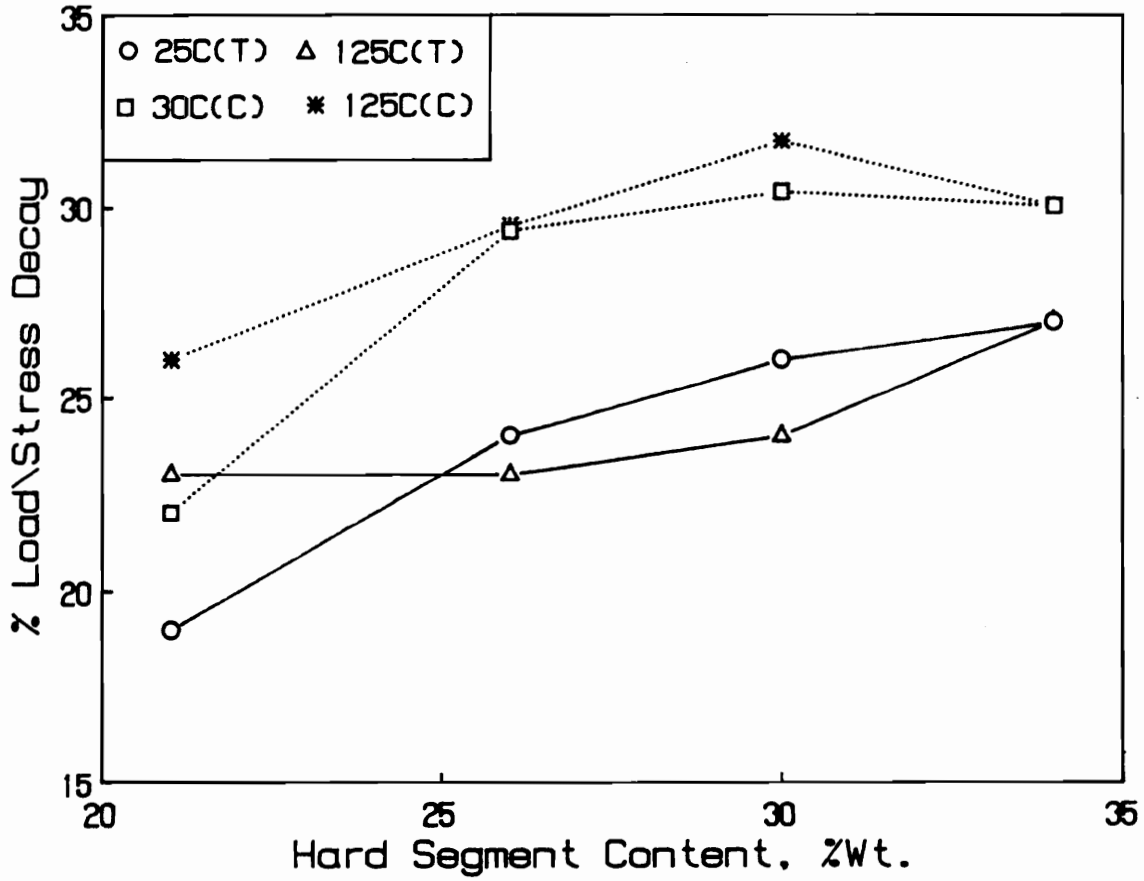

Figure 5.51. Comparison of the Effect of Hard Segment Content on the Relaxation Behavior in Compression and Tension: Behavior in compression obtained at a 65% strain level and that in tension at 25%.

5.3 Compression Creep

In the previous two sections of this chapter, the time dependence of the stress or load of the foam in tension and compression has been presented. In completing the discussion on the viscoelastic behavior for these four flexible foams, results related to changes that occur in the foam's shape while the foam is under a constant load over time are given. For this investigation, the change in the foam's shape has been evaluated by measuring the loss in thickness over time, i.e. the compressive creep behavior. These measurements have been carried out at different constant loads in order to determine the effect of the load and/or the initial penetration on the creep behavior. In addition, the effects of temperature and relative humidity on the creep behavior have also been evaluated. The majority of these tests have been carried out over a three hour time period on foams F1 and F4.

Before discussing the above effects on the creep behavior, a general introduction is given for the behavior of compressive strain with time and the approach utilized in evaluating this behavior. In Figure 5.52, the compressive creep behavior is given for F1 and F4 in the form of compressive strain vs log time after reaching the initial penetration level. This particular plotting scheme is also the same one used by Campbell as well as by Terry for their compressive creep studies on flexible foams as discussed earlier in the literature review(46,58). As shown in Figure 5.52, the behavior is fairly linear for linear strain versus log time after a short induction period(up to -1.0 in log time(min)). During this short induction period, there is very little change in the strain which has been observed for all of foams F1-F4 as well as at all testing conditions. Even though this period is greater for F1 than that of F4 in Figure 5.52, the length of the induction period does not appear to be dependent on hard segment content or the conditions at which the test were conducted under. In general, this period where very little change in the compressive strain is observed, is on the order of 6 seconds(ca. -1.0 in log time(min)) after reaching the initial penetration level. Terry has also reported observing a similar induction period on the order of 6 seconds for a non-crushed sample in his creep study and furthermore an extension of this period upon crushing the foams before

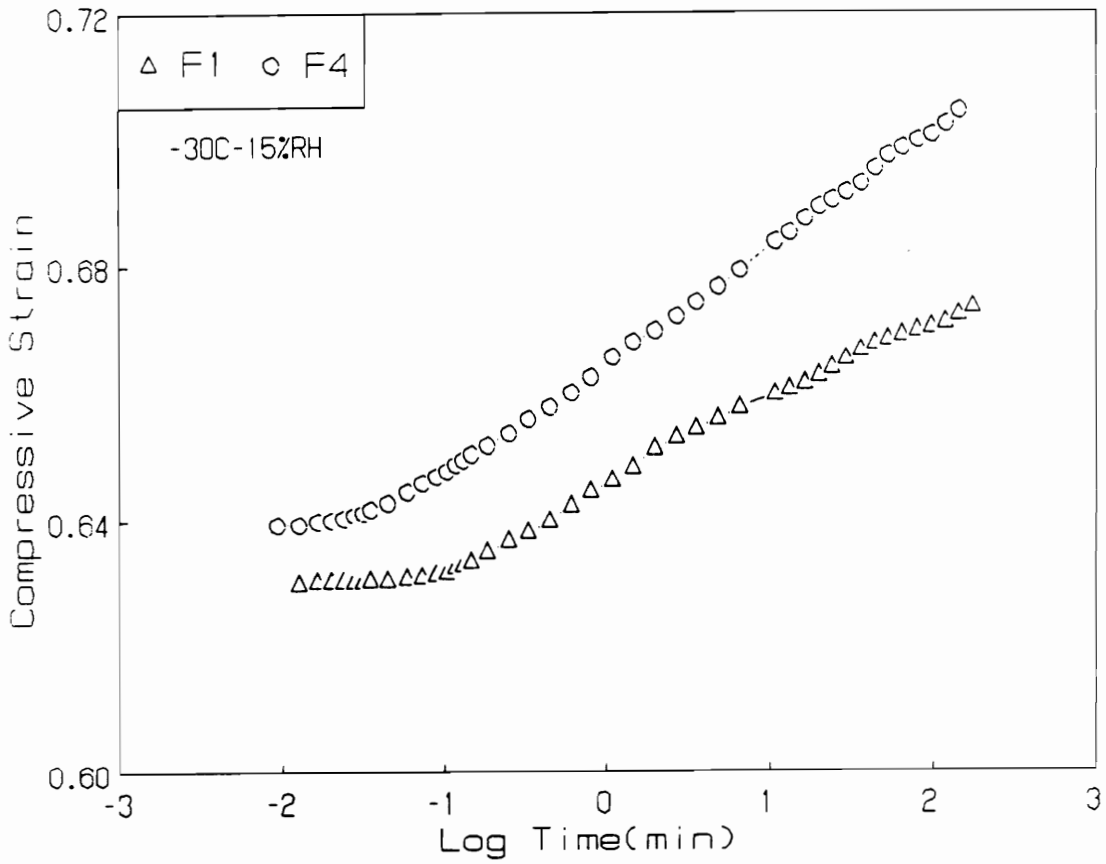

Figure 5.52. Compressive Strain-Log Time Creep Behavior for Foams F1 and F4: Load applied to F1 was 2.7kg and that of F4 was 2.5kg; condition was 30°C-15%RH

testing(46). Though, Terry offered no explanation for this period and the extension of it, it appears at least for his results that this induction period may be a function of fatigue loss. It is also possible that the elastic response of the foam does provide some initial resistance to creep. Thus, to be consistent during the investigation discussed in this dissertation, the foams have were not preflexed before measuring the creep behavior.

In evaluating the results given in Figure 5.52, the slope of the linear portion(data after the induction period) of the curve was measured by linear least squares. This slope represents the initial rate of creep at a given load and better yet the initial strain level. As discussed in the literature review, Campbell showed that the compressive creep behavior was dependent on the initial penetration level, i.e. the initial compressive strain(58). A similar dependency on the compressive creep behavior for foams F1 and F4 is discussed below.

5.3.1 Dependence on Initial Strain Level

In utilizing the above method of evaluation of the strain-log time creep behavior, the dependence of the initial creep rate(Δstrain/Δlog t) on the initial strain level was obtained and is shown in Figures 5.53 and 5.54 for F1 and F4, respectively at 30°C-15%RH. For both F1 and F4, this behavior goes through a maximum near an initial penetration level of 40 percent. Campbell also showed a maximum at a slightly lower compressive strain level for flexible HR foams. In his investigation, Campbell attributed the dependence of the creep rate on the initial penetration to the buckling of the struts(58). This phenomena also appears to be governing the behavior shown in Figures 5.53 and 5.54 for the creep rate as a function of initial strain level(discussed in more detail shortly). As displayed earlier in Figure 5.21, buckling of the struts is thought to occur at strains beginning at 10 percent and on up to strain levels near 60 to 65 percent. On the other hand, the creep rate does not change significantly at initial strains greater than 60 percent where buckling does not take place, - see Figure 5.53 and 5.54. In addition, the creep rate at the lower initial strain levels(near 10 percent) and at 65-70 percent are similar as shown in Figures 5.53 and 5.54 for foams

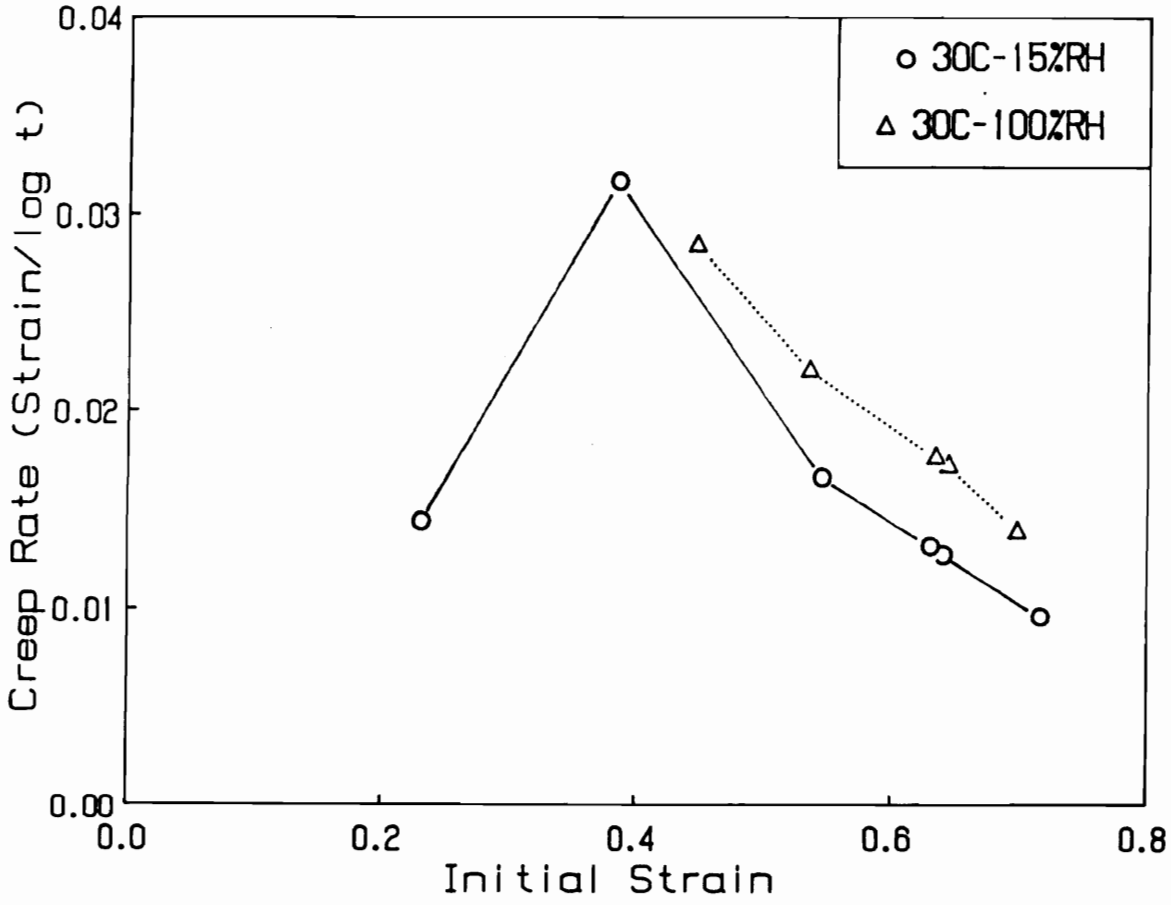

Figure 5.53. Effect of Initial Strain Level on Compressive Creep Behavior for Foam F1 at 30°C: Creep rates based on three hour testing period

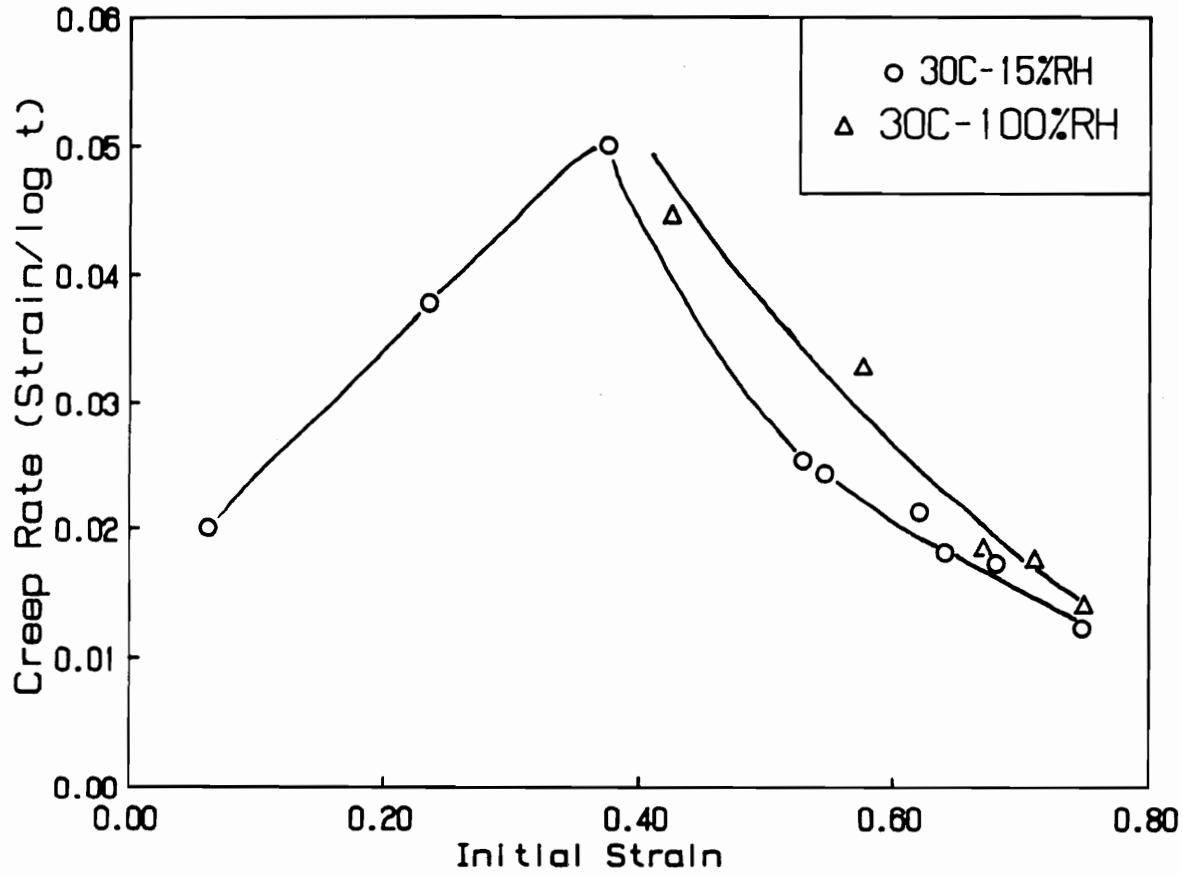

Figure 5.54. **Effect of Initial Strain Level on Compressive Creep Behavior for Foam F4 at 30°C:** Creep rates based on three hour testing period

F1 and F4, respectively. Thus, as Campbell also suggested, it is thought that in these regions, the creep behavior of the solid material of the foams can be evaluated rather independently of the cellular structure(58).

Before showing how the creep behavior is effected by the different variables at initial strain levels near 65 percent, further discussion of the buckling effect and its relation to compressive creep in these materials is given. Campbell qualitatively described the buckling phenomena in flexible foams in terms long column buckling as shown schematically in Figure 5.55(58). In looking at Figure 5.55 or likewise at Figure 2.8(micrograph of cellular textures), as the column or struts are loaded from both ends and enough strain energy is built up, the column or similarly the strut will buckle spontaneously. This buckling phenomena is believed to take place after the force on the struts is greater than a critical value of force which is dependent on the solid wall material(92). In addition, the localized strain on the buckled structure is much greater than before the column buckles. Thus, as Campbell suggested this increase in localized strain brings about a sharp increase in the creep rate as shown in Figure 5.53 and 5.54 beginning with initial strain levels near 10 to 20 percent(58). Thereafter, the rate of creep continues to increase due to an increase in the number of struts that undergo buckling. However, at initial strain levels greater than 40 percent, the number of struts that undergo buckling during creep begins to decrease since the level of strain is approaching a point where densification begins to take place.

5.3.2 Effect of Relative Humidity on Foams F1 and F4

The effect of relative humidity at 30°C and at 85°C on the creep behavior is shown in Figures 5.53-54 and 5.56-5.57 for foams F1 and F4. At both temperatures and for both foams, increasing relative humidity does result in an increase in the creep rate. At 30°C and for a 65 percent initial strain level, the change in the creep rate due to increasing relative humidity is more significant for F1 than for F4. The values for the change in the creep rate with increasing humidity are 30 percent and 18 percent for foams F1 and F4, respectively. At 85°C, this change due to relative humility in

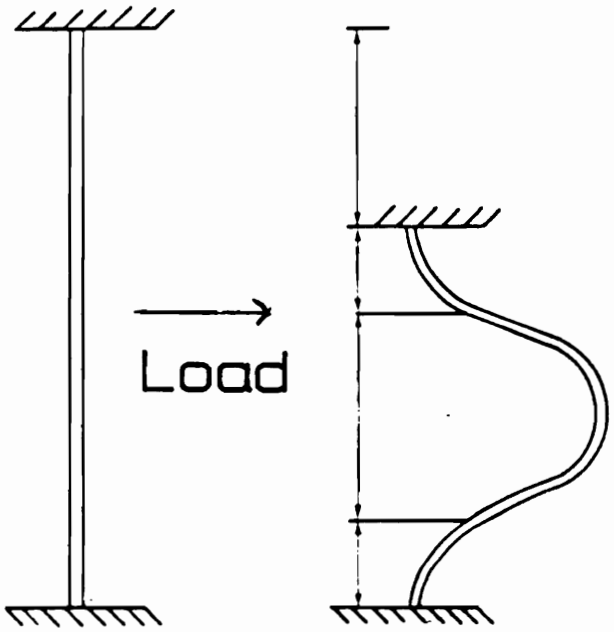

Figure 5.55. Schematic of Long Column Buckling

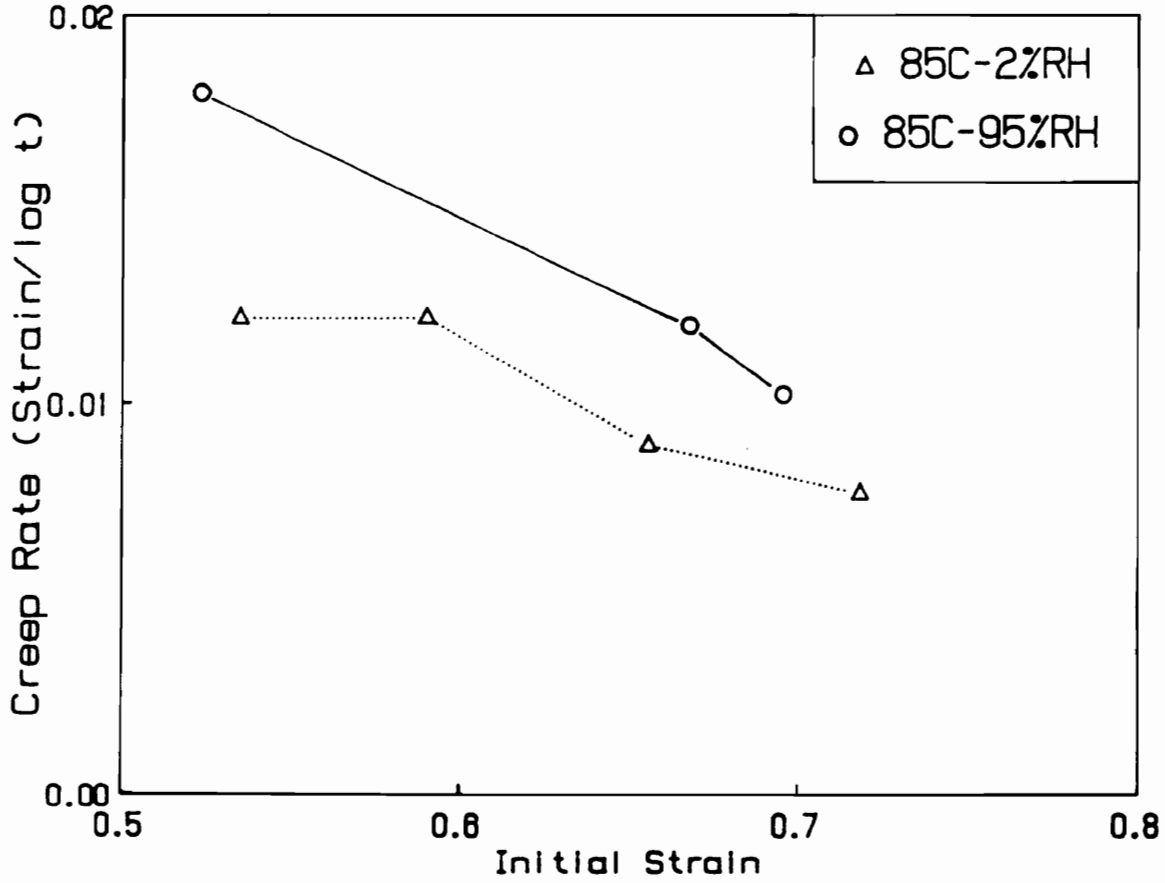

Figure 5.56. **Effect of Initial Strain Level on Compressive Creep Behavior for Foam F1 at 85°C:** Creep rates based on three hour testing period

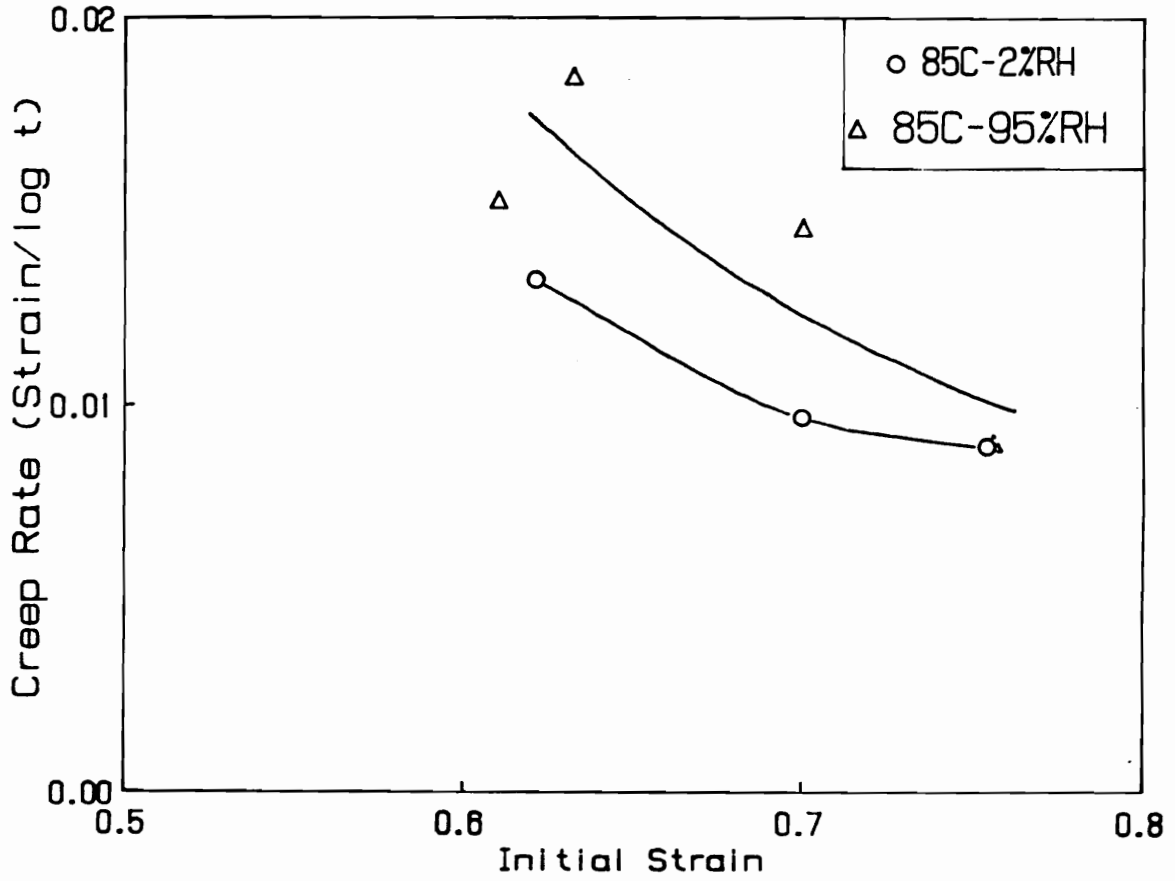

Figure 5.57. Effect of Initial Strain Level on Compressive Creep Behavior for Foam F4 at 85°C: Creep rates based on three hour testing period

the rate of creep appears to be similar and greater than at 30°C for both foams F1(35%) and F4(34%). Before, discussing the results further, it also important to note here that the loads applied at the high relative humidities were lower(ca. 15%) for a given initial strain. One is likely to predict that the creep rate will be less for a smaller load. However, it appears that this difference in loads applied at low and high relative humidity is not influencing the creep rate significantly and that the creep rate is mostly dependent on the initial strain level. Thus, in the discussion to follow it will be assumed that the differences in the creep rates at a given temperature are due to relative humidity and are not effected to any great extent by the differences in the loads applied.

For both foams, it is believed that water is acting as a plasticizer and thus allowing for further chain slippage to occur which will lead to increased amounts of creep. In addition, the change in the rate of creep for foams F1 and F4 due to increasing relative humidity, indicates that the effect of water on the creep behavior for F1 is greater than that of F4 at 30°C and furthermore, that water apparently interacts more extensively with F1 than F4. Also, the increase that is observed in the change in the creep rate from 30°C to 85°C demonstrates that the affinity of water increases with temperature for foam F4 and only changes slightly for that of F1. As suggested earlier in the load relaxation studies, this significant increase in the change of the creep rate for F4 is believed to be related to the greater ability of water to enter into the hard domains due to the weakening of the hydrogen bonds at the higher temperatures. Overall, the above trends are relatively the same to the results obtained for the effects of humidity at 30°C and 85°C for the load relaxation results discussed earlier for F1 and F4. The one exception is the change in the creep rate at 85°C is about the same for foams F1 and F4, whereas the change in the load decay rate is greater for F4(see Table 5.11). This difference could be related to the higher scatter in the results obtained for the compressive creep behavior at 85-95%RH for F4 as shown in Figure 5.57.

The effect of cycling the relative humidity during a compressive creep test has also been evaluated. From the above discussion, one would expect creep to increase by raising the relative humidity. In addition, one would assume by lowering the relative humidity a decrease in the creep rate might be observed. In attempt to confirm these speculations, the compressive creep behavior was monitored at 40°C while cycling the relative humidity from a low level to a high level and then back

to the lower level. The results of this test are exhibited in Figure 5.58 in the form of strain as a function of linear time - Figure 5.58a and log time- Figure 5.58b . In Figure 5.58a the actual timing of the test and the effect of cycling the conditions can be better followed. On the other hand, the change in the creep behavior upon reaching the different conditions is more noticeable in Figure 5.58b.

First, as shown in Figure 5.58b, the creep behavior proceeds with the normal linear behavior for strain-log time up to 200 minutes at 40°C-10%RH. Second, upon rapidly increasing relative humidity to 100% at a time near 200 minutes(see Figure 5.58a), the strain jumps significantly and then begins to take on a higher creep rate(see Figure 5.58b). After maintaining the conditions for 140 minutes at high humidity, the humidity was returned to 10 percent. Upon rapidly returning to low humidity at a time near 400 minutes, the strain continued to increase as demonstrated in Figure 5.58b.

As expected, at an increased relative humidity, the amount of creep in the foam increased. This change is believed to be related to 2 main factors. First, the load that can be withstood by the foam is less at higher relative humidities(recall Figure 5.30b). Second, the creep rate is greater at the higher relative humidities - recall Figures 5.54 and 5.57. Interestingly, by decreasing the relative humidity the strain level also increased. As mentioned above one's first intuition is to predict that the creep rate will decrease. However, when lowering the relative humidity the adsorbed moisture is believed to be released from the foam in a rather reversible fashion based on results obtained for the weight uptake studies on the plaques(see Appendix B). The removal of moisture, appears to facilitate chain slippage very similarly to the water interaction at the high humidities. This hypothesis indicates that the water molecules are physically adsorbed to the molecular structure of the foam and thus by being removed from these structures, a rearrangement of the chains is brought about. Also, this change is most likely to have a greater effect on the hard domains due to the hydrogen bonding between the hard segments.

The compressive creep behavior in Figure 5.58 also resembles the mechano-sorptive creep observed for cellulosic materials as well as other polymeric materials that contain hydrogen bonds(e.g. Aramid fibers)(93-98). This type of creep behavior(usually measured in tension) basically

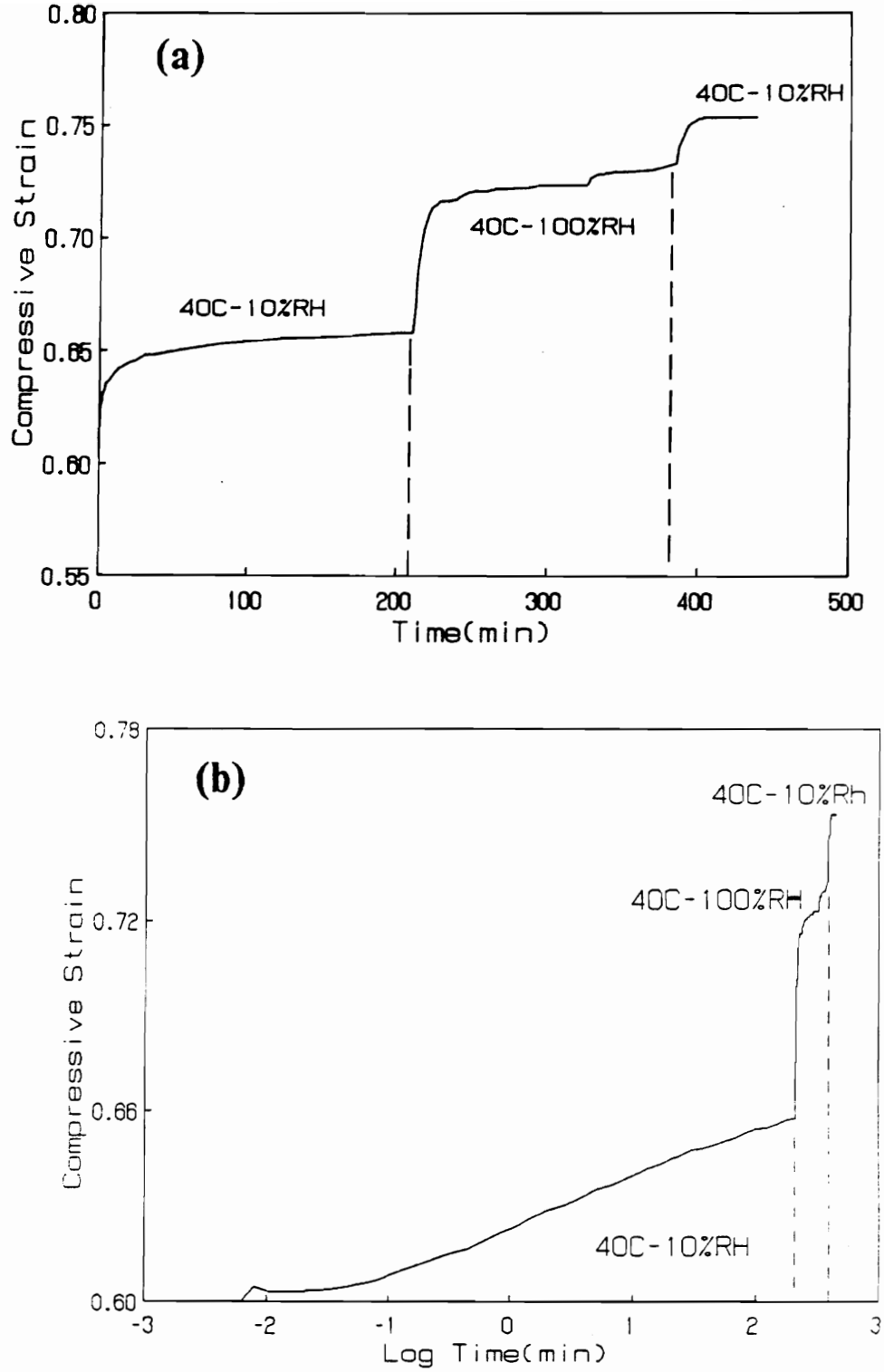

Figure 5.58. Effect of Cycling Humidity on the Compressive Creep Behavior for Foam F4 at 40°C: (a)Strain as a function of time and (b) as a function of log time; humidity cycled to 10%RH to 100%RH then back to 10%RH-20%RH

results in a higher creep rate by cycling relative humidity instead of maintaining conditions near saturation. The authors of these earlier mechano-sorptive creep studies have speculated that this phenoma is a result of swelling(93-96). In addition, it is has been suggested that swelling could add to this creep behavior through free volume and stress field effects(98). The former is thought to be a possible contribution to the creep behavior in Figure 5.58 for foam F4. That is, upon sorption(increase in %RH), swelling is thought to take place at the molecular level and during desorption, some free volume is thought to be created. If free volume is formed during desorption, the relaxation of this free volume is likely to contribute to the increase in the compressive strain level shown in Figure 5.58 at a time near 400 minutes.

Although, only one and a half cycles were carried out for this study, there does appear to be a greater amount of creep occurring in comparison to maintaining the conditions at a constant relative humidity. Thus, future work along these lines will be proposed later in this dissertation to further investigate this unusual creep behavior.

5.3.2 Effect of Hard Segment Content

Similar behavior to that shown for F1 and F4 in Figures 5.53 and 5.54 have also been obtained for F2 and F3 at 30°C-15%RH. Thus, in determining the effect of hard segment content on the creep behavior, values for creep rate were interpolated at a 65 percent initial strain level from plots of creep rate as a function of initial strain level-like the one given in Figure 5.53 for F1. A summary of these results are displayed in Figure 5.59 and given in Table 5.16.

As shown in Figure 5.59, the creep rate at a 65 percent initial strain level does increase with increasing hard segment content at 30°C(15%RH), except at the higher hard segment level. This increase with hard segment content is most significant from 21 wt%(F1) to 26 wt%(F2). The significant increase in the creep rate with hard segment content in the range of 21 wt% to 26 wt% is believed to be mostly related to a greater amount of hydrogen bonds available for disruption in F2(26 wt% HS). By disrupting and reforming the hydrogen bonds, local chain slippage is facilitated

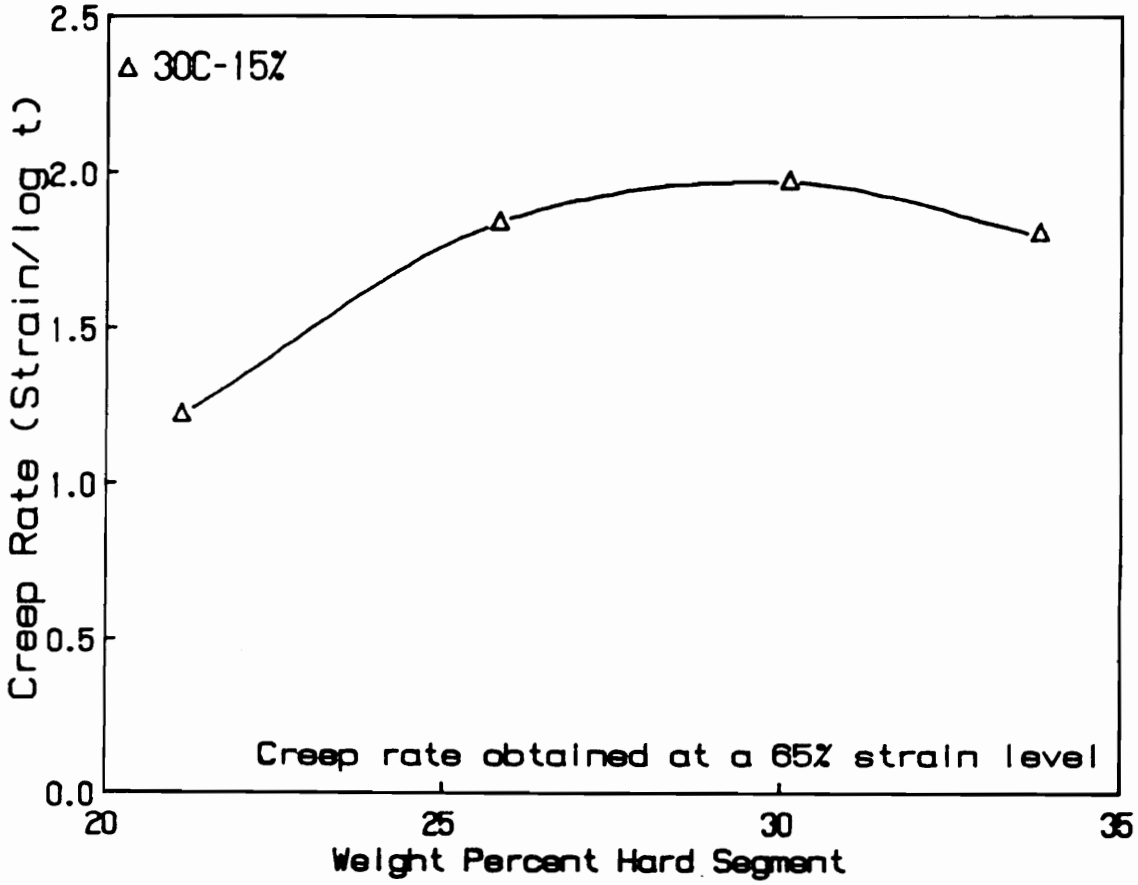

Figure 5.59. Effect of Hard Segment Content on Compressive Creep Behavior: Rates were interpolated from plots of creep rate as a function of initial strain level at a 65 percent strain level at 30°C-15%RH

Table 5.16: Summary of Compressive Creep Results for Foams F1-F4

Condition	Initial Creep Rate x 10^{-2}(180 minutes of testing)			
Foam =	F1	F2	F3	F4
30°C-15%RH	1.24	1.84	1.99	1.8
30°C-100%RH	1.61	2.18	2.3	2.14
85°C-2%RH	0.96	-	-	1.16
85°C-95%RH	1.25	-	-	1.55
125°C	1.37*	-	-	1.57*

* Estimated creep rate
- The initial creep rates are based on values interpolated from creep rate as a function of strain curves like in Figure 5.42 at 65 percent strain

which will lead to a decrease in the amount of load that can be supported by the foam. However, since the load applied to the foams is constant, the foam creeps to higher strain levels where the constant load can be supported. On the other hand, the small change in the creep rate from 26 to 34 wt% hard segment content is not well understood, but is rather consistent with results shown earlier for the compressive load relaxation studies at this same condition -recall Figure 5.36. Several possible factors, i.e. differences in cellular textures and density, were suggested earlier for this behavior at the higher hard segments. However, both of these factors are also not thought to influence the creep behavior for reasons expressed earlier concerning the density of these foams as well as the small influence that the cellular textures are believed to have on the creep behavior at initial strains near 65 percent.

5.3.3 Effects of Temperature on Creep Rate for Foams F1 and F4

The effects of temperature on the creep rate have been measured in the range of 30°C to 125°C for foams F1 and F4. An example of the creep behavior for F1 and F4 at 125°C is shown in Figure 5.60. After the short induction period, the behavior exhibited in Figure 5.60 for both foams is non-linear, unlike the behavior at 30°C and 85°C, and furthermore, similar non-linear behavior has also been observed at other initial penetration levels. The non-linearity observed in Figure 5.60 does indicate that additional causes for creep are occurring at the higher temperatures. These additional causes at 125°C are believed to take place for similar reasons discussed earlier for the compression load relaxation and tensile relaxation studies on these same foams. More discussion on these causes will be given after considering the overall effect of temperature on the creep behavior for foams F1 and F4.

The rate of creep as a function of initial penetration level at the different temperatures is shown in Figures 5.61 and 5.62 for foams F1 and F4, respectively. In determining the creep rates at 125°C, the rate was estimated by calculating the change in strain over the log time period(3 hours) in which this change took place. This simplified method was used since the behavior for strain as a function

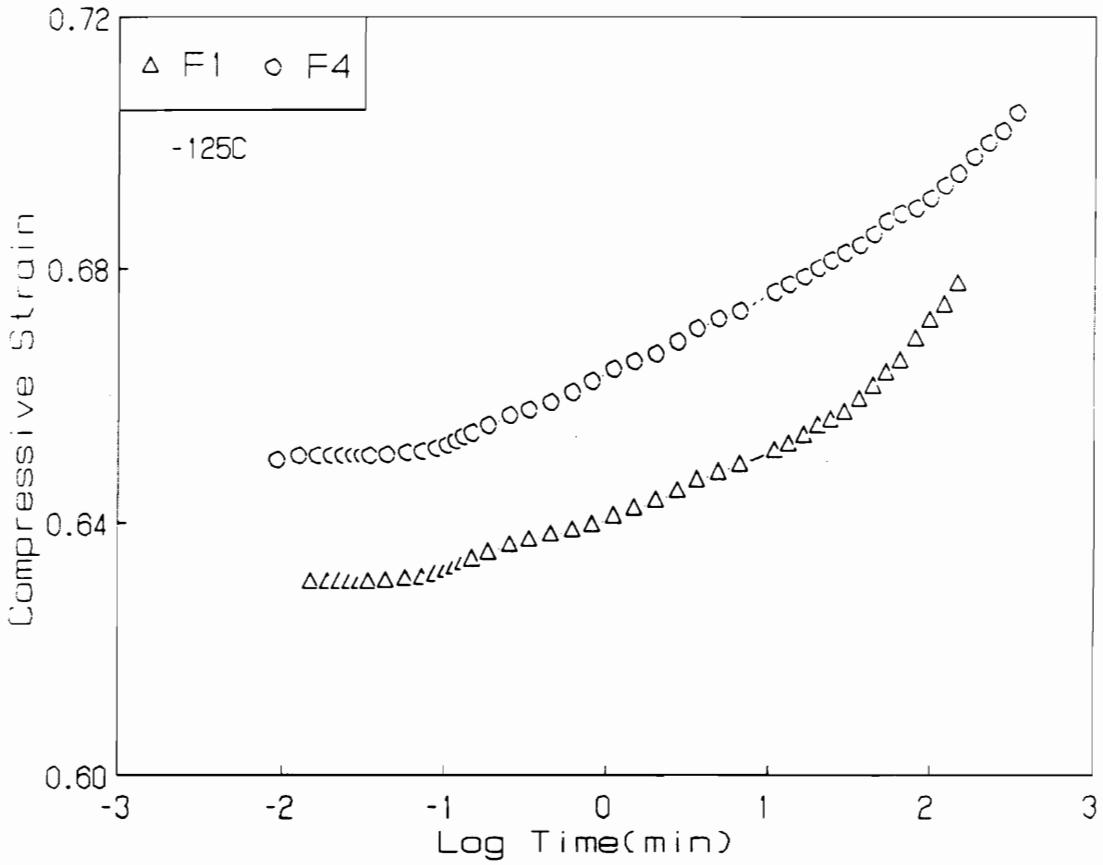

Figure 5.60. Creep Behavior for Foams F1(a) and F4(b) at 125°C: Load applied to F1 was 3500g and that of F4 was 2100g

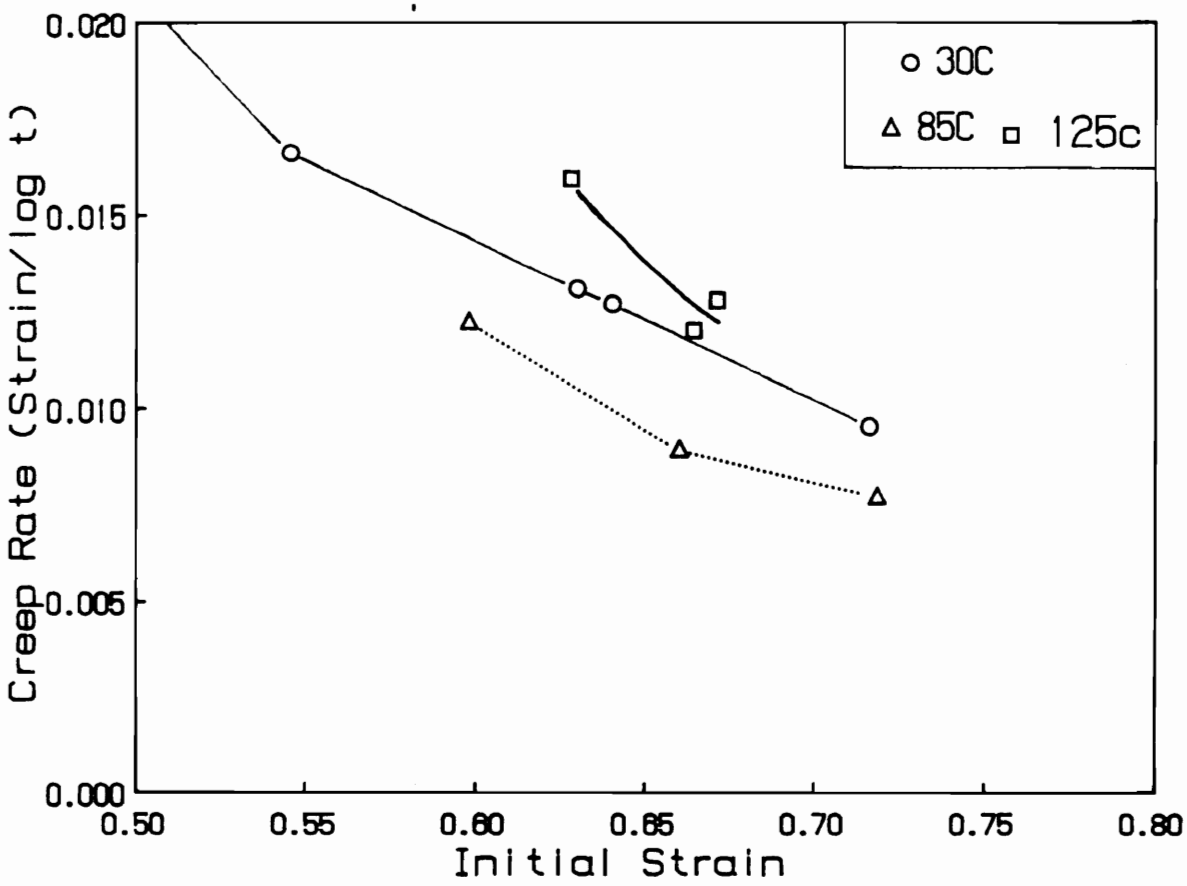

Figure 5.61. Effect of Initial Strain Level on Compressive Creep Behavior at Temperatures Ranging From 30-125°C for F1: Creep rates based on 3 hour testing period; rates estimated at 125°C

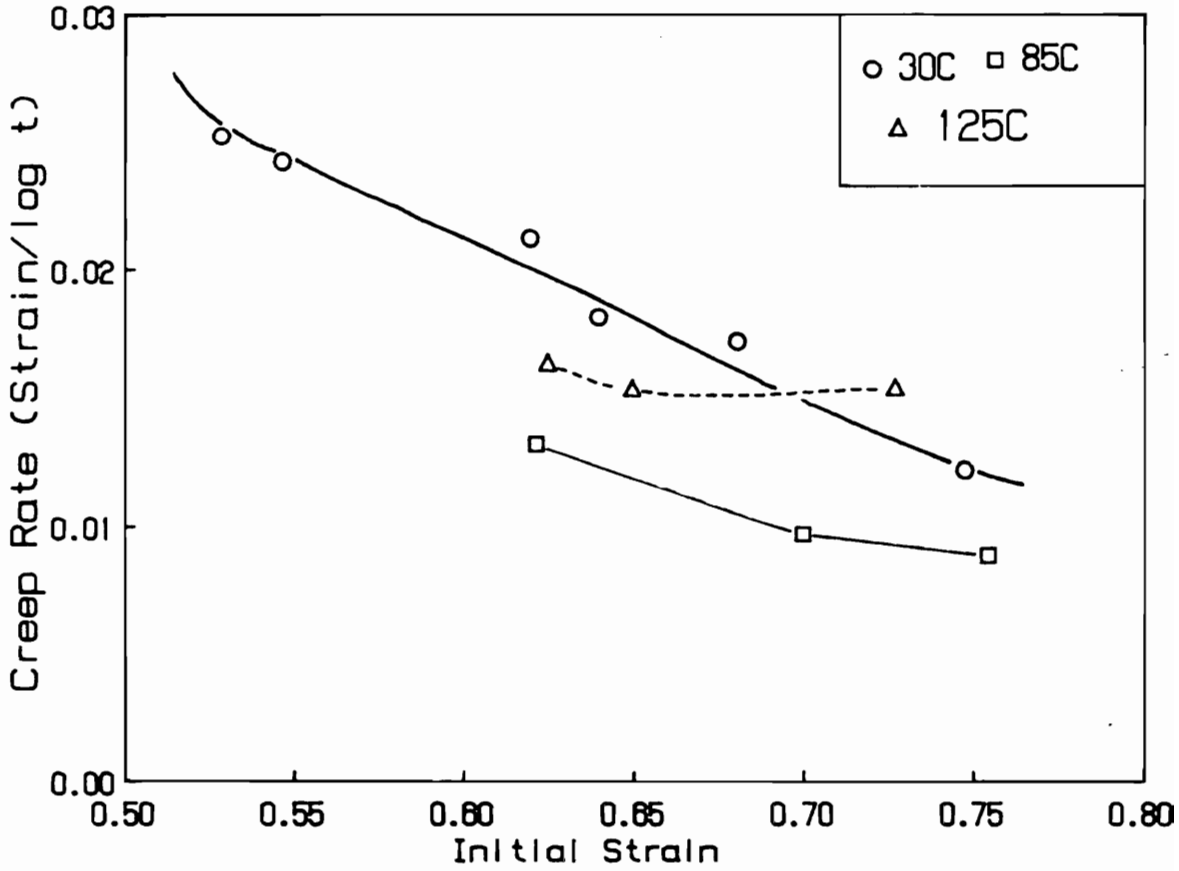

Figure 5.62. Effect of Initial Strain Level on Compressive Creep Behavior at Temperatures Ranging From 30-125°C for F4: Creep rates based on 3 hour testing period; rates estimated at 125°C

log time is non- linear at 125°C as shown in Figure 5.60. From Figures 5.61 and 5.62, the effect of temperature on the creep behavior was determined at a 65 percent initial strain level and is displayed in Figure 5.63. As shown in Figure 5.63, the thermal dependence on the creep rate exhibits a decrease in the amount of creep from 30°C to 85°C and increases from 85°C to 125°C for both foams F1 and F4. The decrease in the rate of creep at 85°C is also thought to be related to similar decreases observed in the rate of load relaxation as well as the stress relaxation in tension over similar temperature ranges. It is also important to note here that the loads applied to F4 at 30°C were slightly higher(ca. 7%) than at 85°C for a given initial strain level. On the other hand, the loads applied to F1 at 30°C were approximately 7 percent lower than at 85°C. While the smaller load applied to F4 at 85°C may contribute to its lower creep rate, this does not appear to be a factor for the creep rate at 85°C for F1. As suggested earlier for the effects of relative humidity on the creep behavior, a small difference in the loads applied at two different conditions is not significantly effecting the comparison of the creep rates at the two conditions. This suggestion also seems applicable to the variable temperature results. Thus, it is believed that the compressive creep behavior is being accelerated by increasing the temperature and therefore it appears that the equilibrium strain level is approached more rapidly.

At the higher temperature of 125°C where additional changes in the network structure have been indicated by the FTIR thermal studies as well as in the relaxation studies, larger amounts of creep are expected to occur. In the case of F1 at 125°C, the estimated creep rate or the amount of creep over three hours at the 65 percent initial level is the highest of the three temperatures. This observation is consistent with the load relaxation results for F1 and furthermore, implies that the structural changes which have been indicated by the FTIR thermal studies are also affecting the compressive creep behavior for this foam. On the other hand, the estimated creep rate for F4 at 125°C is higher than the creep rate 85°C, but, as somewhat unexpected, it is lower than the rate at 30°C(see Figure 5.63). One possible contribution to this difference in creep rates at 30°C and 125°C for F4, is a 15 percent lower load is applied at 125°C. Again, this contribution is not believed to be a major factor, but it can not be overlooked. It is also important to note that this difference in creep behavior at 30°C and 125°C is not observed at the higher strain levels as well as over long time

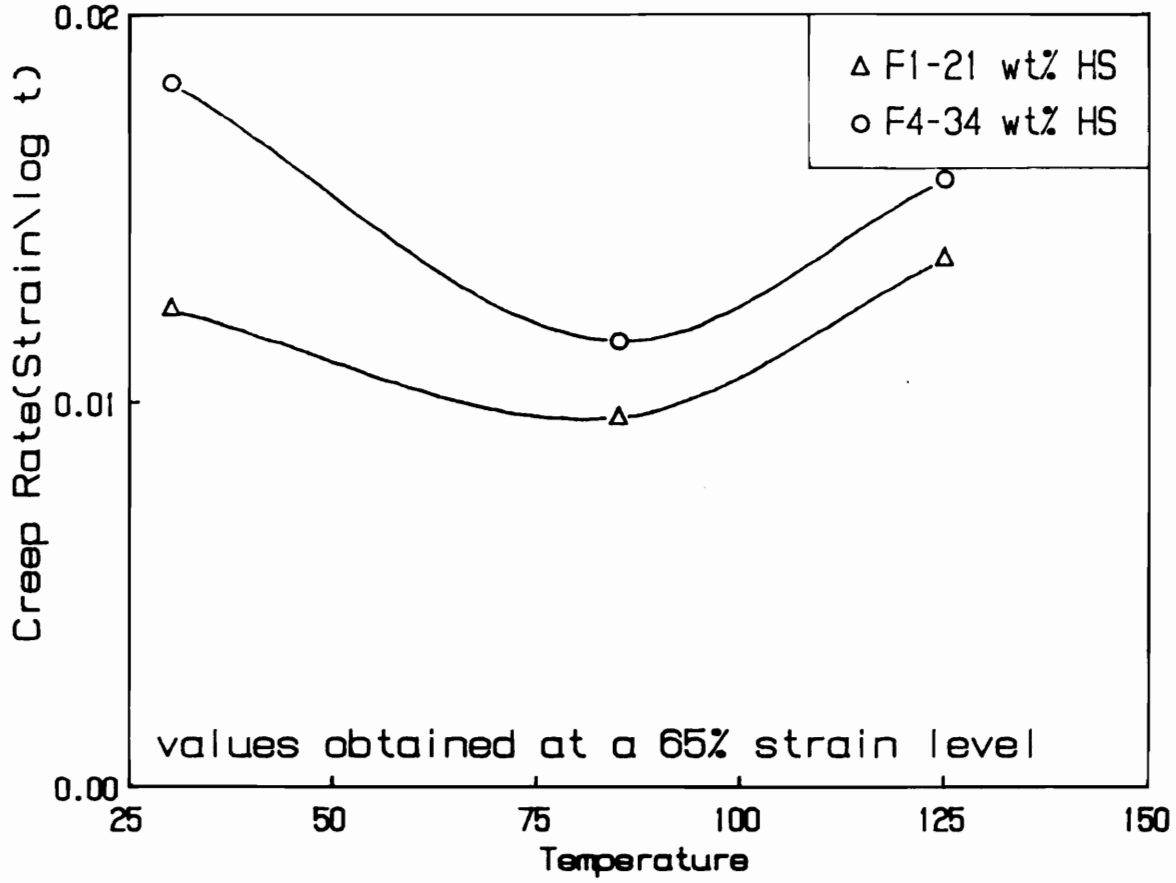

Figure 5.63. Effect of Temperature on Compressive Creep Behavior for Foams F1 and F4: Rates were interpolated from Figures 5.53 and 5.54 at 65 percent strain

periods for a 65 percent initial strain level. As shown in Figure 5.62, one will notice that the estimated rate of creep at 125°C is higher than the creep rate at 30°C for initial strain levels greater than 70 percent. Also, based on results obtained over long time periods at 30°C and 125°C, the amount of creep is similar at a 65 percent strain level after 20 hours of testing and is believed to be greater at 125°C at times longer than 20 hours. This change in behavior over longer time periods is due to the sharp increase in the strain over log time at 125°C, while at 30°C there is a constant change in the strain with log time as will be discussed shortly (see Figures 5.52 and 5.60). Thus, in the case of F4 at 125°C, there is a significant amount of creep taking place, but it is thought to be more noticeable over longer time periods as well as at the higher strain levels.

Further insight can be gained by comparing the effect of temperature on the creep behavior for the two foams F1 and F4. First, the effect of temperature is greater on F4 by increasing the temperature from 30°C to 85°C. This result is consistent with the load decay values from the compression load relaxation studies for foams F1 and F4 as shown in Figure 5.27. Second, the amount of creep is higher at 125°C for F4 than F1 but the increase in the effect of temperature from 85°C to 125°C is greater for F1 than F4. As discussed earlier in the compression load relaxation studies, temperature is believed to have a more significant effect on the viscoelastic behavior of F1 at temperatures above 100°C. This conclusion is supported by the FTIR-thermal studies on the plaques of these foams, i.e. the FTIR-thermal studies indicated that the hydrogen bond disruption is most significant at the higher temperatures(mostly related to urethane groups) and there is possibly some chain scission taking place within the urethane and urea linkages. Both of these structural changes are believed to have a more significant effect on the network structure of F1 than in the case of F4 for reasons that were given earlier. Finally, as discussed above for foam F4, the amount of creep taking place at 125°C for F1 also increases significantly over long time periods as demonstrated by its sharp increase in strain with log time in Figure 5.60. In the next section, further comments on the long term creep behavior at 30°C are made for foams F1 and F4 which will further emphasize the significant effect that temperature has on the amount of creep taking place at 125°C.

5.3.4 Long Term Creep Behavior

In addition to the 3 hour creep period addressed above, more limited longer term behavior of compressive creep response was evaluated at 30°-15%RH for F1 and F4. These results have been obtained over 2 to 3 days of testing for F1 and F4, and are shown in Figure 5.64 for similar initial strain levels. As exhibited for F1 in Figure 5.64a, at times near 5 hours(log time = 2.5) the creep rate begins to take on a slower creep rate and after approximately 30 hours(log time = 3.25) the creep rate begins to level off. The change in the initial creep rate near 5 hours is thought to be related to the effect of strain level on the creep progression in F1. On the other hand, since these materials are networks, they are expected to reach an equilibrium at some extended time period, unless there are some chemical changes occurring. Thus, after 30 hours of creep, F1 appears to show signs of approaching an equilibrium level of strain at this given load.

As shown in Figure 5.64b, foam F4 creeps at an initial rate of creep up to times near 21 hrs(log time = 3.1). At times near 53 hours(log time = 3.5) or slightly greater, foam F4 seems to approach an equilibrium strain level. In comparing the long term behavior for the two foams, it is apparent that the lower hard segment foam, F1, does begin to approach an equilibrium level of strain over a shorter time period than F4 (see Figure 5.64). As discussed earlier, this difference is believed to be mostly related to F4 having a higher hard segment content as well as more available hydrogen bonds; thus, allowing for a more extended rearrangement within its(F4) network structure.

5.4 Summary of Viscoelastic Behavior for Foams F1-F4

In summary, results have been presented and discussed on the viscoelastic behavior for a series of flexible slabstock water-blown polyurethane foams with a systematically increasing hard segment content. Three tests, tensile stress relaxation, compression load relaxation, and compression creep

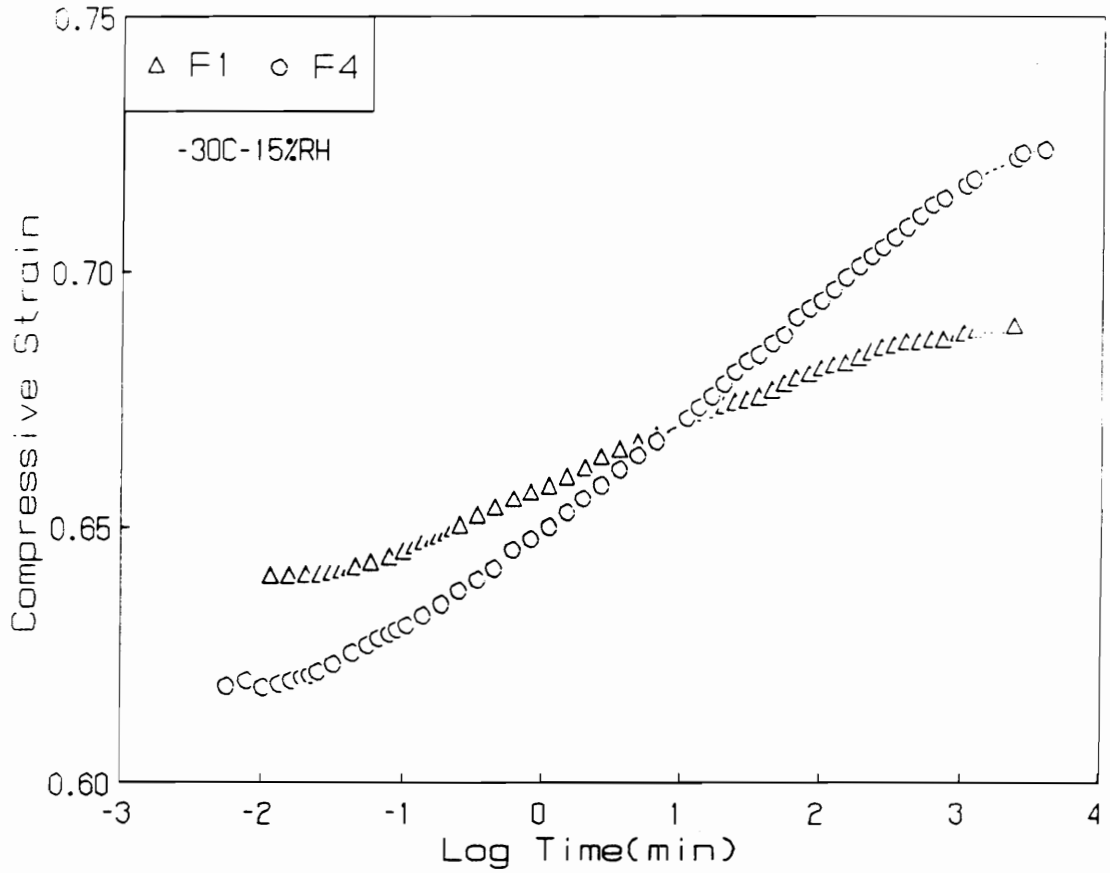

Figure 5.64. Long Term Compressive Creep Behavior For Foams F1 and F4: Load applied to F1 was 3kg and that of F4 was 2.8kg

were utilized to obtain this behavior under controlled conditions of temperature and/or relative humidity. The results obtained from these three tests revealed some similar conclusions on how the viscoelastic behavior of flexible foams is affected. Before summarizing some of these similarities, a review is given for the results that were generally disclosed by only the individual tests.

First, the stress relaxation behavior in tension of foams F1 and F4 and their respective plaques exhibited comparable thermal dependence on stress decay. This result gives further indication that the relaxation behavior in tension is dependent on the solid portion of the foam and thus is independent of its cellular texture. A rather systematic increase in the amount of stress decay over three hours was observed with increasing hard segment content in the range of 22 to 34 wt%. Such an increase was found for temperatures up to 125°C, and at 140°C there was was a minimum in this behavior at 26 wt% hard segment content. As discussed earlier, this minimum was attributed to additional mechanisms for stress relaxation that were believed to be related to possible chain scission in the urea and urethane linkages as well as to further hydrogen bond disruption.

The tensile stress relaxation behavior for foams F1-F4 exhibited a rather linear relaxation for log $\sigma(t)$-log t over most conditions for the three hour testing period. The slope from this rather linear relationship is thought to predict how the relaxation behavior differs with hard segment content and temperature, but not necessarily relative humidity since it is thought to be more a function of weight uptake of water. A similar linear relationship for the log $\sigma(t)$-log t (to that of the foams) was also observed for the PUU elastomer which was utilized to evaluate the viscoelastic behavior of an additional domain forming material. The thermal dependence of the relaxation behavior(log $\sigma(t)$-log t) for the PUU elastomer was comparable to that of the foams; thus, indicating that the changes in the relaxation behavior due to temperature are related to similar structural changes in the two materials. This was believed to be true even though the PUU elastomer has a linear segmented morphology whereas the foams possess a covalent network in addition to a two phase hard/soft domain texture.

For the compression load relaxation behavior of foams F1-F4, a similar relationship to that of the stress relaxation results in tension was observed for the log load vs log t. This rather linear relationship was also seen at most conditions. In addition, the slope of this relationship was found

to be fairly independent of constant strain up to 65 percent. At strains greater than 65 percent, an increase was observed in the slope or load decay rate up to strain levels near 75 percent where a maximum was noticed. The increase in the load decay rate at the higher strains was attributed to an increase in the localized strain on the solid material in the foam. The load decay rates as well as the values for percent load decay also increased rather systematically with increasing hard segment content, except at the higher hard segment contents ranging from 31(F3) to 34(F4) weight percent.

As a result of the decrease in the load relaxation rate up to 100°C, foams F1-F4 were thermally annealed at 100°C and tested at 30°C-15%RH. However, no significant changes in the load relaxation behavior were seen in any the foams which indicated that the annealing process was not causing additional crosslinking to take place. It also gave further credibility to the variable temperature relaxation behavior obtained for these materials.

The hysteresis loss(qualitatively measured) and compression set were also evaluated in addition to the load relaxation behavior. Both of these measurements were rather consistent with the load relaxation results; thus indicating that the hysteresis or fatigue as well as the thickness loss in the shape of the foam are related to the load decay taking place over time.

The compressive creep behavior for foams F1-F4 exhibited a rather linear relationship in the form of strain-log time after a short induction period on the order of 6 seconds. Unlike the dependence of the load decay rate on strain, the initial creep rate was found to be mostly dependent on strain over the range of 10 percent to about 60 percent. Basically, a maximum in this behavior was seen for both foams F1 and F4 near 40 percent. This dependency on strain was attributed to the buckling of the struts which is thought to take place in these foams at strains in the range of 10 to 60-65 percent(58). Thus, it was believed that the creep behavior was rather independent of the cellular textures at the very low strain levels as well as at strains greater than 60 percent. Therefore, in evaluating the effects of temperature, relative humidity, and hard segment content, the initial creep rates at 65 percent strain obtained after 3 hours of testing were utilized.

At a condition of 30°C-15%RH, an increase in the initial creep rate with increasing hard segment content was observed, except at the higher hard segment content from 31 wt% to 34 wt%.

The effect of hard segment content on the creep behavior was similar to that of the load relaxation behavior for the same condition.

Some rather interesting behavior was observed upon cycling relative humidity during a compressive creep test. As expected, when the relative humidity was rapidly increased during the test, the amount of creep was found to increase significantly. On the other hand, upon rapidly decreasing the relative humidity, an increase in the creep or strain level was also observed. Though, somewhat unexpected, it did indicate that the removal of water molecules absorbed to the chain structures was facilitating further chain slippage and thus leading to the increase in creep by lowering %RH. The overall creep behavior observed upon cycling relative humidity was also thought to be similar to the mechano-sorptive creep phenomena that has been observed for some polymeric materials which contain hydrogen bonds.

Up to this point, the effects of temperature and relative humidity on the viscoelastic nature of foams F1-F4 have not been reviewed extensively. The main reason is that these effects were found to be rather similar on the behavior obtained from the three different viscoelastic tests. Some of the key discoveries are summarized below that lead to a better understanding of how temperature and relative humidity effect the viscoelastic behavior and possibly the morphological features of these foams.

For temperatures up to 100°C, a fairly linear relationship was observed over a three hour testing period for the data fits of the three respective viscoelastic tests. From the slopes of these linear relationships, a small decrease in the relaxation rates and the initial creep rate were seen with increasing temperature(3 hr period). These results gave an indication that temperature was accelerating the viscoelastic decay and possibly the approach to equilibrium conditions. Two factors leading to this acceleration that were suggested in the discussion of the stress relaxation behavior were (1) a decrease in the %RH level is taking place with increasing temperature(more so for tensile studies) and (2) an increase in the amount of viscoelastic decay with increasing temperature was occurring upon approaching the constant strain level or the initial compressive strain level. This hypothesis was also confirmed experimentally by additional stress relaxation tests as well as supported by reports in the literature(91).

Within the range of 25°C to 100°C, it was believed that temperature accelerated the viscoelastic decay more so in F4 than in F1. This belief was based on the greater change in the initial creep rate from 30°C to 85°C for F4 in comparison to F1. In addition, the relaxation rate constant, τ_1, obtained from fitting the thermal dependence of the load or stress decay values were lower in the case of F4 than F1. This difference in the temperature dependence on the stress relaxation in F1 and F4 was thought to be related to the higher hard segment content in F4 as well as its higher hydrogen bond content.

At temperatures greater than 100°C, there were signs of significant amounts of viscoelastic decay taking place in foams F1-F4. These signs were indicated by the deviation from linearity for $\log\sigma(t)$ vs log t as well as the log load(t) vs. log t over longer time periods at 100°C and over the three hour testing period at 125°C and 140°C. Also, the compressive strain level as a function of log time exhibited non-linear behavior at 125°C. In addition to observing non-linear behavior, the amount of load and stress decay from 100°C to 125°C increased for the three hour period. In addition, from 85°C to 125°C the amount of creep or the estimated creep rate increased. This increase in viscoelastic decay was thought to be due to additional mechanisms for relaxation and creep. Based on FTIR-thermal studies, these mechanisms were believed to be related to an increase in the disruption of hydrogen bonds with temperature and possibly some chain scission occurring in the urea and urethane linkages.

The thermal effects at temperatures greater than 100°C were also believed to be more significant in the lower hard segment foam, F1, than that of F4. This belief was supported more extensively by the relaxation results obtained in compression and in tension as well as the FTIR-thermal analysis. First, at 140°C, the amount of decay of either the load in compression or the stress in tension was higher for F1 than F4 whereas at temperatures below 140°C it was higher for F4. Second, the relaxation constant, τ_2, of Eq. 5.1 was higher for F1 than for F4. Recall that this constant accounted for the decay that occurs mostly at temperatures greater than 100°C. Also, the results obtained from the FTIR-thermal analysis did indicate that the structural changes were more significant in F1 than in F4.

The effects of relative humidity at various temperatures also revealed similar conclusions by the three different viscoelastic tests. For all three tests it was evident that the load or stress exerted by the foams was less with increasing relative humidity. At 30°C the effect of increasing relative humidity on the change in the viscoelastic behavior was greater for F1 than F4. This result did indicate that water was interacting more effectively with F1 than with F4 at 30°C. At 60°C, the relaxation results(results not obtained for creep) revealed that there was not a significant difference in the effect of relative humidity on the change in the rate of relaxation between foams F1 and F4. However, at the higher temperatures(85°C for compression tests and 90°C for tension), increasing relative humidity did result in greater changes in the load and stress decay rates for F4 than in F1 and there were similar changes observed for both foams in the initial creep rates. In addition, the changes which occurred due to relative humidity were more significant with increasing temperature for F4 than for F1. Thus, it was believed that at the higher temperatures, water was able to interact more with the hard domains due to a weakening of the hydrogen bonds between the hard segments.

In short, the viscoelastic behavior in flexible polyurethane foams is dependent on a number of variables, several of which, have been emphasized in this chapter. As discussed and shown within this chapter, it is important to try to separate the effects of the cellular nature of the foam and that of the solid material contained within the cellular walls when evaluating the effects of these different variables on the viscoelastic nature. Although, in some instances it was not possible to fully separate the two-especially in the compression mode, the effects of the cellular nature were minimized as much as possible in order to determine the effects of hard segment content, temperature and relative humidity on the viscoelastic behavior of foams F1-F4. From these studies, it can be concluded that increasing hard segment content does lead to an increase in viscoelastic decay in tension as well as in compression. At a constant temperature, increasing relative humidity does promote further relaxation and creep in flexible foams - especially at the higher temperatures. In comparison to the effect of relative humidity, temperature does have more significant effect on the viscoelastic decay in flexible polyurethane foams-especially at temperatures greater than 100°C.

Chapter VI

6.0 Characterization of Flexible Foams Containing Lithium Chloride

Over the past 10 years, Dow Chemical and Virginia Tech have worked together to better understand the properties and their relationship to the solid morphology of flexible polyurethane foams - mainly those foams of series F1-F4. As already discussed and reviewed within this dissertation, great progress has been made through this joint venture to further this understanding. As part of a continuation of this joint venture, additional work has been carried out on foams recently developed by Dow Chemical as a result of environmental concerns over CFC's. As discussed in the literature review, CFC's are utilized as chemical blowing agents in making flexible polyurethane foams and serve to lower the density of the foam and "soften" it. Thus, the researchers at Dow Chemical have been working on alternative methods for "softening" the foam, but still retaining important physical properties such as low compression set values.

From the initial morphological investigations of the foam's solid structure carried out by Dow Chemical and Virginia Tech., it was learned that large urea base structures(polyurea aggregates) on the order of 100-300 nm in size were present based on TEM studies. In addition, these polyurea

aggregates structures were believed to act like filler particles therefore giving reinforcement to the foam's stiffness. With this in mind, the researchers at Dow Chemical set out to develop high water(hard segment) content foams and/or lower density foams with less of the urea aggregate structure in order to obtain a "softer" foam. One of these new foam systems involved adjusting the chemical formulation of a standard flexible slabstock foam by adding an extra component, lithium chloride which was dissolved in in water. Although this new foam system provides some of the above desired characteristics, it does have some problems which will become evident in this chapter. However, from a morphological standpoint these new foams are quite interesting - especially the changes that are occurring in the solid portion of the foam which are thought to be related to the urea aggregates whose structure is still not fully understood. In adding to the understanding of the solid structure and the physical properties of these new flexible slabstock foams as well as slabstock foams in general, additional morphological techniques and viscoelastic tests have been carried out on a set of foams with and without lithium chloride in their formulation. The foams utilized for this study are given in Table 4.1 along with composition and density information. As a reminder, all of these foams contain a 5 pphp water in their formulation which results in a 34 wt% hard segment-comparable to foam F4. In addition foams 44-4 and 44-5 contain 0.4pphp and 0.5 pphp lithium chloride in their formulation, while foam 44-0 does not contain any LiCl. The amount of LiCl in foam 44-5 on a molar basis corresponds to approximately 0.012 moles of LiCl to 0.55 mols of urea and urethane linkages. The majority of the results that are presented in the following sections of this chapter are for foams 44-0 and 44-5 - the two extremes for this series.

6.1 Morphological Characterization

In the first part of this chapter, characterization of both the solid and cellular morphology of the LiCl foams and its control are provided. The techniques that have been utilized to characterize the solid morphology are transmission electron microscopy(TEM), small angle x-ray

Table 6.1: Materials

Foam	LiCl Content(pphp)	LiCl Molar Content*	Density(lb/ft^3)
44-0	0.0	0.0	1.36
44-4	0.4	0.02	1.43
44-5	0.5	0.022	1.51

* LiCl molar content is defined as the number moles of LiCl molecules to the number moles of urea and urethane molecules

Comments:

1. All foams were made with 5pphp H_2O and a 100 isocyanate index
2. Hard segment content is 34 wt% for all foams

scattering(SAXS) and wide angle x-ray scattering(WAXS), and differential scanning calorometry(DSC). Scanning electron microscopy(SEM) has also been used to characterize the cellular textures. In some instances, the work presented in this section was carried out at Dow Chemical in Freeport, TX and is shown here in order to aid in the discussion. The results obtained from the above techniques along with some background information are now presented.

6.1.1 TEM

As mentioned earlier, transmission electron microscopy has been useful for analyzing the solid portion of the flexible foams due to the presence of the large urea based structures. These structures have been labeled in many different ways, but will be referred to as the polyurea aggregates in order to be consistent with earlier discussions in this dissertation. In Figure 6.1, the effects of adding 0.5 pphp LiCl to a standard flexible slabstock polyurethane foams formulation can seen by comparing the TEM micrographs for foams 44-0 and 44-5. As shown by these micrographs in Figure 6.1, the differences in the phase segregation are rather significant upon adding the lithium chloride to the formulation. For foam 44-0, the phase segregation is pronounced and the polyurea aggregates are believed to be the darker phases in Figure 6.1a. On the other hand, the phase segregation for 44-5 is diffuse and the more darker regions are not as noticeable. The TEM micrograph for foam 44-4, not shown here, is very similar to that of 44-5, but with slightly better phase segregation. Therefore, it does appear that by adding the LiCl to the formulation that Dow Chemical has effectively dispersed the urea aggregates within the chemical network structure of the solid portion of a high water content flexible slabstock foam. Although, the actual extent of this dispersion is not well understood, it is thought that the polyurea aggregate structure has been reduced in size and/or has not formed at all in the lithium chloride foam.

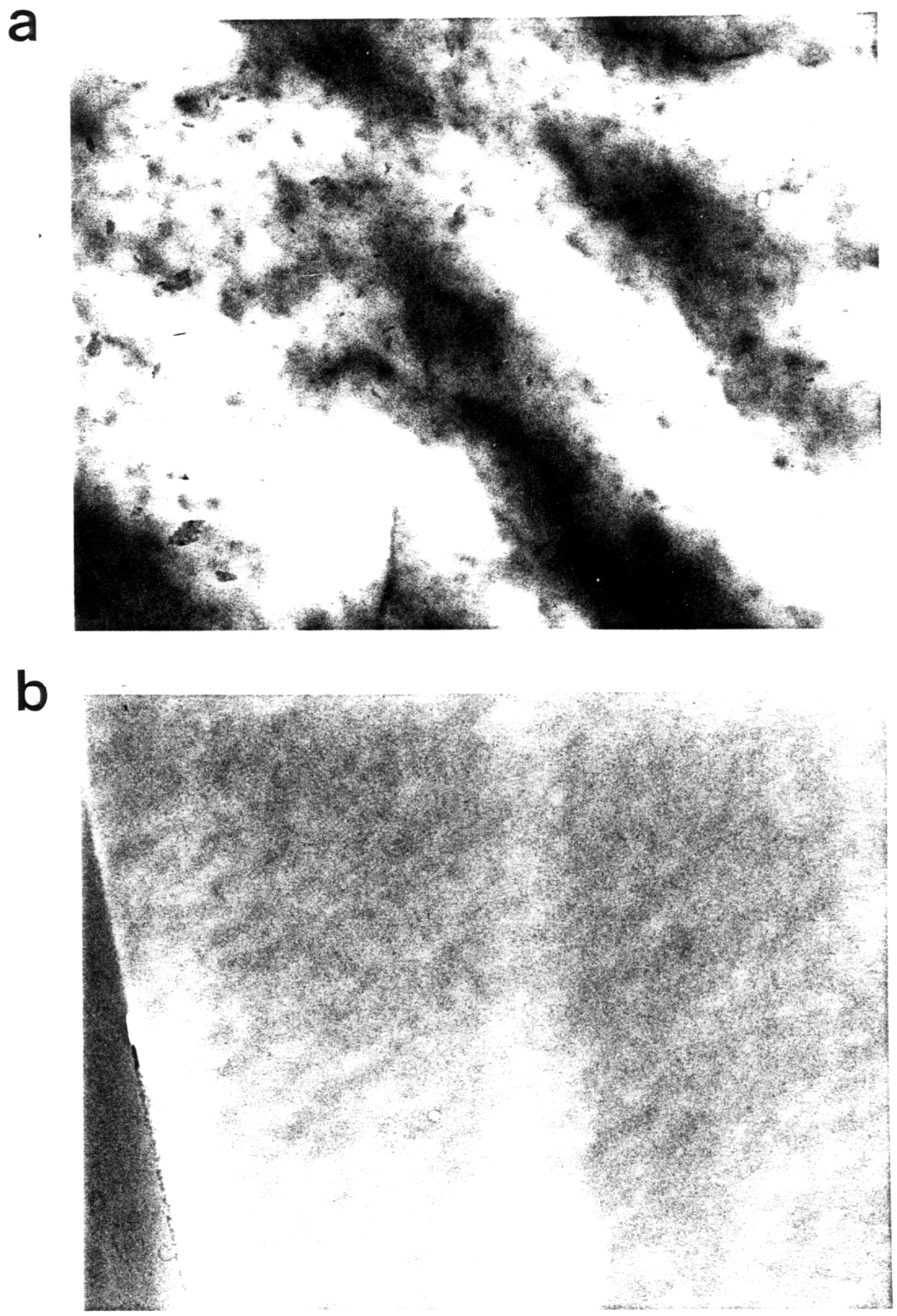

Figure 6.1. TEM Micrographs for Foams (a) 44-0 and (b) 44-5: 1mm = .0333μm

6.1.2 Thermal Analysis

Differential scanning calorimetry was utilized to determine the effect of adding LiCl to the formulation on the soft segment glass transition and the phase separation of the hard and soft segments. The DSC traces are shown in Figure 6.2 for foams 44-0 and 44-5. In comparing the two traces, the soft segment glass transition(near -50 to -45°C) is higher for foam 44-5 and is somewhat broader than that of 44-0. Both of these observations indicate more phase mixing is taking place in the lithium chloride foam. This behavior does seem consistent with the TEM results shown above.

One may also notice that there is broad endotherm near 100°C for foam 44-5 which is not present in the DSC trace for foam 44-0 - see Figure 6.2. In rerunning this test immediately after the first scan this endotherm is reduced considerably. Somewhat similar behavior has also been observed for other flexible foams, e.g foams F1-F4(21). It was speculated that such a broad endotherm as shown in Figure 6.2b is due to bound water being released(21). While additional absorption of water in foam 44-5 could be expected due to the small amount of LiCl present, the thermogravimetric analysis of a fresh sample showed no appreciable weight loss. This result might indicate that the endotherm observed by DSC is not due to moisture being released, but due to the disruption of hard domains that lack thermal stability. Seymour and Cooper have also suggested a similar explanation based on DCS studies of some PTMO/MDI polyurethane elastomers(84).

6.1.3 X-Ray Analysis

Both wide angle x-ray diffraction and small angle x-ray scattering have been utilized to probe possible changes in the structural order of the foams due to the addition of LiCl to its formulation. The WAXS diffraction patterns are shown in Figure 6.3 for foams 44-0 and 44-5. In general, these patterns are similar to those obtained for foams F1-F4. The apparent diffraction peak at 0.45 nm

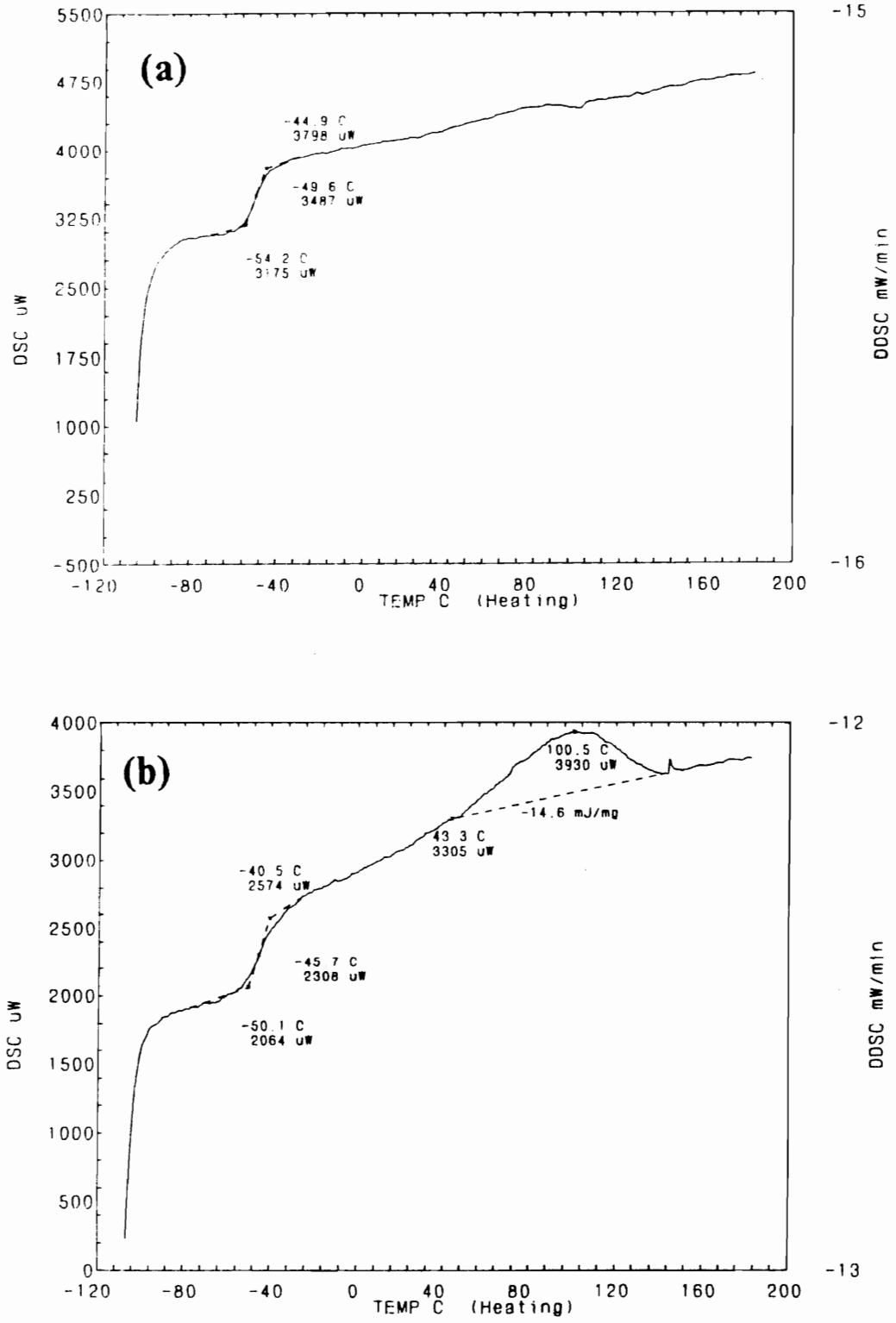

Figure 6.2. DSC Traces for Foams (a) 44-0 and (b) 44-5: Obtained at a 10°C/min heating rate

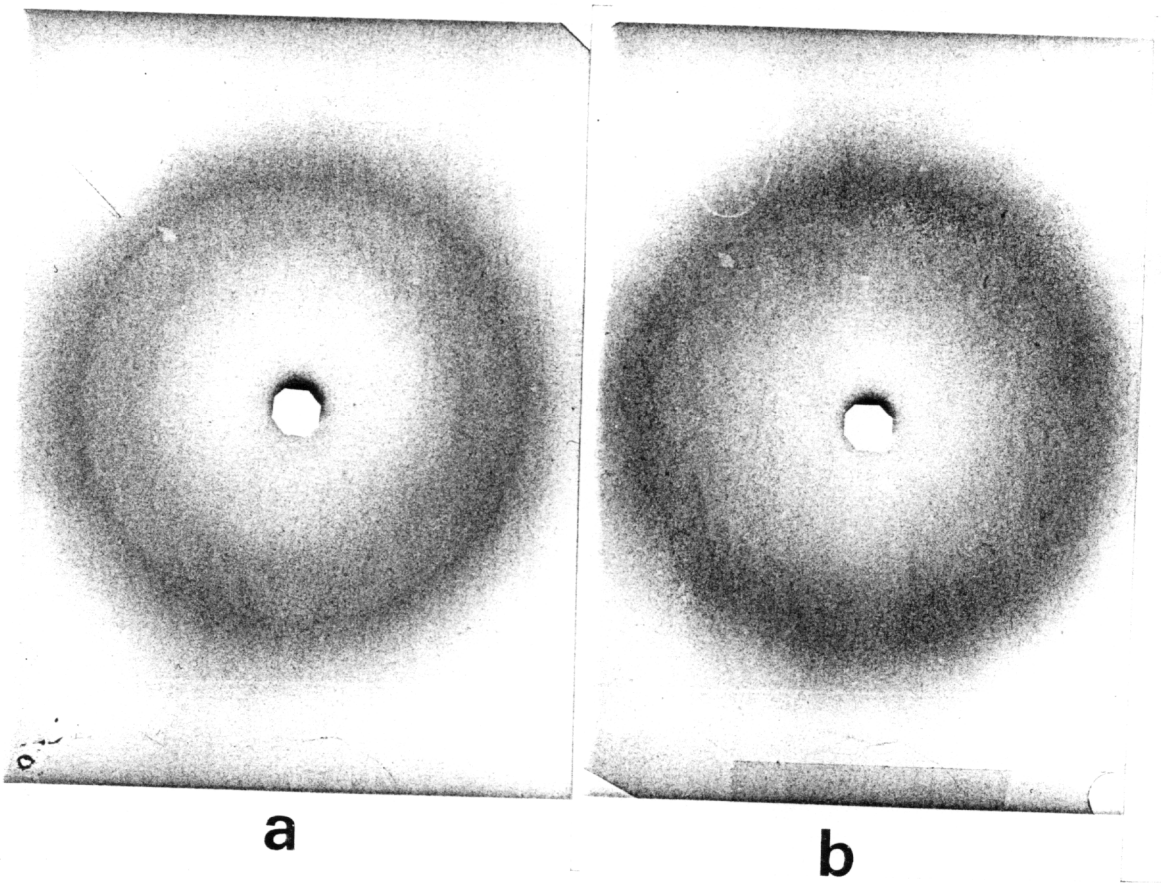

Figure 6.3. WAXS Diffraction Patterns for Foams (a) 44-0 and (b) 44-5

is distinctly sharper for foam 44-0 than 44-5. In addition, there is a sign of a weaker peak at 0.59 nm for foam 44-0 that is not observed in the case for foam 44-5. The differences in the WAXS patterns indicate that the structural order of the hard domains is clearly reduced by adding LiCl to the formulation. In view of the TEM results, this decrease in structural order in foam 44-5 is believed to be related to a significant reduction in the size of the polyurea aggregate and/or a removal of some of these structures. Another possibility is the order of both of the hard domains, aggregates and microdomains, is altered in the lithium chloride foam. This might be a result of a reduction in the formation of hydrogen bonds to the hard segments.

The small angle x-ray scattering profiles are given in Figure 6.4 for foams 44-0 and 44-5 in the form of scattering intensity as a function of scattering vector, s, and s is defined as $2/\ \lambda \sin(\frac{\theta}{2})$ where λ is the wavelength of the x-ray source and θ is the radial scattering angle. Although, neither of the profiles exhibits a sharp peak, both exhibit a shoulder similar to previous foams analyzed in the same manner. As explained in the literature review, the shoulders represent an interference peak which is most likely a result of morphological features not having the same shape, size and distance from one another. The shoulder is sharper for foam 44-5 in comparison to 44-0, but both shoulders appear to occur over the same range of scattering vector, s. By applying Bragg's law to the shoulder region, estimates for the center-to- center(interdomain) spacing between the scattering particles resulted in values on the order of 8 nm for both foams. Also, the scattering intensity in the shoulder region is about 18 percent higher at s equal to 0.081 for foam 44-0 than that of 44- 5. In addition, the interfacial analysis on the SAXS behavior for these materials has been carried out at Dow Chemical and lead to an index of intefacial thickness of ca. 0.7nm for foams 44-0 and 44-5 (99). These results did indicate that a small, but similar amount of phase mixing is taking place at the interface of the soft and hard segments in foams 44-0 and 44-5.

The above results from the SAXS scattering profiles do indicate that the spacing between the micro-hard domains is similar and furthermore signifies that these hard domains are comparable in size for foams 44-0 and 44-5. The higher scattering intensity for foam 44-0 in the shoulder region might suggest that there are more microdomains present in foam 44-0 than 44-5. In addition, this difference might indicate that there is more phase mixing in foam 44-5 in comparison to 44-0. These

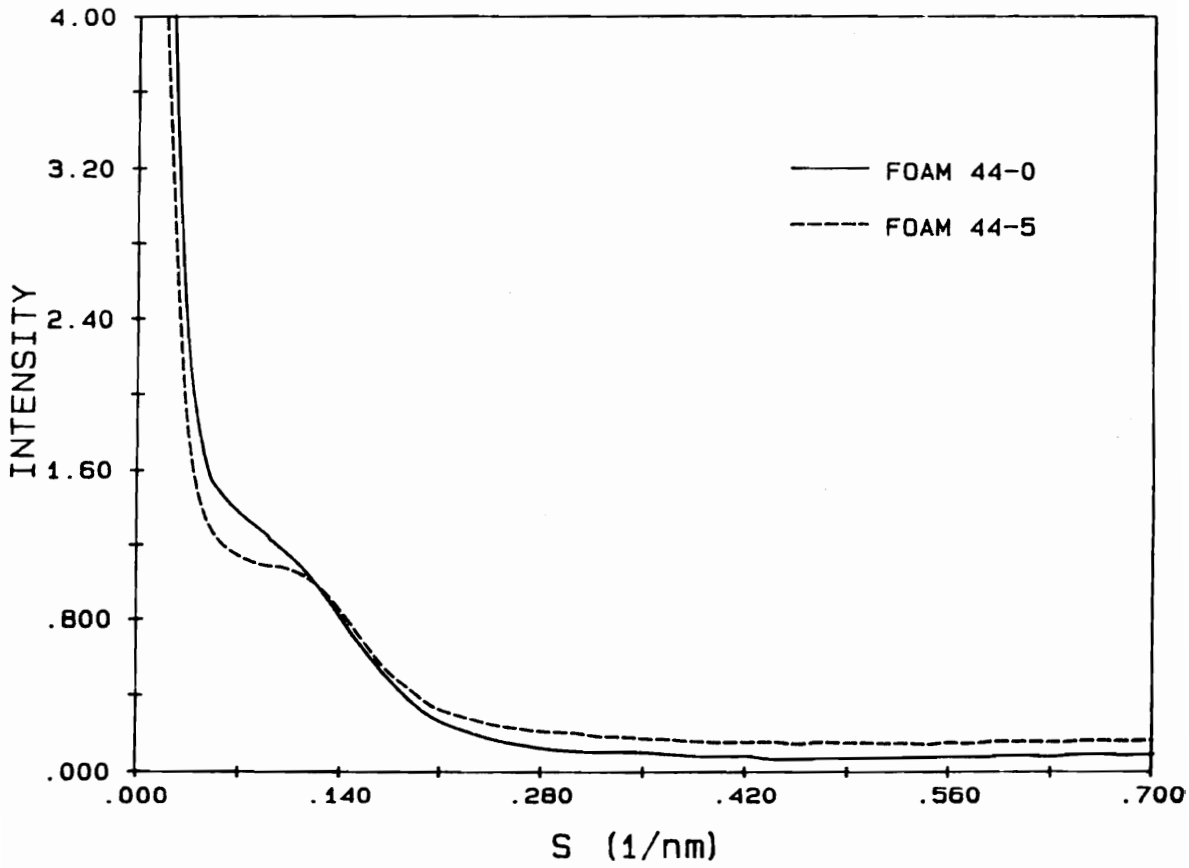

Figure 6.4. SAXS Scattering Profiles for Foams 44-0 and 44-5

speculations would imply that the LiCl addition is not necessarily promoting the formation of the smaller microdomains, but more of the single hard segments units. On the other hand the somewhat more distinct shoulder, would tend to suggest that the hard domains in foam 44-5 are more uniform in size in comparison to foam 44-0.

In short, the results from the above morphological techniques have definitely indicated that some structural changes in the solid portion of the foam have taken place by adding LiCl to the formulation. These changes appear to be mostly related to the polyurea aggregates - suggesting that there is formation of smaller aggregates and/or the hard segments are being dispersed as single units in the network. In addition, based on the TEM micrographs and the DSC traces for foams 44-0 and 44-5 the phase mixing of the soft and hard units is believed to be greater for the LiCl foam. While all the changes are not fully understood and the interpretation of the results is not complete, the suggested modifications in the solid textures due to the addition of LiCl to the formulation, will hopefully aid in the discussion of the viscoelastic properties. Before discussing the effect that the LiCl addition has on the viscoelastic nature of flexible foams, the morphology of their cellular textures will be presented.

6.1.4 Macroscopic Structure

Scanning electron microscopy is a useful technique to evaluate the cellular textures of flexible foams. By utilizing this technique, a better understanding of important mechanical properties and possibly more insight to the foam formation can hopefully be obtained.

The SEM micrographs are shown in Figure 6.5 for foams 44-0 and 44-5 in both the parallel and perpendicular direction to the blow axis. At first glance the cellular textures for these two foams appear to be quite different due to a greater number of filled cell windows in foam 44-5 in comparison to 44-0. This is the main difference, but an important one, between these two foams with regards to their cellular textures. The size of the cells do appear to be similar and possibly slightly

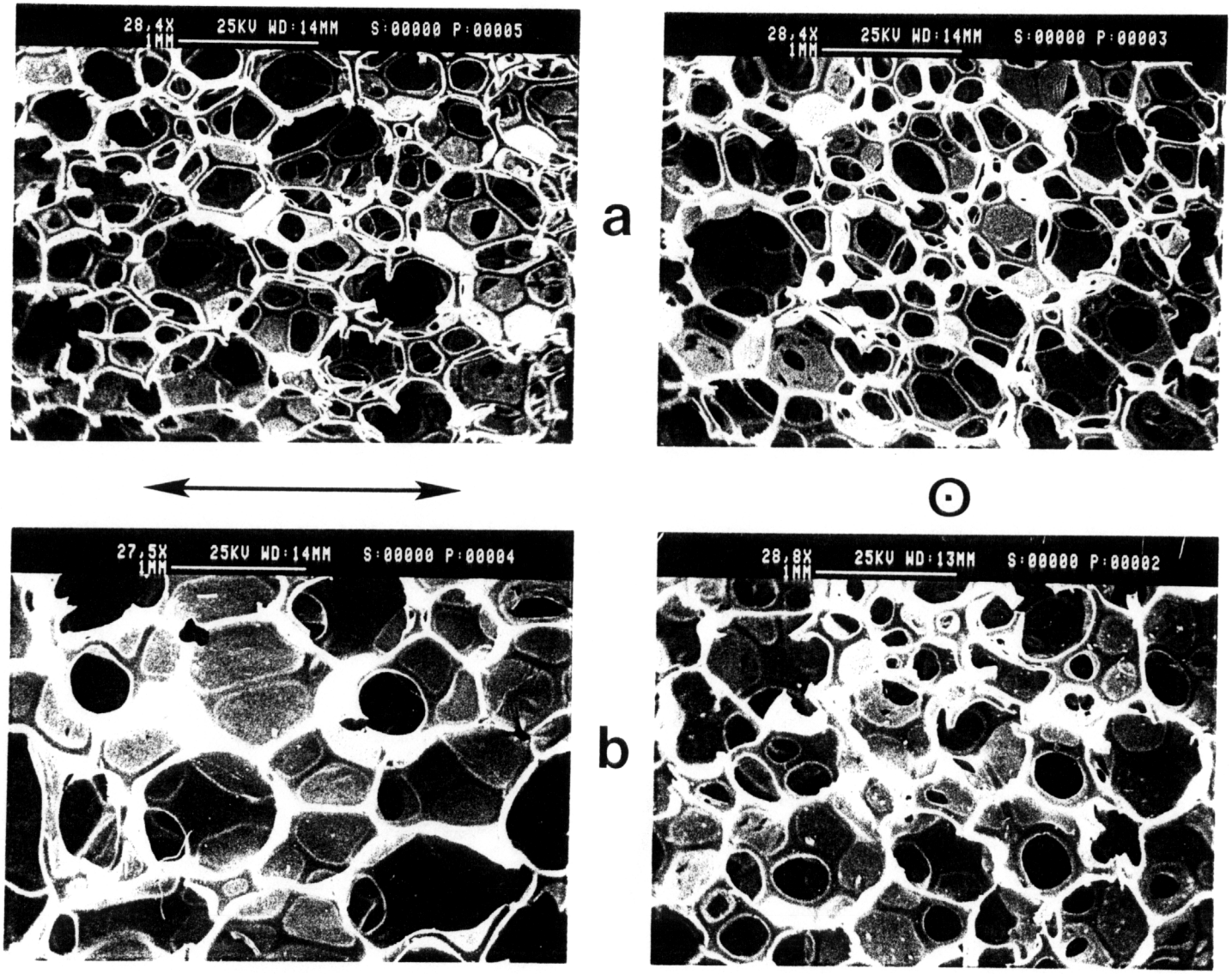

Figure 2.5. SEM Micrographs of Cellular Textures for Foams (a)44-0 and (b)44-5: Shown parallel and perpendicular to blow axis

greater in size for foam 44-5. In addition, the regularity and the shape of the cells in the two directions are comparable for the two foams(see Figure 6.5).

The difference in the amount of cellular windows in foams 44-0 and 44-5 that are filled does appear to be related to the flow of the cellular membrane material into the struts. This step in the formation of an ideal foam is thought to occur after blow off or at the point where gellation takes place. The above process, of course, is dependent on the viscosity of the cell window material and if the viscosity is high, it will prevent some of the flow of this material into the cell wall struts. Thus, it is speculated that the LiCl is possibly promoting gellation to occur more rapidily or earlier in the foam formation and thus bringing about a viscosity build up in the cellular window material. While all the information concerning the foam formation or the chemistry has not been made available, it is known that the tin catalyst level was reduced considerably in making the LiCl foam, 44-5. By adjusting the tin catalyst, one is attempting to obtain a better balance between the two competing reactions, i.e the gelling and blowing reactions, and more specifically, to control the gelling reaction. With this in mind, the addition of LiCl does appear to be promoting or catalyzing the gelling reaction. The above difference in cellular textures also indicates that the LiCl could be acting like a surfactant by "solubilizing" the urea based hard segments in the foaming solution and thus preventing their precipitation. Such precipitation has been suggested by FTIR-kinetic studies on the foaming mixture(10,11,14,15). Also, recall that by adding too much surfactant a foam with a large amount of closed cells is obtained.

The above differences in cellular texture are also believed to reduce the stiffness in foam 44-5 in comparison to 44-0. Basically, the stiffness in open cellular foams is known to be mostly dependent on the struts(33-35). Therefore, the compressive load as well as the tensile stress in these two foams are expected to be higher in foam 44-0 in comparison to 44-5. In the next section, this point is addressed as well as the difference in the viscoelastic behavior of this foams series.

6.2 Viscoelastic Behavior

The effect of lithium chloride on the viscoelastic behavior of flexible foams is now addressed. This behavior has been evaluated by utilizing three tests, tensile stress relaxation, compression load relaxation, and compression creep that were discussed in the previous chapter. Thus, one is referred to the chapter on viscoelastic behavior of flexible foams for the methods of analyzing the data from the three tests. In addition, to evaluating the effect of the addition of LiCl to the formulation on the viscoelastic nature, the effects of temperature and relative humidity have also been measured for the compressive properties of foams 44-0 and 44-5.

As a point of clarification, when the phrase, the "effect of LiCl", is used in the following discussion, it refers to the addition of LiCl to the formulation and the resulting changes in the solid morphology that are brought about by its addition. However, in a few instances which are clearly stated, reference is made to the LiCl molecule acting as a plasticizer in these materials. It is also speculated that the lithium chloride molecules are affecting the hydrogen bonds in the hard domains(both micro and aggregates) and thus it will be referred to as a hydrogen bond(HB) plasticizer.

6.2.1 Tensile Stress Relaxation

The ambient(25°C,20%RH) condition log$\sigma(t)$-log t stress relaxation behavior is shown for foams 44-0, 44-4, and 44-5 in Figure 6.6. As exhibited in Figure 6.6, there is rather linear behavior for all three foams and the initial stress level does decrease systematically with increasing LiCl content. This decrease in stress is believed to be a result of smaller and/or less of the urea aggregate structure present in the solid portion of the foams which in turn is thought to reduce the reinforcement in the foam's struts. The difference in cellular morphology for foams 44-0 and 44-5 is also believed to be another factor as alluded to in the discussion of the SEM micrographs for these

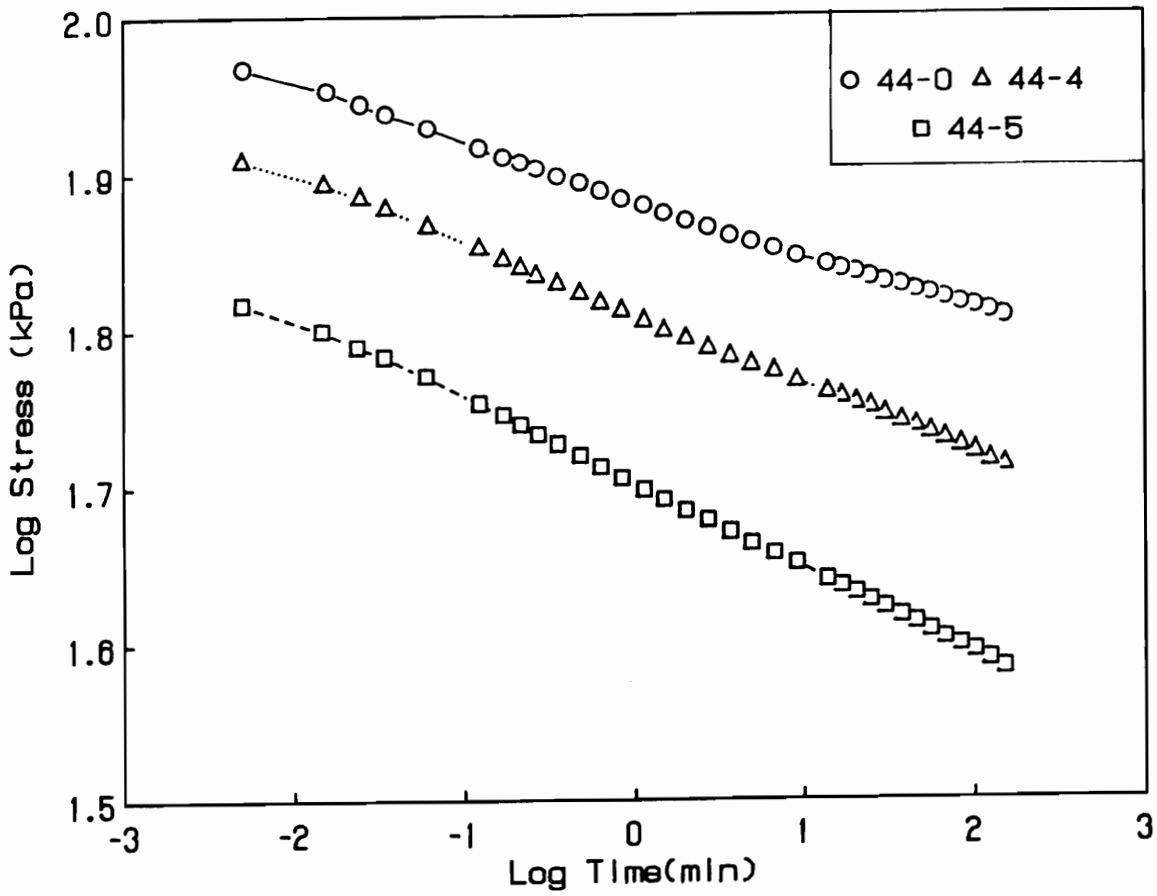

Figure 6.6. Log $\sigma(t)$-Log t Tensile Stress Relaxation Behavior for Foams 44-0, 44-4, and 44-5: Obtained at a 25% elongation and at 25°C-20%RH

foams (recall Figure 6.5 for 44-0 and 44-5). That is, more material appeared to be contained in the cellular window material in foam 44-5 in contrast to 44-0. This observation suggests a lower tensile stress in foam 44-5 versus foam 44-0 would be obtained, since the struts give the foam the majority of its stiffness(33- 35).

As displayed in Figure 6.6, there is also a noticeable difference in the rates of relaxation for the three foams. The stress decay rates as a function of LiCl content are given in 6.7 along with the load decay rates from the compression studies. However, the discussion will continue to focus on the tensile relaxation studies. As shown in Figure 6.7, the stress decay rates do increase systematically with increasing LiCl content. This increase is also rather significant from 0.4 to 0.5 pphp LiCl suggesting that the difference in the solid structure are more significant than they may appear; for example, in TEM micrographs of these two foams exhibited only a slight difference in base segregation. On the other hand, the increase in the stress decay rates with LiCl content does appear to be related to the changes in the solid morphology discussed earlier. That is, the result of reducing and/or removing the urea aggregate structure in the LiCl foam is thought to allow for more mobility of the hard segments. Additional mobility is likely to cause more chain slippage which will lead to further stress relaxation. This increase in the mobility of the hard segments may be a result of a more phase mixing of the soft segments and the hard segments. It could also be a result of a weaker hydrogen bonding network which is likely to allow for more disruption and reformation of hydrogen bonds. Another factor contributing to the increase in the stress relaxation for foams 44-4 and 44-5 is that LiCl could be acting as a "hydrogen bond(HB) plasticizer". By entering into the hard domains it will likely facilitate local chain slippage which, of course, is known to cause additional stress relaxation.

6.2.2 Compression Load Relaxation Behavior

The log load-log t relaxation behavior is shown for foams 44-0, 44-4 and 44-5 in Figure 6.8 at a condition of 30°C and 15%RH. Although there appears to be only a small increase in the initial

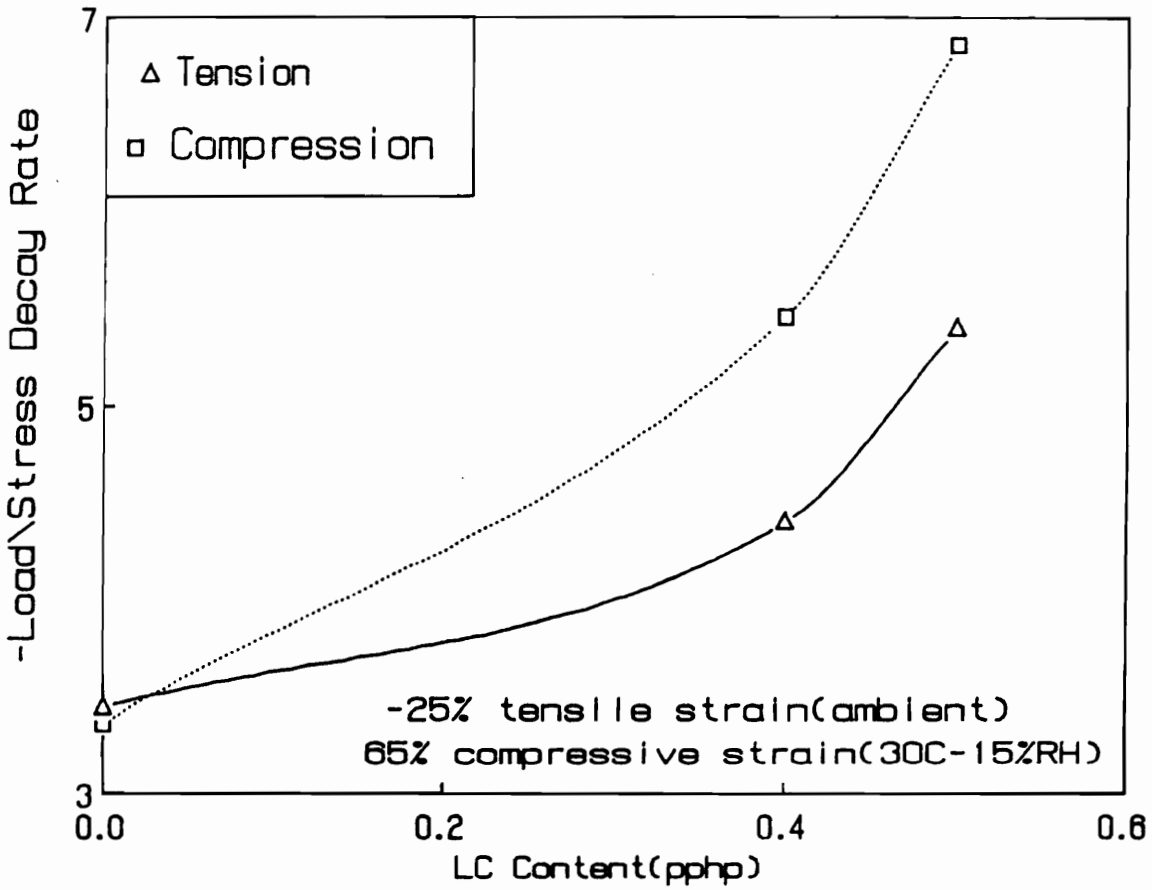

Figure 6.7. Effect of LiCl Content on Relaxation Behavior in Tension and Compression: See discussion in 6.2.2 for compression data.

load levels with decreasing LiCl, it is important to point out that the density of these foams does increase by about 13 percent from foam 44-0(0 pphp LiCl) to 44-5(0.5 pphp LiCl)- see Table 6.1. Thus, if one normalizes on density this increase in the initial load level at 65 percent strain is greater than it appears in Figure 6.8. Regardless, the decrease in the initial load levels due to the addition of LiCl to the formulation is consistent with expectations and is believed to take place for similar reasons discussed above for the decrease in the initial tensile stress levels.

A significant difference in the rate of relaxation is observed in Figure 6.8 for the three foams. Also note that log load-log time behavior is not as near linear for the LiCl foams in comparison to the control foam - especially at short times. The load decay rates as a function of LiCl content are given in Figure 6.7 and exhibit an increase with increasing LiCl content. This increase, like that observed in the tensile stress relaxation study, is thought to be related to the changes that are occurring in the solid morphology. Some of the same factors, e.g. reduction and/or removal of the polyurea aggregate structures are also thought to lead to further relaxation in compression for the LiCl foams. In addition, LiCl may be acting as a HB plasticizer by causing additional chain slippage which will, of course, lead to further load decay.

In comparing the rates of relaxation for the two modes of deformation, there is more relaxation taking place over 3 hours in compression versus tension for the lithium chloride foams whereas the rates are similar for the control foam. The latter is consistent with results shown in the previous chapter which indicated the solid portion of the foam in both tension and compression is governing the relaxation behavior(recall Figure 5.23 (F4)). The rates of relaxation in compression and tension for the LiCl foams are also thought to be mostly governed by the solid material, but it is possible that the cellular morphology is influencing the viscoelastic decay in these materials. Recall, that the LiCl foams have a rather significant amount of cellular window material whereas the foams without LiCl in their formulation do not(see micrographs for foams 44-0 and 44-5 in Figure 6.4). Thus, it is possible that the viscoelastic decay of the cellular windows are effected differently in the compression and tension modes whereas the materials in the struts are not. While there is no proof for this speculation, there are some possible explanations. First, the strain level in compression is higher than in tension and could have a greater effect on the thinner cellular wall materials. It is also pos-

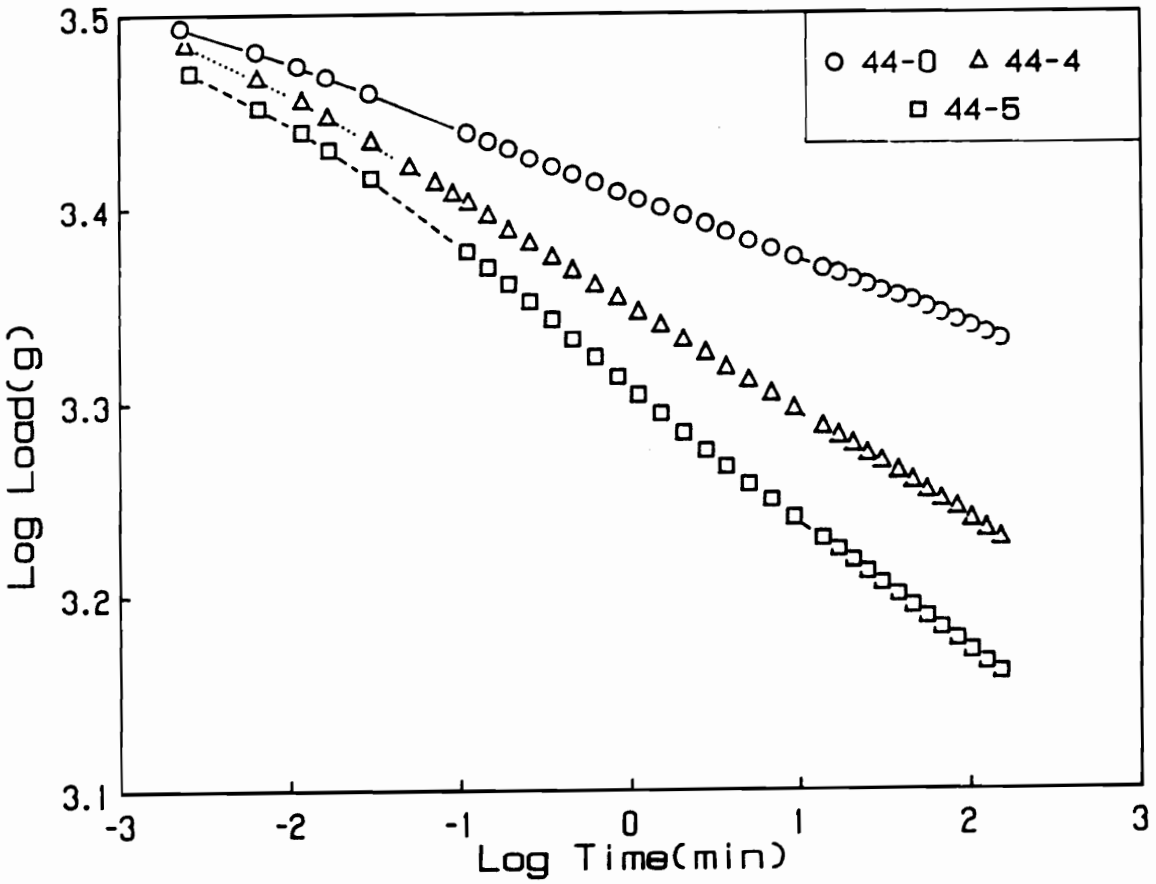

Figure 6.8. Log Load(t)-Log t Compressive Load Relaxation Behavior for Foams 44-0, 44-4, and 44-5: Obtained at a 65% strain and 30°C-15%RH

sible that in the compression of the LiCl foams, the material in the struts as well as in the cellular windows is governing the relaxation. However, in tension, only the material in the struts is contributing to the relaxation behavior.

In short, there are some differences in the relaxation behavior in tension and compression for the LiCl foams which are not fully understood. However, it is believed that the changes which occur in the solid morphology by adding LiCl to the formulation are leading to the majority of the increase in the rate of relaxation in foams 44-4 and 44-5. In the paragraphs to follow, the effect of temperature and relative humidity on the load relaxation behavior are discussed by comparing the results obtained for foams 44-0 and 44-5.

Effect of LiCl on the Variable Temperature Load Relaxation Behavior

The log load-log t variable temperature relaxation behavior is shown in Figures 6.9 and 6.10 for foams 44-0 and 44-5, respectively. Both exhibit a decrease in the initial load level with increasing temperature and this decrease appears to be greater for the LiCl foam(see Tables 6.2 and 6.3). For example, a 26 percent decrease in the initial load is observed from 30°C to 125°C for foam 44-5 and a 23 percent decrease for foam 44-0. In comparing the two surfaces in Figures 6.9 and 6.10, one may notice in the temperature range of 25°C to 100°C that the log load - log time behavior is not as linear in the case of foam 44-5 - especially at short times. At temperatures greater than 100°C, there is negative deviation from the log load vs. log t for both foams - see Figures 6.8 and 6.9. Based on discussions in the previous chapter, this observation suggests that some of the same mechanisms promoted by increasing temperature are also influencing the relaxation in the LiCl foams, i.e. possible chain scission in the urea and urethane linkages at temperatures greater than 100°C.

In contrast, the behavior of the percent load decay and load decay rates differ with increasing temperature for foams 44-0 and 44-5 as shown in Tables 6.2 and 6.3, respectively. This difference can also be observed in Figure 6.11 for the plot of the percent load decay values as a function of temperature. As shown, the behavior does appear to be more scattered and not that systematic for

Table 6.2: Variable Temperature Load Relaxation Results for Foam 44-0

Temp(°C)	L_o(kg)	-Slope(-10^2)*	% Load Decay
30	3.12	3.4	32
85	2.95	2.75	27
100	2.58	2.8	28
125	2.4	-	32

* Correlation function was in the range of 0.995 to 0.999 except at 125°C.

\- Based on data obtained in the previous chapter for foams F1-F4 the range of error for the slope is thought to be ±1 and that of the load decay ±0.7

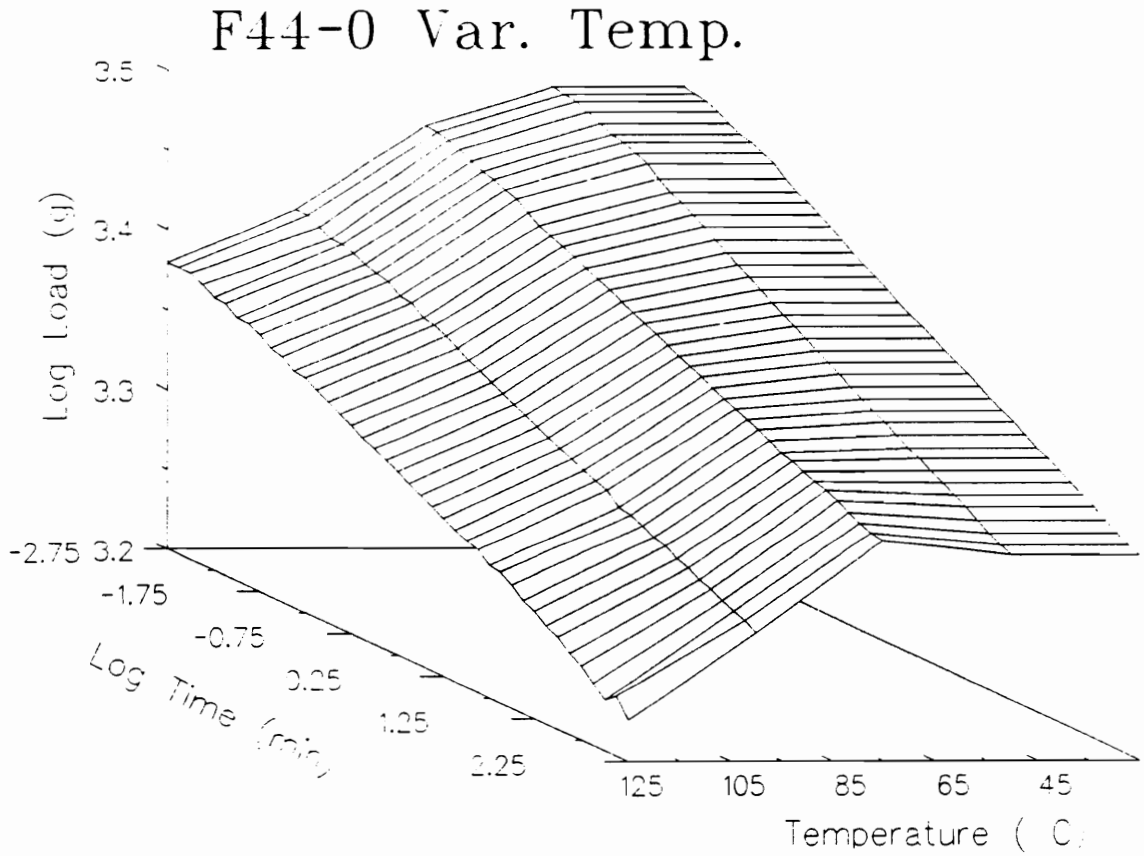

Figure 6.9. Variable Temperature Load Relaxation Behavior for Foam 44-0: Obtained at a 65% strain level

Table 6.3: Variable Temperature Load Relaxation Results for Foam 44-5

Temp(°C)	L_o(kg)	-Slope(x10²)*	% Load Decay
30	2.95	6.8	52
60	2.6	8.2	59
85	2.27	8.0	57
100	2.27	7.5	57
125	2.17	-	62
140	1.95	-	63

* Correlation function was in the range of 0.995 to 0.999 except at 125°C and 140°C

\- Based on two data sets at 85°C the range of error for the slope is on the order of ±0.2 and that of the load decay is ±2.5

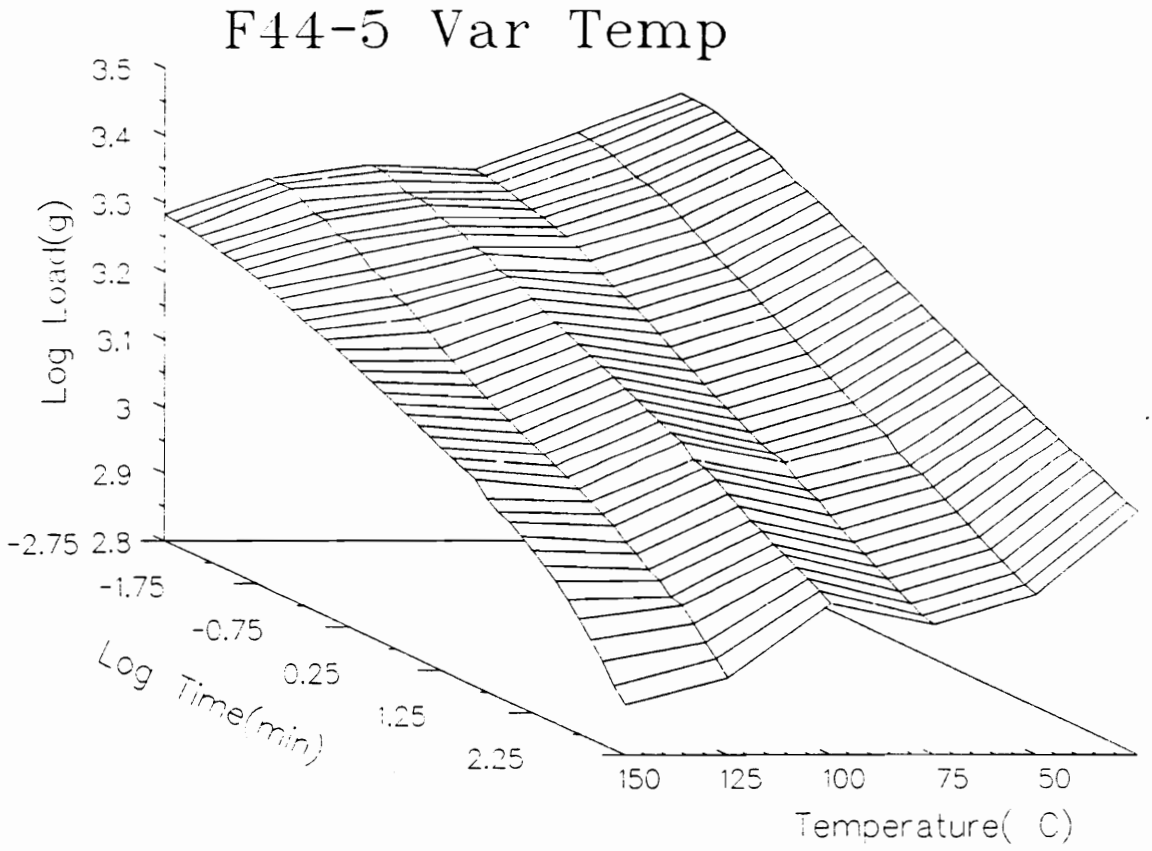

Figure 6.10. Variable Temperature Load Relaxation Behavior for Foam 44-5: Obtained at a 65% strain level

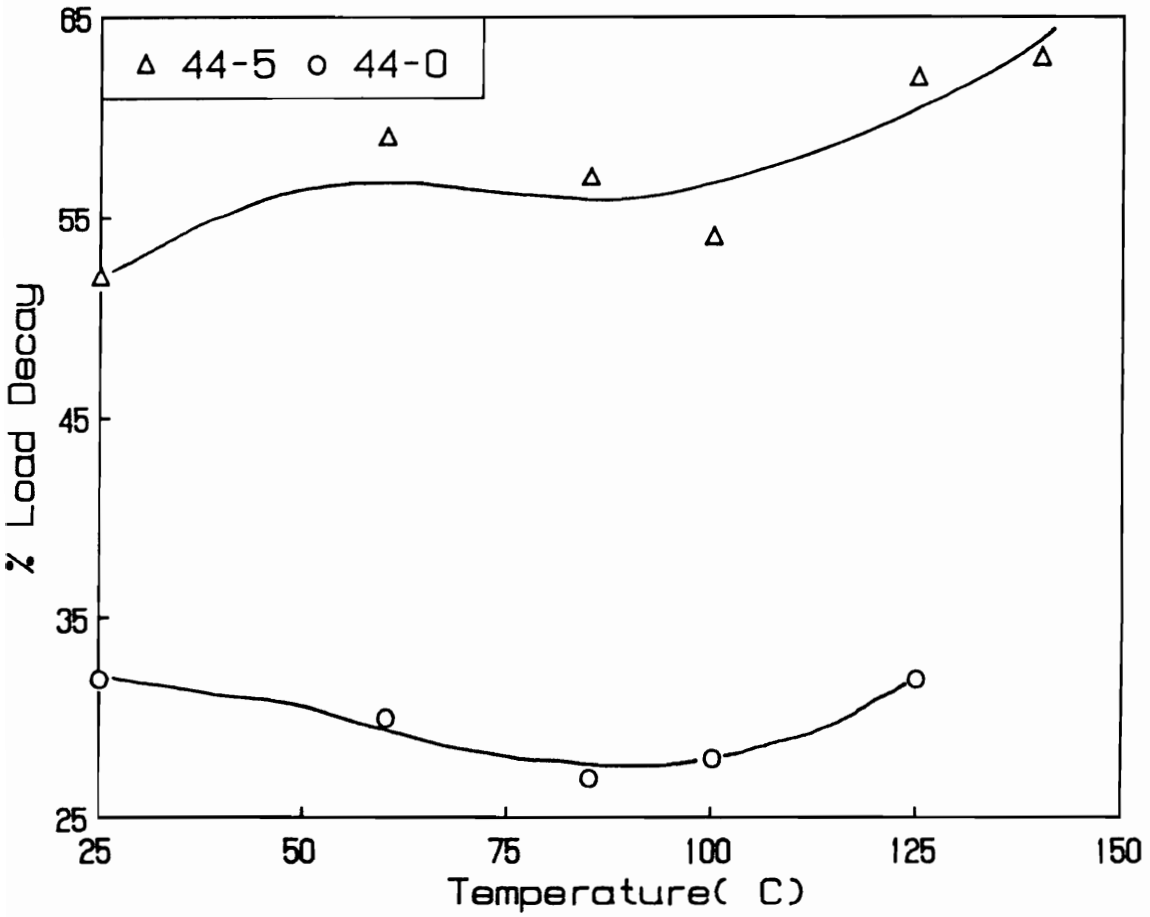

Figure 6.11. Thermal Dependence on Load Decay in Foams 44-0 and 44-5

foam 44-5 in comparison to foam 44-0 as well as the results shown in the previous chapter for foams F1 and F4. However, this irregular behavior in Figure 6.11 for foam 44-5 is believed to fall outside of experimental error based on an additional test performed at 85°C which indicated an error range on order of ±2.5%. On the other hand, the unsystematic behavior for foam 44-5 does make it rather difficult to determine the effect that the LiCl addition is having on the variable temperature relaxation behavior. In comparing the behavior in Figure 6.11 for the LiCl foam and its control, it does appear that temperature has a greater effect on the LiCl foam, 44-5. This effect is most pronounced by comparing the results at 30°C and 125°C for the two foams(see Tables 6.2 and 6.3). The increase that is observed from 30°C to 125°C is possibly a result of more phase mixing and/or more hydrogen bond disruption taking place with increasing temperature in foam 44-5 in comparison to 44-0. Both of these suggestions, are likely to cause additional load decay by increasing the mobility of the hard segments.

Effect of LiCl on Variable Humidity Load Relaxation Behavior

The effect of LiCl on the load relaxation behavior at only low and high relative humidities at 30°C and 85°C has been evaluated. Recall that in the previous chapter measurements were also made at 50 percent relative humidity and thus the 3-dimensional surfaces presented here may seem different for this reason. The results are shown for foams 44-0 and 44-5 in Figures 6.12(30°C) and 6.13(85°C) and summarized in Table 6.4. As exhibited in Figures 6.12 and 6.13, there is a decrease in the load level with increasing relative humidity for both foams at 30°C and 85°C. As discussed in the previous chapter, water is believed to act as a plasticizer in these materials and thus cause a decrease in the load level. The effect of moisture on the initial load level is greater on the LiCl foam at 30°C and about the same at 85°C for the two foams.

At 30°C, the effect of LiCl on increasing relative humidity does result in non-linear behavior for the log load-log t as shown for foam 44-5 at 100%RH in Figure 6.12. In addition, a greater change in the rate of decay for the foam 44-5 is observed with increasing relative humidity in

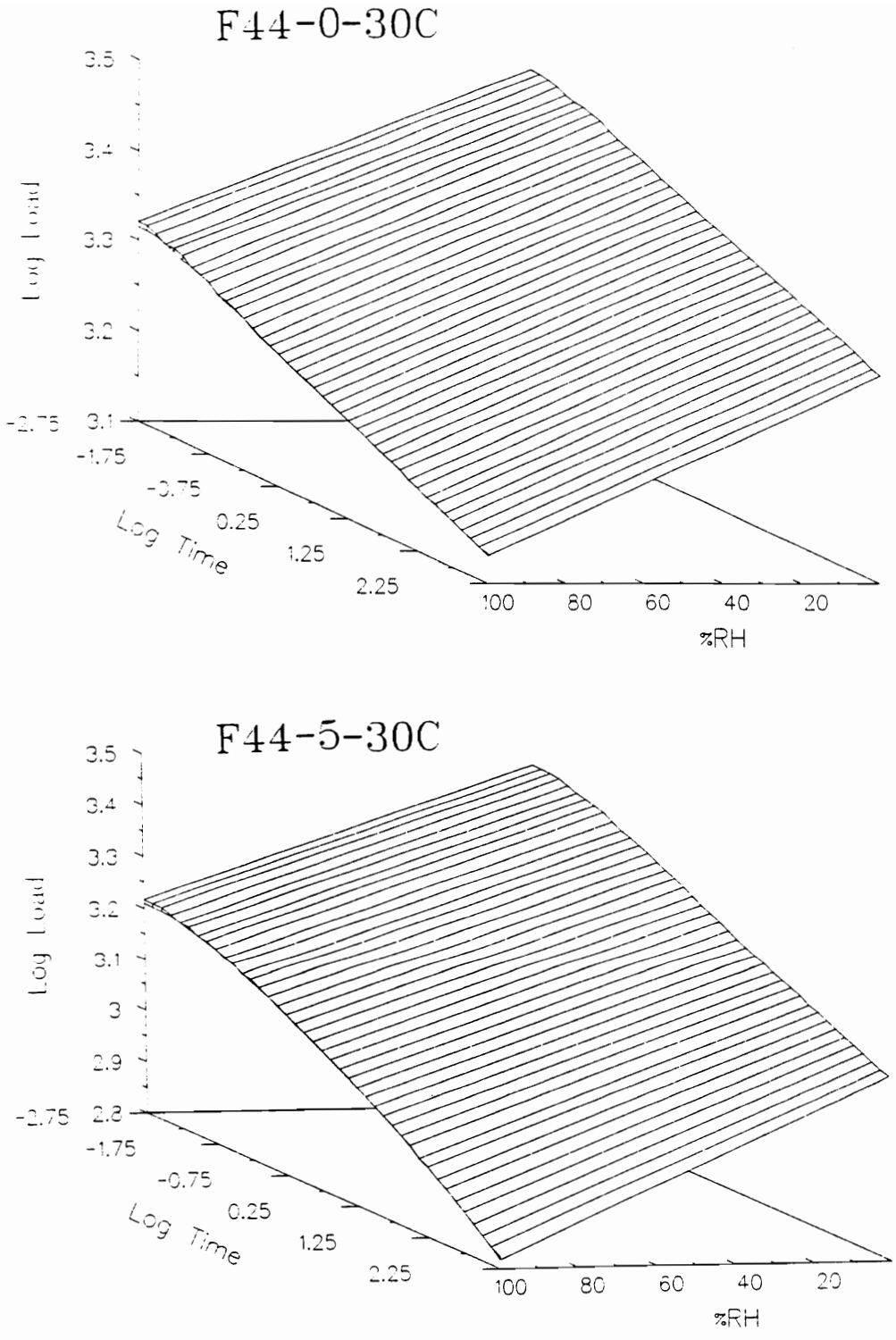

Figure 6.12. Effect of Relative Humidity on Foams 44-0 and 44-5 at 30°C: Obtained at a 65% strain level and at 15%RH and 100%RH

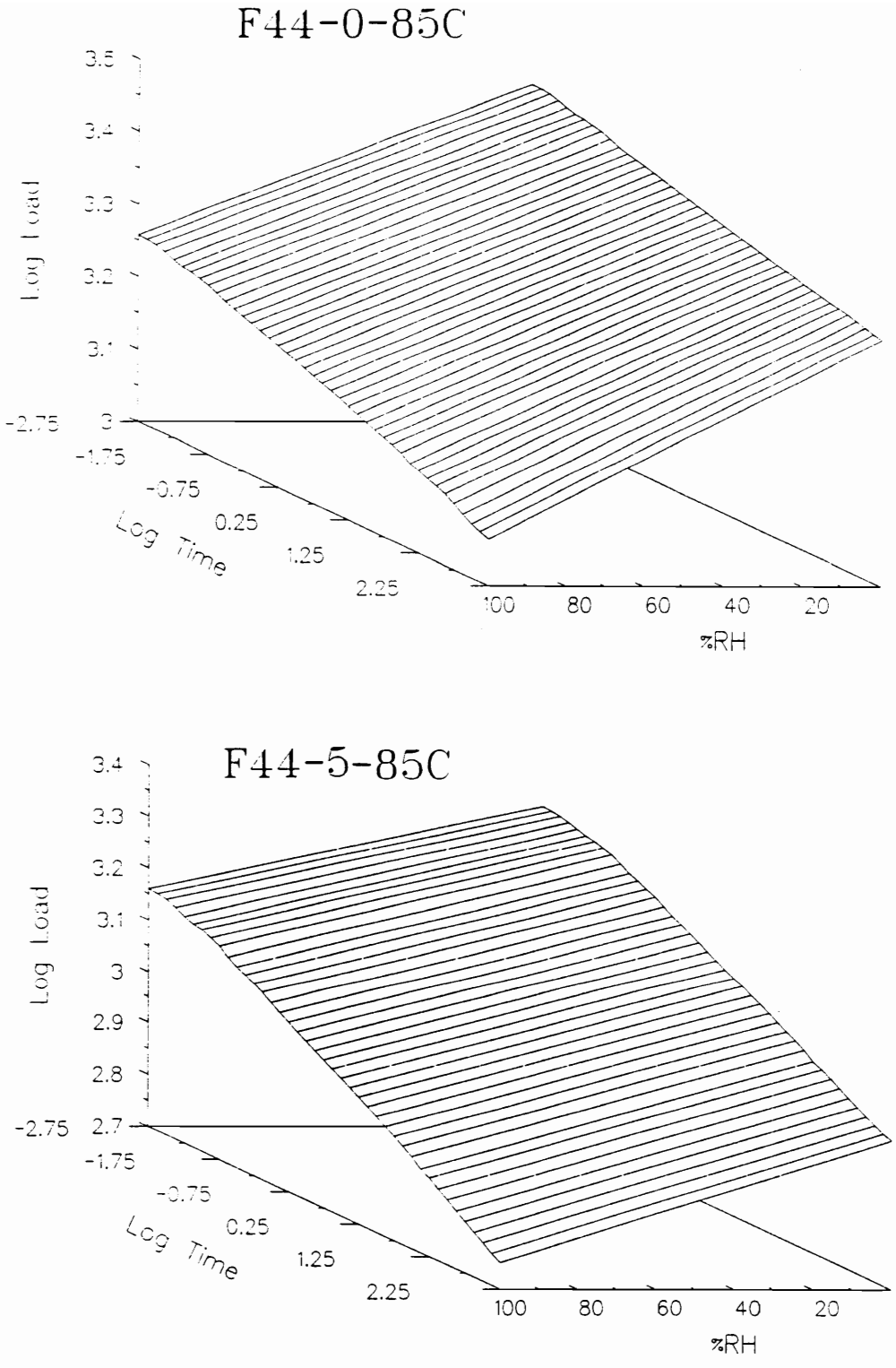

Figure 6.13. Effect of Relative Humidity on Foams 44-0 and 44-5 at 85°C: Obtained at a 65% strain level and at 2%RH and 95%RH

Table 6.4: Load Decay Values for Different Temperature/Relative Humidity Conditions

Condition	% Load Decay(-Load Decay Rate x 10^{-2})	
Foam =	44-0	44-5
30°C-15%RH	32(3.4)	52(6.8)
30°C-100%RH	36(3.9)	62(8.7)*
85°C-2%RH	27(2.75)	57(7.6)
85°C-95%RH	37(4.1)*	63(8.8)*

* Correlation coefficient not within 0.995 to 0.999
- Behavior obtained over a 3 hr time period

comparison to foam 44-0(see Table 6.4). This difference might be a result of water being able to influence the chain slippage more in the hard segments of the LiCl foam, since the majority its hard segments are not believed to be a part of the polyurea aggreagate structures like in the case of foam 44-0. In other words, the hard segments of foam 44-5 are thought to be more accessible by water in comparison to foam 44-0. Another factor is that water may adsorb more to foam 44-5, due to the presence of the hydroscopic LiCl molecules. While the ratio of the LiCl molecules to the other key potential sites, i.e urea and urethane links is 1 to 45, it is still feasible that the presence of LiCl increases the water absorbtion. In addition, since the LiCl molecules are thought to serve as HB plasticizers, the additional absorption of water molecules will likely cause further relaxation.

At 85°C, non-linear behavior is observed in Figure 6.13b upon increasing relative humidity for foam 44-5. In addition, negative deviation from linearity is noticeable at longer times for foam 44-0 - see Figure 6.13a. Also, at 85°C the change in the relaxation rate with increasing relative humidity for foam 44-5 is not as significant as in the case at 30°C. Furthermore, this change at 85°C for the control foam, 44-0, is greater than that of the LiCl foam, 44-5(see Table 6.4). The results from these comparisons are thought to be somewhat misleading due to the effect that temperature also has on the load relaxation behavior of foam 44-5- see Figure 6.11. Thus, the influence of temperature does make it rather difficult to determine the effect of relative humidity on foam 44-5 at 85°C. However, in looking closer at the absolute values for the load decay rates in Table 6.4, one will notice that there is an slight increase from 30°C-100%RH to 85°C-95%RH for foam 44-5 as well as 44-0 - thus indicating that relative humidity does have a rather significant and comparable effect at 85°C on foams 44-0 and 44-5.

Before discussing the compressive creep behavior, it is important to point out that the effects of temperature and relative humidity on the load relaxation behavior for foam 44-0 are comparable to that of foam F4. However, the load decay rate and percent load decay values are slightly higher in the case of foam 44-0. This slight increase was somewhat expected since foam 44-0 has an isocyanate index of 100 and F4 has a 110 index. This difference in isocyanate index would suggests a more complete network is formed in F4.

6.2.3 Effect of LiCl on Compression Creep Behavior

Within this last section on the viscoelastic behavior, the effect of LiCl on the the compressive creep behavior is discussed. To begin with, the creep behavior is shown in the form of compressive strain vs. log t for foams 44-0 and 44-5 in Figure 6.14. As shown, the LiCl foam creeps immediately upon reaching an initial strain level whereas the control foam, 44-0, shows a brief induction period and then begins to creep like the behavior displayed for foams F1-F4 in the previous chapter. In addition, the behavior for foam 44-0 is rather linear for linear strain vs log t after the short induction period. On the other hand, foam 44-5 exhibits linear behavior for approximately the first 10 minutes (log time(min) = 1) and then begins to creep at a slower rate. This difference in behavior is believed to be related to more cellular window material in foam 44-5 in comparison to 44-0. In the case of 44-5, this additional cellular window material is thought to promote creep to take place immediately. That is, this immediate response could be a result of windows continuing to rupture and/or be deformed after applying the constant load and reaching the initial strain level. In looking at the overall progression of the compressive strain over log time for foam 44-5 in Figure 6.14b, it appears that the following changes may be leading to the compressive creep behavior: (1) Initially the collapse and/or rupture of the cellular windows are dominating, (2) after short time periods(ca. 6 seconds) and up to 10 minutes collapse and/or rupture of cellular windows, buckling of the struts, and creep in the solid material are governing the behavior, and (3) after 10 minutes buckling of the struts and creep in the solid material are dominating. The actual extent of the contribution of these factors to the compressive creep behavior is not known, but it is thought to vary depending on the strain level.

From the compressive creep behavior given in Figure 6.14a, the creep rate was determined for foam 44-0 in a similar manner utilized in the previous chapter by taking the slope of the linear portion of the curve. In the case of foam 44-5, an estimate for the creep rate was obtained by calculating the change in the strain over the change in log t, since linear behavior is not observed over the 3 hour testing period. The creep rates were obtained for both foams at the conditions of

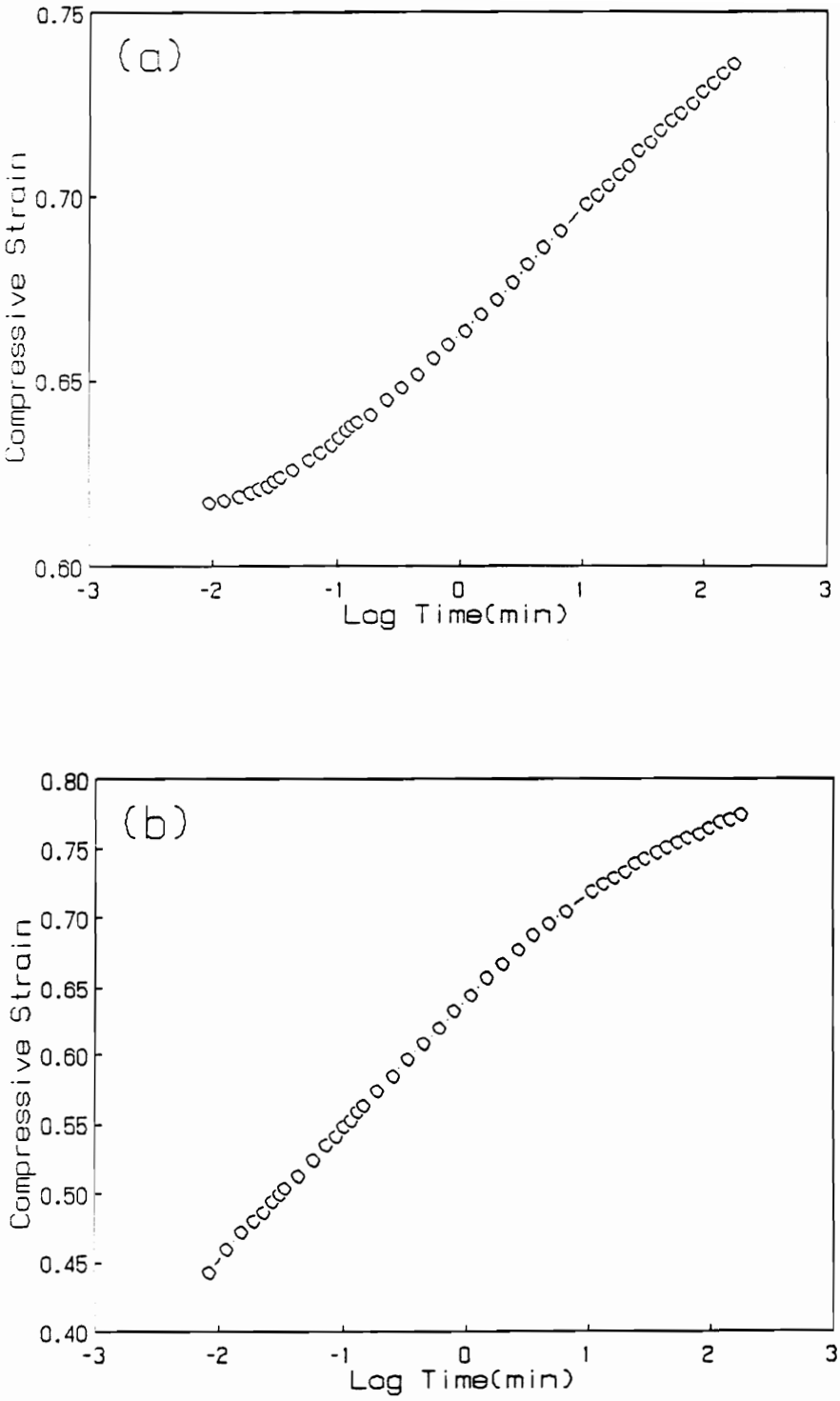

Figure 6.14. Compressive Creep Behavior for Foams 44-0 and 44-5: Weight applied to both foams was 2750 grams

30°C-15%RH for similar constant loads and at 30°C-100%RH for slighly higher constant loads for foam 44-0.

At 30°C-15%RH, the effect of LiCl on the compressive creep behavior is shown in Figure 6.15 by comparing the plots of initial strain level as function of creep rate for foam 44-5 to 44-0. As one would predict, the creep rate is higher at a given initial strain level as well as for equal constant loads applied to the foams for the LiCl foam, 44-5. This behavior is, of course, consistent with those results presented earlier for the tensile stress relaxation and load relaxation studies. The higher creeps rates for foam 44-5 are also thought to be mostly due to the differences in the solid morphology caused by the addition of LiCl to the formulation of foam 44-5. Again these differences in the solid structure are thought to be related to the presence of smaller and/or less of the urea aggregates structures in LICl foam. By reducing the size or amount of these structure, greater mobility of the hard segments is expected which will allow for further creep in in the solid portion of the foams. Another factor that is possibly effecting the creep in the solid portion of the foam is the LiCl molecule acting as a HB plastizer. As mentioned earlier, this type of factor causes additional local chain slippage within the hard domains which, of course, will lead to more creep. One other factor that may contribure to the difference in the creep rates for these foams, is the greater amount cellular window material in LiCl foam versus that of its control. As discussed above, this factor is thought to have a greater influence on the creep rate during the early stages of compressive creep in foam 44-5.

The effect of LiCl on increasing relative humidity at 30°C can be seen by comparing the compression creep behavior for foams 44-0 and 44-5 in Figures 6.16 and 6.17, respectively. This comparison demonstrates that foam 44-5 is affected more significantly by increasing relative humidity than that of foam 44-0. Again, this result is consistent with the results presented earlier for the compression load relaxation behavior at 30°C. It also indicates that water is influencing the creep behavior at 30°C more in the LiCl foam due to the greater accessibility to the hard segments and possibly due to the presence of lithium chloride.

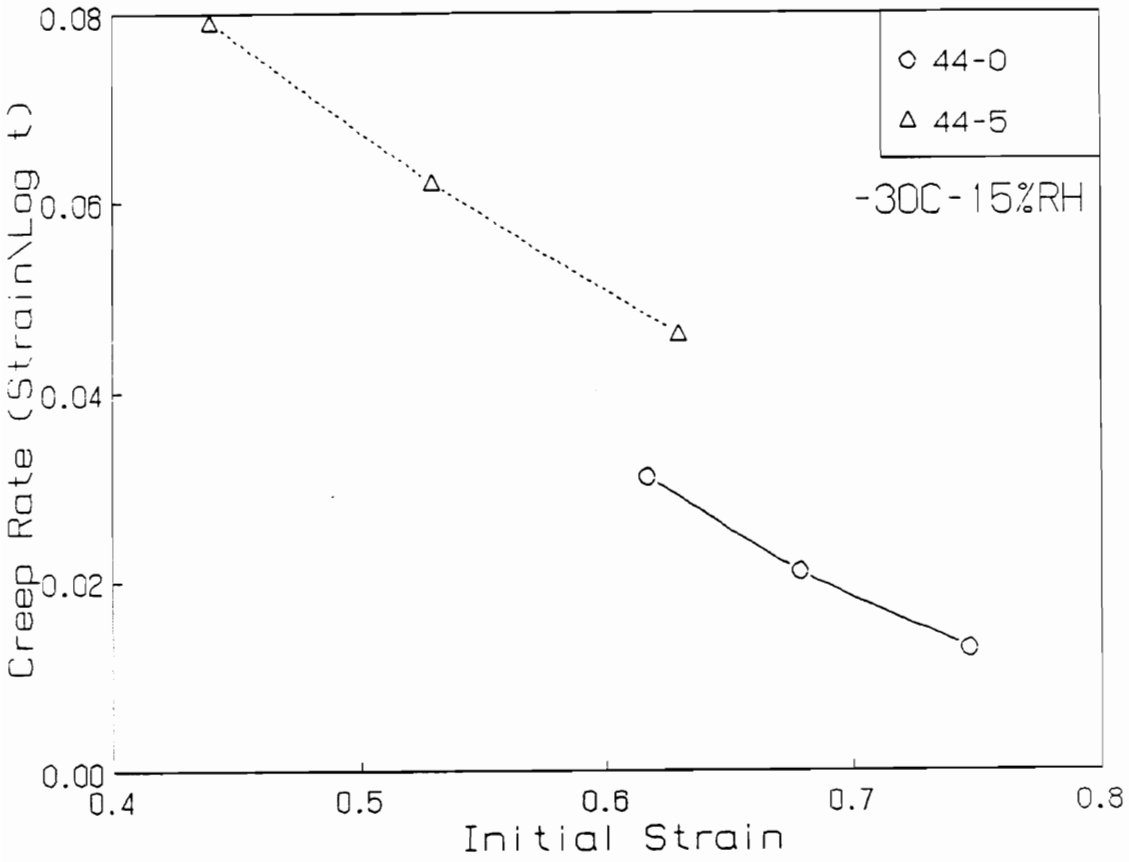

Figure 6.15. Effect of Lithium Chloride on Compression Creep Behavior at 30°C-15%RH: Similar loads applied to both foams

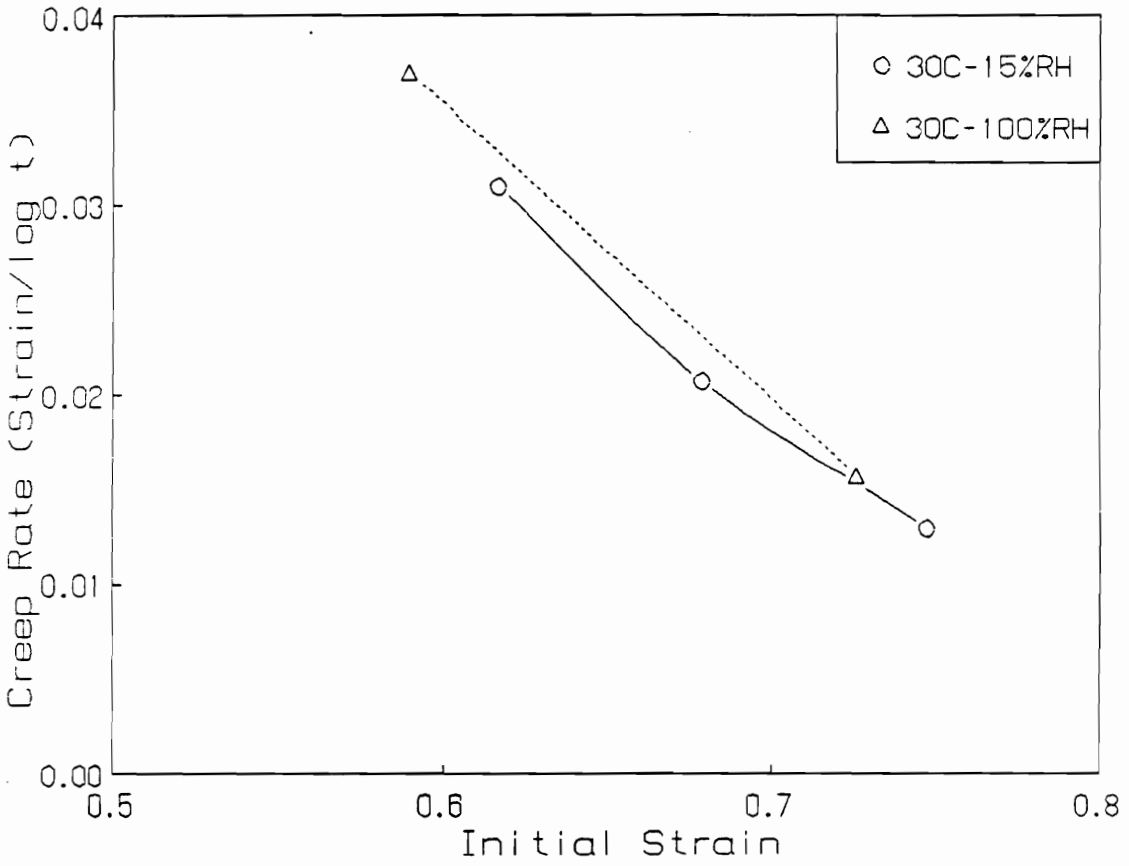

Figure 6.16. Compressive Creep Behavior for Foam 44-0 at 30°C

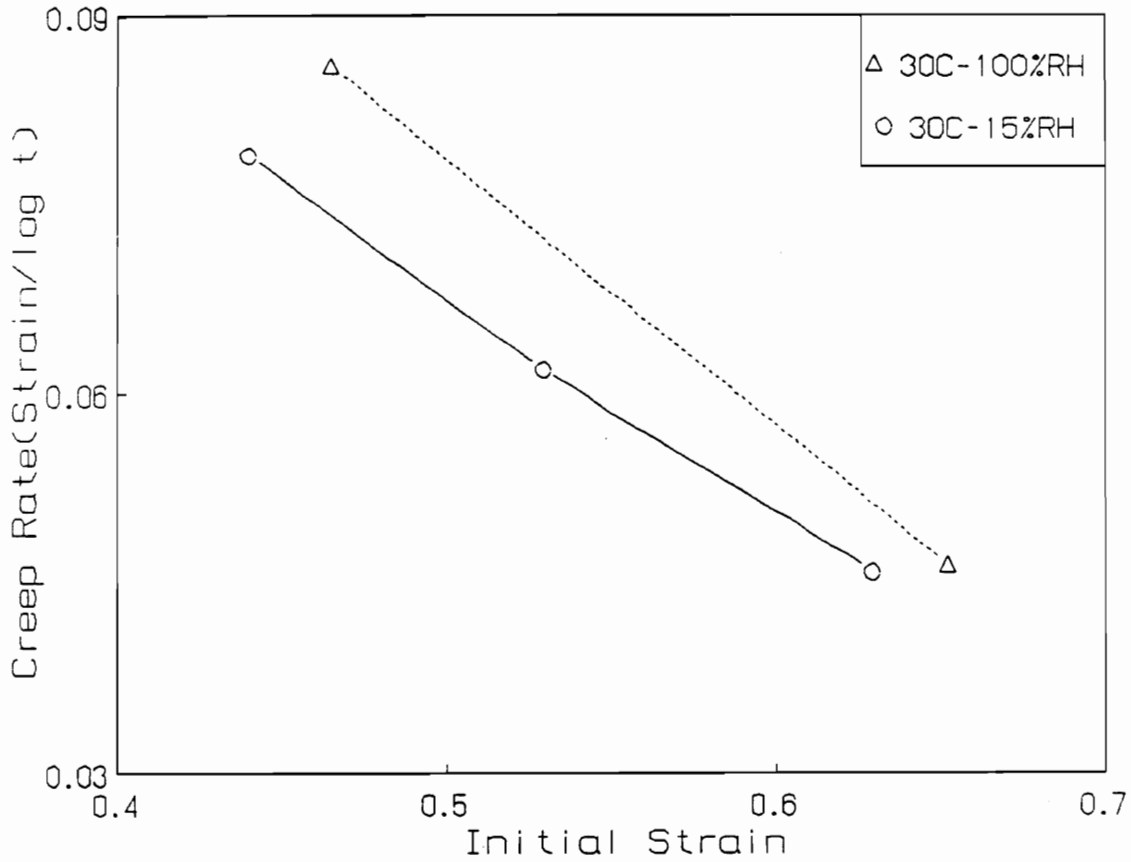

Figure 6.17. Compressive Creep Behavior for Foam 44-5 at 30°C

6.3 Summary

In summary, the addition of LiCl of the formulation does result in some rather interesting changes in the solid morphology of flexible slabstock polyurethane foam. Most of these changes are beleived to be related to the dispersion of the urea aggregate hard domains which were believed to be present in the control foam, 44-0. Based on the different morphological techniques utilized for this study, it was suggested that for the LiCl foams there was formation of smaller aggregates and/or the hard segments were being dispersed as single units within the network. In addition, these results indicated that there was an increase in phase mixing of the hard and soft units due to the addition of LiCl.

Changes were not only detected in the solid morphology, but also in the cellular textures upon addition of LiCl to the formulation of foam 44-5. The key observation from the SEM micrographs was that there is more cellular window material in the LiCl foam(44-5) in comparison to its control(44-0). Also, the greater amount of cellular window material in 44-5 was thought to be due to promotion of the gelling reaction by adding LiCl to the formulation.

The above changes in the solid morphology as well as the cellular textrures did have a rather significant effect on the viscoelastic properties. A signficant increase in the viscoelastic decay was observed for the stress relaxation in tension, compression load relaxation and the compressive creep for the LiCl foams in comparison to their control foam. This increase was attributed to the greater mobility in the hard segments. In addition, it was suggested that the LiCl molecules were acting as a HB plasticizer and thus causing additional local chain slippage. In some instances, the cellular window material was also thought to contribute to this increase - mainly for the properties measured in compression. Temperature was also found to have a more significant effect on the load relaxation behavior of the LiCl foam, 44-5, in comparison to its control. This greater effect was thought to be related to more phase mixing as well as more hydrogen bond disruption in foam 44-5. Relative humidity at 30°C also had a greater effect on the relaxation and creep behavior in the compression mode for foam 44-5 in comparison to foam 44-0. This behavior was attributed to the

hard segments of foam 44-5 being more accessible to moisture than that of foam 44-0. In addition, it was speculated that the HB plasitcizer, i.e. LiCl, was allowing for additional absorption of water molecules.

Chapter VII

7.0 Solid State NMR of Polyurethane Foams

While the main focus of this dissertation has been on evaluating the viscoelastic properties of flexible foams, solid state NMR has also been utilized to aid in the further evaluation of the morphology of the foams as well as in obtaining more information concerning molecular motion in the foam. A better understanding of the molecular motion of the soft and hard segments, would give additional insight into the viscoelastic behavior of the foams. Since very little has been covered on the topic of solid state NMR within this dissertation, a brief introduction is now provided.

Over the past 10 to 15 years, solid state NMR has become a method of great interest and importance for characterizing polymeric materials(100-104). This interest is a result of more advanced techniques which have enabled high resolution NMR spectra to be obtained on solid materials. In the past, there were three main problems that prevented obtaining high resolution spectra as well as important structural information for solid polymers. These problems were (1) line broadening by dipolar and quadrapolar interaction, (2) chemical shift anisotropy, i.e. broadening caused by different orientations of the molecules and (3) long spin lattice relaxation times for the less abundant nuclei such as ^{13}C(100-101). However, in the recent years these problems have been overcome, respectively, by (1) dipolar decoupling which involves applying a strong

radiofrequency(rf) field that overcomes the local fields arising from ^1H- ^1H and ^{13}C- ^1H interactions, (2) magic angle spinning which involves rotating the sample at a 54.7° angle as well as at high rates to reduce anisotropic effects and (3) cross polarization which involves enhancing the signal of less abundant nuclei(^{13}C) by bringing them in contact with a more abundant nuclei(^1H)(100-101). The reader is referred to references 100 and 101 for more detail on these methods. With these more advanced techniques, the ability to obtain information on the structure and motion of polymeric solids has been made possible. For the work presented in this dissertation, a better understanding of the molecular motion within the solid portion, i.e. the soft and hard segments, of polyurethane foams was desired. Such information is usually obtained through relaxation measurements and in the next section, a description of some commonly used relaxation measurements is given. Followed by this discussion, is the presentation of the results obtained from two different relaxation measurements on foams F1-F4 as well as foams 44- 0, 44-4 and 44-5. The results presented in this chapter were measured at the North Carolina State University Chemistry Department by S.S. Sankar and C.G. Moreland and were analyzed in conjunction with the author.

7.1 Nuclear Relaxation-Relaxation Measurements

The molecular motion in solids is known to create a modulation in the local dipolar field which in turn provides a mechanism for nuclear relaxation(100). Alternatively, NMR relaxation time measurements allow a means of quantifying molecular motions in solids(100). A common relaxation time that is measured in solids is $T_{1\rho}$ and it is referred to as the rotating frame spin lattice relaxation time. $T_{1\rho}$ is sensitive to lower frequency motions(in the kilohertz region) which are of interest here since the hard segments in the foams are thought to have relatively little motion(100). In addition, $T_{1\rho}$ measurements are useful when evaluating the relaxation of a dilute spin such as ^{13}C. Thus, for this study two rotating frame relaxation times, $T_{1\rho}(^1H)$ and $T_{1\rho}(^{13}C)$ have been utilized to characterize the motion of the hard and soft segments as well as to further evaluate the

morphological features. The pulse sequences for these two relaxation times were shown earlier in the experimental section. For the following discussion of $T_{1\rho}(^1H)$ and $T_{1\rho}(^{13}C)$, the schematic representation of the magnetization changes in the pulse sequence demonstrated in Figure 7.1 is utilized. As shown, initially a radio frequency(rf) pulse(H_{1y}) is applied at the Larmor frequency of the precessing proton which is enough to tip the protons 90° to the x-axis(see Figure 7.1-A,B). The protons are then spin-locked by phase shifting H_{1y} along the x- axis or along the magnetization vector(see Figure B,C). In the case of the $T_{1\rho}(^1H)$ experiment, the protons are spin- locked for a variable time period, τ, followed by cross polarization with the (spin-locked) carbons. Cross polarization involves transferal of energy from the abundant proton spins to the rare carbon spins under Hartmahn-Hahn conditions(both carbon and proton spins precess about there H_{1y} fields at the same frequency). After cross polarization, acquisition of the carbon signal via free induction decay takes place(see Figure 7.1-C,D). In short, the $T_{1\rho}(^1H)$ experiment is a measurement of the nuclear relaxation of the more abundant proton nuclei through the acquisition of the ^{13}C signal of carbons with strongly coupled protons. On the other hand, for the $T_{1\rho}(^{13}C)$ experiment, cross polarization takes place before the variable delay, τ. During this delay the proton spin lock is turned off while continuing to spin-lock the carbons. After the delay, the carbon signal is then obtained in the form of a free induction decay. Thus, $T_{1\rho}(^{13}C)$ is a measurement of the relaxation of the ^{13}C nuclei. Overall, as stated by Fife, " $T_{1\rho}$ is a characteristic time constant for the decay of the magnetization along the on-resonance rf field (H_{1y}) in the rotating frame"(100).

Recall that a mechanism for the relaxation of nuclear *spins* is a modulation of a local dipolar field, i.e. the *lattice*. Therefore, $T_{1\rho}$ or the rotating frame *spin-lattice* relaxation time does have the potential provide information on the molecular motion in solids. It is also important to point out that $T_{1\rho}$ goes through a minimum with increasing inverse temperature as shown in Figure 7.2. Similarly, $T_{1\rho}$ also goes through a minimum with decreasing frequency of the molecular motion of the local dipolar field, i.e. if this is the main mechanism controlling nuclear relaxation(see Figure 7.2). If the $T_{1\rho}$ value is on the high temperature side(left) of the minimum, the motions of the molecules are thought to be fairly rapid. On the other hand, if the $T_{1\rho}$ values are on the low side,

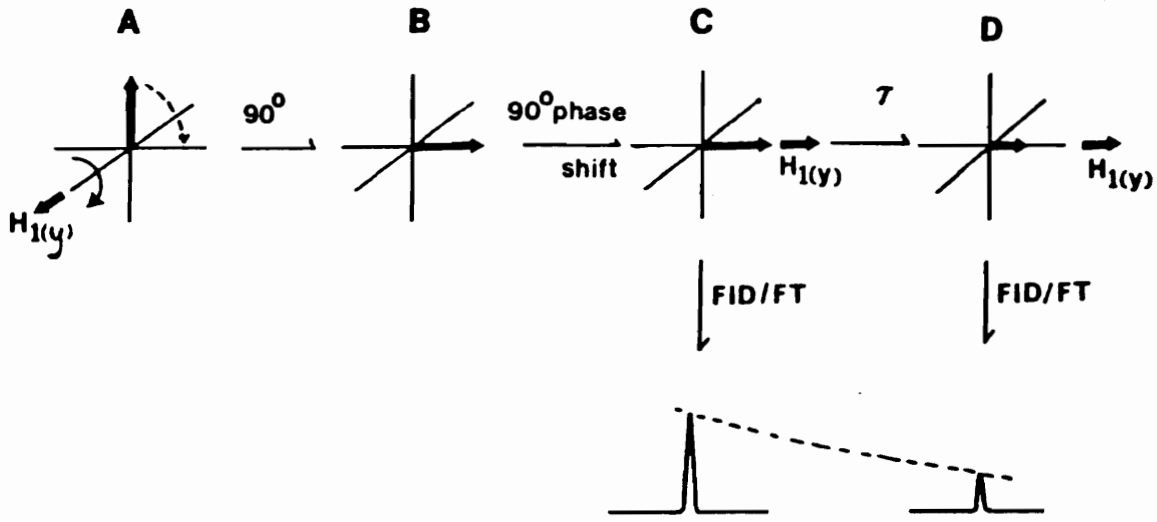

Figure 7.1. Vector Diagram for the Pulse Sequence Utilized for $T_{1\rho}$ Measurements: Taken from ref. 100

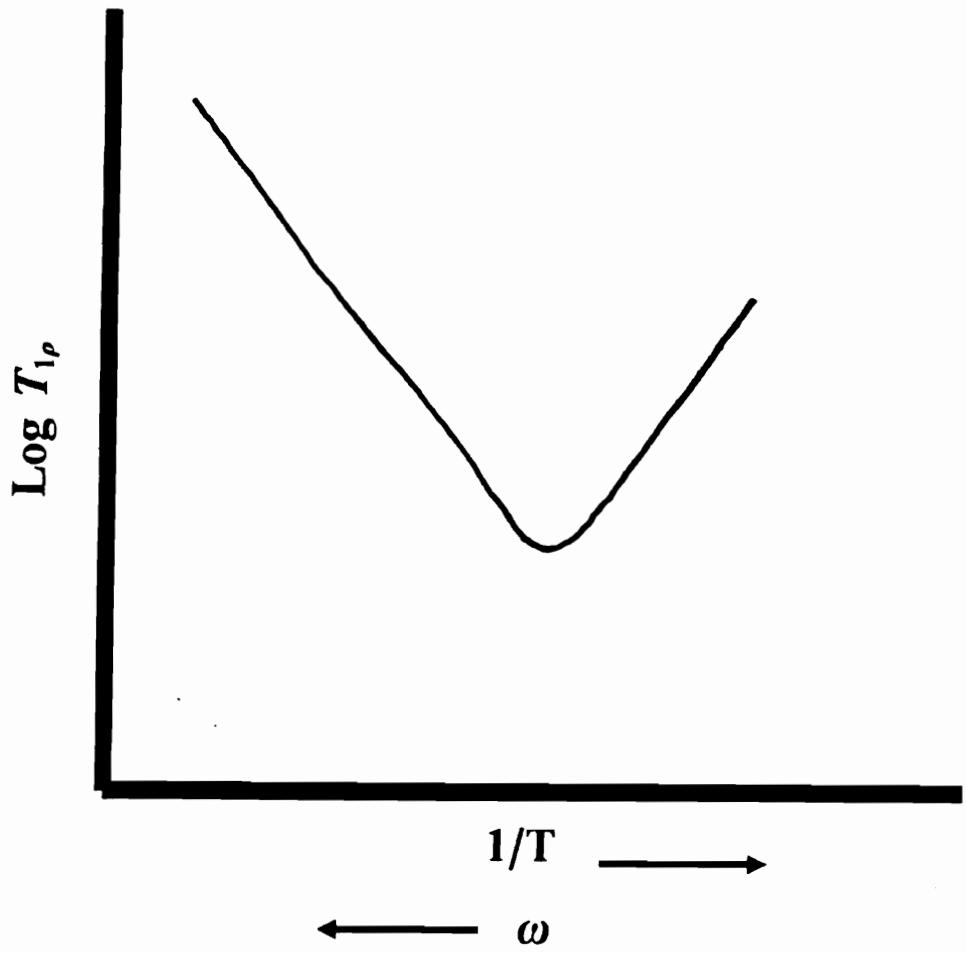

Figure 7.2. $T_{1\rho}$ as a Function of Temperature and Frequency(ω)

the molecular motion is much slower. With a better understanding of nuclear relaxation in solids, the results obtained for two sets of flexible polyurethane foams are now presented.

7.2 Discussion of Results

The foams utilized in this study were foams F1-F4 and foams 44-0, 44-4 and 44-5. Discussion of the morphology of these foams can be found in the literature review as well as in the previous chapter. A typical ^{13}C NMR spectrum for these foams is shown in Figure 7.3 along with the chemical shift assignments in Table 7.1. The carbon assignments are shown in Figure 7.4 for the chemical structures of the soft and hard segments. For most cases in the discussion, the 131 ppm chemical shift is associated with the hard segments and the 73 ppm chemical shift is affiliated with the soft segments -see Table 7.1 and Figure 7.4.

7.2.1 Proton Rotating Frame Spin-Lattice Relaxation Measurements

In Figure 7.5 the $T_{1\rho}(^1H)$ relaxation times for the hard and soft segments are shown as a function of hard segment content. These values given in Figure 7.5 as well as the $T_{1\rho}(^1H)$ values for the other carbons are summarized in Table 7.2. As shown, the $T_{1\rho}(^1H)$ values for the soft segments are rather independent of composition. On the other hand, the $T_{1\rho}(^1H)$ values for the hard segments do increase systematically with increasing hard segment content.

In the determination of $T_{1\rho}(^1H)$, the relaxation of the proton nuclei is detected through acquisition of the ^{13}C signal. Thus proton relaxation is reported by the nearest carbons. $T_{1\rho}(^1H)$ is determined initially by molecular motion, but $T_{1\rho}(^1H)$ measurements are also influenced by spin diffusion between strongly coupled protons. In other words, since the protons(^1H) available for magnetization are in abundance, energy between their spins can be exchanged readily and this tends

Table 7.1: Chemical Shift Assignments

Carbon #	Chemical Shift (ppm)	Segmental Representation
C-8	156	Hard
C-2, C-4(2,4 TDI)	136	Hard
C-2, C-6(2,6 TDI)	136	Hard
C-1, Protonated Aromatic Carbons	131	Hard
C-10	75	Soft
C-9	73	Soft
C-7, C-11	18	Hard,Soft

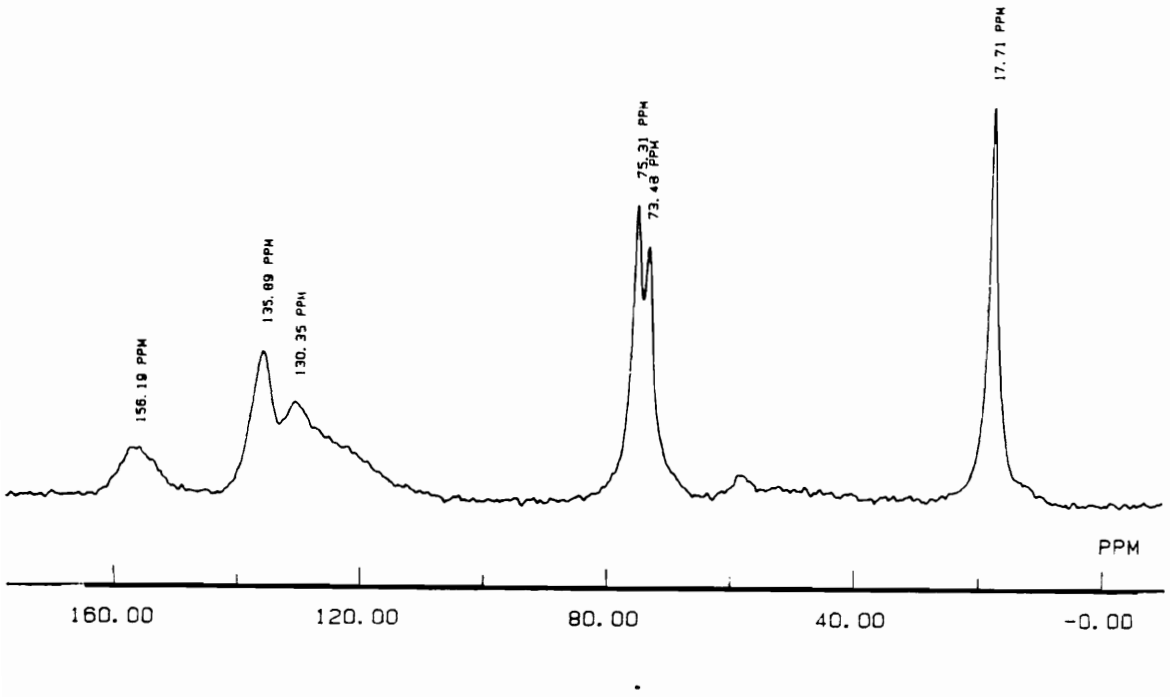

Figure 7.3. Solid State ^{13}C NMR Spectrum for Foam F3

Soft Segment

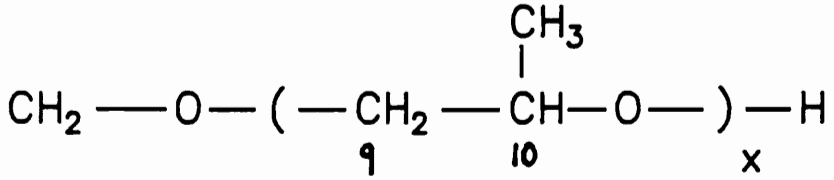

Hard Segment

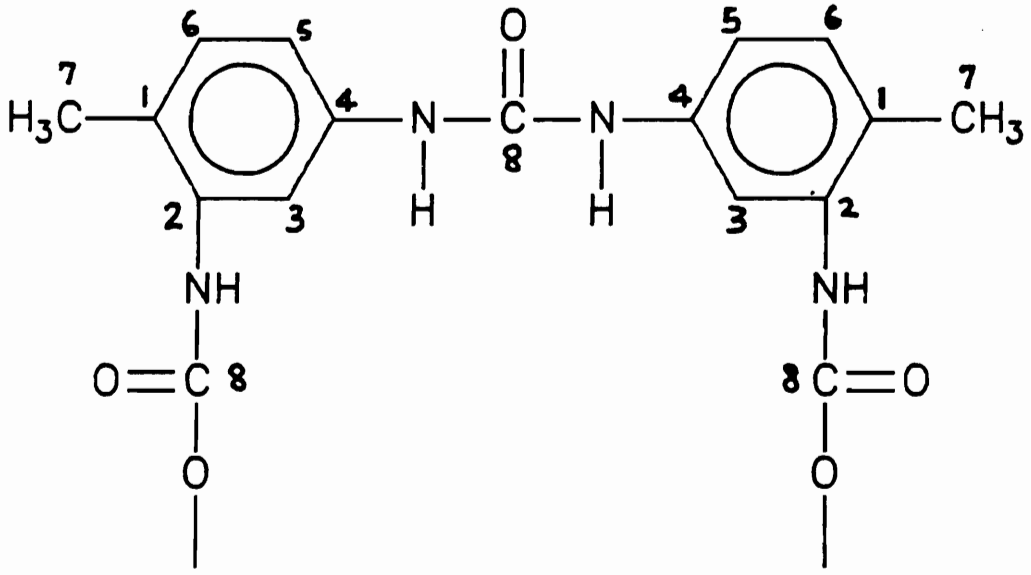

Figure 7.4. Basic Repeat Units for PPO Soft Segment and Polyurea Hard Segment Based on Water Extended TDI-80: Numbers by carbons are listed in Table 7.1

Table 7.2: Proton $T_{1\rho}$(ms)* Values at Ambient Conditions for Foams F1-F4

Foam	wt% HS	18ppm	73ppm	75ppm	131ppm	136ppm	156ppm
F1	21.1	6.4	4.0	4.3	5.4	5.1	6.3
F2	25.8	6.0	4.1	4.6	6.1	5.7	6.9
F3	30.1	5.7	4.1	4.4	6.6	6.2	7.1
F4	33.8	6.1	4.0	4.6	7.2	6.9	6.9

*Error in $T_{1\rho}(^1H)$ values are $\pm$.3 ms

**The band assignments are given Table 7.1 and Figure 7.2

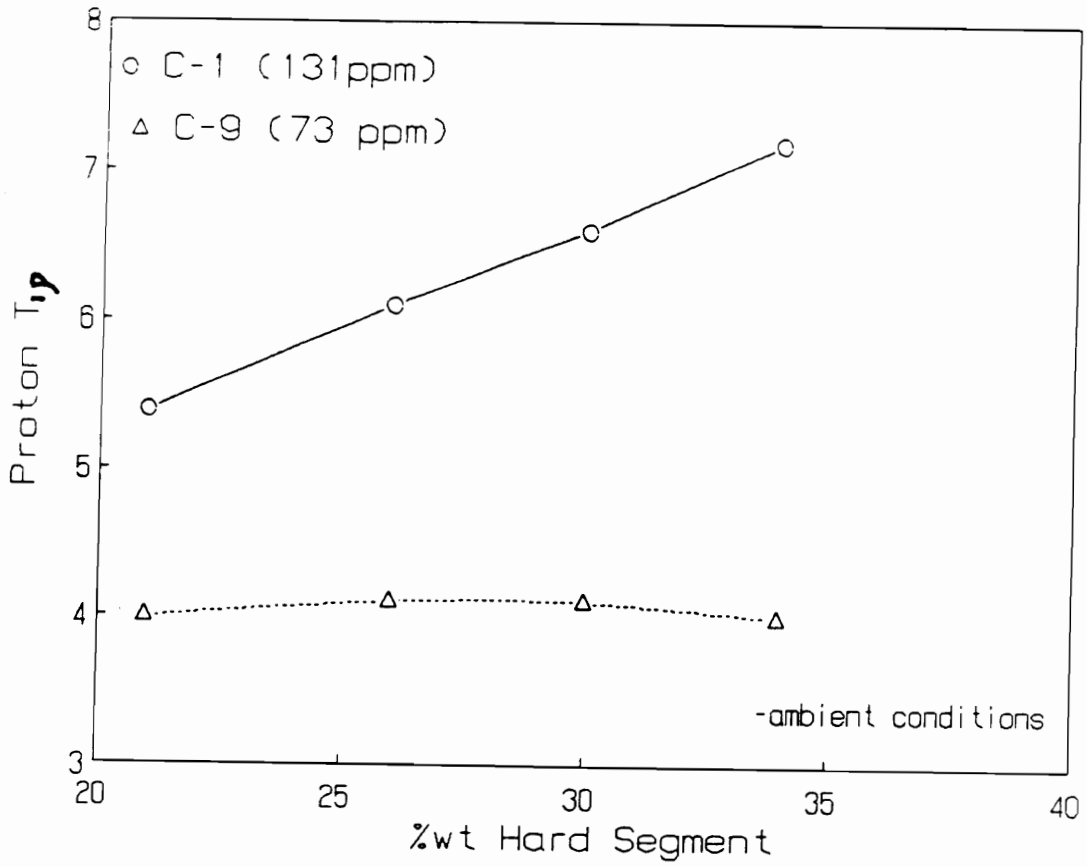

Figure 7.5. Effect of Hard Segment Content on $T_{1\rho}(^1H)$ Values: 131 ppm represents hard segment and 73 ppm represents soft segments; see Table 7.1 for more details

to equalize the relaxation rates. The proximity that this transferal of energy occurs over is thought to be on the order of 1 nm(102). In addition, this transferal of energy can occur between ^1H spins bonded to carbons in different phases or segments(102). Recalling that for foams F1-F4 there is a slight increase in the interfacial region of the hard and soft segments from 0.7 nm to 1.6 nm with increasing hard segment content, one would expect to see changes in the $T_{1\rho}(^1H)$ values for the soft and hard segments with composition. If the thickness of the interface region is important, a decrease in the difference between the hard and soft segment $T_{1\rho}(^1H)$ values with increasing hard segment content would be expected. However, as shown in Figure 7.5 the $T_{1\rho}(^1H)$ values obtained for foams F1-F4 do not agree with this argument - in fact these values exhibit the opposite trend. One possible explanation for this is due to an increase in the size of the urea aggregate structures with increasing hard segment content for foams F1-F4. With the larger aggregate structure present, the influence of spin diffusion from the soft segment to the hard segment is reduced based on the greater distances for spin diffusion to occur over. In an attempt to confirm this speculation, $T_{1\rho}(^1H)$ measurements have also been made on foams 44-0, 44-4 and 44-5 and are discussed below.

The $T_{1\rho}(^1H)$ values for the hard and soft segments of these three foams are shown as a function of lithium chloride content in Figure 7.6. All of the $T_{1\rho}(^1H)$ values obtained for this foam series are also summarized in Table 7.3. As shown in Figure 7.6, there is a steady decrease in both the hard and soft $T_{1\rho}(^1H)$ values with increasing LiCl. This decrease is possibly due to the influence of spin diffusion between the two segments increasing with LiCl content. This explanation does seem plausible based on the morphological changes, i.e reduction and/or removal of the large aggregate structures that are believed to take place upon the addition of LiCl to the formulation. Such changes allow for spin diffusion to be more effective between the soft and hard segments. Another possible explanation is the motion of the soft segments is restricted more by the hard segments with increasing LiCl content. Alternatively, the hard segments may be becoming more mobile or the domains that they are a part of are less cohesive. These changes in the segmental mobility with increasing LiCl content are thought to occur due to more phase mixing which has been indicated by the higher soft segment glass transition temperature obtained from DSC for 44-5 vs. 44-0.

Table 7.3: Proton $T_{1\rho}$(ms)* Values at Ambient Conditions Foams for 44-(0 - 5)

Foam	pphp LiCl	18ppm	73ppm	75ppm	131ppm	136ppm	156ppm
F44-0	0	6.5	4.5	4.7	6.6	6.5	7.2
F44-4	0.4	5.0	3.5	3.6	5.5	5.5	5.2
F44-5	0.5	4.7	3.2	3.3	5.1	4.8	5.4

*Error in $T_{1\rho}(^1H)$ values are $\pm$.3 ms

**The band assignments are given Table 7.1 and Figure 7.2

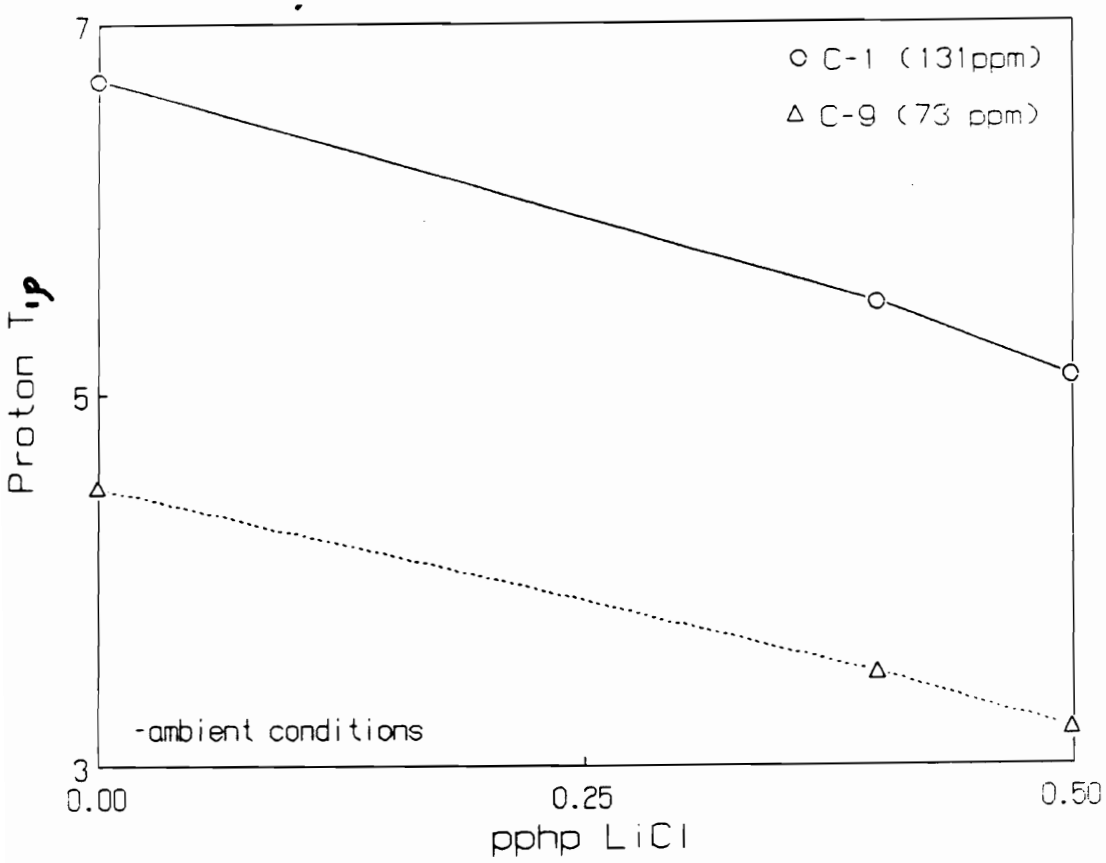

Figure 7.6. Effect of Lithium Chloride Content on $T_{1\rho}(^1H)$ Values: 131 ppm represents hard segment and 73 ppm represents soft segments; see Table 7.1 for more details

This latter explanation does assume that the soft segment $T_{1\rho}(^1H)$ values are on the high frequency side or high temperature side of $T_{1\rho}(^1H)$ minimum whereas the hard segment $T_{1\rho}(^1H)$ values are on the low frequency side(Recall Figure 7.2). In attempt to confirm this assumption, $T_{1\rho}(^1H)$ measurements were made at 70°C. The results did show that the soft segments values were on the high temperature side while the hard segments values changed very little with increasing temperature. This rather small change does indicate that the hard segment values are at or near the minimum of the $T_{1\rho}(^1H)$ inverse temperature curve. In addition, this small change may suggest that this minimum for the hard segment $T_{1\rho}(^1H)$ values is fairly broad. Dickinson et. al. has also shown for a polyurethane network similar behavior as a function of temperature for $T_{1\rho}(^1H)$ values for the soft segments and for $T_{1\rho}(^{13}C)$ values for the hard segments(105). Thus, the high temperature results do indicate that the mobility of the soft segments are being effected with increasing LiCl content for reasons suggested above. On the other hand, it appears that the decrease in the hard segment $T_{1\rho}(^1H)$ values is influenced mostly by spin diffusion, and not by changes in the mobility of the hard segments since the $T_{1\rho}(^1H)$ values show very little dependence on temperature near ambient conditions. This dependence does indicate that the reduction and/or removal of the large aggregate structures is causing the majority of the decrease in the hard segment $T_{1\rho}(^1H)$ values with increasing LiCl content. In addition, since this series of foams (44-0,44-4, and 44-5) has a constant hard segment content, the behavior of their hard segment $T_{1\rho}(^1H)$ values gives further support to the above speculation for foams F1-F4. That is, the polyurea aggregate structure for foams F1-F4 is causing an increase in the $T_{1\rho}(^1H)$ values with increasing hard segment content. In the next section, the topic of mobility is addressed further through discussion of the $T_{1\rho}(^{13}C)$ values.

7.2.2 Carbon-13 Rotating Frame Spin-Lattice Relaxation Measurements

The $T_{1\rho}(^{13}C)$ results have only been obtained for foams F1, F3, 44-0, and 44-5 and are summarized in Table 7.4. $T_{1\rho}(^{13}C)$ values are shown for carbons representing both the soft and hard segments, but the values for the soft segments carbons are only considered here due to the lack of

Table 7.4: Carbon $T_{1\rho}$(msec)* Values at Ambient Conditions

Foam	wt% HS	pphp LiCl	18ppm	73ppm	75ppm	131ppm
F1	21.1	0	23.2	8.1	8.5	(24)
F3	30.1	0	24.0	8.5	9.1	(43)
44-0	34	0	28.7	9.6	10.3	(56)
44-5	34	0.5	19	6.4	6.9	(48)

* Error in $T_{1\rho}(^{13}C)$ is $\pm$0.3msec

**The band assignments are given in Table 7.1 and Figure 7.2

Values in ( ) are inaccurate due to long relaxation times in hard segments

mobility in the hard segments. Furthermore, the $T_{1\rho}(^{13}C)$ values are a measure of the localized motion since ^{13}C is not that abundant and cannot be influenced by spin diffusion.

As shown in Table 7.4, the soft segment $T_{1\rho}(^{13}C)$ values for F1 and F3 do increase slightly, but not within experimental error, with increasing hard segment content. Therefore, this relatively small change in the values for F1 to F3 would indicate that increasing hard segment content has little effect on the motion of the soft segment. For foams 44-0 and 44-5, there is a rather significant decrease in the $T_{1\rho}(^{13}C)$ values for the soft segments with increasing LiCl content(see Table 7.4). This decrease indicates that the motion of soft segments in foam 44-5 is less than that of foam 44-0. As suggested above, the reduction in the mobility of the soft segments of foam 44-5 is most likely brought about by the hard segments restricting the motion of the soft segments. The difference in the mobility of the soft segments in these two foams is believed to be related to the changes which occur in the morphological features upon addition of LiCl to the formulation of foam 44-5. As discussed earlier, these changes are believed to result in a better dispersion of the hard segments and/or formation of smaller aggregate structures within the network structure of the foam.

In summary, from the results for the soft segment $T_{1\rho}(^{1}C)$ values of foams F1-F4 and the $T_{1\rho}(^{1}H)$ values for all of the foams studied, it can be further concluded that the majority of the increase in the hard segment $T_{1\rho}(^{1}H)$ values with hard segment content is due to the polyurea aggregate structures in these foams. Based on the rather small change in the soft segment $T_{1\rho}(^{1}H)$ and $T_{1\rho}(^{13}C)$ values for foams F1-F4, the localized motion of soft segments is not influenced by the increase in the hard segment content. In addition, the $T_{1\rho}(^{1}H)$ and $T_{1\rho}(^{13}C)$ values do indicate that the phase separation of the hard and soft segments is similar for all foams F1-F4. This conclusion is consistent with those of the SAXS and thermal analysis for foams F1-F4 which were mentioned earlier in the literature review. The decrease in the $T_{1\rho}(^{1}H)$ values for the hard segments with increasing lithium chloride content are a result of the morphological changes that occur upon the addition of the lithium chloride to the formulation of foams 44-4 and 44-5. Also, the decrease in the soft segment $T_{1\rho}(^{1}H)$ and $T_{1\rho}(^{13}C)$ values indicate that the motion of the soft segments is restricted more by the hard segments in foams 44-4 and 44-5 in comparison to 44-0. As discussed above, this is believed to be due to more phase mixing in the LiCl foams which corresponds with the SAXS, DSC, and

TEM results shown in the previous chapter. Overall, it has been demonstrated that $T_{1\rho}(^{13}C)$ and $T_{1\rho}(^{1}H)$ values are useful in determining morphological differences in flexible polyurethane foams as well as changes in molecular motion of these materials.

Chapter VIII

8.0 Conclusions and Recommendations

8.1 Conclusions

As a result of the many different tests that were carried out for this dissertation, a considerable number of conclusions and/or suggestions are made here concerning flexible slabstock polyurethane foams. The conclusions for the viscoelastic studies on foams F1-F4 are given first, followed by the effects of LiCl on flexible slabstock foams, and finally conclusions are given for the solid state NMR study of flexible slabstock foams. The conclusions drawn from the FTIR thermal analysis are incorporated with those of the viscoelastic studies.

- The stress relaxation behavior in tension at a 25 percent elongation for flexible slabstock polyurethane foams is dependent on the sclid portion of the foam and thus is independent of its cellular texture. This conclusion is not only supported by previous results obtained by stretching foams F1-F4 parallel and perpendicular to the blow axis, but also by the similar

thermal dependence on stress decay for foams F1 and F4 and their respective compression molded plaques.

- A rather linear relationship exists over a 3 hour time period between the log $\sigma(t)$ vs. log t for the tensile stress relaxation behavior at most conditions for foams F1-F4 as well as their compression molded plaques. The slope of this relationship or the stress decay rate is believed to be of very practical use in predicting the initial short term relaxation behavior. For this rather linear behavior over a 3 hour time period, the stress decay rates are in the range of -2.3x 10^{-2} to -1.7x10^{-2} for foam F1(21 wt% hard segment) and -3.5x10^{-2} to -2.4x10^{-2} for foam F4(34 wt% hard segment).

- An increase in the stress decay rate is observed with increasing hard segment content for foams F1-F4 at ambient conditions. This increase is mostly attributed to the increase in the hydrogen bond content with increasing hard segment content.

- For the load relaxation behavior, a rather linear relationship for the log load - log t response is observed at most conditions and strain levels. For this rather linear behavior over a 3 hour time period, the stress decay rates are in the range of -2.6x10^{-2} to -1.9x10^{-2} for foam F1(21 wt% hard segment) and -3.6x10^{-2} to -2.6x10^{-2} for foam F4(34 wt% hard segment).

- An increase in the hard segment content from 21 to 31 wt. percent does bring about an increase in the load decay rate. However, at hard segment contents ranging from 31 to 34 wt percent there is very little change in the rate of the load relaxation.

- For compressive strain levels up to 65 percent, the compression load relaxation behavior for flexible slabstock foams is mostly independent of their cellular texture. This conclusion is based on the similar relaxation behavior in compression and tension for foams F1-F4 and the conclusion drawn above for the tensile stress relaxation behavior concerning its dependence on the

solid portion of the foam. It is also based on the fact that the compression load relaxation is rather independent of strain up to a 65 percent strain level.

- At strains greater than 65 percent, the compressive load relaxation is dependent on the strain level and exhibits a maximum in the rate of the load relaxation near 75 percent strain. This dependence on strain is believed to be related to a greater localized strain on the solid portion of the foam since the foam is undergoing densification, i.e. the cell walls crush together and the cell wall material itself is compressed.

- After a short induction period(ca. 6 seconds), a near linear relationship between linear strain and log time is observed for the compressive creep behavior for flexible slabstock foams at most conditions. The slope of this relationship or the initial creep rate is dependent on the initial strain level. The initial creep rates at a 65 percent initial strain level for foam F1 range from $0.96x10^{-2}$ to $1.6x10^{-2}$ for foam F1(21 wt% hard segment) and $1.2x10^{-2}$ to $2.1x10^{-2}$ for foam F4(34 wt% hard segment). An increase is observed in the creep rate with hard segment contents in the range of 21 to 31 wt%, but very little change thereafter(up to 34 wt%).

- In the range of 10 to 60 percent strain, the buckling of the struts is believed to govern the compressive creep behavior for flexible slabstock foams. This belief is based on the maximum observed in the creep rate as a function of initial strain near a 40 percent initial strain level for both foams F1 and F4 at 30°C-15%RH. In addition, this observation is supported by the results reported by Campbell on the compressive creep behavior for HR flexible foams as well as the microscopy work in the study by this author (58). At initial strain levels greater than 60 percent and less than 10 percent, the solid portion of the foam is believed to control the compressive creep behavior in flexible foams. This conclusion is based on the fact that there is very little buckling of the struts occurring at strain levels less than 10 percent and greater than 60 percent(33-35,58).

- Temperature as well as relative humidity have similar effects on the tensile stress relaxation, compression load relaxation, and the compressive creep for flexible slabstock foams. Support for this conclusion is given below.

- The effect of temperature on the tensile stress relaxation and compression load relaxation is characterized very well by the following empirical model developed from this study,

$$Stress \vee Load\ Decay = C_1 \exp[\frac{-T}{\tau_1}] + C_2 \exp[\frac{T - T_o}{\tau_2}]$$

This two parameter model accounts for the initial, but rather small, decrease in the load and stress decay values up to 100°C and the significant increase thereafter in the decay. The temperature relaxation constant, τ_1 is believed to represent the small initial decrease in decay values up to 100°C while τ_2 represents the significant increase in the decay values at temperature greater than 100°C. This model and its constants also exemplifies some of the similarities in the thermal dependence of the relaxation behavior in compression and tension. For example, the values for τ_1 and τ_2 for foam F4 in tension are 252 and 18.3, respectively and those in compression for F4 are 274 and 21.5, respectively.

- By increasing temperature in the range of 25°C to 100°C, the viscoelastic decay, i.e. tensile stress relaxation, compression load relaxation and compression creep over 3 hours is accelerated for flexible polyurethane foams. This conclusion is based on the observance of a small decrease in the 3 hour relaxation rates in tension and compression as well as in the 3 hour creep rate with increasing temperature. Also within this same temperature range, the viscoelastic decay is believed to be accelerated more in the higher hard segment foams. This belief is supported by the greater changes detected in the creep rate and relaxation rates for foam F4 in comparison to F1.

- For all three viscoelastic tests, a significant increase in the viscoelastic decay at temperatures greater than 100°C is observed. In addition, temperature has a greater effect on the viscoelastic

decay of the lower hard segment foam, F1, in comparison to foams F2-F4. This latter conclusion is supported especially by the opposite trend in the load and stress decay values for foam F1 and F4 at 140°C, i.e. these values are higher for foam F1 than for F4 at 140°C. Based on the FTIR thermal analysis of the plaques, this significant increase in the viscoelastic decay is attributed to additional hydrogen bond disruption as well as degradation of the urea and urethane links. Furthermore, this analysis revealed that these structural changes are greater for the lower hard segment foam, F1, in comparison to foams F2-F4.

- The unrecoverable compression set at temperatures greater than 100°C for foams F1-F4 is believed to be related to chain scission or degradation taking place in the urea and urethane links. This belief is supported by the observance of free isocyanate band by FTIR at these high temperatures. In addition, this belief is further supported by the observance of residual hard segment orientation after deforming plaque 2-DMF at temperatures greater than 100°C.

- Increasing relative humidity at a given temperature does cause an increase in the viscoelastic decay as well as a decrease in the load of flexible foams. Such changes are believed to be due to water acting as a plasticizer and thus promoting localized chain slippage to take place. The increase in the viscoelastic decay is greater for the lower hard segment foam, F1 in comparison to F4 at 30°C. However, at the higher temperatures(85°C for compression and 90°C for tension), increasing relative humidity does result in greater changes in the load and stress decay rates for F4 than in F1, and there are similar changes observed for both foams in the initial creep rate. Also, from 30°C to 85°C there is a more significant increase in the effect of relative humidity on the viscoelastic decay of foam F4 in comparison to F1. This difference in behavior is believed to be due to water interacting more with the hard domains with increasing temperature. Such interaction is thought to be facilitated by a weakening of the hydrogen bonds between the hard segments.

- Cycling relative humidity in comparison to maintaining humidity at a constant level does have a greater effect on the compressive creep behavior for flexible foams. This conclusion is based

on an increase observed in the strain level by rapidly increasing or decreasing relative humidity. This type of behavior is also thought to be similar to the mechano-sorptive creep phenomena observed for some other polymeric materials that contain hydrogen bonds.

- In comparing the effects of temperature and relative humidity on the viscoelastic decay as determined by stress relaxation, compression load relaxation and compression creep, temperature does have a greater effect than humidity on the relaxation and creep behavior for foams F1-F4 - especially at temperatures greater than 100°C.

- A similar linear relationship to that of the foams is also observed for the log $\sigma(t)$ vs. log t tensile stress relaxation behavior for the PUU elastomer. In addition, comparable thermal dependence on the log $\sigma(t)$ vs. log t behavior exists for the PUU elastomer and foams F1-F4. The results from the FTIR thermal analysis and the orientation changes with deformation also show similar effects are taking place in the PUU elastomer and the plaques of these foams with increasing temperature. However, the changes in the relaxation behavior and the changes observed by the FTIR thermal analysis with increasing temperature are greater for the PUU elastomer. Recall that the foams and the PUU elastomer are chemically different due to the MOCA chain extender utilized in making the PUU elastomer. While the effects of increasing temperature on the PUU elastomer are greater, the forces that govern the structural changes that take place in the PUU elastomer and foams F1-F4 are still thought to be similar; despite the fact that the PUU elastomer contains a linear segmented morphology and the foams possess a covalent network.

- The addition of lithium chloride(LiCl) to the formulation of a flexible polyurethane foam does alter the morphology of solid portion significantly. These changes in the morphology are believed to result in the formation of smaller aggregates and/or the hard segments being dispersed as single units in the network. In addition, more phase mixing of the soft and hard segments is also thought to result due to the addition of LiCl. These suggested changes are supported

by TEM, DSC, SAXS, WAXS, and solid state NMR results obtained on two LiCl foams, 44-4 and 44-5, and their control, 44-0.

- The addition of lithium chloride to the formulation also effects the cellular textures of a foam by causing more cellular window material to be present.

- The addition of LiCl to the formulation also causes a greater amount of viscoelastic decay, i.e. relaxation in both compression and tension as well as in the compressive creep in the LiCl foams in comparison to its control. This difference is believed to be a result of more mobility in the hard segments of LiCl foams which is attributed to the morphological changes. In addition, the LiCl molecule is possibly acting as plasticizer and more specifically a hydrogen bond plasticizer to promote further viscoelastic decay in the foam.

- Temperature and relative humidity effect the LiCl foam, 44-5, more than the that of the control foam, 44-0. The differences in the solid morphology also give support to this conclusion. That is, more phase mixing is likely to occur as one increases temperature in the LiCl foam due to its lower structural order. In addition, the hard segments of the LiCl foams are believed to interact more with water, especially at lower temperatures.

- Solid state NMR is a useful technique to determine morphological differences as well as changes in molecular motion in flexible slabstock foams. The mobility of the soft segments in foams F1-F4 are not affected by the increase in hard segment content. This conclusion is supported by the very little change in the $T_{1\rho}(^{13}C)$ and $T_{1\rho}(^{1}H)$ values obtained for the soft segments of foams F1-F4. The increase in the size of the urea aggregate structures in foams F1-F4 is effecting the $T_{1\rho}(^{1}H)$ values for the hard segments through spin diffusion. This conclusion is supported by the decrease observed in the $T_{1\rho}(^{1}H)$ hard segment values with increasing LiCl content for a set of foams(series 44-0,4, and 5) with a constant hard segment content. The $T_{1\rho}(^{1}H)$ and $T_{1\rho}(^{13}C)$ values for foams F1-F4 also indicate that the phase separation for the hard and soft segment is similar for these foams.

- The mobility of the soft segments for the LiCl foams(44-4 and 44- 5) are thought to be restricted more by the hard segments in comparison to its control foam, 44-0. This suggestion is based on the small decrease in $T_{1\rho}(^{13}C)$ and $T_{1\rho}(^{1}H)$ soft segment values with increasing LiCl content.

8.2 Recommendations for Future Work

Future work should begin by continuing to utilize the above techniques on other flexible foams. In addition, other techniques with the emphasis on evaluating or monitoring the properties of flexible foams over time should also be developed. Some examples of these two suggestions are given in more detail below along with other future considerations.

- The viscoelastic studies utilized in this dissertation should also be applied to additional flexible polyurethane foams where other formulation components have been altered. One modification in the formulation could be made in the polyol, i.e. its functionality, EO/PO content, or endcap it with different functionalized groups (e.g. amine). Other types of flexible foams should also be tested. For example, additional foams related to the CFC issue, foams used for carpet underlay and/or high resilient(HR) foams could be utilized. The latter foams are definitely of interest with regard to viscoelastic properties since they do exhibit high compression set values(37-39,43-44).

- Further testing with regards to cycling relative humidity while measuring the creep behavior should be carried out. The results shown earlier for this type of test are rather interesting and furthermore are thought to be similar to the mechano-sorptive creep phenomena observed for some polymeric materials that contain hydrogen bonds. In investigating this further, a greater number of cycles should be utilized to see if the effect of increasing and decreasing relative

humidity on the creep behavior continues. In this dissertation, the humidity was only cycled from low humidity to high humidity and then back to low humidity. Also other foams, i.e. lower hard segment foams could be characterized in this manner as well. It may also be of interest to see if the load relaxation behavior in compression or tensile stress relaxation is affected by cycling relative humidity. Again, it is thought that a significant decrease in the load or stress level will be observed by rapidly increasing relative humidity, but upon lowering the relative humidity it is not known what is to take place based on the results observed for the creep behavior. Tensile creep on the plaques of these foams as well as the PUU elastomer should also be carried out under cyclic relative humidity conditions. (The reports in the literature for which the mechano- sorptive phenomena has been observed are usually based on data obtained from tensile creep tests(93-98)).

- In further understanding and confirming the compression creep phenomena at initial strain levels of 10 to 60 percent, a video recording during a creep experiment could be made. As discussed in the results and discussion, the buckling of the struts are thought to govern the compressive creep behavior in this range of strain. Thus, a high speed recording would hopefully confirm this phenomena as well as give some idea of the amount of struts undergoing buckling at a given strain level.

- Instead of applying a constant strain level as in the compression load relaxation studies, a small cyclic strain($\pm$2.5%) could be applied to the foam at a 60 to 65 strain level while monitoring the load decay over time. This type of test is thought to give information on the effect of cyclic fatigue on a foam over time. A similar type of test could also be performed for a compression creep test except the strain level would be monitored in this case.

- While a better understanding has been obtained for the effect of relative humidity on the relaxation behavior as well as creep, more data is needed concerning the weight uptake of water in these foams. Such data is of importance since the relaxation behavior is thought to be a function of the weight uptake of water. However, as discussed within this dissertation this type

of data is rather difficult to obtain - mostly related to the experimental apparatus(high temperatures especially) and the foams themselves. It is recommended that these measurements be carried out in an environment where the conditions can be obtained over a large temperature and relative humidity range. In addition, an experimental apparatus should be designed in which the weight uptake can be monitored while the foam or plaque is exposed to the desired conditions.

- The effects of the LiCl in the formulation of the PUU elastomer should also be investigated. Also, additional elastomers should be made from the same chemical components as the PUU elastomer, but with different hard segment contents. The latter suggestion would enable further comparisons to foams F1-F4.

References

1. G. Woods, "The ICI Polyurethanes Book," ICI and John Wiley & Sons, Netherlands, (1987).

2. G. Woods, "Flexible Polyurethane Foams: Chemistry and Technology," Applied Sci. Plublishers, LTD, New Jersy (1982).

3. Dow Chemical Co., "The Flexible Foam Handbook," Dow Chem. USA, Urethane Dept., Midland, MI.

4. K.C. Frisch and J.H. Saunders, "Plastics Foams: Part 1," Marcel Decker, Inc., New York (1972).

5. R.D. Duffy and R.D. Whittman, J. Cell. Plastics, 14(3), 161 (1978).

6. G. Burkhart, H.J. Kollmeier and H.H. Schloens, J. Cell Plastics, 19, 441 (1983).

7. P.S. Zurer, Chemical and Engineering News, 67, 7 (1989).

8. Rubber and Plastics News, October, 15 (1990).

9. Proceedings(Abstracts) of SPI Polyurethane Division Confernce (1990).

10. G. Rossmy, H.J. Kollmeier, W. Lidy, H. Schator and M. Wiemann, J. Cell. Plastics, 17(6), 319 (1981).

11. G. Rossmy, W. Lidy, H. Schator, M. Wiemann and H.J. Kollmeier, J. Cell. Plastics, 13(1), 26 (1977).

12. B. Kanner and T.G. Decker, J. Cell. Plastics, 4, 32 (1969).

13. B. Kanner, B. Prokai, C.S. Eschbach, and G.J. Murphy, J. Cell. Plastics, 15, 315 (1979).

14. F.E. Bailey and F.E. Critchfield, J. Cell. Plastics, 17, 333 (1981).

15. G. Hauptman, K.H. Dorner, J. Hocker and G. Pfister, Proceedings of the 5th. International SPI- Conference, 1980.

16. J. Hocker, J. Appl. Polym. Sci., 25, 2879 (1980).

17. H.W. Illeger, K.H. Dorner, H. Hettel, Polyurethane World Congress, 305 (1987).

18. R.L. Rowton, J. Cell. Plastics, 16, 287 (1980).

19. P. Van Gheluwe and J. Leroux, J. Appl. Polym. Sci., 28, 2053 (1983).

20. J.P. Armistead, MS Thesis, Virginia Polytechnic Institute and State University, Chemical Eng. Dept., Blacksburg, VA (1985).

21. J.P. Armistead, G.L. Wilkes and R.B. Turner, J. Appl. Polym. Sci., 35, 601 (1988).

22. J.C. Moreland, MS Thesis, Virginia Polytechnic Institute and State University, Chemical Eng. Dept., Blacksburg, VA (1989).

23. J.C. Moreland, G.L. Wilkes and R.B. Turner, J. Appl. Polym. Sci., accepted.

24. R.B. Turner, H.L. Spell, G.L. Wilkes, SPI 28th Annual Technical/Marketing Conference, 244 (1984).

25. J.W.C. Van Bogart, A. Lilaonitkul and S.L. Cooper, Adv. Chem., 176, 3 (1979).

26. C.S. Paik Sung, C.B. Hu and C.S. Wu, Macromol., 13, 111 (1980).

27. D. Tyagi, Ph.D. Thesis, Virginial Polytechnic Institute and State University, Chemical Eng. Dept., Blacksburg, VA (1985).

28. R. Bonart, L. Morbitzer and E.H. Muller, J. Macromol. Sci. Phys., B9(3), 447 (1974).

29. G.L. Wilkes and S. Abouzahr, Macromol., 14, 458 (1981).

30. J.T. Koberstein and R.S. Stein, J. Polym. Sci., Polym. Phys. Ed., 21, 1439 (1983).

31. A.N. Gent and A.G. Thomas, J. Appl. Polym. Sci., 1, 107 (1959).

32. A.N. Gent and A.G. Thomas, Rubber Chem. Tech., 36, 597 (1963).

33. M.F. Ashby, Mettalurgical Trans., 14A, 1755 (1983).

34. L.J. Gibson and M.F Ashby, Proc. R. Soc. Lond., 382, 43 (1982).

35. Hilyard, "Mechanics of Celluar Solids," Applied Sci. Publishers, LTD, New Jersey, 1980.

36. K.C. Rusch, J. Appl. Polym. Sci., 13, 2297 (1969).

37. C.B. Wang and S.L. Cooper, Macromol., 16, 775 (1983).

38. W. Patten and D.C. Priest, J. Cell. Plastics, 8, 134 (1972).

39. W. Patten, C.G. Seefried, R.D. Whitman, and D.E. Pollart, J. Cell. Plastics, July, 172 (1974).

40. W. Patten and C.G. Seefried, J. Cell Plastics, 12, 41 (1976).

41. P.E. Kreter, J. Cell Plastics, Sept./Oct., 306 (1985).

42. S. Consoli, P. Pizziolo, and G. F. Martins, Proceedings of the SPI-6th International Tech./Marketing Conf., 230 (1985).

43. R.M. Herrington and D.L. Klarfeld, Proceedings of the SPI-6th International Tech./Marketing Conf., 177 (1983).

44. K. Saotome, K. Matsurbara, and T. Yatomi, J. Cell. Plastics, 13, 203 (1977).

45. J.M. Hogan, C.J. Pearson, T.H. Rogers, and J.R. White, J. Cell. Plastics, Sept., 221 (1973).

46. S.M. Terry, J. Cell. Plastics,12, 156 (1976).

47. F.J. Dywer, J. Cell. Plastics, 12, 104 (1976).

48. B. Beals, F.J. Dywer, and M. Kaplan, J. Cell. Plastics, Jan. (1965).

49. R.P. Kane, J. Cell Plastics, 7, 5 (1971).

50. V.W. Shrichatrapimuk and S.L. Cooper, J. Macromol. Sci. Phys., 15, 267 (1978).

51. W.M. Lee, Proceedings of the SPI-30th Annual Tech./Marketing Conf., 138 (1985).

52. W.J. Dzierza, J. Appl. Polym. Sci., 27, 1487 (1982).

53. R.W. Seymour, G.M. Estes, D.S. Huh, and S.L. Cooper, J. of Polym. Sci., 10(A-2), 1521 (1972).

54. D.J. Doherty and G.W. Ball, J. Cell. Plastics, 3(5) (1967).

55. E.A. Meinecke and R.C. Clark, "The Mechanical Properties of Polymeric Foams," Technomic Publishing Co., Inc., Westport, Conn (1973).

56. J. Miltz and O. Raman, Polym. Eng. and Sci., 26, 1305 (1986).

57. M. Peleg, J. Rheology, 24, 451 (1980).

58. G. Campbell, J. of Polym. Sci., 24, 709 (1979).

59. R.S. Stein, Rubber Chem. and Tech., 44, 458 (1976).

60. G.L. Wilkes, J. Macromol. Sci. Review Macromol. Chem. 10(2), 149 (1974).

61. H.W. Siesler, "Infrared and Raman Spectroscopy of Polymers," New York: Marcel Dekker (1980).

62. R.D.B. Fraser, J. Chem. Phys., 21, 1511 (1953).

63. R.S. Stein , personal communication

64. J.L. White and J.E. Spruell, Polym. Eng. Sci., 21, 859 (1981).

65. J.L. White, J. Polym. Eng., 5, 277 (1985).

66. K. Hoffman and R. Bonart, Colloid and Polym. Sci., 262, 1 (1984).

67. I. Ishihara, I. Kimura, K. Saito and H. Ono, Macromol. Sci.-Phys., B10(4), 591 (1974).

68. I. Kimura, H. Ishihara, H. Ono, N. Yoshihara, S. Nomura, and H. Kawai, Macromol., 7, 355 (1974).

69. V.A. Khranovskii and L.P. Gul'ko, J. Macromol. Sci.-Phys., B22(4), 497 (1983).

70. H.W. Siesler, Ver. Phys. Chem., 92, 641 (1988).

71. M. Shibayama, T. Kawauchi, T. Kotani, S. Normura, and T. Matsuda, Polymer J., 18, 719 (1986).

72. M. Shibayama, Y. Ohki, T. Kotani, and S. Normura, Polymer J., 19, 1067 (1987).

73. R. Bonart, L. Morbitzer, and G. Hentze, J. Macromol. Sci., B3, 337 (1969).

74. R.W. Seymour, A.E. Allegrezza and S.L. Cooper, Macromol, 6, 896 (1973).

75. R.W. Seymour and S.L. Cooper, J. Polym. Sci. Symposium, 46, 69 (1974).

76. R. Bonart and K. Hoffman, Colloid and Polym. Sci., 260, 268 (1982).

77. K. Hoffman and R. Bonart, Makromol. Chem., 184, 1529 (1983).

78. C.S.P. Sung and N.S. Schneider, Macromol., 10, 452 (1977).

79. C.S.P. Sung and N.S. Schneider, J. of Mat. Sci., 13, 1689 (1978).

80. G.A. Senich and W.J. MacKnight, Macromol., 13, 106 (1980).

81. H.W. Siesler, Polymer Bull., 9, 557 (1983).

82. T. Yamamoto, M. Shibayama, and S. Normura, Polymer J., 21, 895 (1989).

83. C.S.P. Sung, T.W. Smith and N.H. Sung, Macromol., 13, 117 (1980).

84. R.W. Seymour and S.L. Cooper, Macromol, 6, 48 (1973).

85. Annual ASTM Standards, 1564 (1981).

86. M.M. Coleman, K.H. Lee, D.J. Skrovanek, and P.C. Painter, Macromol, 19, 2149 (9186).

87. R. Priester of Dow Chemical, personal communication

88. Cohort Software Co., (1989)

89. A.V. Tobolsky, "Properties and Structure of Polymers," Wiley, New York, (1960).

90. R.W. Ramette, "FLEXFIT Software Program," (1988).

91. T.L. Smith and R.A. Dickie, J. of Polym. Sci., Part A-2, 7, 635 (1969).

92. Polakowski and Ripley, "Strength and Structure of Engineering Materials," Printice Hall, Inc., Englewood Cliffs, N.J. 1966.

93. E.J. Gibson, Nature, 4980, 213 (1965).

94. B.H. Mackay and J.G. Downes, J. of Applied Polym. Sci., 2, 32 (1959).

95. L.D. Armstrong, Wood Science, 5(2), 81 (1972).

96. R. Gardner and E.J. Gibson Forest Products Journal, 5, 50 (1967).

97. R. H. Ericksen Polymer, 26, 733 (1985).

98. J.Z. Wang, D.A. Dillard, M.P. Wolcott, F.A. Kamke, and G.L. Wilkes, J. Composite Materials, 24, 994 (1990).

99. M. Heaney of Dow Chemical, personal communication

100. C.A. Fyfe, "Solid State NMR for Chemistry,", Guelph Ontario (1983).

101. J. Schaefer and E.O. Stejskal, Topics in Carbon-13 NMR Spectroscopy,", John Wiley and Sons, Inc., NY, 34 (1979).

102. V.J. McBriety and D.C. Douglass, Macromol. Reviews, 16, 295 (1981).

103. F.A. Bovey and L.W. Jelinski, "Encyclopedia of Polymer Science and Engineering, "Nuclear Magnetic Resonance,, 10, 254 John Wiley and Sons, Inc., NY (1987).

104. T.C. Farrar and E.D. Becker, "Pulse and Fourier Transform NMR," Academic Press, Inc., NY (1971).

105. L.C. Dickenson, P. Morganelli, C.W. Chu, Z. Petrovic, W.J. MacKnight, and J.C.W. Chien, Macromol., 21, 338 (1988).

Appendix A

Components for Experimental Apparatuses for Compression Viscoelastic Tests

A. Compression Load Relaxation

1. Tensile\Compression Tester(Model 1122)
   Manufacturer: Instron

2. Compression Load Cell (MDB-10)
   Manufacturer: Trans Tech, Inc.
   Description: Load cell has a 10lb usuable load range with a 150 percent overload range; Non-linearity is 0.05% of rated output(2mv/v)

3. Analog to Digital Converter(ADM12-10)
   Manufacturer: Qua Tech, Inc.
   Description: The ADM12-10 is a 12-bit A/D conversion module and is used in conjunction with a PXB-721 Parallel Expansion Board. By using the software package, it is capable of a throughput rate of 24 kHz.

4. Environmental Chamber
   Manufacturer: Russells Technical Products
   Description: Sample chamber serves to control humidity and temperature. Temperature can be controlled in the range of -20°C to 300°C. Humidity is controllable in the range of 0-15%RH to 95-100%RH in the temperature range of 4°C to

85°C. An air circulator within the chamber serves to maintain uniform conditions within the chamber. In addition, a Watlow 922 microprosser controller is utlized to set the desired conditions as well as maintain them. Humidity cooling is provided by a 1/3 HP compressor. Humidity is increased by introducing water vapor into the chamber. The chamber has a working space of 11″ wide x 14′ deep x 25″ high and its outer dimensions are 15″ wide x 42 ″ deep x 34 ″ high.

5. Amplifier

Manufacturer: Constructed at Virginia Tech by Riley Chan

Description: Functions as a means to amplify voltage from load cell, as a signal conditioner and as a power source for load cell; has 1% non-linearity

B.Compressive Creep

1. Twin Shaft Rail Assembly

Manufacturer: Thompson

Description: Consists of a carriage with linear bearings which enables frictionless movement on highly precision stainless steel rods

2. Linear Voltage Displacement Transducer(LVDT)

Manufacturer: Schaevitz

Description: Detects a maximum of 0.5 inch movement; accuracy is 0.05% fullscale

3. The above environmental chamber(A.4) was also utilized as well as the A/D card(A.3) for the creep tests

Appendix B
Weight Uptake Measurements

Weight uptake measurements of water into plaques of foams F1 and F4 were performed in order to obtain some estimate of the their difference in affinity for water. In addition, the effect of temperature on the weight uptake of water in these materials was also considered. As stated in Chapter 5, the plaques of these foams were utilized rather than the foams due to problems with separating the surface water from the physically absorbed water. The methods and the results of the weight uptake studies at 23°C and 38°C are presented below.

The weight-uptake measurements at 23°C were made using a manifold system which contained a calibrated quartz spring to determine the weight of water in the sample. The samples utilized for P1 and P4 were both approximately 6 mils in thickness and were cut into small pieces and layered together. This was done since large strips adhered to the glass housing of the manifold system. The measurements were made on P1 and P4 after drying the samples at 110°C for at least 1 hour in order to remove any water that was initially present in these samples. The results obtained for plaques P1 and P4 using this apparatus at saturated conditions exhibited the same percent weight up- take of water which was 0.5 percent. The absorption of water at this condition(23°C, 100%RH) took place within 30 minutes of exposure to the saturated conditions for both plaques. In addition, the water absorbtion was reversible. Measurements at saturated conditions and 38°C were made using an enclosed chamber and with an air circulator. The samples used for this study were approximately 8 mils in thickness for both P1 and P4 which corresponds to about 1 inch in thickness of foam used to compression mold these plaques. After drying the samples in a vacuum over at

110°C for at least 3 hours, the samples were placed in sample chamber which was maintained at 38°C-100%RH. At various time intervals, the samples were removed and immediately patted dry in order to remove any surface water and then weighed. The time to reach "equilibrium" was approximately 30 to 45 minutes of exposure to the condition of 38°C and 100%RH. The weight uptake values using at this condition were 1.3 wt% for P1 and 1.6 wt% for P4.

The few results do indicate that the absorption for water is the same at 23°C for the plaques, but is about 20 percent greater at 38°C for the higher hard segment plaque, P4. A larger weight uptake of water is expected for P4 in comparison to P1 since it's urea content is 4 times greater than that of P1. In addition, the urea hard segments are thought to have higher affinity for water than the soft segments. Thus, it appears with increasing temperature that the access to the urea hard segments is better. This is likely a result of weakening hydrogen bonds within the hard domains and the urea aggregates. The weight up- take results also exhibited an increase with increasing temperature. However, the actual extent of this increase is not known due to using two different experimental apparatuses. For example, in the apparatus where the chamber(38°C) was utilized there was a circulator and in the manifold(23°C) there was not. Also, the sample geometry that was utilized for the two set-ups was different, i.e. 0.5″ x 1″ thin strips were used at 38°C and very small thin strips that had to be layered were used at 23°C.

Vita

John Calloway Moreland was born on August 19, 1963 to Dr. and Mrs. Charles G. Moreland in Gainesville, Florida. He grew up in Raleigh, N.C. where he attended Needham B. Broughton High School. In 1986, he obtained his Bachelor of Science degree in Chemical Engineering from North Carolina State University. He then entered Virginia Tech and in February of 1989 received his Master of Science in chemical engineering. In April of 1991, he completed his Doctorate in chemical engineering at Virginia Tech under the guidance of Dr. G.L. Wilkes. He has accepted a research and development position with Michelin Tire Corporation in Greenville S.C. Cal will also be marrying Ms. Cheryl Whitfield of Roxboro, N.C. on June 1, 1991.